

CTR-C24(1-2)1-271

# COMSAT

## Technical Review

Volume 24 Number 1-2, 1994/1995

*Advisory Board* Joseph J. Duda  
 John V. Evans  
 John S. Hannon  
 Carl M. Jeffcoat

*Editorial Board* Michael Onufry, *Chairman*  
 Dattakumar M. Chitre  
 Calvin B. Cotner  
 Allen D. Dayton  
 Russell J. Fang  
 Ramesh K. Gupta  
 Edmund Jurkiewicz  
 Lewis R. Karl  
 Mark T. Neibert  
 Amir I. Zaghoul

*Past Editors* Pier L. Bargellini, 1971–1983  
 Geoffrey Hyde, 1984–1988  
 Richard A. Arndt, 1989–1993

*Editorial Staff* MANAGING EDITOR  
 Margaret B. Jacocks  
 TECHNICAL EDITOR  
 Barbara J. Wassell  
 PRODUCTION  
 Barbara J. Wassell  
 N. Kay Flesher, *Composition*  
 Virginia M. Ingram, *Graphics*  
 CIRCULATION  
 Merilee J. Worsey

COMSAT TECHNICAL REVIEW is published by COMSAT Corporation. Subscriptions are: one year, \$25 U.S.; two years, \$45; three years, \$60; single copies, \$15; article reprints, \$3. Overseas airmail delivery is available at an additional cost of \$10 per year. Make checks payable to COMSAT and address to: Records Department, COMSAT Corporation, 22300 COMSAT Drive, Clarksburg, MD 20871-9475, U.S.A.

ISSN 0095-9669

© COMSAT CORPORATION 1996  
 COMSAT IS A TRADE MARK AND SERVICE MARK  
 OF COMSAT CORPORATION

# COMSAT TECHNICAL REVIEW

Volume 24 Number 1-2, 1994/1995

## Focus On INTELSAT-K

- v FOREWORD: INTELSAT-K—A UNIQUE ALL-KU-BAND SATELLITE IN INTELSAT'S SPACE SEGMENT  
**A. M. Goldman, Jr. AND A. Ozkul**
- 1 INTELSAT-K SPACECRAFT BUS PERFORMANCE CHARACTERISTICS  
**K. Raghunathan, T. Rush AND A. Ozkul**
- 25 THE INTELSAT-K PAYLOAD  
**R. A. Peters, F. L. Khoo AND A. Ozkul**
- 47 INTELSAT-K COMMUNICATIONS PERFORMANCE FEATURES  
**M. P. Brown, Jr., R. W. Duesing, J. A. Tehrani AND K. Bhatnagar**
- 65 INTELSAT-K TRANSPONDER IN-ORBIT TESTS AND OPERATIONAL CONSIDERATIONS  
**B. Teixeira**
- 79 INTELSAT-K LAUNCH VEHICLE CONSIDERATIONS  
**A. M. Goldman, Jr. AND A. Ozkul**

## Other Topics

- 95 SYSTEM ARCHITECTURES FOR SATELLITE NEWSGATHERING  
**W. A. Sandrin, T. Abdel-Nabi, S. A. Ames, D. V. Haschart, K. M. Price AND A. K. Rao**
- 145 BANDWIDTH ON DEMAND FOR THE INTELSAT NETWORK  
**T. R. Henderson**
- 161 ACOUSTIC ECHO CONTROL CONSIDERATIONS FOR VIDEO TELECONFERENCING  
**C. S. Ravishankar AND M. Onufry**
- 191 COMMUNICATIONS PERFORMANCE OF THE INTELSAT VII AND VIIA SATELLITES  
**S. Jamshidi AND C. B. Cotner**

*Best Paper Award, ICDSC9*

- 221 A BISDN-COMPATIBLE 140/155-MBIT/S MODEM/CODEC  
S. P. Miller, F. Hemmati, D. H. Layer AND P. N. Johnson
- 241 TRANSLATIONS OF ABSTRACTS  
FRENCH 241 SPANISH 246
- 251 AUTHOR INDEX, CTR 1993
- 253 INDEX OF 1993/1994 PUBLICATIONS BY COMSAT AUTHORS

**Foreword**

***INTELSAT-K—A unique all-Ku-band satellite in  
INTELSAT's space segment***

A. M. GOLDMAN, JR., Co-Editor, COMSAT  
A. OZKUL, Co-Editor, INTELSAT

In 1989, INTELSAT purchased the partially completed GE SATCOM K4 satellite from General Electric Technical Services Corporation (GETSCO) with the intention of modifying its payload to carry primarily leased video and business services traffic over the Atlantic Ocean Region. As part of these modifications, the antenna subsystem was changed to provide high-power coverage over Europe and North America using a dual-beam deployable antenna, and split-beam downlink-only coverage to South America using a fixed antenna. A new transponder subsystem was implemented consisting of 16 channels with power amplifiers configured in two sets of 11-for-8 redundancy, providing up to 47-dBW edge-of-coverage specified effective isotropically radiated power (EIRP). The high-power payload is accommodated on a Series 5000 bus, which underwent little change from K4 except for the incorporation of improved electrostatic discharge protection and momentum wheel lubrication.

From the signing of the construction contract through delivery of the spacecraft, the INTELSAT-K procurement cycle took 28 months. The satellite was launched on June 9, 1992, from Cape Canaveral, Florida, by an Atlas II-A launch vehicle, to begin service at 338.5°E longitude in mid-September 1992. An orbital maneuver life in excess of 9 years was projected after launch. The spacecraft design life is 10 years. INTELSAT-K is currently operating at the 338.5°E orbital slot, collocated with an INTELSAT V spacecraft.

During construction of INTELSAT-K, the INTELSAT Program Office (ISPO) was established at the GE Astro plant in East Windsor, New Jersey, to monitor the construction and testing of the spacecraft. The office was also instrumental in the successful completion of launch site tests and in launch mission control, which was conducted from the Astro Spacecraft Operations Center. The ISPO initiated and maintained technical contact with the owners of the already operational sister spacecraft to INTELSAT-K—ASTRA-1B, and ANIK E1 and E2—to learn more about Series 5000 spacecraft performance during the launch mission and in-orbit operations. Valuable lessons learned through this interface were applied to improve spacecraft integration, test, and operational



**COMSAT**  
Technical Review

Volume 24 Number 1-2, 1994/1995

procedures, and even to correct some manufacturing concerns that improved INTELSAT-K mission reliability.

Although several challenges were encountered during construction of INTELSAT-K, they were successfully met by the dedicated staffs at GE-Astro and INTELSAT. Today, INTELSAT-K is operating successfully over the Atlantic as the first all-Ku-band spacecraft in INTELSAT's space segment, providing video and other network services to a large number of international customers. As one customer representative explained recently, "INTELSAT-K is a reliable and unique satellite which is capable of providing total connectivity on one hop between three continents." Another customer praised INTELSAT-K's efficient operability by saying "In addition to its wider coverage, INTELSAT-K is a newsgatherer's dream for flexibility and switchability, providing quick access to virtually all points within its coverage at a reasonable cost."

The first five papers in this issue of *COMSAT Technical Review* discuss INTELSAT-K. COMSAT and INTELSAT authors summarize highlights of the spacecraft's manufacture, as well as the launch and postlaunch operational experiences gained with this uniquely successful satellite.

Index: INTELSAT, broadcast satellites

## **INTELSAT-K spacecraft bus performance characteristics**

K. RAGHUNATHAN, T. RUSH, AND A. OZKUL

(Manuscript received January 17, 1995)

### **Abstract**

The INTELSAT-K spacecraft is a GE/Martin Marietta Series 5000 three-axis-stabilized platform equipped with four 22-cell, 50-Ah batteries and capable of providing 3.5 kW of solar array power after 10 years in orbit. The main spacecraft body contains the central cylinder, propulsion tanks, and thrusters. The thrusters include twin 490-N, dual-mode, liquid apogee engines and four improved electrothermal hydrazine thrusters for inclination control. The spacecraft mass at liftoff was 2,925 kg, with a dry weight of 1,250 kg. The general design characteristics of INTELSAT-K are described, with emphasis on spacecraft bus capabilities as they relate to the on-orbit operations of the satellite.

### **Introduction**

INTELSAT-K is a three-axis-stabilized spacecraft based on the General Electric (GE)/Martin Marietta Series 5000 platform employing both fixed and deployable communications antennas. The spacecraft is modular in design, with most of the payload components being located on the north and south panels, which provide large radiating surfaces to facilitate on-orbit thermal control. Command security is provided by the KI-23 command encryption algorithm. The deployable solar arrays are designed to provide more than 3.5 kW at the end of life, with four independently charged 50-Ah nickel-hydrogen (Ni-H<sub>2</sub>) batteries for full-eclipse operation.

Onboard attitude control employs GE/RCA-designed three-axis attitude control techniques. A dual-mode propulsion subsystem uses two bipropellant liquid apogee engines (LAES) for orbit-raising operations, and monopropellant

thrusters for attitude and orbit control. Following transfer orbit operations—including apogee and other maneuvers—INTELSAT-K had sufficient propellant remaining to meet its design life for an Atlas II-A launch. The mass and electrical power budgets for INTELSAT-K are given in Table 1.

### Antenna

INTELSAT-K has two communications antenna systems that provide the coverage shown in Figure 1. The east/west antenna is a 2.15-m deployable dual-grid reflector with four feed horn arrays. It provides both Europe and North America coverage, as well as telemetry and command functions during on-station operations. The orthogonal polarization grid networks are carried on two separate reflectors which overlap with sufficient offset to separate their respective focal points. This dual-grid/dual-reflector arrangement minimizes the overall volume of the spacecraft while providing for optimal frequency reuse. Each feed array is connected to a low-loss, lightweight, monolithic beam-forming/combining network housed in a tower structure on the earth-facing panel. The east/west antenna provides 47-dBW edge-of-coverage effective isotropically radiated power (EIRP) for the North America and Europe beams, with a minimum flux to saturate of  $-93$  dBW/m<sup>2</sup> and a gain-to-noise temperature ratio,  $G/T$ , of 3.0 dB/K.

The transmit-only South America antenna is rigidly mounted on the earth-facing panel. It consists of a  $91 \times 78$ -cm elliptical reflector fed by two pairs of feed horns housed in a separately mounted lightweight graphite tower assembly. This antenna provides 45-dBW edge-of-coverage EIRP. When combined variable power divider operation is selected to broadcast to North and South America simultaneously, both beams have an edge-of-coverage EIRP of 42.7 dBW. An omnidirectional antenna provides telemetry and command capability during transfer orbit operations and emergency in-orbit operations.

### Mechanical subsystem

The stowed and deployed configurations of INTELSAT-K are shown in Figures 2 and 3, respectively. The omni antenna, east/west (E/W) antenna, and solar arrays are stowed in their launch configuration. The omni antenna is attached to the earth-facing overhang of the south panels and uses a two-stage deployment system with transfer orbit and on-station deployed configurations. The east/west reflector stows above the earth panel and is supported at six points. The solar arrays are stowed to the north and south panels and are restrained by two wrap cables and supported by four shear ties.

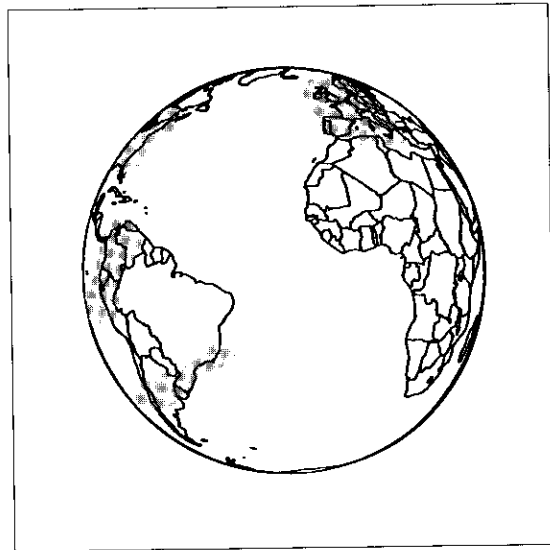
All deployments are initiated with pyrotechnic cable-cutting mechanisms. Three classes of mechanisms are used on INTELSAT-K. Single-operation

TABLE 1. INTELSAT-K MASS AND POWER BUDGETS  
(a) Mass Budget

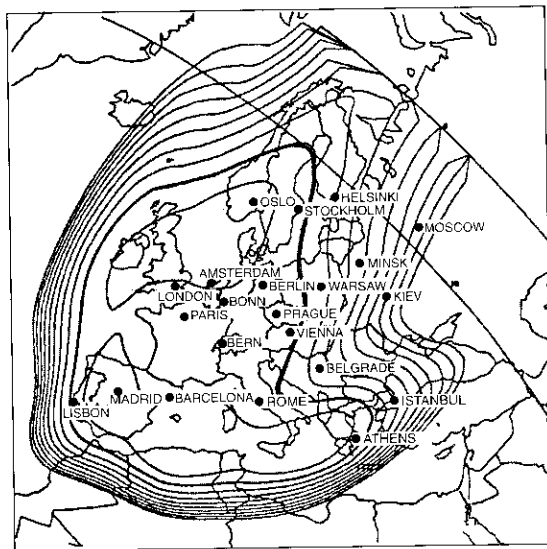
SUBSYSTEM	VALUE (kg)
Primary Structure	205.3
Secondary Structure	19.5
Mechanical Assemblies	27.5
Attitude Control	69.8
Telemetry, Command, and Ranging (TC&R)	42.9
Propulsion	138.6
Power System	306.9
Thermal	65.2
Harness	75.9
Communications	216.8
Antennas	48.4
Solar Array Wrap Cables	2.0
SUBSYSTEM TOTAL	1,218.8
Balance Weights	26.4
Pressurant	4.8
SPACECRAFT DRY WEIGHT	1,250.0
Oxidizer (N <sub>2</sub> O <sub>4</sub> )	668.0
Hydrazine (N <sub>2</sub> H <sub>4</sub> )	1,007.0
SPACECRAFT LIFTOFF WEIGHT	2,925.0

(b) Electrical Power Budget: Autumn Equinox, Year 10

SUBSYSTEM	VALUE (W)
Payload	2,749.0
TC&R	54.6
Attitude Control	58.5
Propulsion	1.3
Thermal	237.4
Electrical Power	45.1
Bus Heater	44.3
Battery Charge Power	355.0
TOTAL	3,545.2
+ 3% Margin	3,651.5
Solar Array Power Available	3,786.3
Margin	134.8

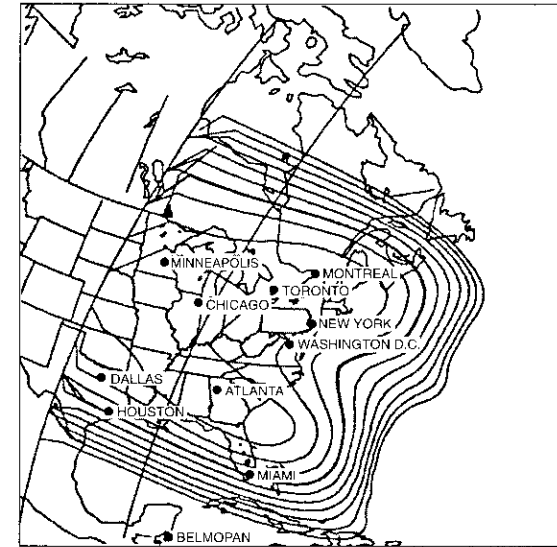


(a) Overview

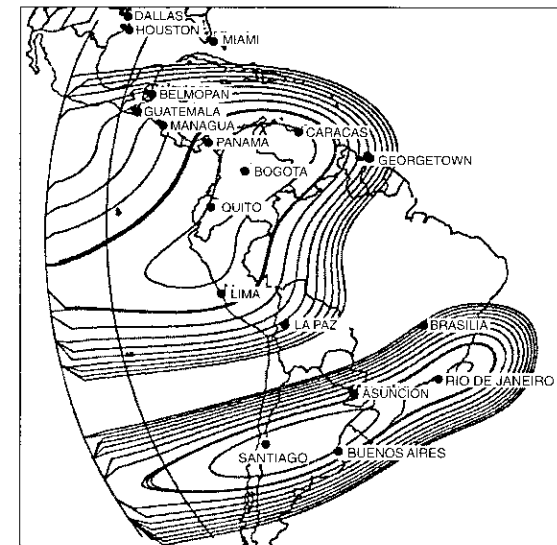


(b) Europe

Figure 1. *INTELSAT-K Antenna Coverage*



(c) North America



(d) South America

Figure 1. *INTELSAT-K Antenna Coverage (Cont'd)*

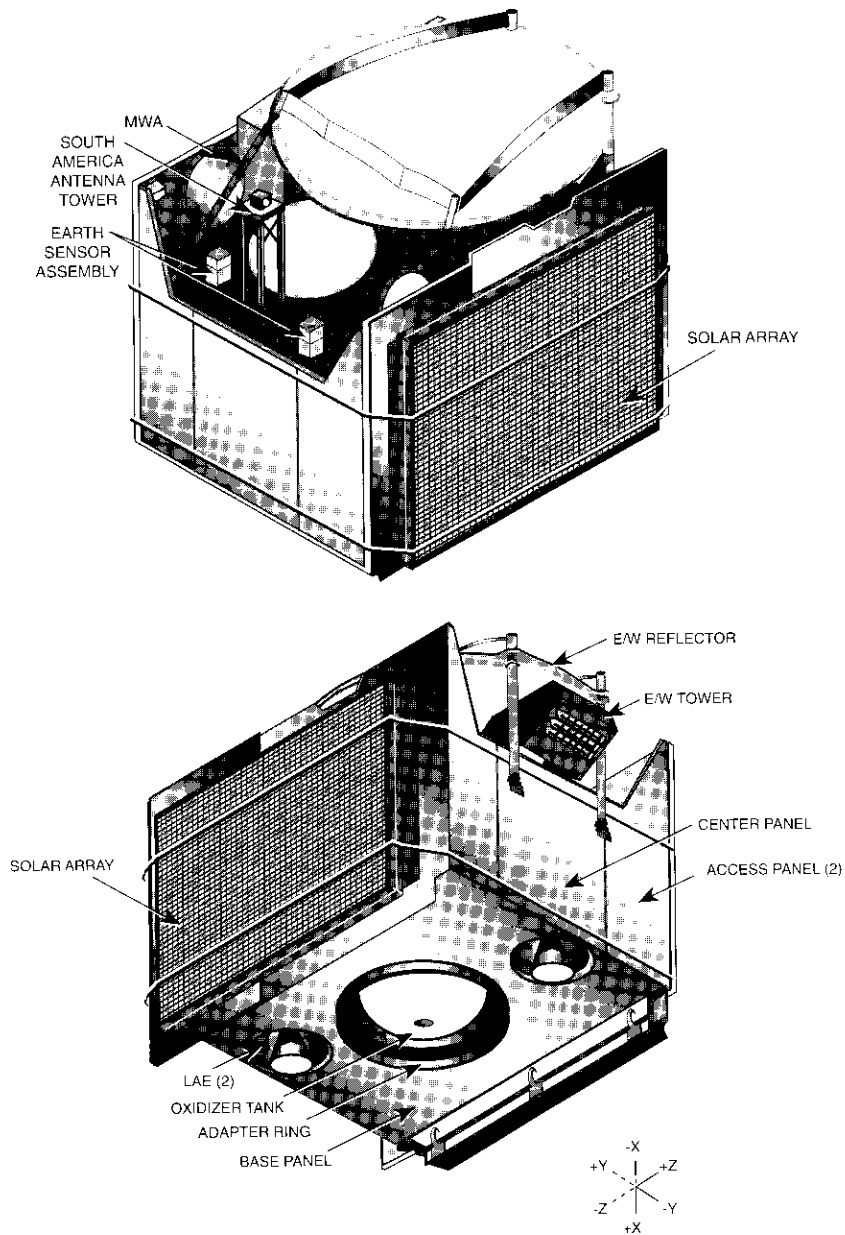


Figure 2. *INTELSAT-K Stowed Configuration*

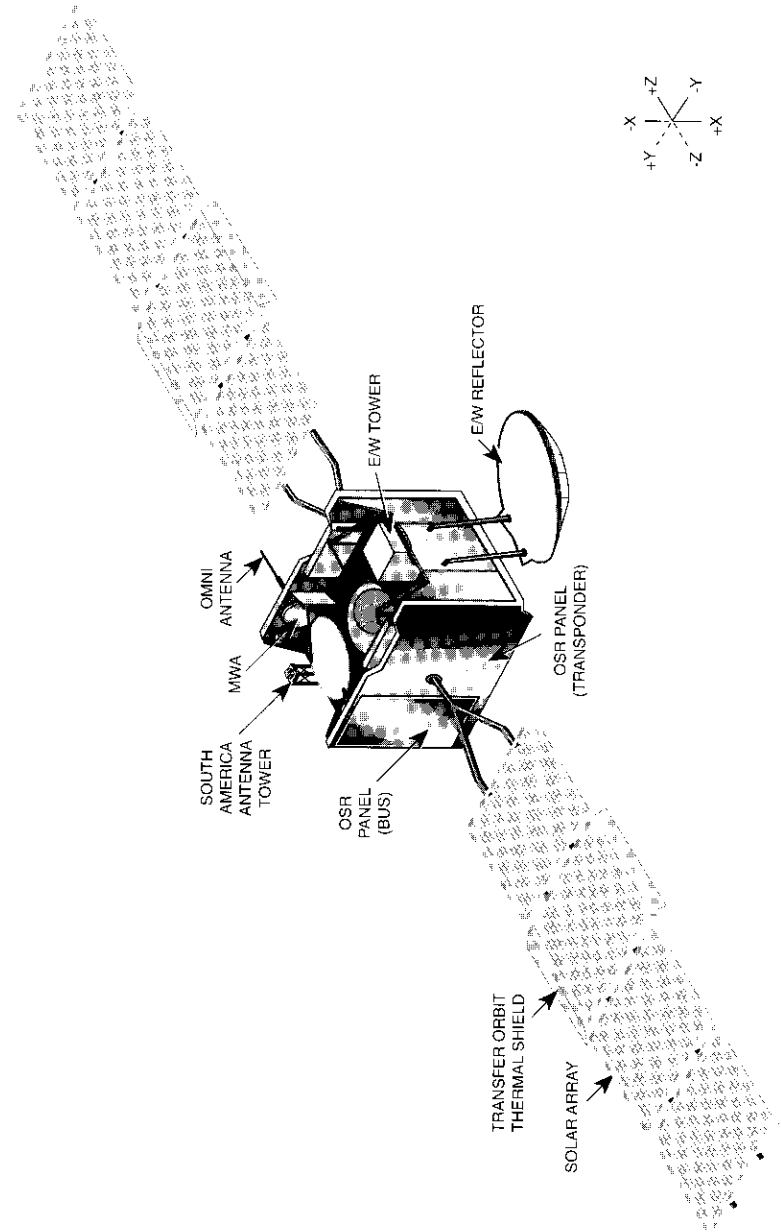


Figure 3. *INTELSAT-K Deployed Configuration*

devices are used for deployments and momentum wheel assembly (MWA) release. Deployment actuators are all spring-driven, viscous-damped mechanisms. The momentum wheel pivot is a stepper-motor-driven, occasional-use linear actuator. The solar array drive and the momentum wheel are continuous-operation, motor-driven mechanisms.

### Structure subsystem

The INTELSAT-K structure is built up from a core assembly consisting of a magnesium and aluminum central cylinder with aluminum honeycomb bulkheads and base panel. The core assembly is surrounded on the remaining five sides with additional bonded aluminum panels attached to the radial bulkheads and/or the central cylinder rings. The propulsion tanks and plumbing, as well as several bus components, are located on the core assembly. The spacecraft north and south sides consist of two removable equipment panels, one bus panel, and one transponder panel on each side. The east and west sides contain a combination of fixed panels and removable access panels, with the deployable east/west reflector extension arms hinged at the fixed west panel. The earth panel supports the South America antenna systems and a variety of payload and bus equipment.

### Thermal subsystem

The INTELSAT-K thermal control subsystem was designed and tested to maintain temperatures within required limits during all phases of the mission. Temperature control is achieved with passive features, active and ground-commandable heaters, and heat pipes. Figure 4 shows an overview of the thermal control subsystem. This relatively simple design provides both high reliability and sufficient flexibility to accommodate the many payload operating modes of the INTELSAT-K spacecraft.

The north and south panel exterior surfaces are covered with optical solar reflectors (OSRs) to radiate excess heat. Payload equipment with high dissipation is located on the north and south transponder panels, which are also equipped with heat pipes. The rear surfaces of the deployed solar arrays have a high-emittance coating for thermal control. Spacecraft areas requiring minimum coupling to the external environment are covered with multilayer insulation (MLI) blankets. To minimize the potential for electrostatic discharge, the outermost layer of the blankets is coated with a transparent indium-tin-oxide (ITO) conductive coating.

Active thermal control is achieved by using film strip heaters, dual thermal controllers, and temperature sensors. The thermal controllers provide ground-

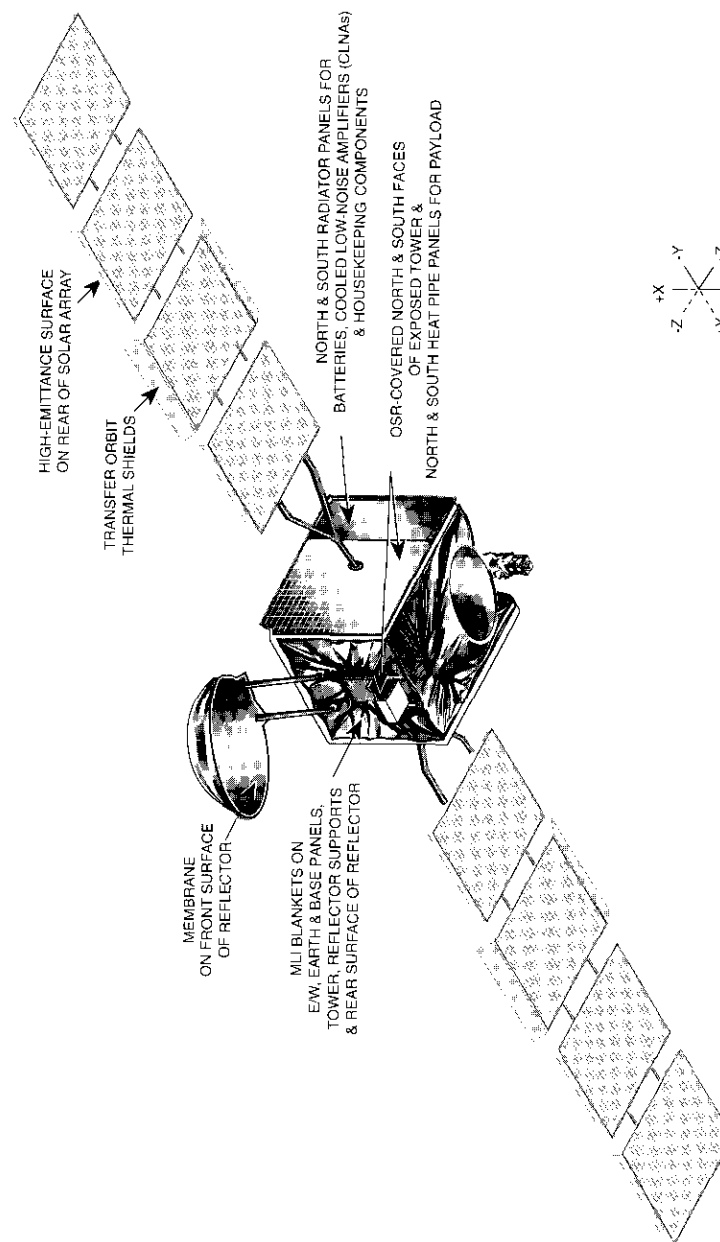


Figure 4. External Thermal Control Surfaces

overrideable proportional heater control based on temperature sensors. All heaters are sized to maintain acceptable thermal conditions in an environment 10° below the minimum predicted spacecraft environment. Heaters for components associated with ground-commanded events are themselves controlled by ground command.

Integral heat pipes are bonded within the north and south transponder panels. These axial-groove ammonia pipes can achieve thermal efficiencies greater than 90 percent. Temperatures were measured during panel-level testing to verify individual heat pipe operation and the thermal quality of the heat-pipe-to-honeycomb bond. The system can tolerate the failure of any single heat pipe and still maintain acceptable temperatures for all units.

**Power subsystem**

The INTELSAT-K electrical power subsystem (EPS) uses solar arrays and batteries in a direct energy transfer configuration to provide full power to the spacecraft at all times. The EPS is designed to support the spacecraft with all 16 transponders operating after 10 years of life, and has a limited capability to detect and correct failures. A single-bus configuration is used, with a bus voltage range of 23.5 to 35.5 V. The key features of the subsystem are listed in Table 2. Figure 5 is a block diagram of the EPS.

The solar arrays consist of 38,976 N-on-P solar cells, each 2 3 4 cm. The arrays are designed to provide more than 3.5 kW at the end of 10 years. The solar cells are shallow-junction devices with blueshifted response characteris-

TABLE 2. INTELSAT-K ELECTRICAL POWER SUBSYSTEM KEY FEATURES

FEATURE	DESCRIPTION
System Type	Direct energy transfer
Solar Array	2 3 4 panel
Cells	N-on-P
Area	34.69 m <sup>2</sup>
BOL* Power	4,844 W
EOL* Power	3,639 W
Shunt System	Partial linear (transfer orbit) Partial linear/switched sequential (on-station)
Array Drive	DC stepper motor
Battery	4 Ni-H <sub>2</sub> batteries
Cells	22 50-Ah cells per battery
Depth of Discharge	70%
Charge Rates	C/10, C/20, C/60, C/90

\* BOL: beginning of life; EOL: end of life.

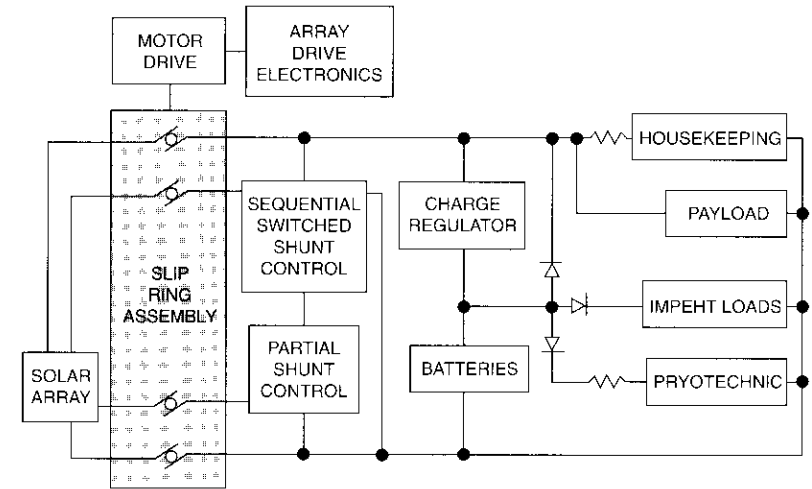


Figure 5. Power Subsystem Block Diagram

tics, connected into 448 parallel strings of 87 series cells. The interconnections are made with a 2-mil-thick expanded silver mesh. The cells are mounted on eight 2.6-cm-thick aluminum honeycomb panels with Kevlar graphite face skins. Each solar cell is protected by an 8-mil-thick fused silica coverglass, sized larger than the cell to ensure radiation protection. The coverglass utilizes a multilayer antireflective coating (MgF<sub>2</sub>) on the sun-facing side, and an ultraviolet-rejection film on the cell-facing side.

During transfer orbit, the panels are folded and stowed by restraint cables against the north- and south-facing sides of the spacecraft. The outermost panels are illuminated as the spacecraft spins, to provide housekeeping power during transfer orbit. Once geosynchronous orbit is attained, the solar arrays are deployed and rotated to face the sun, and full power is available. The arrays are rotated by a single-axis, clock-rate-controlled DC stepper motor. Each array is driven by independent motors with redundant drives and electronics.

INTELSAT-K uses a combination of partial linear shunts and sequential switched shunts to control power output from the arrays. During transfer orbit, the two strings on each of the outer panels are controlled with switched shunts. After the solar panels are deployed, the sequential shunts on the innermost string on each of the two outer panels are reconfigured into switched-shunt configurations to minimize thermal dissipation inside the spacecraft body due to excess solar array power.

Four Ni-H<sub>2</sub> batteries, each containing twenty-two 50-Ah cells, are provided—for a nameplate capacity of 200 Ah. The batteries can be charged independently at one of four charge rates: \* C/10, C/20, C/60, or C/90. The charge rates are regulated to accommodate array degradation. The C/10 and C/20 rates also have optional voltage-temperature limiting. Each battery cell has its own resistor for reconditioning, and a C/20 rate is available to pull up the battery voltage after reconditioning. The batteries provide payload and housekeeping power to the bus during eclipse and when higher-than-usual daytime loads are present. In addition, the augmentation heater of each improved electrothermal hydrazine thruster (IMPEHT) is powered directly from a single battery. The battery power to an IMPEHT can be assisted by the solar arrays by using the commandable C/20 charge rate during inclination maneuvers when the thrusters operate continuously.

**Propulsion subsystem**

The INTELSAT-K dual-mode propulsion subsystem incorporates highly efficient bipropellant LAEs to raise the transfer orbit apogee for orbit circularization, and simple monopropellant reaction control thrusters for stationkeeping and on-orbit attitude control. All components are supplied from common fuel tankage which can be isolated into redundant half-systems. Figure 6 is a block diagram of the INTELSAT-K propulsion subsystem.

The LAEs, which burn hydrazine (N<sub>2</sub>H<sub>4</sub>) and oxidizer (N<sub>2</sub>O<sub>4</sub>), operate in a pressure-regulated mode and are used only during multiple apogee injection maneuvers. At the end of transfer orbit operations, the LAEs, oxidizer tank, and pressurant tank are isolated, reverting to a monopropellant blowdown reaction control subsystem (RCS) during geosynchronous operation.

The INTELSAT-K LAE, built by TRW, is a high-performance engine that burns an industry-unique combination of N<sub>2</sub>H<sub>4</sub> and N<sub>2</sub>O<sub>4</sub>. The TRW LAE has demonstrated a nominal specific impulse of over 3,040 N/kg·s (314 lb<sub>f</sub>/lb<sub>m</sub>·s), with greater than 490-N thrust. The tightly regulated feed system maintains the mixture ratio to 1.05 ± 1 percent. The LAE chamber temperature typically runs less than 2,350°C, which is conducive to long engine coating life.

The RCS is fully redundant, with 16 catalytic reaction engine assemblies (REAs). These assemblies, manufactured by Rocket Research Corporation, range in size from 1 to 22 N and provide attitude and orbit control. The thruster utilization matrix is given in Table 3. Four IMPEHTs are used for north-south stationkeeping; the remainder are used for east/west stationkeeping and altitude-keeping during all maneuvers. Each REA and IMPEHT has

\* The current rate (in A) that will return the given percent (10, 20, 60, or 90 percent in this case) of the battery capacity (in Ah) in 1 hr.

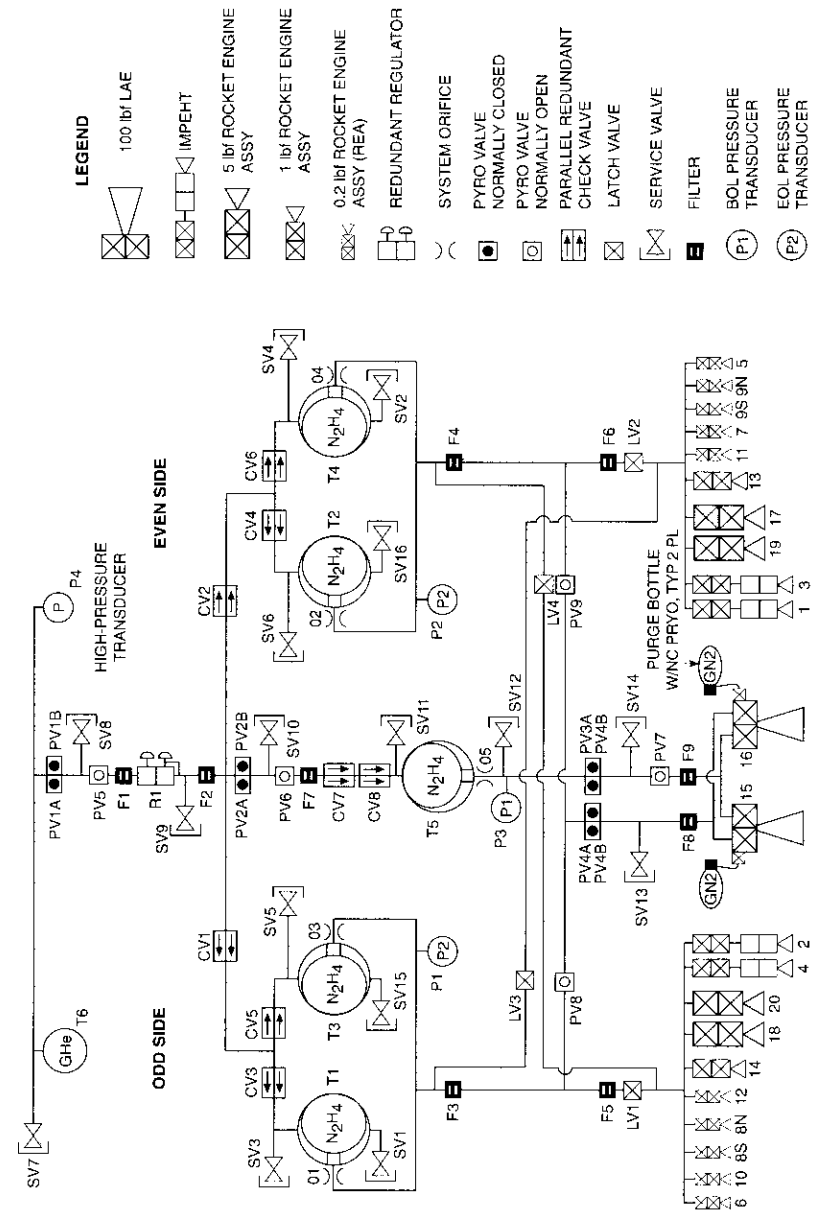


Figure 6. Propulsion Subsystem Diagram

TABLE 3. THRUSTER UTILIZATION MATRIX

THRUSTER MODE	THRUSTERS
<b>Spin Precession Maneuvers</b>	
Coarse Primary	18 and 20, 17 and 19
Coarse Odd Half-System	17 and 19
Coarse Even Half-System	18 and 20
Fine Primary	8 and 11, 6 and 9
Fine Odd Half-System	11 and 9
Fine Even Half-System	8 and 6
<b>Spin Rate Control</b>	
During LAE Burns	
Primary	17, 18, 19, 20
Odd Half-System	17, 19
Even Half-System	18, 20
Fine Spin Rate Adjustment	
Primary	5 and 12 or 7 and 10
Odd Half-System	5 or 7
Even Half-System	12 or 10
<b>LAE Burns</b>	15 and/or 16
<b>Thruster-Assisted Pitch Capture</b>	
Primary	13 and 14
Odd Half-System	9 and 11
Even Half-System	6 and 8
<b>Backup Roll Control</b>	
Odd Half-System	5, 7
Even Half-System	10, 12
<b>North-South Stationkeeping</b>	
Primary	1, 2, 3, 4
Odd Half-System	1, 3, 5, 7
Even Half-System	2, 4, 10, 12
Alternate Primary Mode	1, 2, 3, 4 (5 and 7 or 10 and 12)
<b>East-West Stationkeeping</b>	
Correct Eastward Drift	
Primary	9, 11, 1, 2, 3, 4
Odd Half-System	9, 11, 1, 3
Even Half-System	10, 12, 2, 4, (6 or 14), 8
Correct Westward Drift	
Primary	6, 8, 1, 2, 3, 4
Odd Half-System	5, 7, 1, 3, 9, (11 or 13)
Even Half-System	6, 8, 2, 4
<b>Timed Pulse Mode</b>	1-20 (selectable)
<b>Automatic Pitch Error/Momentum Adjust</b>	
Combined	6, 8, 9, 11
Odd Half-System	9, 11
Even Half-System	6, 8
Auxiliary	13, 14
<b>Pitch Impulse Balancing</b>	
Odd Half-System	11 or 13
Even Half-System	6 or 14

redundant catalyst bed heaters, and all engines have temperature telemetry for ground verification of thruster operation. In the highly unlikely event of external thruster leakage, thruster bank isolation can be commanded through latch valve operation.

The IMPEHTs used for north-south stationkeeping are derived from the early Rocket Research electrothermal-hydrazine thrusters, with augmentation heater power increased significantly. An IMPEHT operated with the augmentation heater delivers a specific impulse of 2,925 N/kg-s (301 lb<sub>f</sub>/lb<sub>m</sub>s). The beginning of life (BOL) thrust of the IMPEHT is 0.5 N, decreasing as the system pressure blows down to 0.35 N at the end of life (EOL).

#### Attitude control subsystem

The INTELSAT-K attitude control subsystem (ACS) maintains spacecraft pointing and control throughout all mission phases. It has the following key features:

- Spin-stabilized in transfer orbit.
- Active spin control during LAE burns.
- Three-axis-stabilized on station using a momentum bias system.
- 11.0-kg-m/s momentum provided by 6,000-rpm MWA.
- Roll/yaw control provided by magnetic torquers in normal mode.
- MWA pivot augments roll control, allowing for easy inclined orbit operation.
- Several thruster modes available for on-orbit stationkeeping.
- Selectable attitude thresholds available for terminating thruster operation.
- Time-varying pitch and roll offsets available for diurnal pointing corrections.
- Loss of earth lock automatically switches telemetry beacons to high power.
- Capability to monitor and switch sensors, actuators, and control electronics.

Table 4 lists the components of the ACS.

The ACS operating modes can be separated into preoperational modes used in transfer orbit through earth acquisition, and operational modes active during drift orbit and geosynchronous orbit. In the preoperational mode in transfer orbit, the spacecraft is spin-stabilized at 10 rpm about its X-axis, and data

TABLE 4. ACS COMPONENTS

COMPONENT	QTY	CHARACTERISTICS
Sun Sensor Assembly	1	Internally redundant with a measurement accuracy of 0.1°.
Horizon Sensor Assembly	1	Internally redundant operating at spacecraft rates of 4.5 to 16 rpm and 45 to 66 rpm.
Spin Measuring Assembly	2	Accelerometer unit with digitizing electronics.
Earth Sensor Assembly	2	Lockheed scanning infrared sensor with 8-Hz scan rate and 4-Hz output rate. Measurement range $\pm 6.60^\circ$ in pitch and $\pm 2.24^\circ$ in roll.
Rate Measuring Assembly	3	Northrop rate integrating gyro with integrated drift of $<0.015^\circ$ over 15 minutes.
Momentum Wheel Assembly	2	11.0 kg-m/s at 6,000 rpm with 0.014 kg-m motor.
MWA Pivot Assembly	2	Pivots wheel through $\pm 2.8^\circ$ using a stepper motor.
Roll and Yaw Control Torquers	1	Internally redundant magnetic torquers of 300 and 600 atm <sup>2</sup> , respectively.
Attitude System Processor	2	RCA 1802 microprocessor-based attitude control electronics.

from the horizon and sun sensors are telemetered for ground determination of the spin axis attitude. The spin axis attitude and spin rate are controlled with thrusters. During apogee motor firing using LAEs, the spin rate is held constant through closed-loop thruster operation. Spin-up and spin-down can be performed to attain desired momentum levels. At the end of transfer orbit operations, the spacecraft spin axis is reoriented to orbit normal by a dual spin turn (DST) operation in preparation for performing earth acquisition using thrusters.

During on-station operation in normal mission mode, the satellite is in an earth-oriented attitude with the momentum wheel axis nominally oriented along orbit normal. The satellite is three-axis-stabilized, with an earth sensor providing attitude reference, the momentum wheel providing the required gyroscopic stiffness and momentum exchange for pitch control, and autonomous magnetic torquing providing roll and yaw control. Thrusters can provide backup three-axis control, but nominally are used only during stationkeeping maneuvers.

Three-axis attitude is sensed during stationkeeping maneuvers by using the rate maneuvering assemblies for roll and yaw sensing, in addition to the earth sensor assembly (ESA). The ACS also provides the capability to monitor the

redundant attitude system processor (ASP) and ESA. The following modes have been implemented in the ASP to accomplish the ACS functions:

- *North/south stationkeeping* (primary, alternate, odd, and even half-systems). Roll and yaw attitude control during primary stationkeeping is obtained by off-pulsing the four IMPEHTS used for velocity incrementing.
- *East/west stationkeeping* (primary, odd, and even half-systems) is used to generate east or west velocity increments.
- *Automatic pitch error momentum adjust control* is used to control pitch attitude and momentum during stationkeeping.
- *Magnetic control and active nutation damping* (MAND) uses a "bang-bang" control law with hysteresis to control roll and yaw attitude and to damp residual nutation.
- *Backup roll control and pitch impulse balancing* are employed for roll and yaw attitude control using the thrusters, and to act as a backup to MAND.
- *Pivot-enhanced roll control* augments the magnetic roll control provided by MAND by pivoting the momentum wheel in response to sensed roll errors that exceed a ground-selectable threshold.
- *Pivot-actuated nutation damping* provides active nutation damping through the momentum wheel pivot, using the gyro as a sensor. This mode is nominally used following the DST maneuver prior to earth acquisition.
- *Thruster-assisted pitch capture* is performed to acquire the earth in pitch following the DST.

Offset pointing is provided to accommodate possible station changes and/or inclined-orbit operation, and to correct detectable on-orbit biases. Pitch offsets of up to  $\pm 6.00^\circ$  can be implemented by commanding a bias to the earth sensor pitch channel. Roll offsets of up to  $\pm 2.20^\circ$  are provided by pivoting the momentum wheel and biasing the roll channel of the earth sensor. Time-varying roll and pitch offsets can also be commanded in the ASP to compensate for diurnal variations.

#### Telemetry, command, and ranging subsystem

Figure 7 is a block diagram of the INTELSAT-K telemetry, command, and ranging (TC&R) subsystem. Key subsystem features are listed in Table 5. The

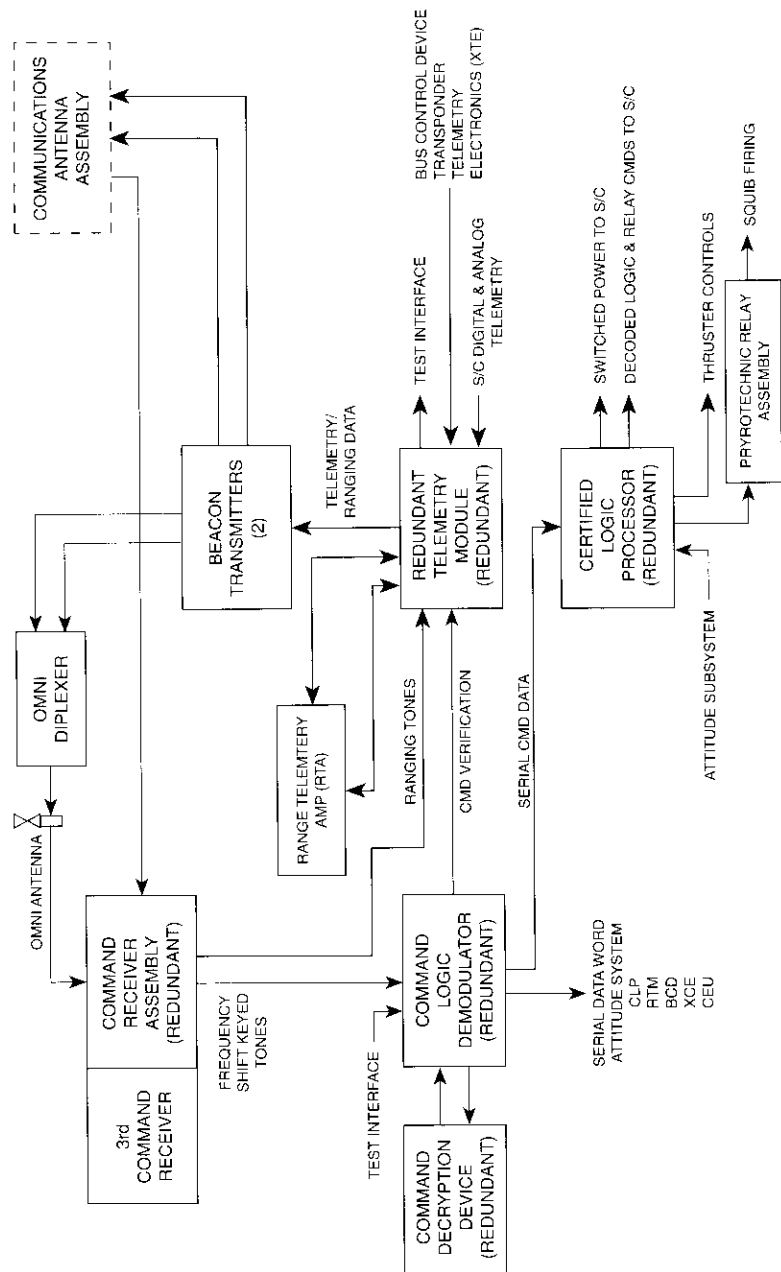


Figure 7. TC&R Subsystem Block Diagram

TABLE 5. TC&R SUBSYSTEM OPERATIONAL FEATURES

FEATURE	INTELSAT-K
Command Frequencies	K-band
Command Format	FM
Telemetry Frequency	11.4 GHz for beacon transmitter 1 11.7 GHz for beacon transmitter 2
Telemetry Format	1-kb/s pulse code modulation (PCM)
Frame	256 words, 8 bits/word
Subcommutation	25 levels
Range Tones	35 Hz through 28 kHz
Command Threshold	-80 dBW/m <sup>2</sup> omni, -87 dBW/m <sup>2</sup> main antenna
Beacon EIRP	1-dBW omni, <13.5-dBW main antenna
Simultaneous Ranging	Yes

satellite receives the frequency-modulated command carrier through either a deployable omni antenna during transfer orbit and contingencies, or through the narrow beamwidth east/west antenna from either Europe or North America at all times.

The uplinked commands are received by the three redundant command receivers, and the demodulated command frequency tones are sent to both command logic demodulators (CLDs). Beyond the CLDs, the two sides of the command system are completely independent. The CLD sends all command data to the redundant telemetry module (RTM) to be downlinked for command verification. When the next command is received, the CLD sends the 8-bit command upcode to the central logic processor (CLP) for decoding. The CLP decodes the command message and transmits an execute pulse. At the same time, the CLD sends the extended command (if present) to the bus control device (BCD), the command extender unit (CEU), or the north or south transponder command electronics (XCE).

The capability for secure commanding is available. Encryption is performed using the KI-23 algorithm, and decryption is performed by the command decryption device before the command is processed by the CLD.

The command system has no provisions for storing commands or for onboard intelligence to execute commands in response to a change in spacecraft state. However, if earth lock is lost, the system will switch the telemetry beacon transmitters to a high-power mode, and the signal will be transmitted through both the east/west and omni antennas.

The ranging function is implemented by measuring the slant ranges from the ground station sites to the spacecraft, for precise transfer orbit and geosynchronous orbit determination. The ranging tones uplinked with the command carrier are stripped from the carrier in the command receivers and sent to the RTMs via cross-strap relays. The RTM sends to the beacon transmitters either the range tones alone, or the range tones combined with the telemetry data.

The telemetry system receives the status of all satellite subsystems and transmits this information for use in attitude determination and the evaluation of subsystem performance. The two RTMs form the heart of the telemetry system. Each has eight different operational modes, which provide the flexibility to switch from processing the normal spacecraft telemetry data to processing range data, dwell data from a single telemetry point, or command verification data. The RTM telemetry modes are as follows:

- *PCM High-Priority*. Produces a normal telemetry data stream, containing command verification data, once per second (*i.e.*, twice per frame).
- *PCM Low-Priority*. Produces a 14.5-kHz frequency modulated with command verification data when the CLD is receiving valid commands; otherwise provides a normal telemetry data stream.
- *PCM Dwell*. Produces a telemetry stream, but samples only one data point. The frame still contains RTM internal telemetry and command verification data, but the rest of the telemetry frame is filled with samples of the selected dwell data point.
- *Subcarrier Dwell*. Produces a 14.5-kHz subcarrier which is frequency modulated with the dwell telemetry point data.
- *Special Sensor*. Same as subcarrier dwell, except that the dwell telemetry points are preselected to be ESA scan data.
- *Attitude Monitor*. Same as subcarrier dwell, except that the dwell telemetry points are preselected to be SSA and HSA data (used for transfer orbit).
- *Ranging*. Sends out ranging tones received from the command receivers.
- *Simultaneous Ranging and PCM Telemetry*. Adds range tones to the normal PCM telemetry data stream.

The two RTMs nominally operate independently, transmitting primarily the same data. However, thermal data points are typically sent through only one

RTM, with each RTM having a representative sample for the whole spacecraft. The RTMs receive telemetry point data directly from the north and south transponder telemetry electronics (XTE) and the BCD. The RTM formats the telemetry into a PCM biphasic-L data stream with a 1-kb/s data rate. The data stream consists of 256 eight-bit words per 2-s frame, with 25 levels of sub-commutation. The telemetry data stream is then sent to redundant beacon transmitters, where the data are phase-modulated and transmitted to the ground.

### **ESD control measures**

The INTELSAT-K Program Office, which monitored spacecraft construction at the GE-Astro plant, actively sought operational performance data—especially regarding electrostatic discharge (ESD)-related anomalies encountered in previously launched Series 5000 spacecraft—for the purpose of correcting potential generic problems on INTELSAT-K. As part of this activity, formal contacts were established with TELESAT of Canada and SES of Luxembourg, which owned and operated the ANIK E1/E2 and ASTRA-1B satellites, respectively. The data obtained from these contacts, as well as INTELSAT's experience in satellite operation, led to design changes and the implementation and testing of ESD protection measures on certain INTELSAT-K spacecraft hardware. Table 6 lists the design changes and hardware modifications incorporated into INTELSAT-K for improved ESD protection.

Since the INTELSAT-K launch in June 1992, the satellite's in-orbit performance has been critically examined to evaluate the benefits of these ESD protection measures. Results have shown reduced susceptibility to solar storms and other ESD disturbances, especially in regard to mechanism and ACS performance.

TABLE 6. INTELSAT-K ESD PROTECTION IMPROVEMENTS

**Design and Hardware Improvements**

Subdivided OSR panels with ITO-coated OSRs

Attacks ESD threat at the source

Reduces peak magnitude of transients by 75%

Reduces coupling to components to 36 V

OSR discharge is responsible for Series 5000 anomalies

MWA filter board and harness shielded

Filters execute command lines to momentum wheel electronics (MWE) and pivot

Reduces coupling on bus-to-MWE harness

Reduces coupling on MWE-to-pivot harness

ESA filter board and harness shielded

Corrects ESA design flaw

Filters telemetry lines to RTM

Reduces coupling on bus harness

Attitude determination electronics (ADE) filter board

Filters command lines to ADE

Series 3000 anomaly

Bus external harness shielded

Increases ESD margin

Payload external harness not shielded

Analysis indicates positive margin

Zener diode added to XTE-to-RTM interface

Added margin to circuits

Not required with OSR change

Improved earth panel blanket grounding

Ground added every 20 cm

**Additional Analyses and Performance Verification**

Solar array harness

Analysis and test demonstrate 6-to-1 margin on RTM circuits

Mutual coupling to spacecraft harness <30-V transient

Does not pose a threat to spacecraft components

Zener diodes on BCD-to-RTM interface

OSR change reduces this threat to acceptable levels

BCD not on OSR panel

Solar array threat <30 V

Margin >6 to 1 exists

Temperature sensor shielded

OSR change reduces threat to acceptable levels

Sensors on mux shelf; decoupled from OSR panels

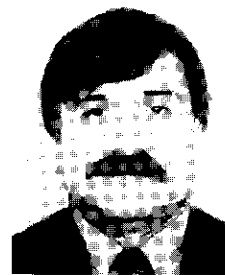
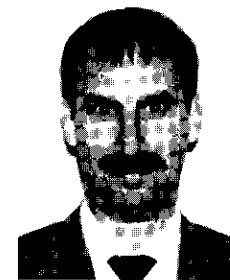
Blanket grounding improves 3 dB over Series 5000 design

No anomalies observed on Series 5000



*Krishnaswamy Raghunathan earned an MSc from Annamalai University, India, and subsequently graduated from Fairleigh Dickinson University and Northwestern University with MS and PhD degrees in physics. Prior to joining INTELSAT in 1979, he worked at Systems and Applied Sciences Corporation for NOAA Satellite Services. At INTELSAT, Dr. Raghunathan has worked in both ground segment and space segment programs. He served as Deputy Program Manager for the INTELSAT-K program, after which he was Subsystem Manager for the SCE/TC&R subsystems for the INTELSAT VII/VIIA programs. He is currently System Engineering Manager for the INTELSAT VIII/VIIIA programs.*

*Timothy Rush received a Bachelors degree from the University of Delaware and a Masters degree from the University of Maryland. He is currently a Principal Engineer in the INTELSAT Spacecraft Engineering Department (SED). As part of INTELSAT's matrix organization, SED provides technical support to Flight Operations, the Spacecraft Program Offices, and the Launch Vehicle Program Office. Mr. Rush served as INTELSAT-K Systems Engineer involved with mission planning and testing. He is a member of the INTELSAT VI, VII/VIIA, and VIII/VIIIA launch teams, and has participated in all INTELSAT VI and VII/VIIA missions to date.*



*Ahmet Ozkul received a BSAE from the California Institute of Technology in 1971 and was employed at JPL, Applied Mechanics Laboratories, working on nondestructive testing of components for the Shuttle and other aerospace vehicles. He received the MSAE and ApSc degrees from George Washington University in 1974 and 1977, respectively, while employed at NASA Langley Research Center in Hampton, Virginia. In 1978, Mr. Ozkul joined INTELSAT's Systems Planning Division, where he conducted space/ground segment configuration studies to optimize INTELSAT system growth. After transferring to the Satellite Operations Department in 1983, he supported numerous launch missions and was involved in software-based projects related to satellite in-orbit operation,*

including performance modeling based on historical telemetry data, and electrostatic discharge mitigation onboard INTELSAT satellites. He served as Project Manager for INTELSAT-K at GE-Astro in East Windsor, New Jersey, from 1989 through the successful launch in 1992.

Mr. Ozkul is currently a Principal Engineer in the Engineering and Spacecraft Programs Division at INTELSAT, where he works on satellite system engineering and the feasibility study and implementation of special projects to enhance INTELSAT's space segment. He has authored numerous technical papers as a member of AIAA, IEEE, JIAFS, and other organizations.

Index: transponders, in-orbit testing,  
INTELSAT

## **The INTELSAT-K payload**

R. A. PETERS, F. L. KHOO, AND A. OZKUL

(Manuscript received January 17, 1995)

### **Abstract**

The INTELSAT-K satellite supports intercontinental communications applications such as video distribution, very small aperture terminals, international business services, and satellite newsgathering, which employ small, low-cost receive terminals and thus require high downlink EIRP. The payload consists of sixteen 60-W, 54-MHz channel transponders providing receive and transmit coverages to Europe and North America, and transmit coverage to South America. Flexible beam connectivity allows a variety of uplink and downlink connections, including combinations of the three beams. The amplifiers in one transponder panel have limiter circuits to compensate for decreases in uplink signals, such as are caused by propagation fading. The payload features of INTELSAT-K are described in detail, and performance verification testing of the satellite is discussed.

### **Introduction**

The INTELSAT-K satellite provides advanced intercontinental communications designed specifically for applications that require high downlink effective isotropically radiated power (EIRP), such as video distribution, very small aperture terminals (VSATs), international business services (IBS), and satellite newsgathering (SNG) [1]. The high EIRP allows the use of small, low-cost receive terminals. Currently, antennas as small as 60 cm in diameter are receiving high-quality video downlinks from INTELSAT-K, as discussed in a companion paper by Brown *et al.* [2].

The INTELSAT-K payload consists of sixteen 60-W, 54-MHz channel transponders that can provide receive and transmit coverages to Europe and North America, and transmit coverage to South America. An exceptionally flexible

connectivity scheme allows a variety of beam connections from the uplink to the downlink, including combinations of the three beams which permit simultaneous transmission to all coverage regions. The output amplifiers are arranged in two banks with 11-for-8 redundancy. The amplifiers in one transponder panel have limiter circuits that can maintain a constant EIRP, even in the presence of uplink fade or other variations in uplink power.

Major components of INTELSAT-K had already been completed as part of the GE-Astro SATCOM K4 satellite—a U.S. Ku-band satellite designed for video distribution. To meet INTELSAT's requirements, the antenna coverages and frequency plans were modified, and additional receivers and low-noise amplifiers were added, along with an additional antenna to provide coverage of South America. Use of the K4 components and design allowed INTELSAT-K to be completed within 28 months after the effective date of the contract.

The transponder panels were tested in thermal vacuum, and again at spacecraft level, as part of an environmental testing program which also included vibration testing. Antenna performance was evaluated on the far-field antenna range, and again on the near-field range, to verify spacecraft-level performance. Special tests were conducted to measure the thermal and hygroscopic distortions of the deployable antenna. The tests measured the actual deflections of the antennas over a temperature variation of 90°C. Results were then fitted to a model to predict non-equilibrium distortion. During the payload in-orbit test, the performance of the entire payload was verified, and the thermal distortion of the deployable antenna was measured in the space environment.

This paper highlights the unique features of the INTELSAT-K payload and describes both the developmental and in-orbit verification testing of payload performance.

### **Antennas and coverages**

INTELSAT-K provides coverage to Europe and North America from a 2.2-m-diameter deployable, dual-gridded offset reflector. Coverage of South America (downlink only) is provided by a fixed antenna mounted on the earth-facing deck. Both antennas are fabricated from a Kevlar composite that is transparent to RF energy. Copper lines were deposited on a Kapton film, which was then glued to the Kevlar. The orientation of the lines determines the polarization reflected. The deployable antenna uses two reflectors, one above the other, with orthogonal polarization. The South America antenna, which was made available from a previous program, has a single reflecting surface but a dual grid for use with vertical or horizontal polarization. Only the vertical polarization of this antenna is used in INTELSAT-K.

The K4 reflector used for INTELSAT-K has two reflecting surfaces, with one surface offset with respect to the other, as shown in Figure 1. Offsetting the vertical and horizontal feed elements by the same amount as the two surfaces enables the elements to illuminate the same region. A new beam-forming network (BFN) was designed and fabricated to meet the coverage requirements of INTELSAT-K. Diplexers were used to provide transmit and receive functions from the same feed elements. At the start of the program, it did not appear possible to provide the desired coverage because size limitations of the bus constrained the spacing of the horns. Receiving in both polarizations from North America and transmitting in both polarizations to Europe required greater separation of the horizontal and vertical feed elements than could be accommodated by the structure. However, by optimizing the design, Astro was able to fit an additional horn into the feed, resulting in performance that exceeded the specifications.

High-power downlinks and very sensitive uplinks, combined with an extremely flexible connectivity of Western Europe, eastern North America, and the high population regions of South America, make the INTELSAT-K ideally

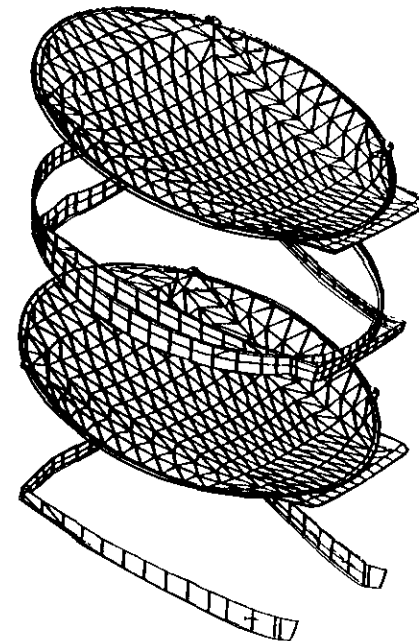


Figure 1. *Dual Offset Reflector Used on INTELSAT-K*

suiting for video distribution, SNG, VSAT, and other applications requiring high satellite performance.

At the time the specification was developed for INTELSAT-K, the satellite's orbital location was not fixed, but 310°E, 319.5°E, and 338.5°E were candidates. The 338.5°E location was ultimately selected, with coverages as shown in Figure 2. This location provides excellent coverage of Europe, South America, and eastern North America. Several customers are successfully using INTELSAT-K to access areas significantly outside the nominal coverage region, even as far as Moscow.

Thermal distortion of the deployable reflector was of special concern during the program, and a special test used to characterize the distortion is discussed in detail later in this paper.

### **Frequency plan and connectivities**

The frequency plan for INTELSAT-K is given in Figure 3. A quick count reveals 28 possible downlinks. Since there are only 16 transponders, switching and power-splitting must be used. The Europe and North America downlink frequency plans reflect the different International Telecommunication Union (ITU) guidelines for fixed satellite service for the two regions.

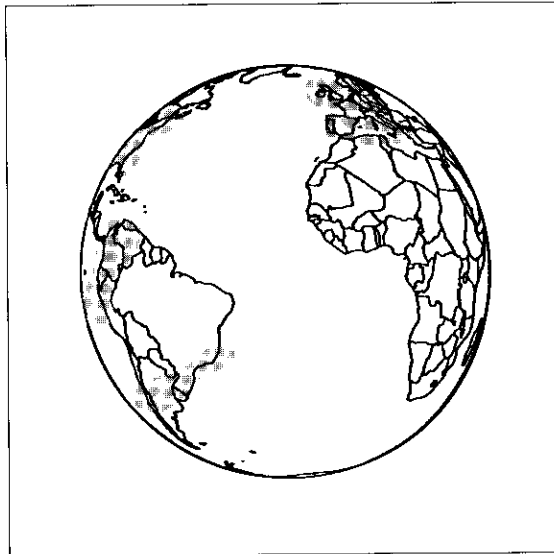


Figure 2. *INTELSAT-K Antenna Coverages*

Figure 4 is a block diagram of the INTELSAT-K communications payload. There are eight transponders on the north panel (lower portion of the figure) and eight transponders on the south panel (upper portion). The nominal configuration of INTELSAT-K is eight west-to-east transponders (north panel) and eight east-to-west transponders (south panel). However, channels 5 through 8 of the south panel can be switched, on an individual basis, to an east downlink. Using this feature, there can be up to 12 west-to-east transponders, with a corresponding decrease in the number of east-to-west transponders.

The western downlinks (south panel) are switchable, using a variable power divider (VPD), between North America, South America, and the North/South America split mode. VPDs cannot be used with an east downlink on the south panel. The VPD, manufactured by COMDEV, handles the full 60 W from the traveling wave tube (TWT). A conservative design permits the VPD to survive, even when all the RF power is reflected back into it. In the split mode, the VPD divides the power to provide equal EIRP downlinks to North and South America.

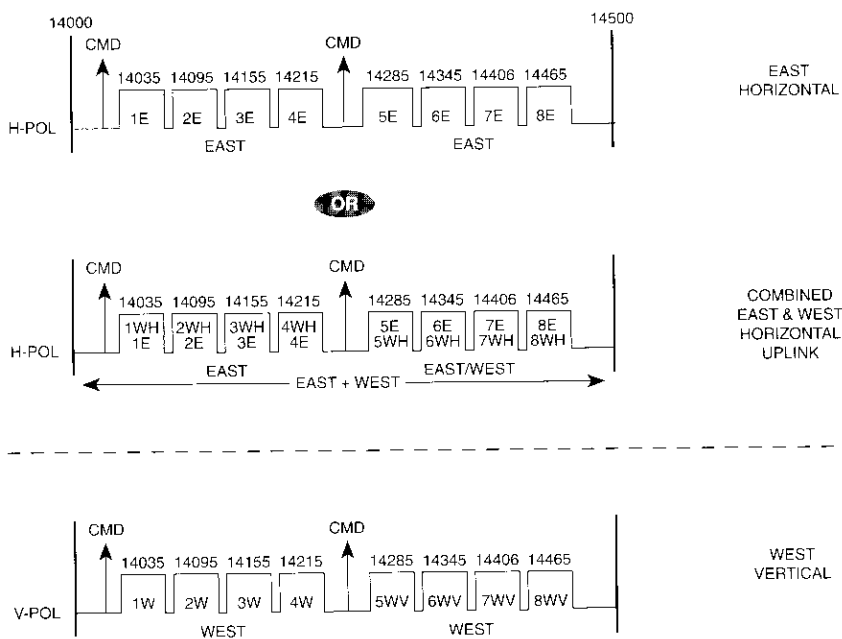
Unlike some of its competitors who specify EIRP under the best set of conditions, INTELSAT specifies EIRP as worst-case temperature, worst-case redundancy, and worst location in the coverage, based on end-of-life (EOL) values. The worst-case EOL, edge-of-coverage EIRPs for the different INTELSAT-K coverages are:

North America	47.0 dBW
Europe (vertical and horizontal)	47.0 dBW
South America	45.0 dBW
Combined North and South America	42.7 dBW

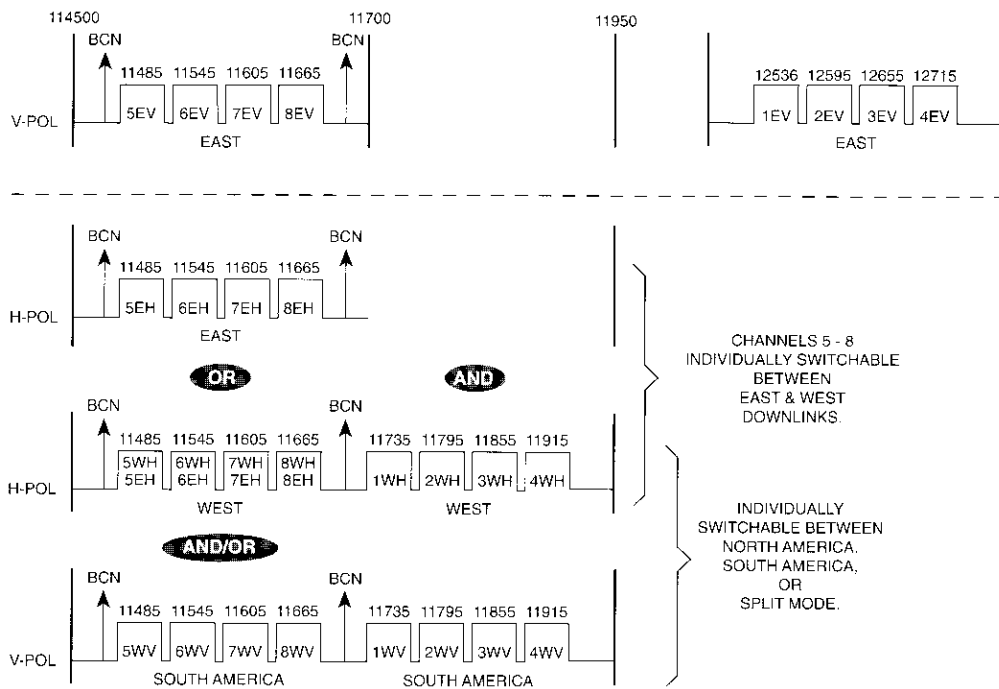
These values are guaranteed to customers under all situations. For comparison, typical peak EIRP values measured in orbit exceed the 47 dB requirement by more than 4.3 dB.

The unique flexible connectivity of INTELSAT-K is achieved through a combination of hybrids and switches. The hybrids, located after the receivers and before the traveling wave tube amplifiers (TWTAs), accommodate only low-power signals, to minimize losses. Through the use of hybrids, any uplink can be connected to any downlink, or to all three downlinks simultaneously. Besides providing this broadcast capability, the use of hybrids improves the reliability of the transponder by minimizing the need for mechanical switches.

There is an additional switchable hybrid on the Europe and west horizontal polarization uplinks. When this hybrid is selected, the uplink can be received from either or both regions without the need to reconfigure the satellite. In



(a) Uplinks



(b) Downlinks

Figure 3. INTELSAT-K Frequency Plan

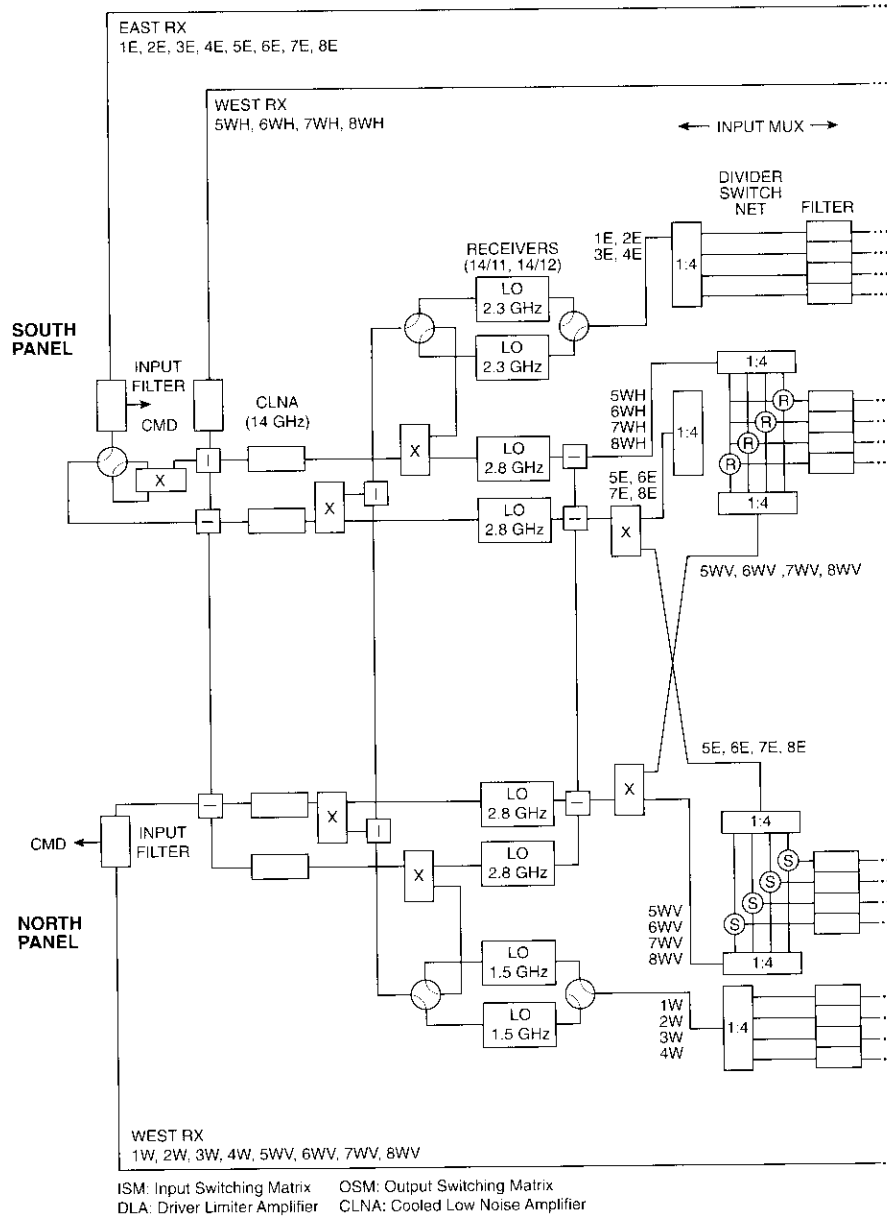
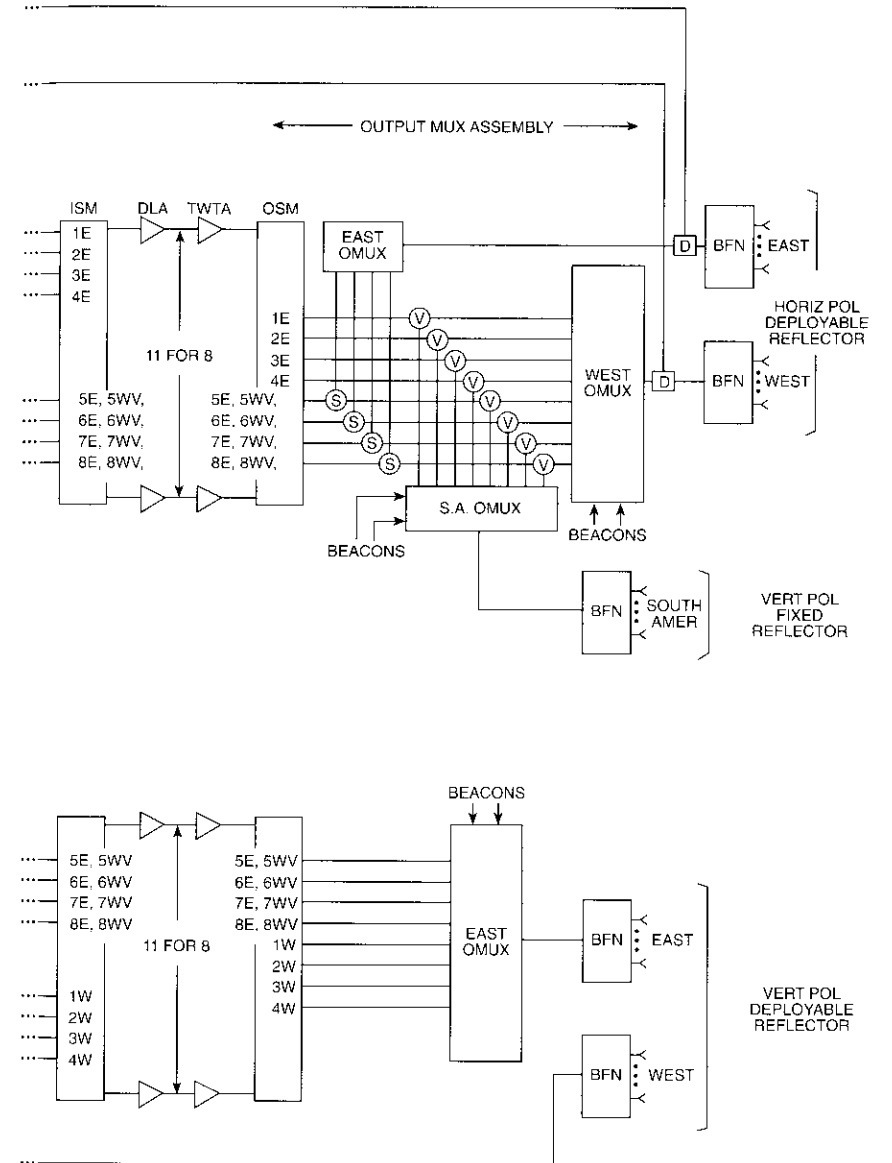


Figure 4. Communications Subsystem



Functional Block Diagram

addition, both uplinks can access the same transponder simultaneously. This hybrid can be switched in or out by ground command. When it is switched in, the saturation flux density (SFD) and gain-to-noise temperature ratio, *G/T*, of the affected transponders are reduced by about 3.2 dB.

Channels 1 through 4 of each panel must be switched as a block of four transponders, while transponders 5 through 8 are individually switchable. A matrix showing the possible connectivities is given in Table 1. Once a row or column of the table is selected for a given channel, it cannot be reused for the second transponder of the same channel. For example, if channel 5 is connected from the EUH beam to the NAH and SAV beams in one transponder, the EUH beam in the uplink and the NAH and SAV beams in the downlink cannot be used in the co-channel transponder.

TABLE 1. INTELSAT-K BEAM AND TRANSPONDER INTERCONNECTION CAPABILITIES (14-GHZ UPLINKS)

SATELLITE TRANSMISSION: DOWNLINK		SATELLITE TRANSMISSION: DOWNLINK											
		NORTH AMERICA		EUROPE			SOUTH AMERICA		NAH +		NAH +		NAH +
		NAH		EUH	SAV		SAV	EUH	EUH	SAV	SAV	EUH	SAV
		1-4	5-8	1-4	5-8	5-8	1-4	5-8	1-4	1-8	1-4	5-8	
SATELLITE TRANSMISSION: UPLINK	XPDR												
Europe EUH	1-4 5-8	I	I	G	I	I	I	I	I	I	I	I	
N. America NAV	1-4 5-8	I	I	G	I	I	I	I	I	I	I	I	
N. America NAH	1-4 5-8	I	I	G	I	I	I	I	I	I	I	I	
NAH + EUH	1-4 5-8	I	I	G	I	I	I	I	I	I	I	I	

- Notes:**
1. EU = Europe; NA = North America; SA = South America. Thus, for example, EUH = Europe horizontal polarization.
  2. G: Selectable as a group of four transponders.
  3. I: Selectable on a channel-by-channel basis.
  4. The NAH + EUH uplink must be selected as a group of eight transponders.

**Amplifiers**

Downlink power is generated by forty-eight 60-W TWTs manufactured by AEG (Germany). The minimum efficiency is 48 percent. These TWTs feature a three-collector design and are mated with a high-efficiency (88-percent) electronic power conditioner (EPC) designed and built by Astro. The TWTAs use a mixed-metal matrix dispenser cathode with active cathode current regulation via anode control to support in-orbit operations for up to 17 years. In the event that cathode decay exceeds expectations, the filament power to the cathode can be raised in three steps.

Since the anode voltage is available from telemetry, cathode performance can be monitored. Throughout more than 2 years of in-orbit experience, changes in cathode performance have been well within expected bounds. Helix current telemetry is also provided.

The TWTAs were built and optimized for the K4 frequency plan. Initially, channels 1 through 4 of the eastern downlink were considerably outside the K4 frequency range. However, by careful selection of the TWTs, the required power was obtained for all transponders.

The TWTs are driven by solid-state driver limiter amplifiers (DLAs). Those on the south panel provide the customer the option of a limiter mode of operation. In this mode, the DLA maintains a constant output signal, even if the input signal decreases—providing either 15 or 25 dB of additional gain. This allows constant output power from the satellite in the presence of uplink fades due to rain or other causes. In the presence of such fades, the signal-to-noise ratio (*S/N*) degrades somewhat, but the limiter reduces the amount of degradation. The limiter is used only for single-carrier uplinks because of the intermodulation products generated by the limiting action. For this reason, use of the limiting feature is optional and the DLA can be commanded into the linear mode by ground command. Figure 5 is a block diagram of the DLA configured in the limiter mode.

In the limiter mode, the DLA output is constant over a wide range of input power. Since increasing the uplink power does not increase power to the TWT input, there is a commandable output power attenuator, as well as telemetry on the RF output power. The attenuator is commandable in discrete steps over a 10-dB range. The DLA RF output power is obtained from the diode voltage (see Figure 5) and is available in both the limiter and linear modes of operation. In addition, telemetry of the RF power prior to the limiter is available to verify that the uplink power is correct in the limiter mode.

There is an additional commandable attenuator on the input of the driver amplifier, which is used to set the transponder gain to provide the best link

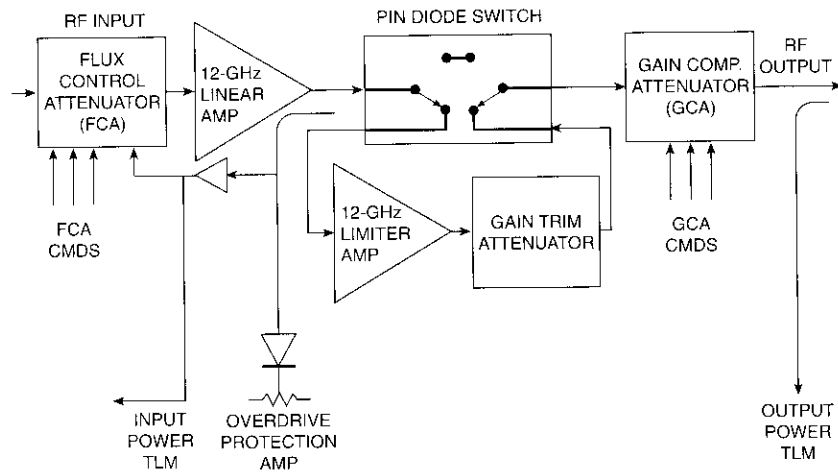


Figure 5. *INTELSAT-K DLA Block Diagram: Limiter Mode*

budget for the current combination of active earth stations. This attenuator provides up to 22 dB of attenuation, which, with the high sensitivity of an SFD of  $-93 \text{ dBW/m}^2$ , allows the satellite to be optimized for a broad range of applications.

Because of the wider frequency band (11,450 to 12,750 MHz) of the transponders on the north panel, the limiter option could not be provided. In all other respects, operation of the driver amplifiers on the two panels is equivalent. The use of RF telemetry, with the DLA in the limiter and linear modes, has allowed INTELSAT to assist users in troubleshooting problems. This telemetry is particularly useful because INTELSAT's communications system monitoring (CSM) network is capable of monitoring only C-band links.

An overdrive protection circuit adds additional attenuation when the power level reaches 6-dB overdrive (exceeding the power required to saturate the TWT by 6 dB). This protects the TWT from signals of 20 dB or more overdrive.

The low-noise amplifiers (LNAs) used on INTELSAT-K employ Pettier coolers to improve noise performance. The effect of this improvement is difficult to observe in practice because the modifications to the K4 layout resulted in significantly longer waveguide runs prior to the LNA, raising the input noise temperature to nearly  $300^\circ\text{C}$ .

## Reliability

High reliability for INTELSAT-K customers is ensured through the use of highly reliable components (Class S parts) wherever possible, conservative design practices, thorough testing, and a high level of redundancy for all critical parts, as follows:

LNA	1 for 1
Receiver	2 for 1
TWTA	8 for 11

All units have a design life of 10 years or greater. There has not been a single payload-related failure on the satellite after more than 2 years in orbit. The calculated reliability for all transponders operating at specification is 0.65 after 10 years in orbit.

Historically, the most troublesome components of a satellite payload are the high-power amplifiers (HPAs), with TWTAs being somewhat more reliable than solid-state power amplifiers (SSPAs) [3]. The major failure mechanism for TWTs has been the cathodes. The cathodes used in the INTELSAT-K TWTs built by AEG were fabricated using an advanced mixed metal. This cathode was extensively tested over several accelerated and unaccelerated temperatures within the operational range by using test triodes and TWT-like fixtures. Following the accelerated temperature tests, selected cathodes were allowed to establish a new equilibrium at the nominal operating temperature and their performance was recharacterized. In this way, they were "aged" but tested at their nominal operating point. This rigorous test established the robustness and durability of the cathodes [4].

## Manufacture and test

The high reliability of INTELSAT-K was further ensured by a thorough test plan. All active boxes were tested in thermal vacuum over thermal cycles. The hot and cold temperature limits were determined by adding  $3^\circ$  to the thermal predictions to account for uncertainty in the models, and then adding  $5^\circ$  margin to that value. Performance was measured at the temperature extremes.

The LNAs and receivers are mounted on the earth-facing deck. The rest of the transponder components (input multiplexers, DLAs, TWTAs, output multiplexers, variable power dividers, redundancy, and connectivity switches) are mounted on the north and south transponder panels. Figure 6 shows the layout

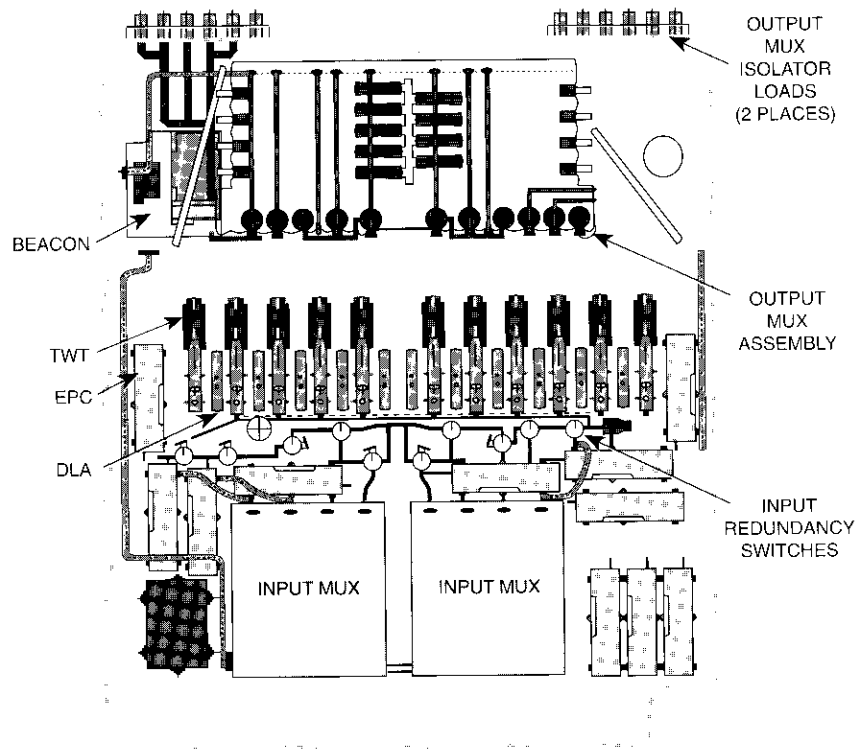


Figure 6. Typical Transponder Panel

of a typical panel. This construction allowed the north and south panels to be integrated in parallel with the spacecraft bus and tested in thermal vacuum prior to spacecraft integration.

After the bus and payload panels were integrated (Figure 7), the entire spacecraft was given an environmental test which included a thermal vacuum test and vibration testing (launch environment and pyrotechnic shock). All significant performance parameters were measured during both the hot and cold plateaus. Units powered during the launch were also powered during the vibration and pyrotechnic testing.

A special power stability test was run on the power subsystem to verify its performance in time-division multiple access (TDMA) operation. In this test, a pulsed load consisting of a 500-Hz, 50-percent duty cycle was applied to the power harness to simulate the effects of TDMA traffic on the power system.

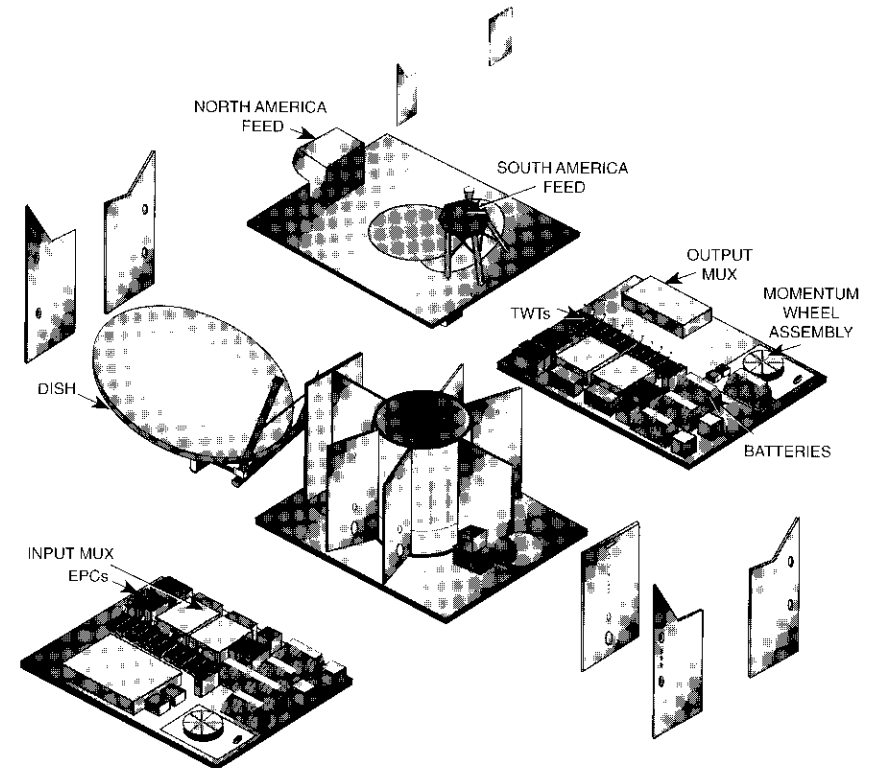


Figure 7. Spacecraft Equipment Layout

Results showed no impact on power buses when the payload was operated in TDMA mode.

### Antenna design and test

Ensuring the performance of the antenna subsystem proved challenging for two reasons. First, there was concern about thermal distortion of the antenna boresight angle of the deployable antenna. Second, there was no positioner at Astro capable of holding the spacecraft for far-field antenna range measurements, so it was necessary to verify antenna performance at the spacecraft level using the near-field range. Since the absolute accuracy of this range proved to be inadequate for these measurements, a differential test approach was used, as described below.

There was particular concern that the coefficient of thermal expansion (CTE) of the reflector surface would be different than that of the other structural members. Differential expansion or contracting would cause cupping of the surface (see Figure 1). Since the deployable antenna is supported at its edge, even mild cupping could change its boresight angle significantly. The Kapton film on the surface, and the extra adhesive used to attach it to the surface (the CTE of Kevlar can change with the percentage of adhesive), could cause a differential CTE.

To determine if there would be problems in orbit, an antenna distortion measurement program was set up in a thermal chamber using a dry nitrogen atmosphere. The motion (distortion) of the reflector was measured from  $-50^{\circ}$  to  $90^{\circ}\text{C}$  at nine points over the surface of the reflector using linear variable differential transformers (LVDTs). Considerable effort was put into designing a jig to hold the reflector so that it was not more constrained than it would be in orbit, and yet would allow measurement of the motion. (A completely free suspension of the reflector would not have allowed measurement of the reflector.) The test fixture was designed so that it did not induce thermal motion of its own. The fixture and the positioning of the LVDTs are shown in Figure 8.

Hygroscopic distortion was also determined as part of this measurement. This is distortion caused by differential swelling of the structure due to water vapor in the air. While the amount of boresight shift due to hygroscopic distortion was within the pointing budget, spacecraft alignment procedures were modified to correct for this change.

Coupons (small test pieces fabricated in the same manner as the antenna) were tested to determine their CTEs. Additional coupons were tested that had a Kapton face sheet glued to their surface, representative of the reflector surface. CTEs derived from the reflector thermal distortion measurements had to be consistent with the coupon data, which meant that the coupon data limited the values used to match the reflector measurements. With this limitation, quite good agreement with measurements was obtained.

Since the test was conducted under ambient pressure, it was not possible to simulate the thermal gradients that are experienced in orbit. The goal of the measurements was to model the actual distortion of the reflector over the temperature range and determine the CTE of the reflector and its ribs. The model was then used to predict thermal behavior under the anticipated in-orbit gradients. Close agreement to the measured data was obtained by selecting CTEs for the ribs and shell that were within the range of values obtained from the coupon test.

To gain increased confidence in the modeling, in-orbit-measured thermal distortion of other Astro spacecraft was modeled, with the CTEs for the ribs

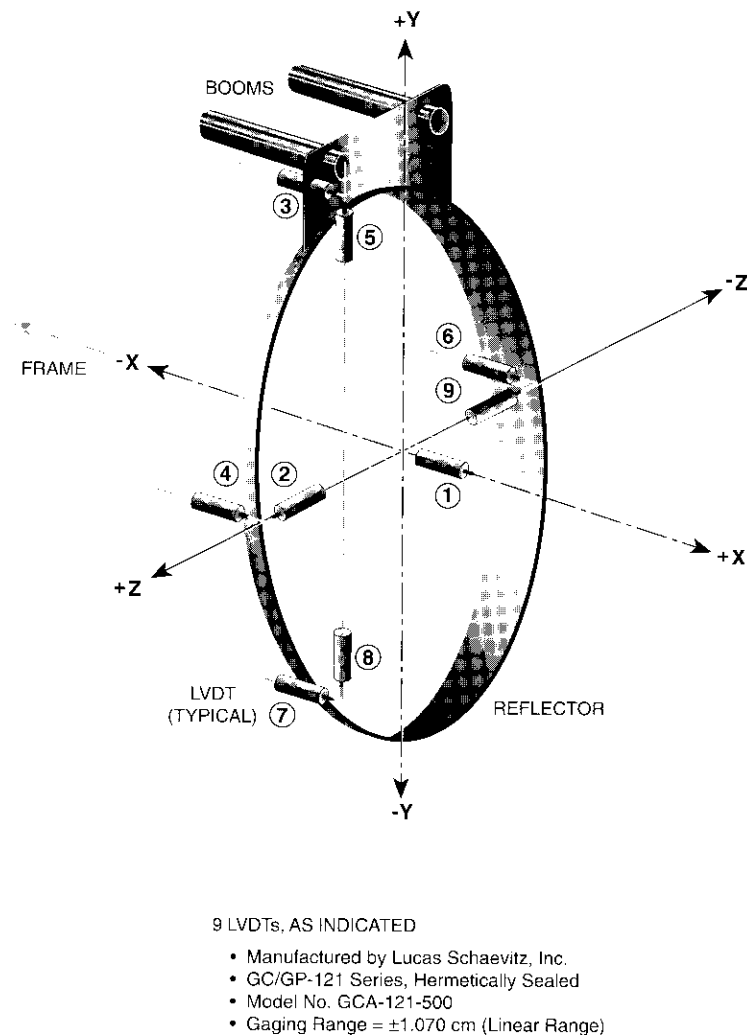


Figure 8. *INTELSAT-K Test Fixture and Displacement Transducer Locations During Reflector Distortion Test*

and shell considered as variables. The range of possible CTEs was estimated based on the coupon test data. The CTEs necessary to fit the data for the in-orbit satellites were within the range of coupon test data.

The modeling revealed that the thermal gradients created when the reflector emerged from the shadow cast by the spacecraft caused a significant change in the antenna boresight angle in the baseline design. To reduce these gradients, the reflector sunshield was changed from a single layer of Kapton to a sandwich of three layers of Kapton separated by two layers of a quartz insulating material. To reduce EOL temperatures, the sun shield coating was changed from Z202 to a germanium coating, which undergoes less ultraviolet degradation.

As a result of this test program, the predicted thermal distortion of the antenna was  $0.12^\circ$  peak-to-peak and was accounted for in the pointing budget. In-orbit measurements showed a larger than expected value of  $0.22^\circ$  peak-to-peak.\* The discrepancy is now believed to be due to thermal distortion of the spacecraft body and hinge mechanism.

There was much less concern about the South America antenna thermal performance because this antenna is symmetrically supported, and any cupping would not change the boresight angle. Since the antenna is mounted on the earth-facing panel, it also experiences fewer temperature extremes, further reducing the possibility of thermal distortion. There was concern regarding "RF spillover" in that, since the antenna is recessed into the multilayer insulation (MLI) blanket, spillover from the feed might be reflected into the coverage area, degrading sidelobe polarization and cross-polarization purity. A full-scale mock-up of the earth-facing deck was fabricated with the antenna mounted on it, and the assembly was wrapped in MLI in the same way it would be on the spacecraft. Tests showed that antenna performance was not degraded.

Concern that the EOL temperature of the South America antenna would exceed the acceptance temperature resulted in changing the coating of its sun shield. The high EOL temperature would result from blackening of the white Z202 thermal coating on the Kapton sun shield due to ultraviolet radiation. For this reason, the sun shield on the reflector was changed to the germanium-based S13GLO material, which exhibits better EOL performance. The germanium coating used on the deployable antenna had not been qualified by Astro at the time the decision was made to change coatings on the South America antenna.

The absence of a positioner capable of holding the INTELSAT-K satellite eliminated the possibility of testing antenna performance on the far-field range at spacecraft level. Only the near-field range could be used at this level; however, this range did not have sufficient absolute accuracy to verify antenna performance. INTELSAT and Astro agreed to a test program in which the far-field range was used for antenna subsystem measurements prior to integration

with the spacecraft. The antenna acceptance and performance predictions were based on these tests. Immediately following the far-field tests, near-field range measurements were conducted.

Following integration with the spacecraft, the near-field range measurements were repeated to verify that there was no change in performance due to the spacecraft structure. This procedure relied on the assessment that, although the absolute accuracy of the near-field range was insufficient to verify performance, its relative accuracy in detecting changes was sufficient to identify any changes in performance. Both the deployable and South America antennas were tested in this way.

The in-orbit tests on the antenna verified the effectiveness of these steps. Except for thermal distortion, the in-orbit measurements agreed well with predicted values. Thermal distortion measured in orbit was almost two times greater than expected; however, conservative design practices allow the satellite to meet or exceed all of its performance specifications.

## Conclusions

The performance of the INTELSAT-K payload has been verified by in-orbit tests and, more importantly, demonstrated by customer satisfaction. Since its launch in the summer of 1991, all performance requirements have been met or exceeded. The integration and test program described has produced a highly reliable payload, with no in-orbit failures to date. RF power telemetry has proved useful in helping INTELSAT-K customers to troubleshoot any difficulties they may encounter in setting up a link.

## References

- [1] T. Rush *et al.*, "INTELSAT-K: INTELSAT's First All K-Band Satellite," AIAA 14th International Communications Satellite Systems Conference, Washington, D.C., March 1992, *A Collection of Technical Papers*, Pt. 2, pp. 1008-1018, AIAA Paper No. 92-1944-CP.
- [2] M. P. Brown *et al.*, "INTELSAT-K Communications Performance Features," *COMSAT Technical Review*, Vol. 24, No. 1-2, 1994/1995, pp. 47-64 (this issue).
- [3] R. Strauss, "Orbital Performance of Communication Satellite Microwave Power Amplifiers (MAPs)," *International Journal of Satellite Communications*, Vol. 11, July 1993, pp. 279-285.
- [4] J. L. Stevenson *et al.*, "Reliability Assessment of Dispenser-Type Thermionic Cathodes," *Quality and Reliability Engineering International*, Vol. 4, 1988, pp. 347-366.

\* Also see: B. Teixeira, "INTELSAT-K Transponder In-Orbit Tests and Operational Considerations," *COMSAT Technical Review*, Vol. 24, No. 1-2, 1994/1995, pp. 65-78 (this issue).



*Robert A. Peters received a PhD in physics from the Stevens Institute of Technology in 1973 and became an Assistant Professor of Physics at Catholic University of America, where he initiated a solid-state research program. Joining INTELSAT's R&D Department in 1979, he developed total-dose and cosmic ray radiation test and hardening techniques, TWT cathode test techniques, solid-state earth horizon sensors, onboard carrier regeneration hardware, and optical intersatellite link components, and conducted system studies. In 1989 he became Payload Manager for the INTELSAT-K satellite program. Following successful completion of that program in 1992, he served as manager of INTELSAT Headquarters' Payload Engineering Section, where his responsibilities included preparation of payload specifications for new spacecraft RFPs and subsequent proposal evaluations, technical support for satellites under construction (particularly the INTELSAT VIII spacecraft series), in-orbit testing of new satellites, in-orbit payload anomaly investigations, and providing customer support for link problems. He left INTELSAT in 1995 and is currently providing consulting services in the above areas.*

*F. Lin Khoo received a BSEE in 1983 and an MSEE in 1987, both from the George Washington University. She is currently a Spacecraft Payload Engineer in INTELSAT's Spacecraft Communications and Payload Engineering Department, where her responsibilities include payload performance specification and evaluation, as well as monitoring of the payload during integration and test. In addition, she supports spacecraft launches, payload testing, monitoring, operation, and anomaly investigations of all INTELSAT in-orbit satellites. She has also participated in INTELSAT R&D activities involving emerging spacecraft payload technologies.*



*Prior to joining INTELSAT in 1986, Ms. Khoo was employed by Satellite Business Systems, where she was involved with the testing and evaluation of digital applications equipment for satellite communications. From 1983 to 1985, she was an engineer in COMSAT's World Systems Division, where she was involved with the design, implementation, and testing of the COMSAT TDMA/DSI system. She is a member of Tau Beta Pi and Eta Kappa Nu.*



*Ahmet Ozkul received a BSAE from the California Institute of Technology in 1971 and was employed at JPL, Applied Mechanics Laboratories, working on nondestructive testing of components for the Shuttle and other aerospace vehicles. He received the MSAE and ApSc degrees from George Washington University in 1974 and 1977, respectively, while employed at NASA Langley Research Center in Hampton, Virginia. In 1978, Mr. Ozkul joined INTELSAT's Systems Planning Division, where he conducted space/ground segment configuration studies to optimize INTELSAT system growth. After transferring to the Satellite Operations Department in 1983, he supported numerous launch missions and was involved in software-based projects related to satellite in-orbit operation, including performance modeling based on historical telemetry data, and electrostatic discharge mitigation onboard INTELSAT satellites. He served as Project Manager for INTELSAT-K at GE-Astro in East Windsor, New Jersey, from 1989 through the successful launch in 1992.*

*Mr. Ozkul is currently a Principal Engineer in the Engineering and Spacecraft Programs Division at INTELSAT, where he works on satellite system engineering and the feasibility study and implementation of special projects to enhance INTELSAT's space segment. He has authored numerous technical papers as a member of AIAA, IEEE, JIAFS, and other organizations.*

## ***INTELSAT-K communications performance features***

M. P. BROWN, JR., R. W. DUESING, J. A. TEHRANI,  
AND K. BHATNAGAR

(Manuscript received January 17, 1995)

### ***Abstract***

INTELSAT-K is a high-power, all-Ku-band satellite located at 338.5°E which has unique beam interconnectivity features among groups of its sixteen 60-W, 54-MHz transponders. The major communications performance features of INTELSAT-K are described, and the typical analog and digital television quality achievable over a range of receive earth station sizes is illustrated for services such as satellite newsgathering (SNG), cable head-ends, and direct-to-home (DTH) reception.

### ***Introduction***

INTELSAT-K is a high-power satellite with 60-W traveling wave tubes (TWTs) for each of its sixteen 54-MHz bandwidth transponders. It was purchased by INTELSAT in June 1989 to meet anticipated Ku-band television lease requirements in the Atlantic Ocean Region (AOR). INTELSAT-K is intended primarily for full- or fractional-transponder leased international television service between Europe, North America, and South America, but can also support other analog and digital services offered by INTELSAT, such as intermediate data rate (IDR) and international business services (IBS). The orbital maneuver life for the satellite is more than 9 years, with a stationkeeping tolerance of  $\pm 0.05^\circ$  (east/west and north/south). Figure 1 illustrates the INTELSAT-K antenna coverage from 338.5°E and depicts one of its beam connectivities. Figure 2 shows the satellite's transponder channelization and possible beam

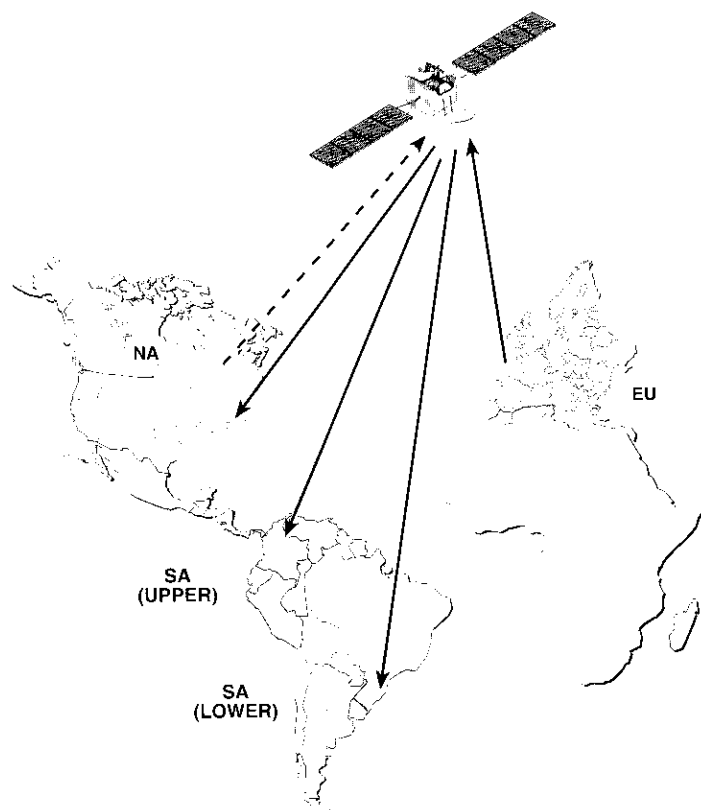


Figure 1. Earth Coverage Regions of the INTELSAT-K Satellite, Showing One Connectivity Option

connections.\* The 16 transponders operate over the uplink frequency band of 14.0 to 14.5 GHz from North America and Europe, and the downlink frequency bands of 11.45 to 11.70 GHz to North America, South America, and Europe; 11.70 to 11.95 GHz to North and South America; and 12.50 to 12.75 GHz to Europe. Depending on the transponder connection, two-times frequency reuse is achieved by either orthogonal linear polarization or spatial isolation.

The spacecraft beam connectivity capability affords combinations of west-to-east, east-to-west, west-to-west, and east-to-east configurations. INTELSAT-K

provides selectable transmit coverages of Europe, North America, and South America, and can receive from North America or Europe, but not South America. The high effective isotropically radiated power (EIRP) available from the satellite can support a variety of television services, including satellite newsgathering (SNG) and direct-to-home (DTH) broadcasting.

#### Communications parameters, beam connectivity, and coverage

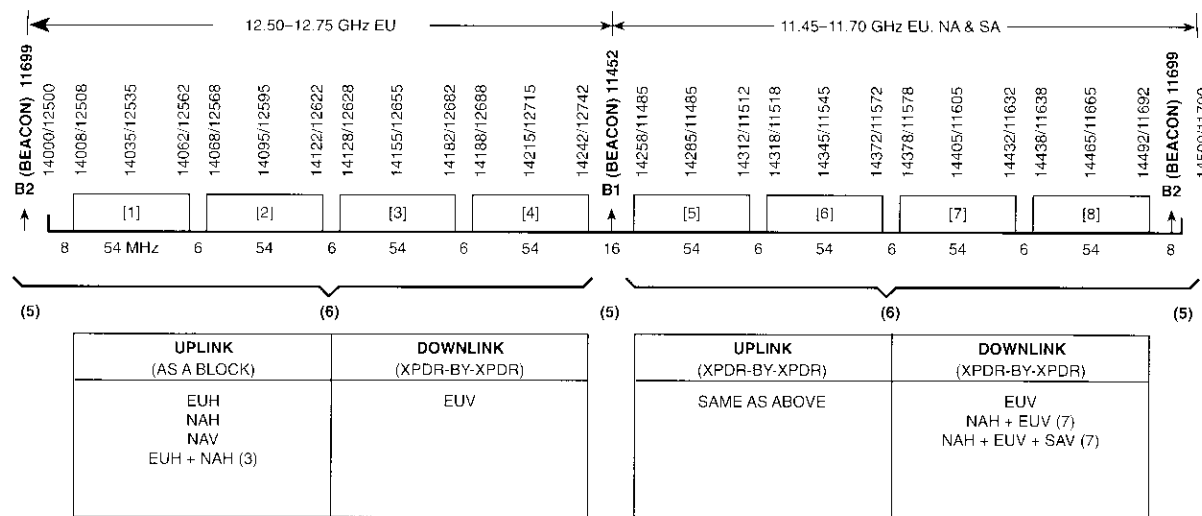
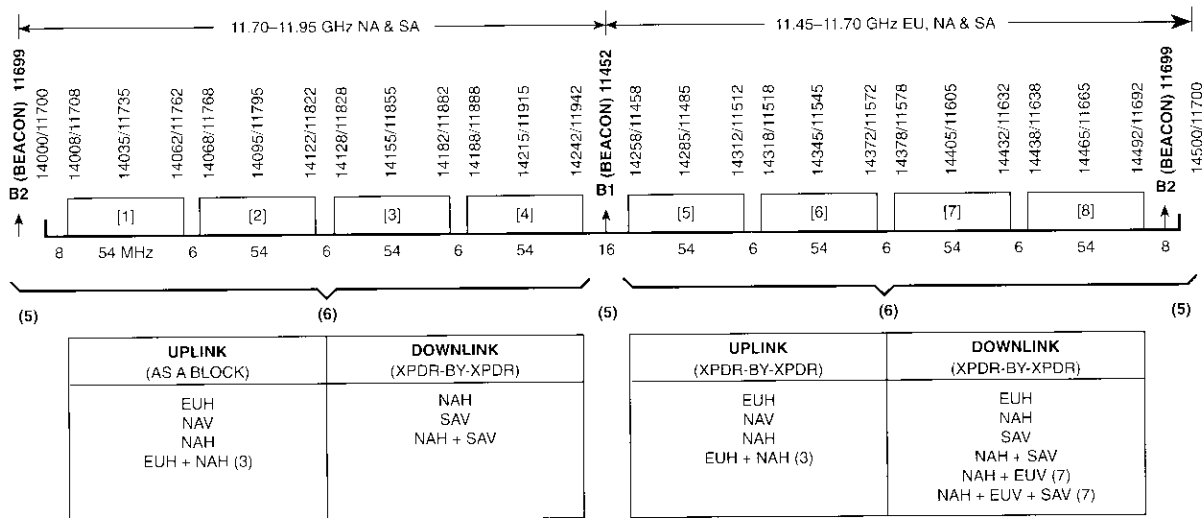
Table 1 shows the various up and downlink beams available on INTELSAT-K, along with their associated polarizations, connectivities, and specified communications parameters [saturation flux density, gain-to-noise temperature ratio ( $G/T$ ), and EIRP]. Depending on the geographical location of an earth station within the satellite antenna pattern, the parameters can typically be 1 to 3 dB better than those specified for the edge of the coverage area.

This spacecraft offers considerable flexibility for uplink and downlink beam configurations for North America, South America, and Europe. The INTELSAT-K beam nomenclature is based on a combination of the coverage area and polarization. For the uplink, the North America Horizontal (NAH), North America Vertical (NAV), and Europe Vertical (EUV) beams are available. For the downlink, Europe Horizontal (EUH), EUV, NAH, and South America Vertical (SAV) are available.

INTELSAT-K beams are not steerable; however, a platform bias which affects all beams may be applied in the east/west and north/south directions to achieve the coverages desired at given locations. INTELSAT-K transponders can also be configured for combined uplinks and broadcast downlinks. On the uplink, the NAH and EUH beams can be combined for simultaneous or alternating uplinking from North America and Europe. For the downlink, NAH and EUV can be combined, or NAH and SAV can be combined, or optionally all three beams (NAH, EUV, and SAV) can be combined to provide broadcast coverage.

Typical measured downlink (satellite transmit) antenna pattern coverage diagrams for the INTELSAT-K satellite at 338.5°E are shown in Figure 3. The diagrams illustrate constant gain contours for each beam, projected on the earth's surface with the appropriate spacecraft platform biasing. The pointing bias is 0.11°E, 0.16°N, but may change with time depending on service requirements. The contours were generated from prelaunch antenna gain data for each beam, measured at a given frequency over a range of azimuth and elevation points. The uplink (satellite receive) coverage diagrams are essentially the same as the transmit diagrams, except that the two coverages shown for South America (Figures 3c and 3d) are not available on the uplink.

\*See also: R. A. Peters, F. L. Khoo, and A. Ozkul, "The INTELSAT-K Payload," *COMSAT Technical Review*, Vol. 24, No. 1-2, 1994/1995, pp. 25-45 (this issue).



Notes: [ ] = Transponder frequency slot.

(1) See Table 1 for further information.

(2) EU = Europe; NA = North America; SA = South America; H = Horizontal polarization; V = Vertical polarization. Thus EUH = Europe Horizontal polarization.

(3) Uplink connections of EUH + NAH are switchable only on a group basis for transponders 1-8.

(4) 14000/11700 = 14,000-MHz (uplink) / 11,700-MHz (downlink).

(5) Beacons are transmitted via the communications antenna.

Polarization of the NA beacons is Horizontal. Polarization of the EU and SA beacons is Vertical.

(6) Only one beam configuration may be selected from each uplink and downlink column.

(7) Downlink broadcast mode.

Figure 2. INTELSAT-K Transponder Channelization and Beam Connections

TABLE I. INTELSAT-K TRANSMISSION PARAMETERS: CONTRACTUAL SPECIFICATIONS

(a) Uplink

BEAM/POLARIZATION*	EUH, NAH, NAV, or EUH + NAH	EUH, NAH, NAV, or EUH + NAH
Frequency (GHz)	14.0-14.25	14.25-14.5
Transponders (54 MHz)	1-4	5-8
Saturation Flux Density (dBW/m <sup>2</sup> )**		
Lowest Flux, Gain Step = 16	-70.5	-70.5
Highest Flux, Gain Step = 1	-93.0	-93.0
Gain Step Size (dB)	1.5	1.5
G/T (dB/K)**	3.0	3.0

(b) Downlink

BEAM/POLARIZATION*	EUH, NAH, SAV	NAH + SAV	EUV, EUH, NAH, or SAV	NAH + EUV	NAH + SAV + EUV or NAH + SAV
Frequency (GHz)					
Europe	12.5-12.75	—	11.45-11.7	11.45-11.7	11.45-11.7
North and South America	11.7-11.95	11.7-11.95	11.45-11.7	11.45-11.7	11.45-11.7
Transponders (54 MHz)	1-4	1-4	5-8	5-8	5-8
Saturation EIRP at Beam Edge (dBW)	<u>EU</u> <u>NA</u> <u>SA</u>	<u>NA</u> <u>SA</u>	<u>EU</u> <u>NA</u> <u>SA</u>	<u>EU</u> <u>NA</u>	<u>EU</u> <u>NA</u> <u>SA</u>
	47.0 47.0 45.0	42.7 42.7	47.0 47.0 45.0	47.0 47.0	47.0 42.7 42.7

\* EU = Europe, NA = North America, SA = South America; H = Horizontal polarization; V = Vertical polarization. Thus, EUH = Europe horizontal polarization, for example.

\*\* EUH + NAH = Combined uplink beams, which reduces the satellite saturation flux density and G/T by 3 dB.

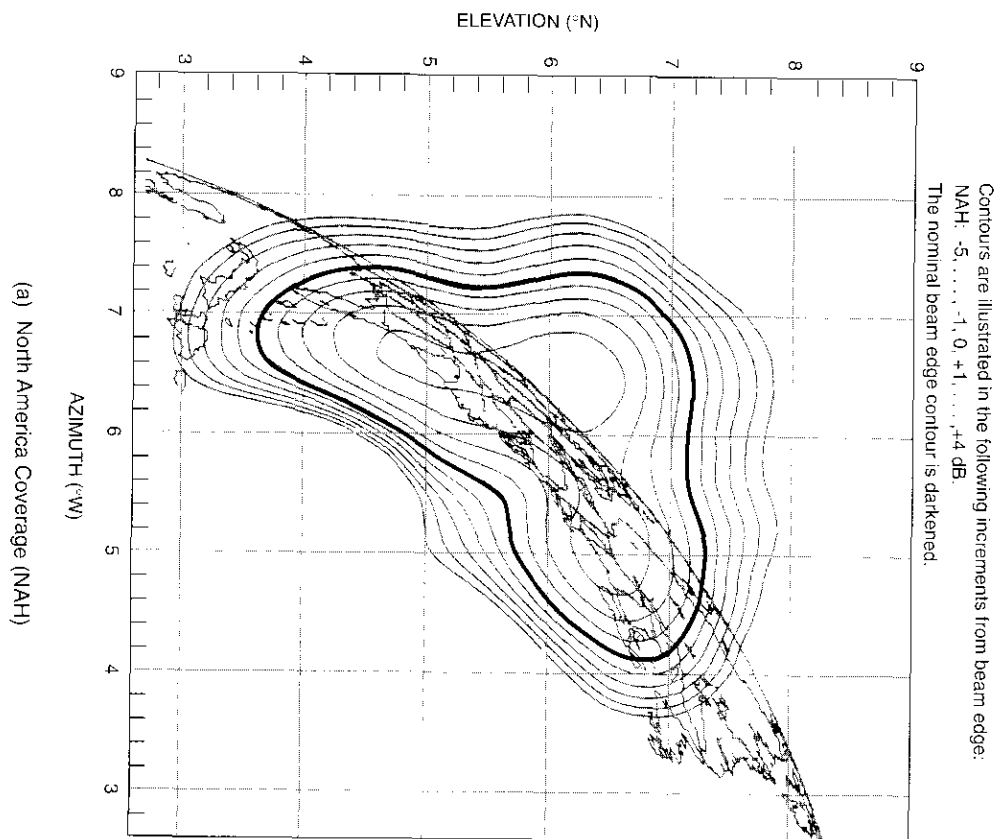
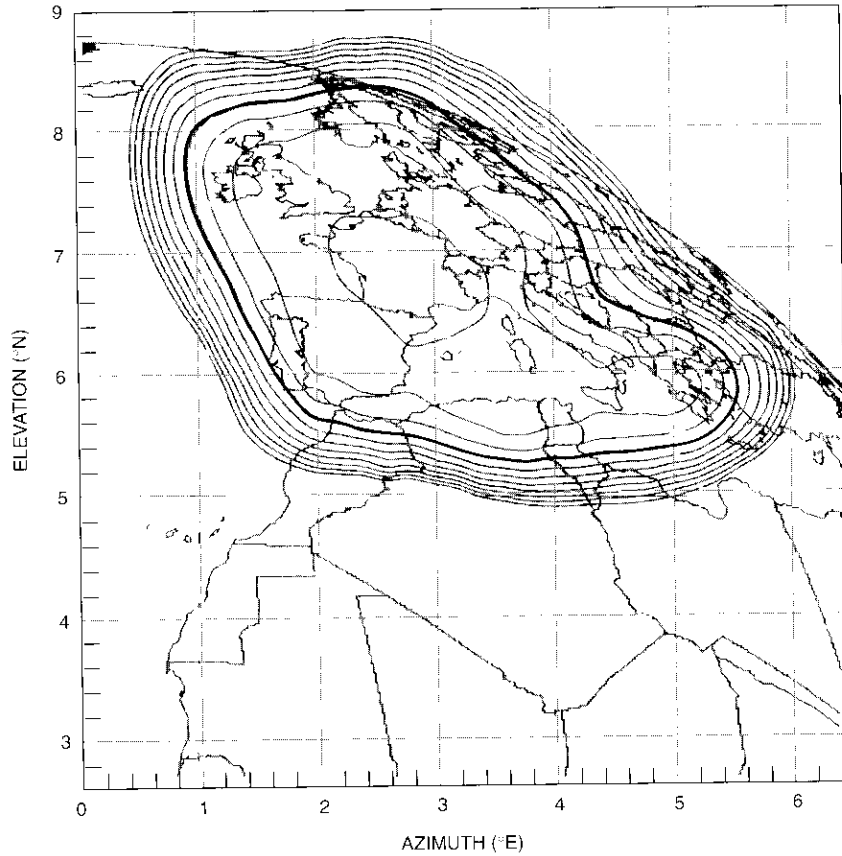


Figure 3. Typical Measured INTEL-SAT-K Transmit Beam Coverages for the Atlantic at 338.5°E

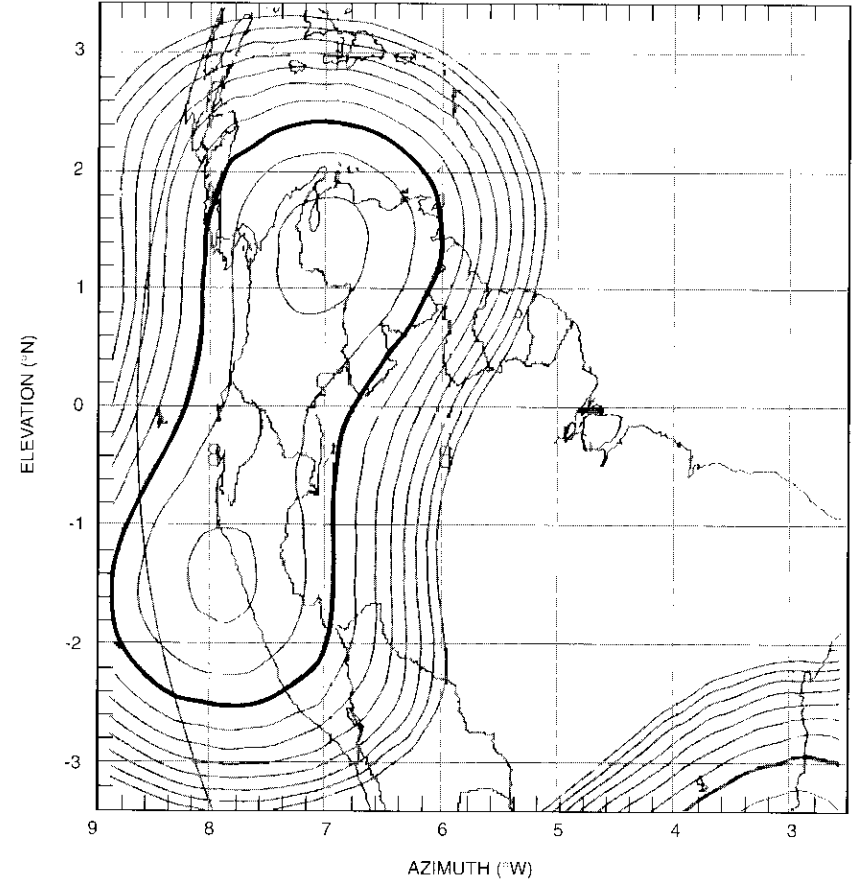
Contours are illustrated in the following increments from beam edge:  
 EUH: -7, ..., -1, 0, +1, ..., +3 dB.  
 The nominal beam edge contour is darkened.



(b) Europe Coverage (EUH)

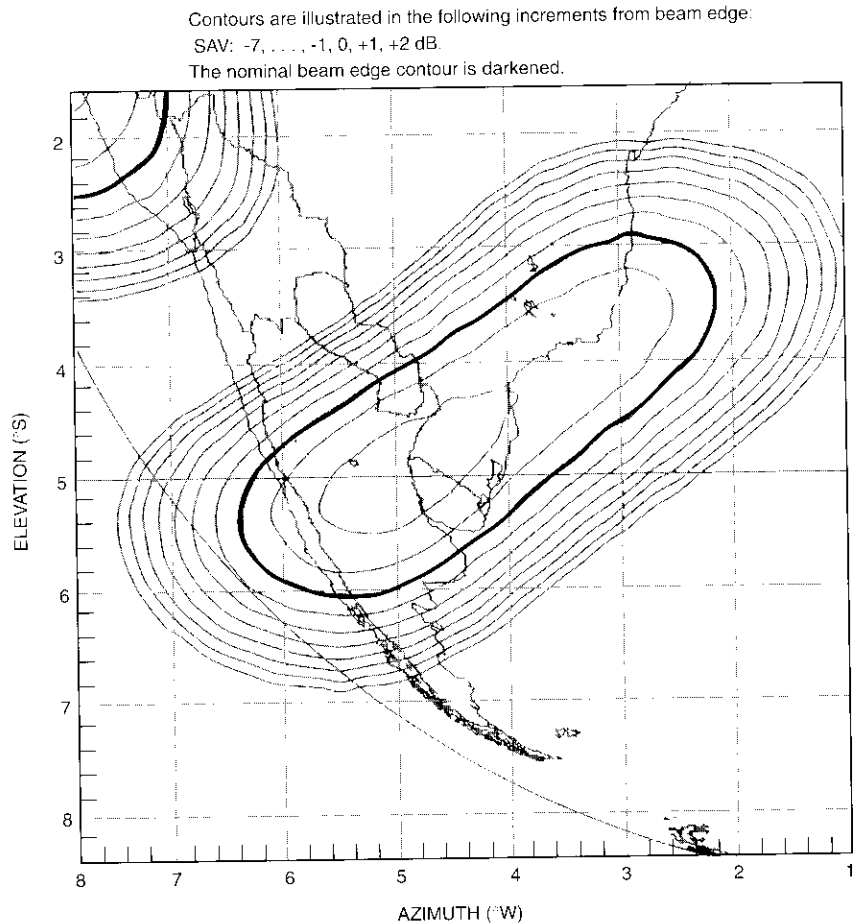
Figure 3. Typical Measured INTELSAT-K Transmit Beam Coverages for the Atlantic at 338.5°E (Cont'd)

Contours are illustrated in the following increments from beam edge:  
 SAV: -7, ..., -1, 0, +1, +2 dB.  
 The nominal beam edge contour is darkened.



(c) South America Coverage: Upper Beam (SAV-Upper)

Figure 3. Typical Measured INTELSAT-K Transmit Beam Coverages for the Atlantic at 338.5°E (Cont'd)



(d) South America Coverage: Lower Beam (SAV-Lower)

Figure 3. Typical Measured INTELSAT-K Transmit Beam Coverages for the Atlantic at 338.5°E (Cont'd)

### Level-limiting circuit

An important communications feature of the INTELSAT-K satellite is the input level-limiting circuit, which is available as a ground-commandable option. For single-carrier-per-transponder operation, this uplink fade control circuit will hold the downlink EIRP to within 3 dB of its original setting for uplink fades of up to 25 dB. The level-limiting circuit is not recommended for use with two or more carriers per transponder because excessive intermodulation products are generated, and because the control circuit will affect all carriers within the transponder when it reacts to a fade on a particular carrier.

The level-limiting circuit is available in transponders connected to the NAL, EUH, and SAV downlink beams. It is not available in transponders connected to the EUV downlink beam.

### Frequency planning

INTELSAT-K became operational in 1992 and has since been used mainly to transmit analog TV. Some of the 54-MHz transponders support a single TV carrier, while others carry two TV carriers per transponder. Although the user can generally select any TV modulation technique and RF bandwidth, many of the TV services in the operational plan use 27- and 30-MHz TV/FM carriers, while one transponder supports a digital TV carrier. Co-channel interference among the TV carriers is minimized by offsetting the co-channel carrier center frequencies.

### Transponder gain step increments and selection process

The INTELSAT-K spacecraft has a wide range of gain steps that can be selected by ground command for any transponder input. The gain step increments are 1.5 dB, which allows the specified edge of coverage saturation flux density to vary from -93.0 to -70.5 dBW/m<sup>2</sup>. An appropriate gain step is selected for a given application through coordination between INTELSAT Operations and the users. For example, for SNG where a small earth station transmits to a large earth station, gain steps corresponding to high uplink sensitivity (1 through 5) are appropriate. These steps keep the uplink EIRP relatively low. In the case of a large earth station transmitting to a small earth station (e.g., DTH), gain steps corresponding to somewhat lower uplink sensitivity (6 through 9) may be appropriate. In this case, the gain steps keep the uplink EIRP and uplink carrier-to-noise ratio, C/N, relatively high compared to the low downlink C/N to a small terminal.

### Initial utilization

During its first 3 years of operation, INTELSAT-K has been used to transmit one or two analog TV carriers per transponder. Leases supporting transmission to North America are configured in the combined uplink connectivity, referred to as EUH + NAA in Figure 2 and Table 1. Thus, these transponders may be used to support simultaneous transmission of two TV carriers per transponder, such as one from Europe and one from North America. Optionally, the combined uplink beams can transmit a single TV carrier through the transponder, with the carrier originating alternately from Europe and North America. Such operation allows greater flexibility because full transponder power is needed to deliver the required  $C/N$  at the small receive terminal.

### Transmission design

Table 2 provides sample link budgets for single-carrier-per-transponder television operation of TV/FM and compressed digital TV. These budgets were developed to illustrate the television performance expected at receive earth stations of various sizes. Under these conditions, the transmission design assumes that the uplink earth station is large enough to transmit sufficient EIRP to operate the transponder at saturation while using a transponder gain step that will keep the uplink  $C/N$  relatively high, since the overall link is downlink-limited.

Figures 4 and 5 compare analog and digital television performance vs gain step and earth station size. For digital TV, a 25.5-Mb/s compressed digital TV carrier using rate 1/2 forward error correction (FEC) and a Reed-Solomon (RS) outer code has been considered. Depending on the receive antenna size and the availability requirements, different carrier sizes and coding schemes can be adopted. For the analog TV computation, a 30-MHz bandwidth TV carrier with a receive filter bandwidth of 22.5 MHz has been used in the link budgets. A 22.5-MHz filter is used for the small television receive-only antennas (TVROS) to improve their  $C/N$  (but with a slight deterioration in signal quality).

### Summary

INTELSAT-K's orbital location at 338.5°E places it in a position to provide high Ku-band EIRP over key geographical areas in North America, South America, and Europe. The initial loading of INTELSAT-K is predominately leased transponder operation using analog television for services to cable heads and DTH. SNG is also supported. It is expected that the modulation technique used on this spacecraft will shift toward compressed-digital TV when this technology becomes widely available.

TABLE 2. PER-CARRIER DTH LINK BUDGETS: SINGLE-CARRIER-PER-TRANSPONDER 30-MHZ ANALOG TV AND 25.5-MB/S DIGITAL TV

NO.	PARAMETER	DIGITAL	ANALOG	UNIT
<b>General</b>				
1	Satellite Type	K	K	
2	Type of Service	CDTV	TV/FM	
3	Uplink Beam	NAV	NAV	
4	Downlink Beam	EUU	EUU	
5	Frequency (up)	14.0	14.0	GHz
6	Frequency (down)	11.2	11.2	GHz
7	Transponder Bandwidth	54.0	54.0	MHz
8	No. TV Carriers	1	1	
9	Transponder Amplifier Type	TWTA	TWTA	
10	Gain Step	4	4	
11	Transmit Earth Station Size	Any	Any	
12	Receive Earth Station Size	0.85	0.85	m
<b>Uplink</b>				
13	Total Uplink EIRP	75.4	75.4	dBW
14	Path Loss (up) at 10° Elevation	208.3	208.3	dB
15	Earth Station HPA IM Limit	10.0	10.0	dBW/4 kHz
16	C/T HPA IM	-127.2	-127.2	dBW/K
17	Gain of 1 m <sup>2</sup>	44.4	44.4	dB/m <sup>2</sup>
18	Operating Flux Density	-88.5	-88.5	dBW/m <sup>2</sup>
19	Saturation Flux Density (BE)	-88.5	-88.5	dBW/m <sup>2</sup>
20	Antenna Pattern Advantage (up)	0.0	0.0	dB
21	Input Backoff (total xpdr)	0.0	0.0	dB
22	Spacecraft G/T (BE)	3.0	3.0	dB/K
23	C/T Thermal (up)	-129.9	-129.9	dBW/K
24	Spacecraft Spatial Beam Isol. (up)	N/A	N/A	dB
25	Spacecraft X-Pol. Beam Isol. (up) <sup>a</sup>	33.0	33.0	dB
26	Earth Station X-Pol Isol. (up)	30.0	30.0	dB
27	Misalign Angle (dual pol. lin.) (up)	1°	1°	
28	Net Isolation (up) <sup>b</sup>	25.0	28.0	dB
29	C/T Co-Channel (up)	-128.0	-127.1	dBW/K
<b>Intermodulation</b>				
30	Saturated EIRP (BE)	47.0	47.0	dBW
31	Output Backoff (total xpdr)	0.0	0.0	dB
32	C/T IM (one carrier/xpdr)	None	None	dBW/K

TABLE 2. PER-CARRIER DTH LINK BUDGETS: SINGLE-CARRIER-PER-TRANSPONDER 30-MHZ ANALOG TV AND 25.5-MB/S DIGITAL TV (CONT'D)

NO.	PARAMETER	DIGITAL	ANALOG	UNIT
<b>Downlink</b>				
33	Spacecraft Spatial Beam Isol. (dn) <sup>a</sup>	30.0	30.0	dB
34	Spacecraft X-Pol Beam Isol. (dn)	N/A	N/A	dB
35	Earth Station X-Pol Isol. (dn)	N/A	N/A	dB
36	Misalign Angle (dual pol lin.) (dn)	N/A	N/A	deg
37	Net Isolation (dn)	30.0	33.0	dB
38	C/T Co-Channel (dn)	-123.0	-122.1	dBW/K
39	Antenna Pattern Advantage (dn)	2.0	2.0	dB
40	Elevation Angle (dn)	10.0	10.0	deg
41	Path Loss (dn)	206.1	206.1	dB
42	Earth Station G/T	18.0	18.0	dB/K
43	C/T Thermal (dn)	-139.1	-139.1	dBW/K
<b>Totals</b>				
44	C/T Sum	-140.1	-140.1	dBW/K
45	Other Losses <sup>c</sup>	2.5	1.9	dB
46	C/T Total (available)	-142.6	-142.0	dBW/K
<b>Summary</b>				
47	C/T Threshold per Carrier	-149.0	-145.1	dBW/K
48	System Margin	6.4	3.0	dB
49	C/T per Carrier	-142.6	-142.0	dBW/K
50	Carrier Receive Noise Bandwidth <sup>d</sup>	36.0	22.5	MHz
51	C/N per Carrier	10.4	13.1	dB
52	S/N (525/60 unified weighting)	N/A	47.8	dB
53	S/N (625/50 unified weighting)	N/A	46.0	dB

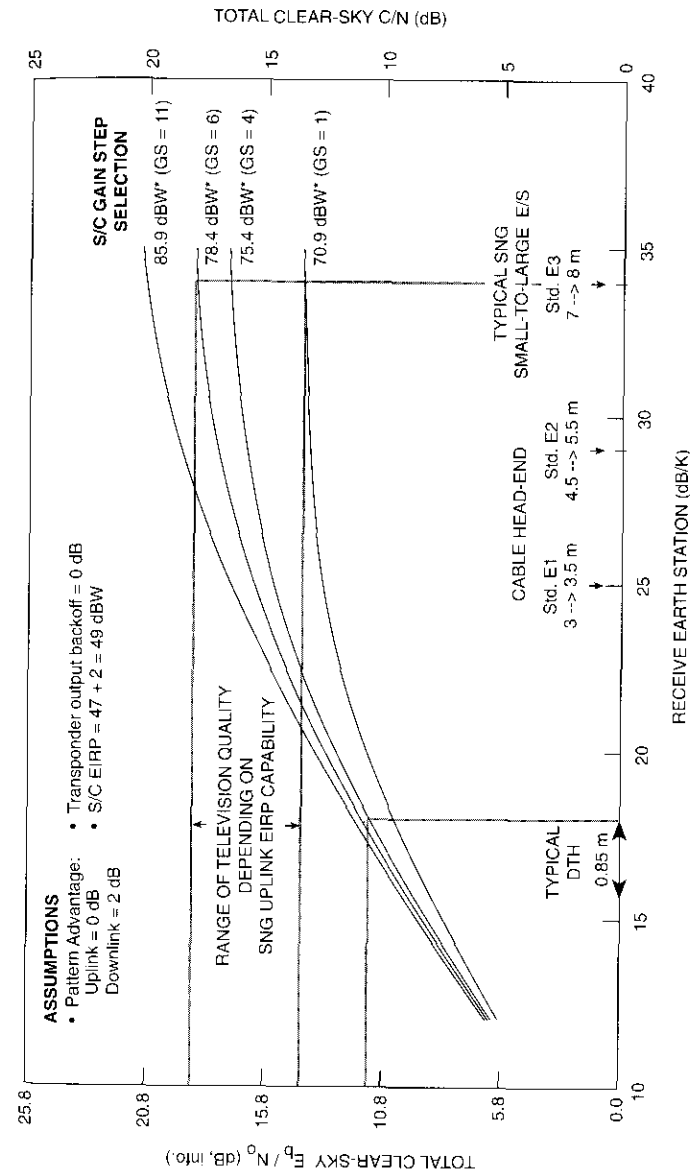
**Notes:**

<sup>a</sup> The co-channel transponder is assumed to be NAH on the uplink and SAV on the downlink.

<sup>b</sup> For analog TV, an improvement of 3 dB has been assumed for the uplink and downlink co-channel isolation due to the frequency interleaving advantage available.

	Digital	Analog
	TV	TV
<sup>c</sup> "Other Losses" includes the following:		
1. Effect of downlink tracking loss on total link	0.8	0.8
2. Uplink tracking loss and HPA instability	0.5	0.5
3. 5% earth station equipment noise [-10 log (1-0.05)]	0.2	0.2
4. 10% of total noise for ASI for analog TV; 20% for digital TV	1.0	0.5
5. 10% of total noise for terrestrial interference. [-10 log (1-0.1)]	0.5	0.5
Items (1), (2), and (3) are root-sum-squared and then added to items (4) and (5) to yield:	2.5 dB	1.9 dB

<sup>d</sup> The receive bandwidth of the TV/FM carrier is assumed to be 22.5 MHz, to improve the TV C/N for small receive antennas. For larger antennas, a bandwidth of 30 MHz should be used.



\* Uplink EIRP needed to saturate the satellite transponder for a given gain step (GS).

Figure 4. Television Quality vs Earth Station G/T for Compressed Digital TV (25.5 Mb/s, rate 1/2 FEC with Reed-Solomon outer code, North America downlink)

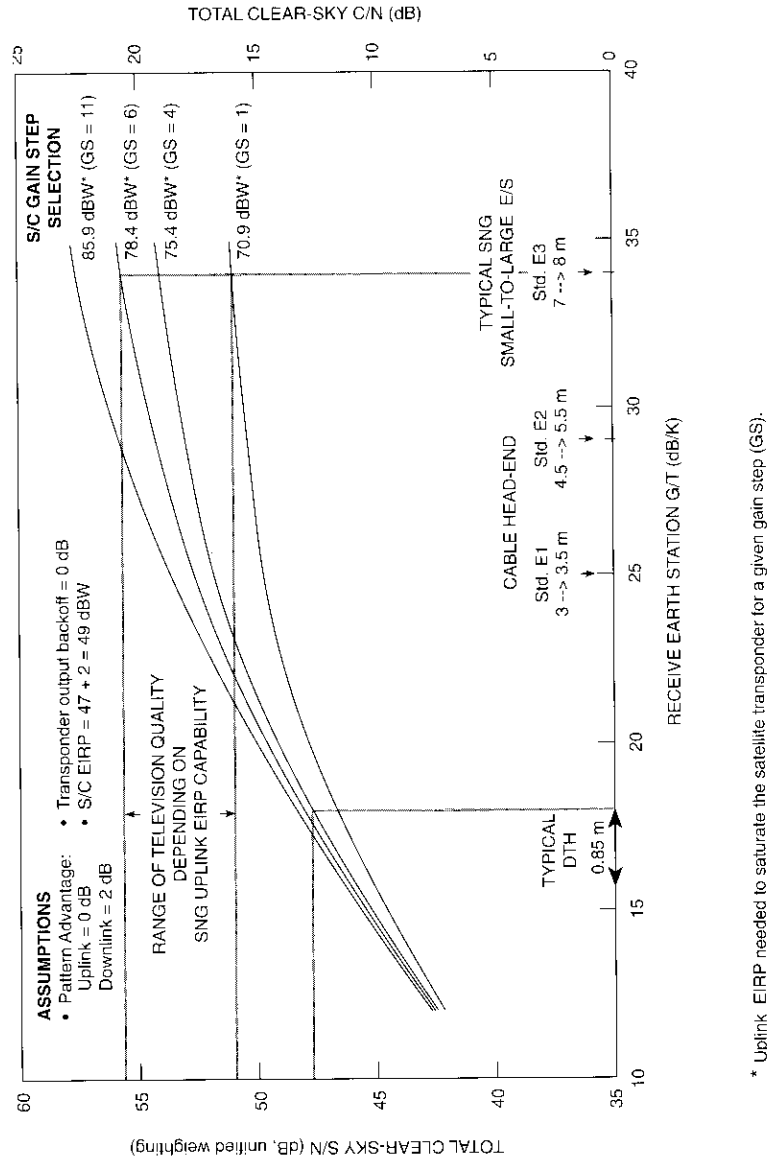
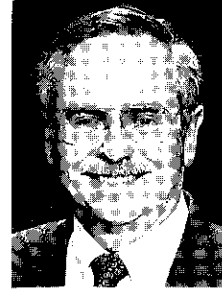


Figure 5. Television Quality vs Earth Station G/T for a Single TV/FM Carrier per Transponder to North America (11.7-11.95 GHz, 30-MHz NTSC TV)



Martin P. Brown, Jr., received a BEE from the Georgia Institute of Technology in 1966. Prior to entering military service, he was employed by IBM at Cape Kennedy, where he was involved in construction of the first Saturn V launch vehicle. From 1967 to 1971, he served as an engineering communications officer with the U.S. Air Force. In 1971 he joined COMSAT Laboratories, where he was primarily involved in transmission design for INTELSAT IV, IVA, and V. He joined INTELSAT in August 1978 to become Manager of the Satellite Transmission Engineering and Modeling Section, where he was responsible for the FDMA transmission design for the INTELSAT VI, VII, VIII, VIIIA, and K satellites, and for preparing the required earth station performance characteristics associated with each of these spacecraft series. He was also involved in designing most of the analog and digital modulation techniques employed by INTELSAT, and in developing computer system models for satellite communications.

In 1995, Mr. Brown joined the Systems Development Division at COMSAT Laboratories as a Program Manager, and is currently involved in studies relating to the management, control, and monitoring of military circuits on DSCS III and various commercial satellites. He is a past Chairman of the IEEE Communications and Broadcast Satellite Systems Committee and a Registered Professional Engineer.

Richard W. Duesing received a BS in mathematics from Youngstown University in 1962. He then worked at McDonnell-Douglas Astronautics, where he developed software models for digital filtering, telemetry data reduction, acoustic and vibration analysis, and weight control applications. He was subsequently employed at Computer Sciences Corporation in 1969 as a Department Manager, and participated in developing models in support of the defense communications satellite system, orbit determination applications for the NASA/JPL deep space probes, and real-time message switching and scientific systems.



In 1979, Mr. Duesing joined INTELSAT as a Principal Engineer in the Transmission Engineering and Modeling Section, where he was responsible for the management and implementation of computer system models pertaining to communications engineering and transmission analysis. He was also involved in the transmission planning and development of satellite characteristics modules for the INTELSAT V, VI, VII, VIII, and K series satellites. Mr. Duesing is currently a Program Manager at COMSAT Laboratories, primarily involved with the implementation of burst time plan generation software in support of INTELSAT's upgraded TDMA system.



leased transponders. Mr. Tehrani is a member of IEEE.

*Jahangir Anvari Tehrani received a BSEE from Oklahoma State University in 1977, and an MS from George Washington University in 1979. In 1978 he worked at COMSAT, where he was involved in intersystem coordination between INTELSAT and the USSR. He joined INTELSAT in 1979 and is currently a Principal Engineer in the Transmission Engineering and Laboratory Department. He has worked in the areas of transmission planning for INTELSAT VI, VII, VIII, and K; design of the digital modulation techniques employed with these spacecraft; and evaluation of the transmission plans for the*

*Krishan L. Bhatnagar received a BSc in physics and mathematics from the University of Delhi, and an EE and PhD from the University of Toronto. From 1970 to 1974 he was a Member of the Technical Staff at COMSAT Corporation, where he studied the use of predictive and transform encoding techniques in image processing, and simulated digitized television signals. Subsequently at Computer Sciences Corporation, he worked on modification of a channel model simulation program, and the computation of inter-modulation effects in satellite transponders. As a Senior Systems Engineer/Member of the Technical Staff at CONTEL ASC (formerly American Satellite Co.), Dr. Bhatnagar was responsible for the communications payload portion of the ASC-1 and ASC-2 satellites, and participated in their procurement and launch.*



*Since 1988, Dr. Bhatnagar has been a Senior Communications Engineer with COMSAT World Systems. He has conducted transmission analyses and provided link budgets for digital data services and analog/digital video services that resulted in their successful implementation on INTELSAT's multibeam satellites. He participated in INTELSAT's Board of Governors' Technical Advisory Committee, conducted feasibility studies on transmission issues, and managed a number of COMSAT World Systems' development projects at COMSAT Laboratories. Dr. Bhatnagar is a member of IEEE.*

Index: in-orbit testing; INTELSAT; telemetry, tracking & command; transponders

## **INTELSAT-K transponder in-orbit tests and operational considerations**

B. TEIXEIRA

(Manuscript received January 17, 1995)

### **Abstract**

The general measurement methods used, and results obtained, during RF in-orbit testing of the INTELSAT-K satellite communications payload (antennas and transponders) and telemetry, command, and ranging (TC&R) subsystems are described. All repeater, antenna, and TC&R subsystems performed within specifications. Additional antenna tests conducted to measure the contours of the Europe beam within the fringe areas of the main beam are discussed, and INTELSAT's operational support provisions to ensure proper beam connectivity changes on an as-needed basis, as requested by some customers, are explained.

### **Introduction**

When a new spacecraft is launched for INTELSAT, in-orbit testing is routinely conducted to verify that the stress loads imposed by launch have not affected the onboard subsystems, and to ensure that the satellite is capable of supporting the traffic services it is intended to carry. One such series of tests is the RF in-orbit test (IOT), which verifies the performance of the communications payload (antennas and transponders) and the telemetry, command, and ranging (TC&R) subsystems. To attain the desired level of confidence, it is necessary to check the correct operation, in orbit, of all units of the RF subsystems, as well as the performance of other subsystems which have direct impact on the RF performance seen by ground stations. This can only be accomplished by performing the IOT before traffic operation commences.

The INTELSAT-K RF IOT was performed during the period July 8 through August 4, 1992, and the results were compared with data obtained previously from ground-based tests conducted by the manufacturer during spacecraft construction. The IOT measured satellite payload RF performance with a high degree of accuracy, showing the effects of the spacecraft body and blankets on the operational performance of the antennas.

Because of the limited attitude bias capabilities of INTELSAT-K ( $\pm 5^\circ$  in pitch and  $\pm 2^\circ$  in roll), it was necessary to use a dedicated test station for each beam measurement. The Europe beam was tested using the Fucino, Italy, IOT station; each North America beam was tested using the Clarksburg, Maryland, USA, communications system monitoring (CSM) station; and the South America beams were tested using a portable antenna and test setup flown to the Tangua and Manaus facilities provided by the Brazilian signatory, EMBRATEL. Reference 1 provides details on the Fucino IOT system. The Clarksburg CSM station was used to perform saturated flux density, effective isotropically radiated power (EIRP), and antenna pattern measurements only. The portable station in the South America coverage region was employed to perform saturated EIRP measurements (using test signals transmitted from Fucino) and antenna pattern measurements.

The INTELSAT-K IOT was performed in two phases. Phase 1 consisted of communications (repeater and antenna) subsystem performance tests using the three earth stations—one for each communications beam. Phase 2, comprising the TC&R subsystem performance tests, was conducted from the Clarksburg, Maryland, tracking, telemetry, and command (TT&C) station. Repeater performance was confirmed by measuring the transponders' gain-to-noise temperature ratio ( $G/T$ ), saturation flux density, saturation EIRP, and frequency response for all channels. Antenna performance was confirmed by measuring the copol and cross-pol antenna patterns for all beams.

The IOT measurements taken showed that all repeater, antenna, and TC&R subsystems performed within specifications. A week-long series of antenna cut measurements of the Europe beam were carried out at 2-hour intervals at seven discrete elevation offset points. A new "centroid" measurement method was successfully implemented to analyze the results, in order to determine the Europe beam boresight position and the daily pointing stability. Complete characterization of the daily antenna pointing variations was conducted to provide better, more well-defined service in the future. This approach was prompted by the new Europe/North America antenna design, which uses a single antenna with dual offset gridded reflectors to produce beams having orthogonal polarities.

This paper describes the general measurement methods used, and the results obtained, during the INTELSAT-K payload IOT. The rationale and the basic results for additional antenna tests to measure the contours of the Europe beam within the fringe areas of the main beam are also discussed. In addition, INTELSAT's operational support provisions to ensure proper beam connectivity changes on an as-needed basis, as requested by some customers, are explained. (See References 2 and 3 for further details.)

### **INTELSAT-K subsystems**

The INTELSAT-K payload IOT evaluated the performance of the satellite's communications payload (transponders and antennas) and TC&R subsystems. The measurement methodologies used are explained in detail in Reference 1.

#### **Communications subsystem**

The INTELSAT-K communications subsystem is described in a companion paper by Peters *et al.*\*

#### **TC&R subsystems**

The INTELSAT-K TC&R subsystems consist of the telemetry, command, and ranging components described below.

##### TELEMETRY SUBSYSTEM

Figure 1 is a block diagram of the telemetry subsystem on board INTELSAT-K. Two redundant telemetry modules (RTMs) are cross-strapped to two telemetry transmitters, which provide the two commandable telemetry beacons for the spacecraft. The INTELSAT-K beacon 1 frequency is 11,452.0 MHz, and the beacon 2 frequency is 11,699.0 MHz. When the transmitter is commanded to the high-power mode, the beacons are transmitted by the relevant communications antennas, as well as by an omnidirectional antenna having vertical polarization. Each RTM can operate independently in eight different modes:

- *Pulse Code Modulation (PCM), High-Priority.* Produces a digital stream at 1,024 b/s in biphas-L format which modulates a 32-kHz subcarrier. Each telemetry frame consists of 256 eight-bit words. The nominal frame size is 2 s.
- *PCM, Low-Priority.* The power-on default mode. Identical to the high-priority mode, except that the RTM turns off the 32-kHz

\* R. A. Peters, F. L. Khoo, and A. Ozkul, "The INTELSAT-K Payload," *COMSAT Technical Review*, Vol. 24, Nos. 1/2, 1994, pp. 25-45 (this issue).

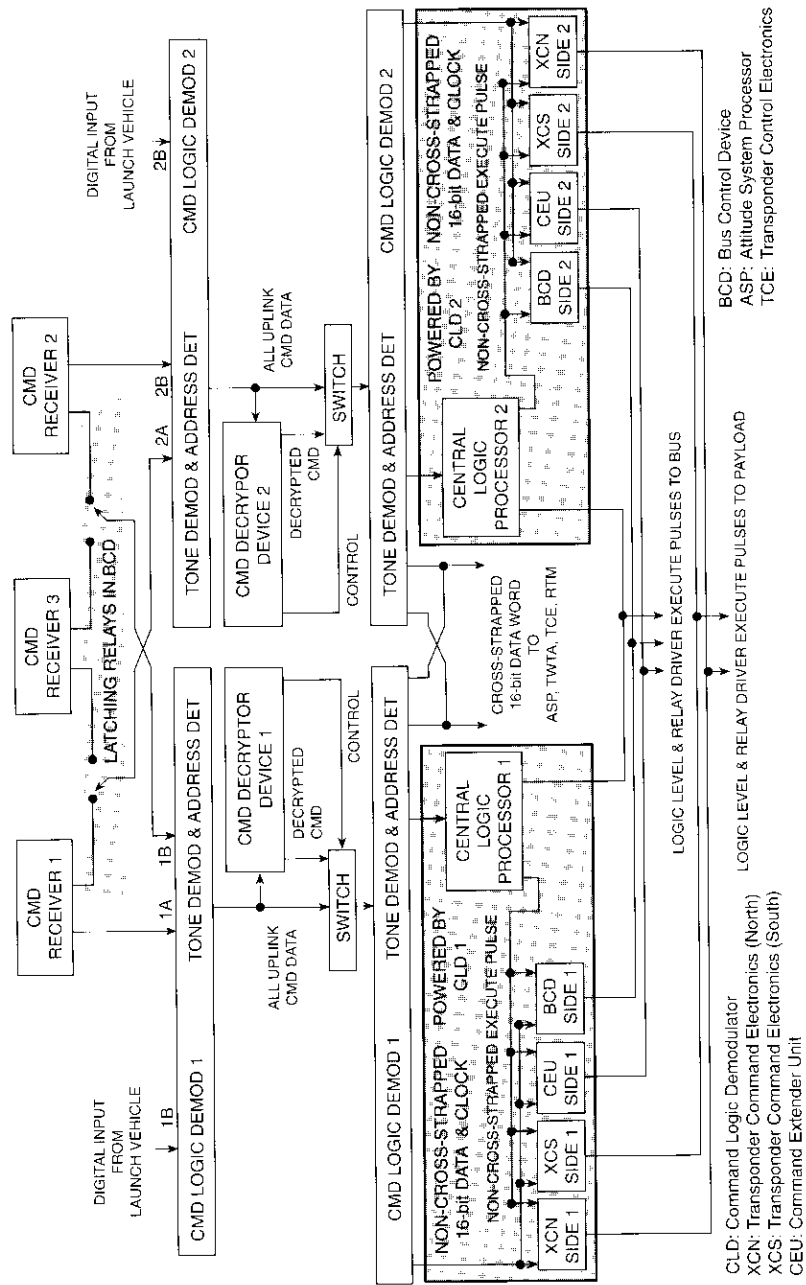


Figure 1. INTELSAT-K Telemetry and Ranging Subsystems Block Diagram

#### COMMAND AND RANGING SUBSYSTEMS

Figure 2 is a block diagram of the command subsystem. (The transmit portion of the ranging function is performed by the telemetry subsystem and was depicted in Figure 1.) This subsystem provides ground control of all commandable spacecraft functions. Commands can be transmitted to the spacecraft via two different command carrier frequencies in the 14-GHz range. They are received by a horizontally polarized dual-mode toroidal bicone omnidirectional antenna (frequency 1) and/or by the North America Vertical or Europe Horizontal beams (both frequencies). The antenna outputs are directed to three separate redundant receivers. The uplink carrier frequency determines the choice of command receiver, since the receivers are tuned to two different frequencies (*i.e.*, receivers 1 and 2 are tuned to frequency 1, and receiver 3 is tuned to frequency 2).

telemetry subcarrier and substitutes a 14.5-kHz subcarrier which contains the command data bits in the uplink and the execute pulse. The telemetry subcarrier is restored when the command registers are cleared.

- *PCM Dwell.* Telemetry data in this mode are identical to data in the high-priority mode, except that the multiplexer continuously samples any one of the 256 telemetry words specified by command.
- *Subcarrier Dwell.* Produces a 14.5-kHz subcarrier modulated directly by the selected telemetry word, instead of being processed into PCM data.
- *Special Sensor.* Produces a 14.5-kHz subcarrier modulated directly by the analog output of earth sensor assembly (ESA) 2 and 1 north scans for RTMs 1 and 2, respectively.
- *Attitude Monitor.* Produces a 14.5-kHz subcarrier modulated directly by either the sun sensor assembly/horizon sensor assembly (SSA/HSA) (transfer orbit sensors) or the earth sensor's south scan, when it is on.
- *Ranging.* All internally generated telemetry is replaced by the third video output of the selected command receiver, which passes through a 12-kHz high-pass filter. This mode is used to provide a narrowband transponder for ranging.
- *Simultaneous Ranging and PCM Telemetry.* The range tone from the selected command receiver is added to the 32-kHz PCM data subcarrier. Filters in the ground station equipment separate the two. This is the nominal operational mode for beacon 1.

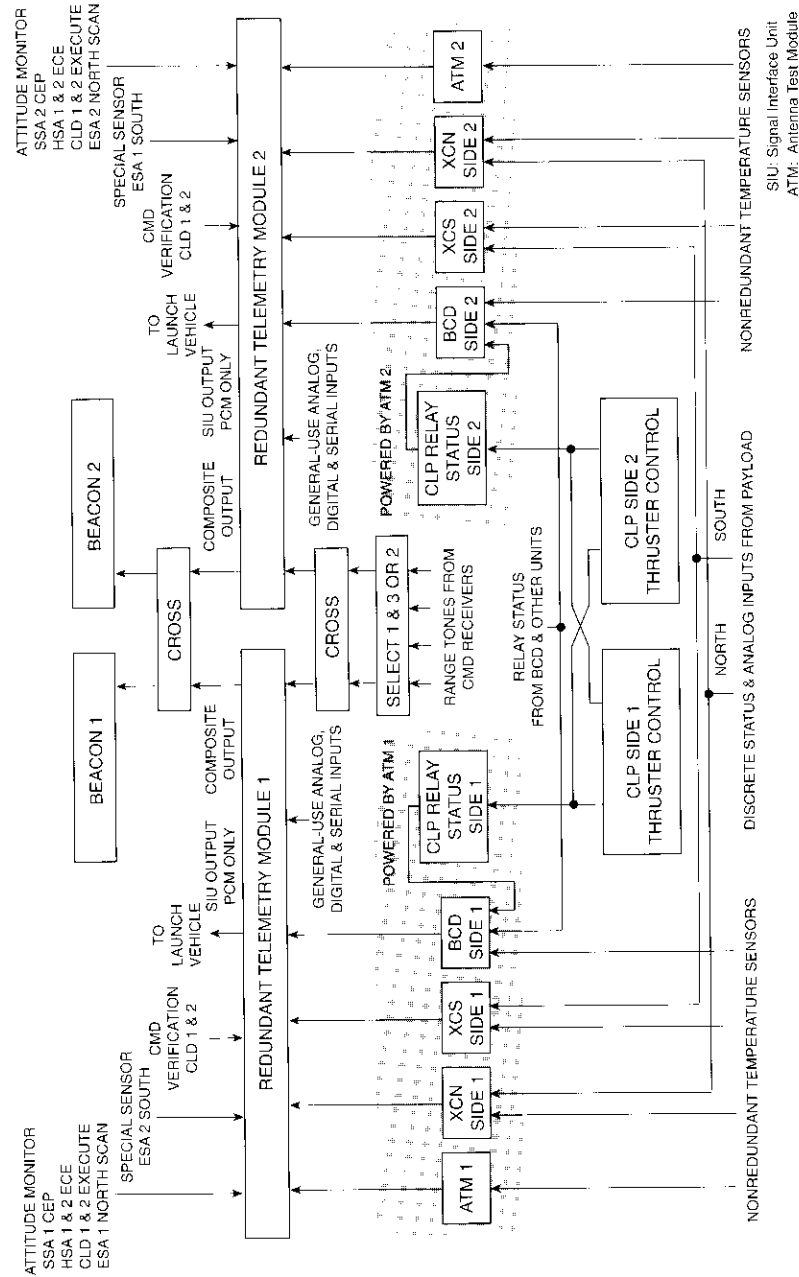


Figure 2. INTELSAT-K Command Subsystem Block Diagram

Three separate command tone frequencies are used (corresponding to 0, 1, and Execute) which frequency-modulate the command carrier. The chosen command receiver demodulates the command tones and feeds them to each of the two redundant command logic demodulators (CLDs). The CLDs then feed the commands, in the form of a PCM-RZ data stream, to the corresponding central logic processor (CLP). CLD selection information is contained within the command message. The receivers and CLDs are fully cross-strapped for high reliability.

The command receivers also provide a separate output to a selected telemetry transmitter for ranging operation, which is available when any of the beacons are operated in the ranging (or simultaneous PCM and ranging) modes. An encrypted command data format can be used for added security.

### **INTELSAT-K payload IOT results**

#### **Transponder RF testing**

All transponder units [e.g., receivers and traveling wave tube amplifiers (TWTAs)] are tested during the IOT. In addition, all alternate paths through the various switch combinations are verified such that every switch is exercised and every switch contact is used at least once.

When the IOTs are performed, the measured data are automatically compared against data taken during factory testing of the spacecraft (prelaunch data). The prelaunch data are stored in a database called the Test Data Handling System (TDHS). The IOT system automatically retrieves the TDHS data for the measured configuration, calculates the spacecraft antenna gain for the position of the testing station in the beam, performs the comparison, and then prints the test results in tabular and graphical formats.

All in-band/out-of-band frequency responses, step attenuator values, and translation frequency measurements showed good agreement with the prelaunch data. Table 1 gives the average deltas between measured and prelaunch data for EIRP, saturation flux density, and  $G/T$ .

#### **Antenna testing**

The three main antenna coverage beams on INTELSAT-K are called the Europe, South America (dual), and North America beams. (The Peters *et al.* paper, cited earlier, provides detail on the antenna designs and shows their coverage on the earth as seen from the operational longitude of 338.5°E.) All of these beams were tested during the payload IOT by measuring copol and

TABLE 1. AVERAGE DELTAS BETWEEN IOT MEASURED DATA AND PRELAUNCH DATA

BEAM	EIRP (dB)	FLUX DENSITY	G/T (dB)
North America Horizontal	+0.8	-0.4	—
North America Vertical	—	+1.3	—
Europe Horizontal	-1.2*	0.0	+0.6
Europe Vertical	0.0	—	—
South America Vertical	-0.6	—	—

\*Prelaunch data suspected too high by 1 dB.

cross-pol antenna patterns at discrete pointing offsets. The results were in good agreement with prelaunch data.

#### EUROPE BEAMS

A total of 84 different antenna cuts were taken for the Europe Horizontal receive to Europe Vertical transmit beams, in groups of 12 daily cuts taken every 2 hours during seven consecutive days. On each day, the spacecraft roll offset was changed so that the antenna cuts would be performed on a different elevation offset on the beams. Figure 3 shows the position of the seven azimuth cuts performed, and their elevation offsets. At the conclusion of the monitoring, the data taken at the same hour daily (seven cuts) were combined and the beam shape was reconstructed. This produced 12 beam contours (Figure 4) showing the beams' pointing at 2-hr intervals, which made it possible to determine pointing stability and average offset.

In addition to the 7 days of centroid data, pointing stability was also confirmed by offsetting the spacecraft attitude so as to place the Fucino IOT station on points of the beam that had high gain slopes on either the elevation or azimuth planes. The saturated EIRP level was monitored for 24 hours and then correlated with the antenna beam movement. The results agreed very well with predictions based on the data obtained from the 7-day measurements. The daily pointing fluctuation of  $\pm 0.11^\circ$  fell outside the range specified for pointing accuracy, while RF performance inside the specified coverage region still met specifications.

INTELSAT is now conducting a long-term monitoring study of daily pointing shifts in order to build a database for the automatic hourly correction of spacecraft pointing, thus reducing daily pointing error. This should improve

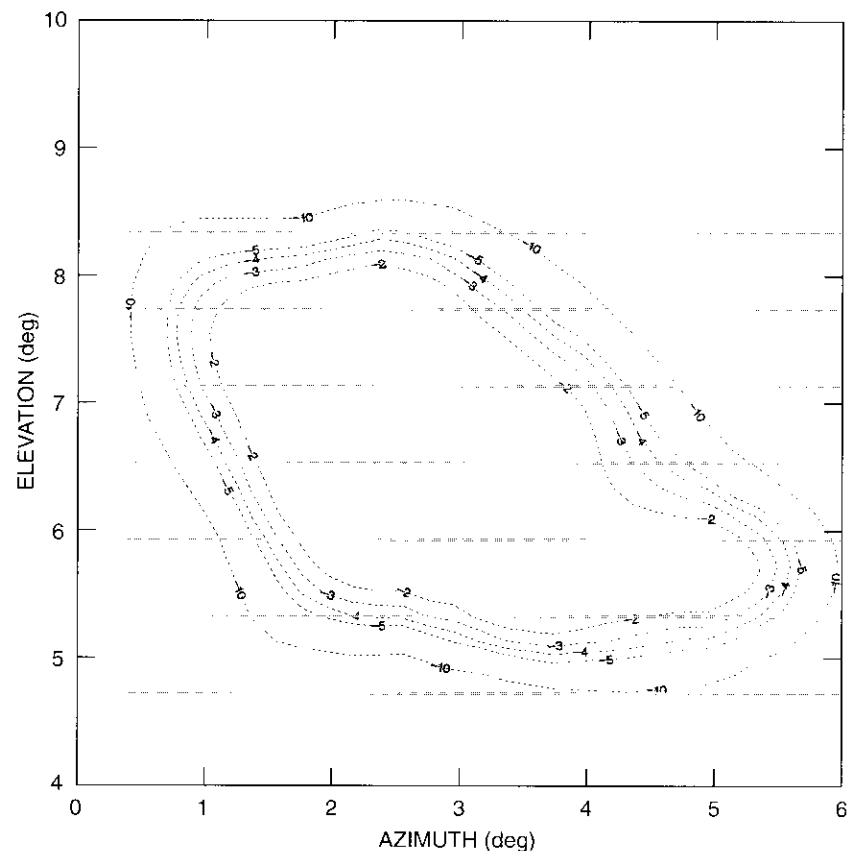


Figure 3. *INTELSAT-K Europe Antenna Cut Scan Positions*  
(Small numbers on contours correspond to rolloff from peak gain)

performance for stations located on the edge of coverage, and even beyond—for example, in the Eastern European countries.

#### SOUTH AMERICA BEAM(S)

The pointing of the South America beams was verified by performing a single centroid measurement similar to the one used for the Europe beam. The method required seven azimuth cuts,  $0.5^\circ$  apart in elevation, resulting in the contours shown in Figure 5. The solid lines indicate the measured performance, while the dashed lines represent predictions calculated from the

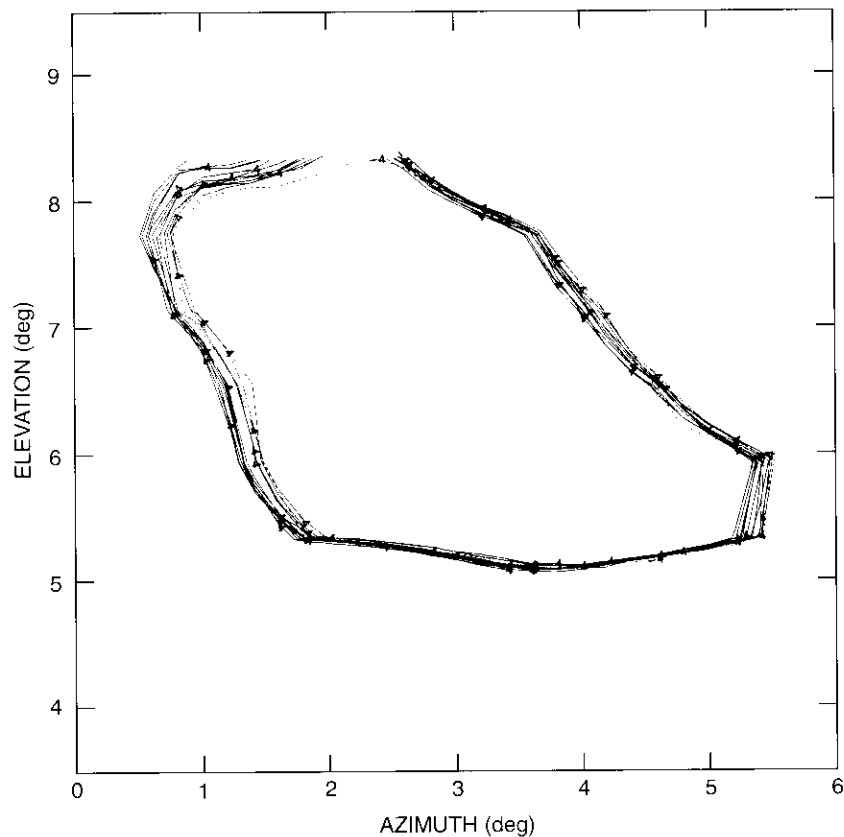


Figure 4. *Overlay of the 12 Reconstructed Europe Beam Contours*

prelaunch data. Again, the IOT results were in good agreement with the prelaunch data.

#### NORTH AMERICA BEAM

The North America beam is produced by the same reflector that produces the Europe beams. This reflector was extensively characterized during the 7 days of centroid measurements. Therefore, only three antenna pattern cuts, at different elevation offsets (Figure 6), were needed to confirm the relative offset between the North America and Europe beams and to check cross-pol performance. The results showed good agreement with the prelaunch data, as

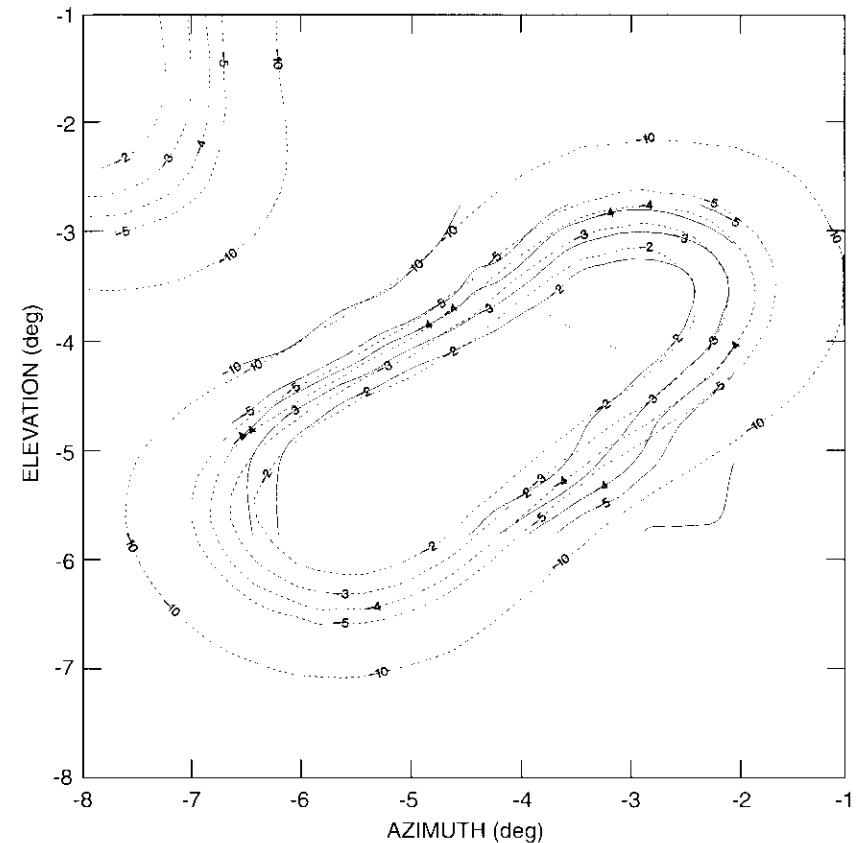


Figure 5. *South America Beams Antenna Cut Scan Positions*

illustrated in Figure 7 which compares the measured and predicted antenna azimuth cuts at an elevation offset of  $4.8^\circ\text{N}$ .

#### Spacecraft reconfiguration

Reconfiguration commands are generated using the PC-based Repeater Command Assistance Program (RCAP), which provides a graphic or tabular representation of the spacecraft payload (transponders) that can be manipulated by the operator to the desired configuration. RCAP then produces, in a format recognizable by the spacecraft, the appropriate command lists to enable this configuration to be achieved. A file of commands, called a command

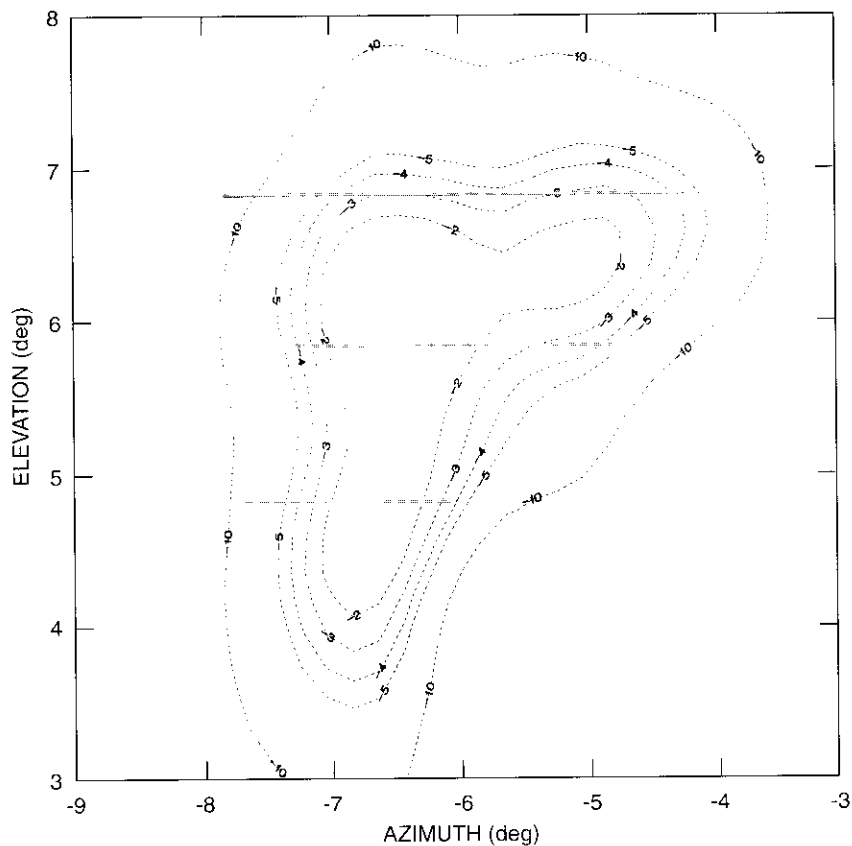


Figure 6. *INTELSAT-K North America Antenna Cut Positions*

queue, can be electronically transferred to the command coordination system at the Spacecraft Control Center (SCC) in Washington, D.C., for future execution.

Different sets of command queues have been produced to accommodate all of the spacecraft configurations coordinated with international users. Thus, whenever there is a need to reconfigure the transponders, the SCC operator schedules the appropriate command queues and the desired configuration is quickly achieved. This expands satellite capabilities by enabling transponders to be connected to different beams daily, allowing for more efficient use of capacity for the type of traffic the satellite attracts (satellite newsgathering, video distribution, etc.). Safety features contained in each command

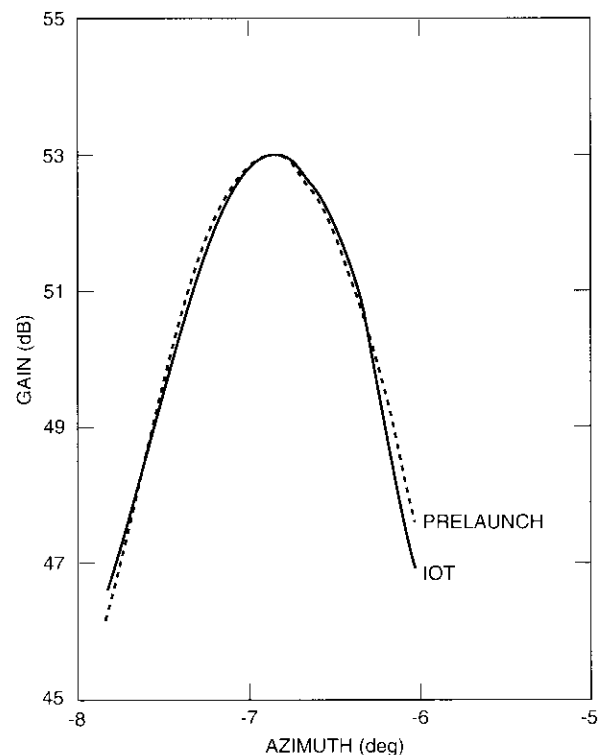


Figure 7. *Prelaunch and IOT Cuts for the North America Beam at 4.8°N*

queue “mute” the driver for the affected traveling wave tube amplifier (TWTA) during the reconfiguration, allowing for “hot” switching with no danger to the spacecraft components.

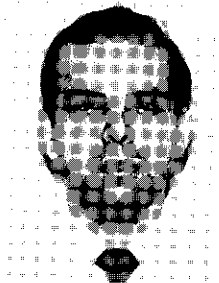
### **Acknowledgments**

*The INTELSAT-K IOT testing was a team effort. The author would like to express his gratitude to many of his colleagues at INTELSAT—in particular to K. Betaharon, R. Peters, and A. Ozkul—and also to M. McGovern from GE-Astro, for their support and helpful discussions throughout the preparations for the INTELSAT-K IOT. Thanks are also due to K. Lindqvist of INTELSAT for support at the Fucino IOT site, and to the Flight Operations and Spacecraft Control Center staff for support at INTELSAT Headquarters in Washington, D.C. Further, the support by the local station staffs at the Fucino,*

Clarksburg, Tangua, and Manaus sites is greatly appreciated. Particular thanks also go to T. Brigagão from EMBRATEL, who assisted in coordinating the shipment of the portable test station, site logistics, and travel for testing the South America beams at EMBRATEL's facilities in Brazil.

## References

- [1] B. Teixeira *et al.*, "In-Orbit RF Test of an INTELSAT VI Spacecraft," *COMSAT Technical Review*, Vol. 21, No. 2, Fall 1991, pp. 339-388.
- [2] G. E. G. Rosell, "INTELSAT K (101) In-Orbit Test Report," INTELSAT Technical Memorandum, No. IFO-TM-93-01, January 1993.
- [3] GE Aerospace, Astro-Space Division, "INTELSAT-K Program Spacecraft System Summary," January 1992.



*Basilio Teixeira is a Senior Engineer with the Spacecraft Engineering Department at INTELSAT. His primary functions include operation of the payload of all in-orbit INTELSAT satellites, definition of tools needed for the proper monitoring and operation of new satellite series, and support for the payload IOTs, including responsibility for spacecraft safety and the provision of command support. He was responsible for the integration and testing of all new equipment installed at the Fucino IOT station, as well as all of the IOT software upgrades and the migration of the hard copy in-plant test data to the TDHS format to support the INTELSAT-K IOT. Previous assignments included development of payload concepts and performance specifications for future satellites, and participation as Software Engineer and Payload Specialist for the IOTs of new INTELSAT satellites. He was stationed at the INTELSAT TTC&M/IOT facilities at Fucino and Beijing for a period of 8 years. Prior to joining INTELSAT in 1981, Mr. Teixeira was employed by EMBRATEL, working on the installation, acceptance testing, and maintenance of the equipment provided by the signatory and INTELSAT at the Tangua TTC&M station in Brazil.*

Index: celestial mechanics, propulsion, launchers

## INTELSAT-K launch vehicle considerations

A. M. GOLDMAN, JR. AND A. OZKUL

(Manuscript received January 17, 1995)

### Abstract

The INTELSAT-K communications satellite was successfully launched in June 1992 using an Atlas II-A launch vehicle. The launch campaign began about 1 year prior to delivery of the spacecraft and included launch site testing to verify spacecraft health, as well as preparation and loading of the spacecraft onto the launch vehicle. Details of launch site testing are discussed, and a comprehensive description is given of the Atlas II-A launch vehicle, including its flight performance until separation and injection of the spacecraft into transfer orbit.

### Introduction

The INTELSAT-K communications satellite was successfully launched on June 9, 1992, from Cape Canaveral, Florida, on a General Dynamics/Martin Marietta Atlas II-A vehicle. It reached preoperational drift orbit 11 days later on June 20, and became operational on July 15, 1992.

The INTELSAT-K launch campaign began about 1 year prior to delivery of the spacecraft. In line with INTELSAT's strategy of maintaining dual launch vehicle compatibility for its spacecraft launches, both Ariane and Atlas launchers were considered for INTELSAT-K during the feasibility studies. However, at the time of contract signing and during subsequent months, the spacecraft configuration, on-station availability requirements, and other INTELSAT launch schedule constraints dictated selection of the Atlas II-A vehicle.

Following selection of the launch vehicle, the INTELSAT Launch Vehicle Program Office (LVPO) assumed responsibility for ensuring the compatibility

of the spacecraft with the Atlas II-A. A team consisting of INTELSAT, General Electric/Martin Marietta, and support staff conducted launch site testing to verify spacecraft health following transportation from the manufacturer's facilities, and prepared and loaded the spacecraft onto the launch vehicle. All launch vehicle/spacecraft interface documents and specifications were reviewed, and detailed launch dynamics analyses and tests were jointly prepared, performed, and verified. Assessment of liftoff mass and volume constraints, coupled with the spacecraft geometry, resulted in optimum orientation of the spacecraft with only minor modifications to the launch vehicle fairing and plumbing.

INTELSAT-K underwent detailed launch site testing, propellant loading, and encapsulation at Lockheed/Martin Marietta Astrotech facilities in Titusville, Florida. Final compliance with the required specifications was validated there before the spacecraft was transported to Space Launch Complex-36B (SLC-36B) at Cape Canaveral Air Force Station (CCAFS) for mating and electrical/mechanical interface tests.

This paper discusses details of the launch site testing and provides a comprehensive description of the Atlas II-A launch vehicle, including its flight performance until separation and injection of the spacecraft into transfer orbit.

### **Prelaunch test activities**

INTELSAT-K was shipped from the GE/Martin Marietta Astro plant on March 31, 1991, to arrive at the Astrotech Launch Processing Facilities on April 2, 1992. The entire spacecraft checkout station (SCS) used in the testing at the Astro plant was also shipped to Astrotech for prelaunch testing. Following verification by the SCS and other launch site equipment (LSE), launch site spacecraft electrical performance tests (SEPETs) were begun on April 3. The initial spacecraft bus SEPET was conducted during April 3-7, and the communications SEPET began on April 7.

Table 1 lists the procedures used in the prelaunch tests, as well as those functions that were excluded from the launch site test plans due to spacecraft launch configuration and deployment/pyrotechnic requirements. Table 2 lists the functions tested under each spacecraft bus subsystem, and Table 3 lists the communications payload SEPETs performed, as well as those excluded from the test plan.

The INTELSAT-K spacecraft bus SEPET went extremely well. No major SCS/LSE difficulties were experienced during a total of 65 bus tests. Test discrepancy reports (TDRs) were closed after additional verification by testing or analyses.

TABLE 1. INTELSAT-K PRELAUNCH TESTS

Thermal Blanket Continuity
SEPETs
Battery Charge/Capacity
Launch Site Equipment
Launch Stand Test
Solar Array Edge Illumination
Launch Site Rehearsal: Power Up/Down
Launch Site Rehearsal: Main Enable
Launch Site Rehearsal: Arm Plug Installation
Squib Stray Voltage
Reaction Control Subsystem (RCS ) Pressure Test Setup
Install Shipping
<b>Functions Not Tested</b>
Momentum Wheel Assembly (MWA) Pivots—Pivots captive
Pyrotechnics—Pyro valve and solar array center pull pyrotechnics connected
Deployments—Array/reflector/omni in launch configuration
Solar Array Drive Rotation—Spacecraft and solar arrays in launch configuration
Full Array Current; Partial Shunt Current; Switched Shunt Sequence—Spacecraft and solar arrays in launch configuration

The communications portion of the launch site SEPET was started on April 7 and completed on April 16 (including retests). This SEPET is a complete performance test of the payload and repeats all measurements made in previous thermal vacuum and ambient SEPETs. All test results were reviewed to confirm that communications performance was in agreement with previous SEPET results.

Following spacecraft health verification in SEPETs, final launch preparations were completed, consisting of the following activities:

- Wet spacecraft spin/final balancing and final wet weigh. The final measured spacecraft weight was 2,930 kg.
- Final spacecraft closeout and inspection. A visual inspection was performed by both GE/Martin Marietta and INTELSAT after closeout. The inspection particularly focused on thermal blankets, clearances around shear ties, and deployment mechanisms, including close-up photographs of all critical visible hardware.
- A spacecraft readiness review between GE/Martin Marietta and INTELSAT representatives to confirm spacecraft readiness for mating with the launch adapter.

TABLE 2. INTELSAT-K PRELAUNCH BUS SUBSYSTEM TESTS

**Attitude Control Subsystem (ACS) Tests**

Earth Sensor Assembly (ESA) 1 & 2 Command & Output Check  
 Roll, Pitch & Yaw Gyro  
 Sun Sensor 1 & 2  
 Tap Cap, Side 1 & 2  
 Horizon Sensor  
 Tadoc  
 Torquer Test, Side 1 & 2 Check  
 MWA 1 & 2 Command Check  
 Attitude System Processor (ASP1) Telemetry & MWA Cross Strap  
 ASP Control of High Beacon  
 ASP2 Telemetry & MWA Cross Strap  
 Pitch Capture Test  
 Pitch Offset Test  
 Spin Precession Test  
 ASP Timed Pulse Mode  
 North/South Stationkeeping (N/S SK) Logic Checks  
 Backup Roll Control  
 East/West SK Logic Checks  
 Auto Pitch Error Test  
 ASP Ram/Command Input Check

**Telemetry, Command & Ranging (TC&R) Tests**

Decoder Redundancy  
 Redundant Telemetry Module (RTM) Modes  
 Beacon Functional  
 Command Threshold  
 Ranging Threshold  
 RTM1 vs RTM2  
 Beacon Modulation Index  
 Subcarrier Dwell  
 Pulse Code Modulation (PCM) Dwell  
 Low Voltage TC&R  
 Launch Vehicle Int.  
 Command Encryption

**Power Subsystem Tests**

Power Telemetry  
 Charge Regulator  
 Shunts/Failures  
 N/S SAD  
 Battery Heaters

TABLE 2. INTELSAT-K PRELAUNCH BUS SUBSYSTEM TESTS (CONT'D)

Load Profile  
 Fail Detection  
 Battery Taper Charge

**Reaction Control Subsystem (RCS) Tests**

Reaction Engine Assembly Firing  
 Electrothermal Hydrazine Thruster (EHT) Firing  
 Liquid Apogee Engine (LAE) Fire Control  
 Catalyst Bed Heaters  
 Line Heaters  
 Tank Heaters  
 Thruster Valve Heaters  
 Thruster Flow

**Heater Tests**

Solar Array & Reflector Heater (HTR1)  
 Omni & MWA Heater (HTR2)  
 Auxiliary Heater System (HTR3)

TABLE 3. INTELSAT-K PRELAUNCH COMMUNICATIONS TESTS

Input Power  
 Output Power  
 Intermodulation Distortion  
 Driver Limiter Amplifier (DLA) Attenuator Steps  
 Group Delay  
 Amplitude Response  
 Spurious Outputs  
 Command & Telemetry  
 Linear Transfer Response  
 Limiter Transfer Response  
 TWTA Undervoltage Turnoff  
 DC Power Drains

**Functions Not Tested**

Timer Override  
 Anode Voltage Control Loops (command verified)  
 Cooled Low-Noise Amplifier Cooler Operation (verified in thermal vacuum)

- Mechanical and electrical mating of the spacecraft with the adapter, verification of umbilical interface after mating, installation of the battery enable relay box (BERB), and powering-up of the spacecraft for electrical tests.
- Post-mate launch site electrical tests, including commanding the spacecraft into launch configuration.
- Establishing voice and data links between Astrotech and the SLC-36B blockhouse, as well as between Astrotech and GE/Martin Marietta Astro Spacecraft Operations Center (ASOC).
- Demating of the BERB and installation of the spacecraft and adapter onto the ground transport vehicle (GTV). Final spacecraft closeout, including removal of holding fixtures and omnidirectional antenna and liquid apogee engine (LAE) protective covers.
- Installation of the fairing to the GTV.
- Verification of the RF link through the omni antenna.
- Installation of the GTV with the fairing/spacecraft on the trailer.

All of these activities went smoothly and were performed according to schedule to support the June 9 launch date.

The following spacecraft activities were performed as part of the final readiness for INTELSAT-K AC-105 Atlas II-A launch:

- |        |  |
|--------|--|
| May 20 | Verify RF link check under different operating contingencies.  |
| May 21 | Power-on spacecraft to support combined electrical readiness test (CERT).<br>Start battery charging (battery charging activities are continued until liftoff). |
| May 23 | Spacecraft terminal countdown rehearsal.   |
| May 28 | Install enable plugs (MEP1, MEP2, and SEP1).   |
| June 9 | INTELSAT-K/AC-105 launch.  |

### **Launch mission**

INTELSAT-K successfully flew on General Dynamics Commercial Launch Services flight AC-105, the first Atlas II-A, from Cape Canaveral, Florida, on June 9, 1992, following a liftoff attempt on May 29, 1992, that was suspended due to inclement weather. INTELSAT-K had a separated spacecraft weight of 2,930 kg, which was a good match to the capabilities of the Atlas II-A.

The Atlas II-A launch vehicle consisted of an Atlas first stage powered by three Rocketdyne MA-5A liquid propellant engines consuming RP-1 fuel and liquid oxygen; a Centaur upper stage powered by two Pratt & Whitney RL10-A-4 liquid hydrogen and liquid oxygen engines; and a 4.27-m-diameter metal payload fairing that protected the INTELSAT-K spacecraft during the ascent. Figure 1 shows the preparation activity flow of the AC-105 launch vehicle for the INTELSAT-K launch.

### **Atlas II-A launch vehicle description**

Atlas is the name of a family of booster stages, while Centaur is a family of high-energy, restartable upper stages. Atlas II-A is the designation for an Atlas II booster combined with a Centaur II-A upper stage. The Centaur upper stage is mounted on top of the one-and-one-half-stage Atlas booster to form a two-and-one-half-stage vehicle. The Atlas booster is 3.05 m in diameter and 24.9 m long. The propellant tanks are a thin-wall, fully monocoque, corrosion-resistant stainless steel construction. The fuel tank, which contains RP-1, and the oxidizer tank, which contains liquid oxygen, are separated by an ellipsoidal intermediate bulkhead. The structural integrity of the tanks is maintained in flight by internal pressure or by the application of mechanical stretch.

The Atlas uses the Centaur avionics system for guidance, flight control, and sequencing functions. An external equipment pod houses Atlas systems such as range safety, propellant utilization, pneumatics, and instrumentation.

Atlas booster propulsion is provided by the Rocketdyne MA-5A engine system, which includes a sustainer engine and two booster engines. All engines are ignited prior to liftoff and develop a total sea-level rated thrust of 2,110,576 N. The section containing the booster engines is jettisoned [booster package jettison (BPJ)] approximately 170.6 s into flight, at an axial acceleration of 5.5 g. Flight continues, powered by the sustainer engine ("sustainer phase" flight) until propellant depletion.

The Atlas is structurally linked to the Centaur by an aluminum interstage adapter, and is separated from the Centaur by a flexible linear-shaped charge system attached to the forward ring of the interstage adapter.

The Centaur upper stage is 3.05 m in diameter and 10.06 m long. It employs high-energy liquid hydrogen and liquid oxygen propellants separated by a double vacuum-insulated intermediate bulkhead. The propellant tanks (like those of the Atlas stage) are constructed of thin-wall, fully monocoque, corrosion-resistant stainless steel. Tank stabilization is maintained at all times by internal pressurization or the application of mechanical stretch.

The Centaur avionics package, mounted on the equipment module, monitors and controls all vehicle functions. It performs the inertial guidance and

ACTIVITES	WEEKS												
	1	2	3	4	5	6	7	8	9	10	11	12	
AC-72 Launch													
Pad Conversion to Atlas II-A		13	14	22									
Erect Atlas 105				24									
Erect Interstage Adapter				24									
Erect Centaur				25									
Erect Boattail				26									
Powered Avionics Compatibility Test				1									
SIM Flight							24						
Wet Dress Rehearsal								1					
Encapsulate Spacecraft									7-8				
Erect Spacecraft										11			
Composite Electrical Readiness Test											13		
F - 4 Days, N <sub>2</sub> H <sub>4</sub> Sampling												14	
F - 3 Days, RP - 1 Tanking & Ordnance													15
N <sub>2</sub> H <sub>4</sub> Loading													16
N <sub>2</sub> H <sub>4</sub> Cleanup													17
F - 2, F - 1 Day													18-19
Launch													20

Figure 1. INTELSAT-K Launch: Atlas II-A/AC-105 Launch Preparation Activity Flow

attitude computations for both the Atlas and Centaur, and monitors tank pressures and propellant use.

The Centaur propulsion system uses two RL10A-4 engines manufactured by Pratt & Whitney. Each engine has a rated thrust of 92,518 N. The Centaur engines are restartable and capable of multiple firings in space, separated by coast phases.

The stub adapter and equipment module are attached to the forward end of the Centaur. The adapter is bolted to the forward ring of the Centaur tank and supports the equipment module and payload fairing. The equipment module attaches to the forward ring of the stub adapter and has provisions for mounting the Centaur avionics and the spacecraft adapter.

The payload fairing protects the spacecraft from the time of encapsulation through atmospheric ascent. The fairing used by the INTELSAT-K mission was a 4.27-m-diameter, two-half-shell aluminum structure with vertical, split-line longerons. It consisted of a cylindrical section topped by a conical nose cone and spherical cap.

The fairing provides thermal and acoustic enclosures for the payload and launch vehicle electronic compartments during prelaunch and ascent. Portions of the external surface of the fairing are insulated with cork to limit temperatures to acceptable levels. Noncontaminating thermal control coatings are used on internal surfaces to reduce incident heat fluxes to the spacecraft. The payload fairing is jettisoned approximately 55 s after Atlas booster jettison.

The mechanical interface between the INTELSAT-K spacecraft and the launch vehicle was provided by a standard adapter built by General Dynamics Space Systems. In transfer orbit, the Centaur issues separate commands to release and separate the spacecraft from the forward adapter.

Atlas and Centaur launch vehicles and components are produced by the GE/Martin Marietta Corporation/General Dynamics Space Systems Division in San Diego, California, Vandenberg Air Force Base, California, and Harlingen, Texas. The launch vehicles were transported to CCAFS for final assembly and checkout at SLC-36.

#### Launch mission profile

The Atlas II-A carrying INTELSAT-K was launched from SLC-36B at CCAFS. The mission used a parking orbit ascent trajectory with the first Centaur burn, which placed the vehicle into an 150-km perigee altitude parking orbit. After a 15-min coast period, the Centaur second burn injected the satellite into a geosynchronous transfer orbit with a 35,788-km apogee and 187-km perigee

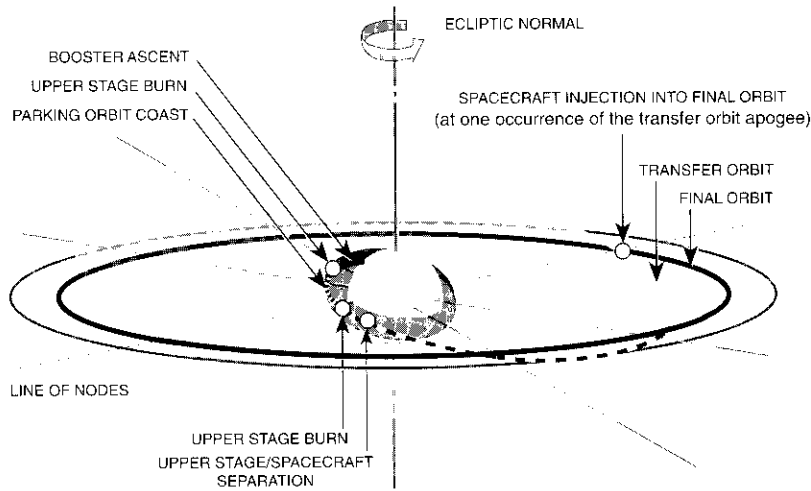


Figure 2. Orbital Planes During Mission Launch of INTELSAT-K

altitude, as shown in Figure 2. The nominal Atlas II-A transfer orbit parameters at spacecraft separation were:

Apogee Altitude	35,945 km
Perigee Altitude	185 km
Transfer Orbit Inclination	25.5°
Transfer Orbit Period	634 min.
Argument of Perigee	179.3°
Longitude of Ascending Node	173.5°

The AC-105 mission ascent profile, shown in Figure 3, includes 10 mission mark events. Figure 4 shows general Atlas-Centaur II-A hardware and indicates the hardware involved in each mark event. Figure 5 shows the nominal vehicle ground trace. The AC-105/INTELSAT-K mission sequence of events is given in Table 4. Note that the entire sequence, from liftoff through spacecraft separation, took place in only 29 minutes. During this time, enormous quantities of propellant were consumed, as shown in the weight history in Table 5.

The INTELSAT-K launch followed a standard Atlas II-A ascent profile. The flight began with a short vertical rise. During flight between  $T + 2$  and  $T + 15$  s, the vehicle rolled from its launch pad alignment of  $115^\circ$  to its mission-specific flight azimuth of  $97.5^\circ$ , followed by pitch and yaw programs under

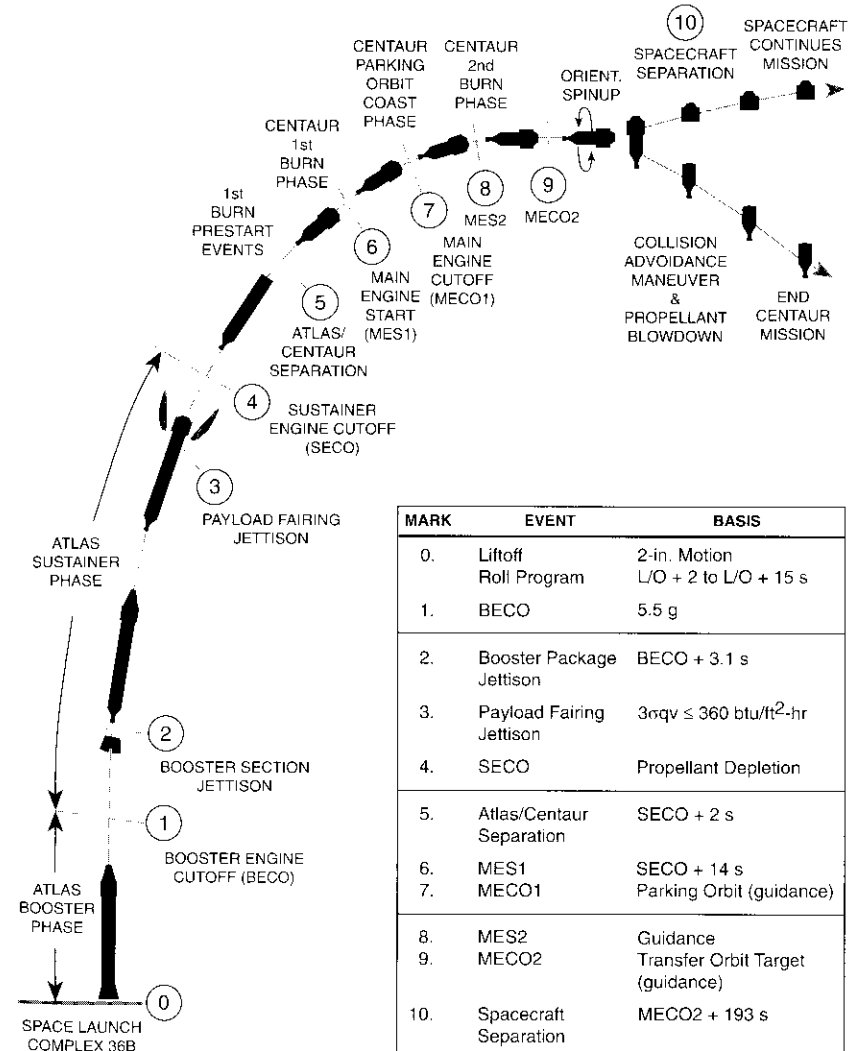


Figure 3. Mission Ascent Profile

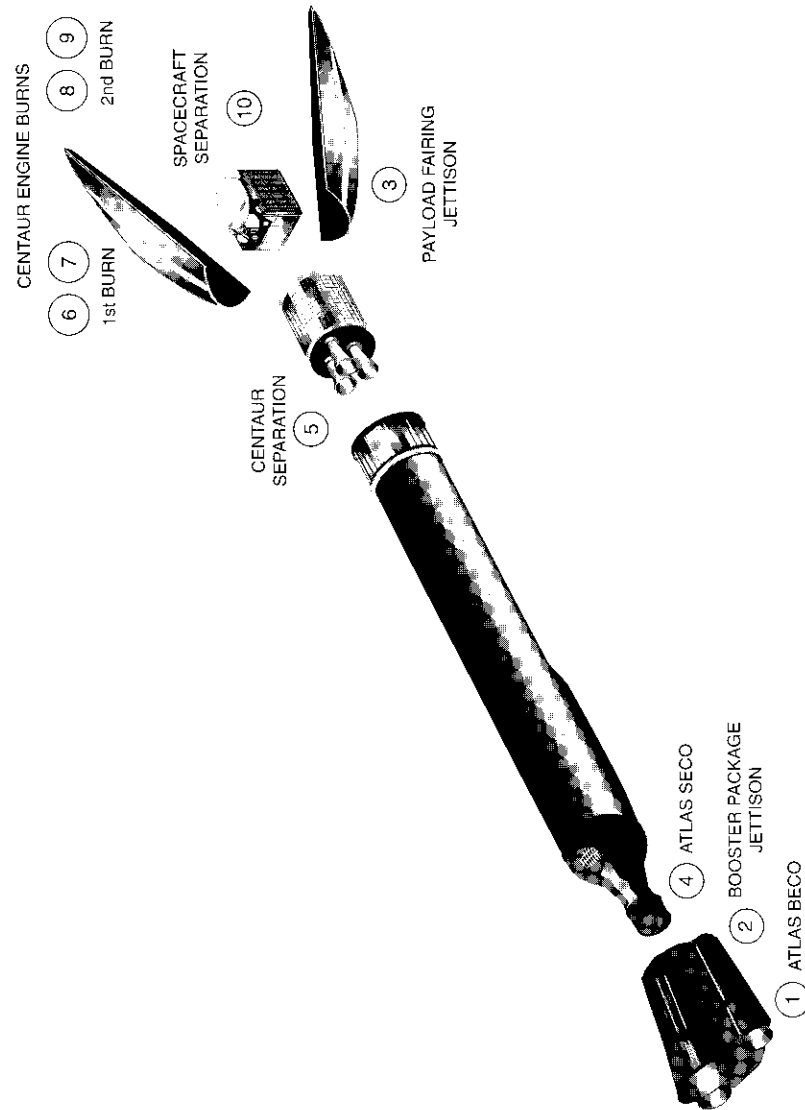


Figure 4. Hardware Involved in Mark Events

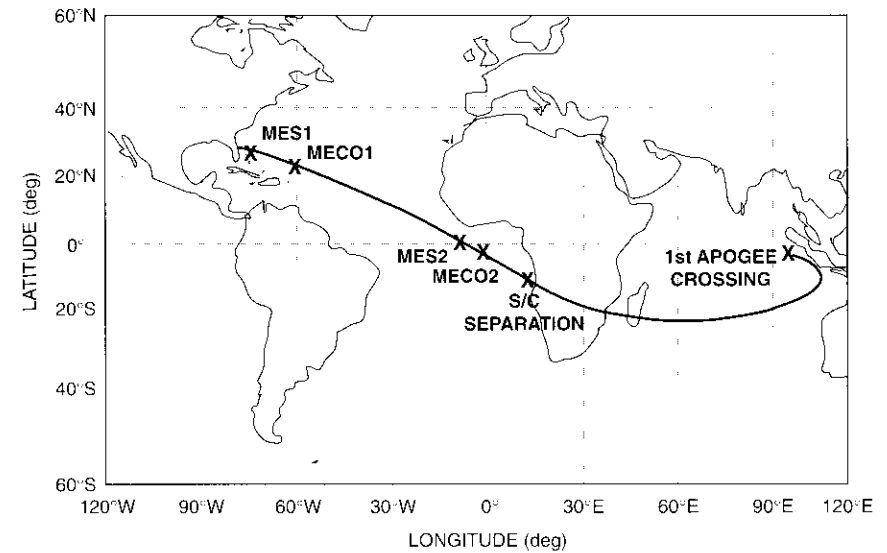


Figure 5. Subvehicle Trace: Launch to Spacecraft First Apogee

control of the Centaur inertial guidance system. Atlas booster engine cutoff (BECO) occurred upon attainment of an axial acceleration of 5.5 g. During the Atlas sustainer phase, the payload fairing was jettisoned when heating dropped to predetermined levels. Atlas sustainer engine cutoff (SECO) occurred based on sensing the minimum residual propellant. Atlas/Centaur separation occurred at SECO + 2 s, and the Centaur first main engine start (MES1) occurred at SECO + 14 s.

The Centaur first burn consisted of a 311-s firing of the Centaur main engines to inject the combined Centaur/spacecraft vehicle into a low-altitude parking orbit of  $150 \times 2,361$  km. During the burn, guidance steering was applied in an orbit inclination of  $28.4^\circ$ . Following Centaur first main engine cutoff (MECO1), the vehicle coasted in parking orbit over the mid-Atlantic for approximately 14.4 min prior to arriving at the required location for Centaur second burn. Throughout this otherwise zero-g coast, the Centaur hydrazine 27-N axial thrusters (S-engines) fired, either in groups of four for propellant settling or in groups of two for propellant retention.

The Centaur second burn occurred over the Atlantic Ocean between the African Ivory Coast and Ascension Island, prior to the vehicle's first passage over the equator. This burn, lasting approximately 90 s, accelerated the combined Centaur/INTELSAT-K vehicle into a  $185 \times 35,945$ -km transfer orbit at spacecraft separation.

TABLE 4. AC-105/INTELSAT-K MISSION SEQUENCE OF EVENTS

EVENT	MARK EVENT	EVENT SEQUENCE	TIME FROM LIFTOFF (s. nominal)
Liftoff			0.0
Start Roll			2.0
End Roll, Start Open-Loop Pitch & Yaw Steering			15.0
Atlas Booster Engine Cutoff at 5.5 g	1	BECO	167.5
Jettison Booster Package	2	BECO + 3.1	170.6
Jettison Payload Fairing	3		226.3
Atlas Sustainer Engine Cutoff	4	SECO	273.9
Atlas/Centaur Separation	5	SECO + 2.0	275.9
Start Extendible Nozzle Deployment		SECO + 3.5	277.4
Centaur 1st Burn, LO <sub>2</sub> Prestart		SECO + 3.5	277.4
Centaur 1st Burn, LH <sub>2</sub> Prestart		SECO + 6.7	280.6
End Extendible Nozzle Deployment	5A, 5B	SECO + 10.5	284.4
Centaur 1st Main Engine Start (MES1)	6	SECO + 14.0	287.9
Centaur 1st Main Engine Cutoff (MECO1)	7	MECO1	598.5
Start Reorient to MES2 Attitude		MES2 - 600	858.7
Centaur 2nd Burn, LH <sub>2</sub> Prestart		MES2 - 17.2	1,441.6
Centaur 2nd Burn, LO <sub>2</sub> Prestart		MES2 - 12.0	1,446.8
Centaur 2nd Main Engine Start (MES2)	8	MES2	1,458.7
Centaur 2nd Main Engine Cutoff (MECO2)	9	MECO2	1,548.1
Start Alignment to Separation Attitude		MECO2 + 2.0	1,550.1
Start Spinup to 5.0 rpm		MECO2 + 112	1,660.1
Separate Spacecraft	10	MECO1 + 193	1,741.1

BECO: Booster engine cutoff, Atlas    MES: Main engine start, Centaur  
 SECO: Sustainer engine cutoff, Atlas    MECO: Main engine cutoff, Centaur

TABLE 5. WEIGHT HISTORY DURING LAUNCH

ITEM	WEIGHT (kg)
Liftoff	187,853
Centaur Separation	21,848
Centaur MECO1 + Decay	8,812
Centaur MES2	8,732
Centaur MECO2	5,060
Centaur/Spacecraft Separation	5,051
Separated Spacecraft	2,930

Following MECO2, Centaur reoriented to the attitude required for spacecraft separation, and then used its reaction control system thrusters to initiate a controlled spinup to 5 rpm. Separation occurred at MECO2 + 193 s. After a short coast, Centaur despun and then performed a series of maneuvers, called collision and contamination avoidance maneuvers, to preclude recontacting or contaminating the free-flying spacecraft. At the end of this sequence, the Centaur mission was complete, and Centaur unlocked its vent valves and terminated its programmed flight sequence.

The launch of INTELSAT-K using the Atlas II-A vehicle was a complete success, delivering the spacecraft to the desired transfer orbit as planned. At the conclusion of transfer orbit activities, an apogee motor maneuver, and a short east/west drift, INTELSAT-K was placed at the proper orbital location about 11 days following launch.



*Alfred M. Goldman, Jr., holds bachelor's and master's degrees from the California Institute of Technology, and did additional graduate work at Stanford University, the University of Southern California, and CALTECH. He joined COMSAT World Systems (CWS) in April 1989 and managed CWS engineering and operations R&D projects conducted at COMSAT Laboratories. As a Principal Engineer with COMSAT World Systems Engineering and Operations Department, he performed satellite and launch vehicle systems engineering in support of COMSAT's role as U.S. Signatory to INTELSAT. He also served as a U.S. Delegate to the INTELSAT Board of Governors' Technical Advisory Committee. His previous systems engineering experience included Boeing & Hamilton, CONTEL-ASC, Jet Propulsion Laboratory, General Dynamics, Hughes Aircraft, and service as an officer in the U.S. Air Force.*

*Mr. Goldman retired from COMSAT Laboratories in February 1996. He is an Associate Fellow of AIAA and a Senior Member of IEEE.*



*Ahmet Ozkul received a BSAE from the California Institute of Technology in 1971 and was employed at JPL, Applied Mechanics Laboratories, working on nondestructive testing of components for the Shuttle and other aerospace vehicles. He received the MSAE and ApSc degrees from George Washington University in 1974 and 1977, respectively, while employed at NASA Langley Research Center in Hampton, Virginia. In 1978, Mr. Ozkul joined INTELSAT's Systems Planning Division, where he conducted space/ground segment configuration studies to optimize INTELSAT system growth. After transferring to the*

*Satellite Operations Department in 1983, he supported numerous launch missions and was involved in software-based projects related to satellite in-orbit operation, including performance modeling based on historical telemetry data, and electrostatic discharge mitigation onboard INTELSAT satellites. He served as Project Manager for INTELSAT-K at GE-Astro in East Windsor, New Jersey, from 1989 through the successful launch in 1992.*

*Mr. Ozkul is currently a Principal Engineer in the Engineering and Spacecraft Programs Division at INTELSAT, where he works on satellite system engineering and the feasibility study and implementation of special projects to enhance INTELSAT's space segment. He has authored numerous technical papers as a member of AIAA, IEEE, JIAFS, and other organizations.*

**Index:** digital transmission; INTELSAT; modulation, demodulation, modems; satellite newsgathering; transponders

## **System architectures for satellite newsgathering**

W. A. SANDRIN, T. ABDEL-NABI, S. A. AMES, D. V. HASCHART,  
K. M. PRICE, AND A. K. RAO

(Manuscript received May 2, 1994)

### **Abstract**

The demand for satellite newsgathering (SNG) services—where mobile units using small antennas transmit programming material to a broadcast center via satellite—is growing rapidly. A study was conducted to examine satellite system architectures appropriate for this type of service. Topics addressed include the modulation and multiple-access transmission format; selection of the uplink frequency band for the SNG-to-satellite link; spacecraft implementation issues such as transponder channelization and antennas (with emphasis on add-on packages); and the provision of an auxiliary or coordination channel in the direction of the broadcast-center-to-SNG site. Other issues presented include rain impairment and uplink margin requirements for the SNG-to-satellite link operating at both Ku- and Ka-band, a comparison between channelized transponders implemented with surface acoustic wave filters and those with onboard digital processors, and considerations related to the placement of spacecraft antennas on an SNG add-on package.

Based on the study results, an architecture consisting of digitally compressed video carriers operating in a frequency-division multiple-access mode, in combination with channelized transponders that apply automatic gain control to carriers on an individual basis, was recommended. This architecture maximizes uplink margins against rain impairment.

### **Introduction**

Satellite newsgathering (SNG) services are expected to become a major market for INTELSAT. As the demand for SNG services increases, INTELSAT's interests will best be served if it can provide this service to customers in a

cost-effective and reliable manner. This paper summarizes a study performed by COMSAT Laboratories and Space Systems/Loral for INTELSAT. Although organized to illustrate the methodology employed in the study, the paper also describes a variety of topics relevant to the design of future SNG satellite systems.

An SNG service is characterized by the transmission of real-time programming material from small transportable earth stations located at the site of a news event. The information from the SNG site is relayed by satellite to a broadcast center, where it is integrated into the broadcast programming material. For SNG service, it is important that the remote earth station be easily transportable, that operating costs be relatively low, and that operations can be conducted on demand with as few restrictions as possible.

The requirements of an SNG system are very different from those of a direct broadcast satellite (DBS) system. In an SNG system, information from a relatively few small remote earth stations is uplinked to a broadcast center via a satellite, while in a DBS system programming is broadcast from a center to a large number of very small receive-only earth stations via a single satellite uplink. Because of this fundamental difference, each service requires a different system architecture. This study addressed SNG systems only.

SNG services using Ku-band have grown rapidly because spacecraft with high antenna gain-to-noise temperature ratio,  $G/T$ , values are available; compact earth station designs are available; and frequencies can be used with relatively few restrictions. For similar reasons, it is anticipated that Ka-band will also be used for future SNG services.

To operate an SNG service at either band, the satellite transmission channel must be designed with a reasonable margin against rain impairments, and the satellite system must be able to provide, on demand, the required connectivity between the SNG site and the broadcast center. This study was conducted to recommend SNG system designs that best meet these objectives. Although many aspects of SNG services were considered, the study focused on selecting the uplink frequency band to be used from the SNG unit to the satellite, the modulation and multiple-access format, the spacecraft architecture, and spacecraft considerations related to implementation. Problems related to establishing a relatively low-rate auxiliary channel from the broadcast center to the SNG site were also investigated.

In phase 1 of the study, candidate SNG system architectures consisting of specific combinations of uplink and downlink frequencies, various modulation and multiple-access techniques, and different transponder architectures were evaluated and parametrically compared. A total of 36 different system architectures were examined, and a limited set of preferred architectures was identified for further investigation. In phase 2, the selected set was examined

with emphasis on refining the recommended system architectures and investigating specific issues related to spacecraft implementation.

### **Phase 1: Evaluation of candidate SNG architectures**

The SNG architectures examined in this phase of the study consisted of various combinations of the following:

- SNG uplink frequency band (Ku-band or Ka-band)
- Downlink frequency band (C-band or Ku-band)
- Modulation (digital using compressed video or TV/FM)
- Multiple-access technique (frequency-division multiple access [FDMA] or time-division multiple access [TDMA])
- Either conventional or channelized automatic gain control (AGC), or onboard regeneration (OBR) transponder architectures.

The preferred architectures were selected by first developing a baseline link budget for each. Then, propagation data (quantifying rain impairments) and a series of parametric tradeoffs (to determine the sensitivity of parameters such as uplink rain margin to various link design parameters) were used to compare the relative performance of the candidates. Table 1 identifies the 36 specific system architectures studied and provides a key to the nomenclature used to identify them. Figure 1 illustrates these architectures in tree form.

The basic methodology of this study was to first narrow the options for an SNG system to a small set, and then develop the recommended options in greater detail. As a first step in this process, prior to examining the initial tradeoffs, a set of assumptions and baseline parameters were defined by selecting basic system parameters and parametric ranges that reflected practical designs.

Another preliminary step involved quantifying the effects of rain impairments. At both Ku- and Ka-band, rain impairments are so severe that the amount of margin a candidate system design could provide against uplink fades was a major factor in evaluating system alternatives.

### **Rain impairments and margin requirements**

A key factor in the design of a satellite link operating at either Ku- or Ka-band is rain fading, and the consequent value of the power margin required to protect against fades. Quantitative estimates of rain impairment are needed to determine the requirements of links operating at each frequency. Rain fading at these frequencies is very sensitive to three factors: frequency band, elevation angle, and local climate.

TABLE 1. THE 36 SNG SYSTEM ARCHITECTURES INVESTIGATED IN THE PHASE I STUDY

	SATELLITE ARCHITECTURE NO.											
	1	2	3	4	5	6	7	8	9	10	11	12
Spot Beam												
Ka-Band Uplink	Yes	Yes	Yes				Yes	Yes	Yes			
Ku-Band Uplink				Yes	Yes	Yes				Yes	Yes	Yes
Satellite Transponder												
With AGC		Yes			Yes			Yes			Yes	
With OBR			Yes			Yes			Yes			Yes
C-Band Downlink	Yes	Yes	Yes	Yes	Yes	Yes						
Spot Beam												
Ku-Band Downlink							Yes	Yes	Yes	Yes	Yes	Yes
Analog FM TV												
FDMA, No OBR	1a	2a	NA	4a	5a	NA	7a	8a	NA	10a	11a	NA
Digital TV												
FDMA, No OBR	1b	2b	NA	4b	5b	NA	7b	8b	NA	10b	11b	NA
TDMA, No OBR	1c	2c	NA	4c	5c	NA	7c	8c	NA	10c	11c	NA
TDMA OBR	NA	NA	3d	NA	NA	6d	NA	NA	9d	NA	NA	12d
FDMA Uplink, TDM Downlink, OBR	NA	NA	3e	NA	NA	6e	NA	NA	9e	NA	NA	12e
FDMA Uplink, FDM Downlink, OBR	NA	NA	3f	NA	NA	6f	NA	NA	9f	NA	NA	12f

To illustrate the magnitude of rain impairments, a computer program (RAIN) based on the COMSAT/INTELSAT propagation analysis package (PAP) rain impairment model, was used with three representative example climates:

*Climate 1.* Western Europe, which has little thunderstorm activity.

*Climate 2.* The U.S. Mid-Atlantic region, which has moderate rainfall and moderate thunderstorm activity.

*Climate 3.* Tropical and semitropical areas, which have larger amounts of rainfall and thunderstorm activity.

Although a wide range of climates is covered by these examples, none represents the extremes of either very dry or very wet climates. Figures 2a and 2b illustrate approximate rain attenuation vs percentage of time for various elevation angles for Ka- and Ku-band, respectively.

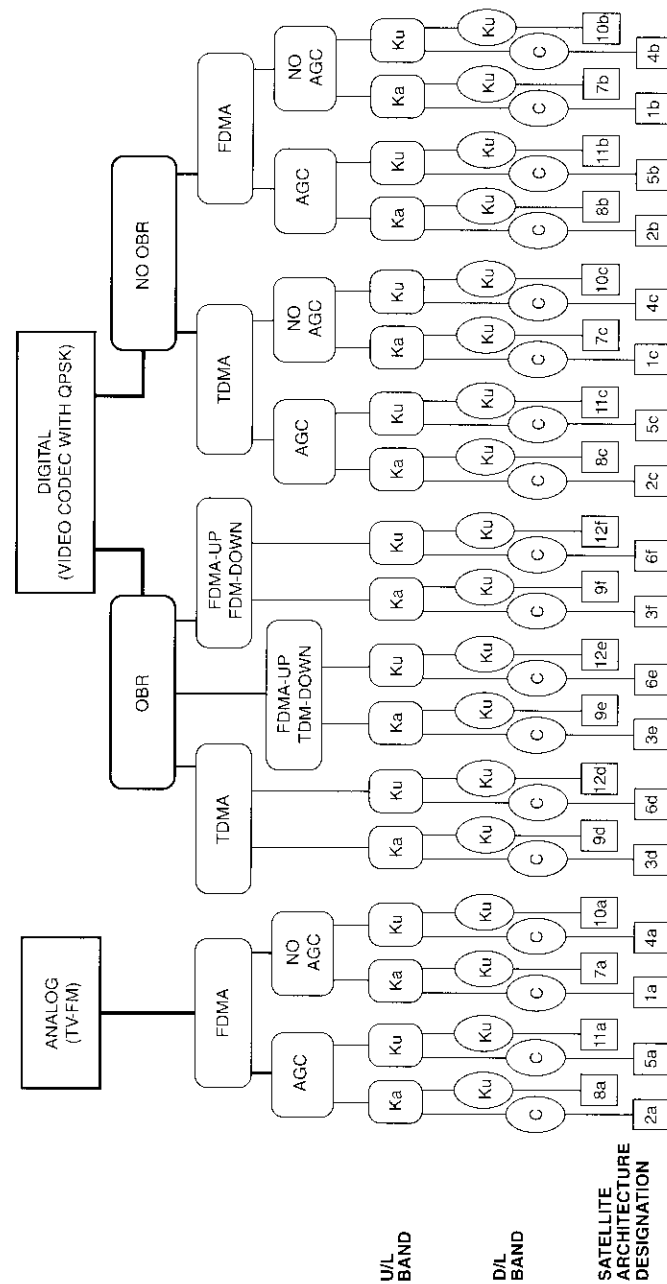


Figure 1. Breakdown of the 36 SNG System Architectures

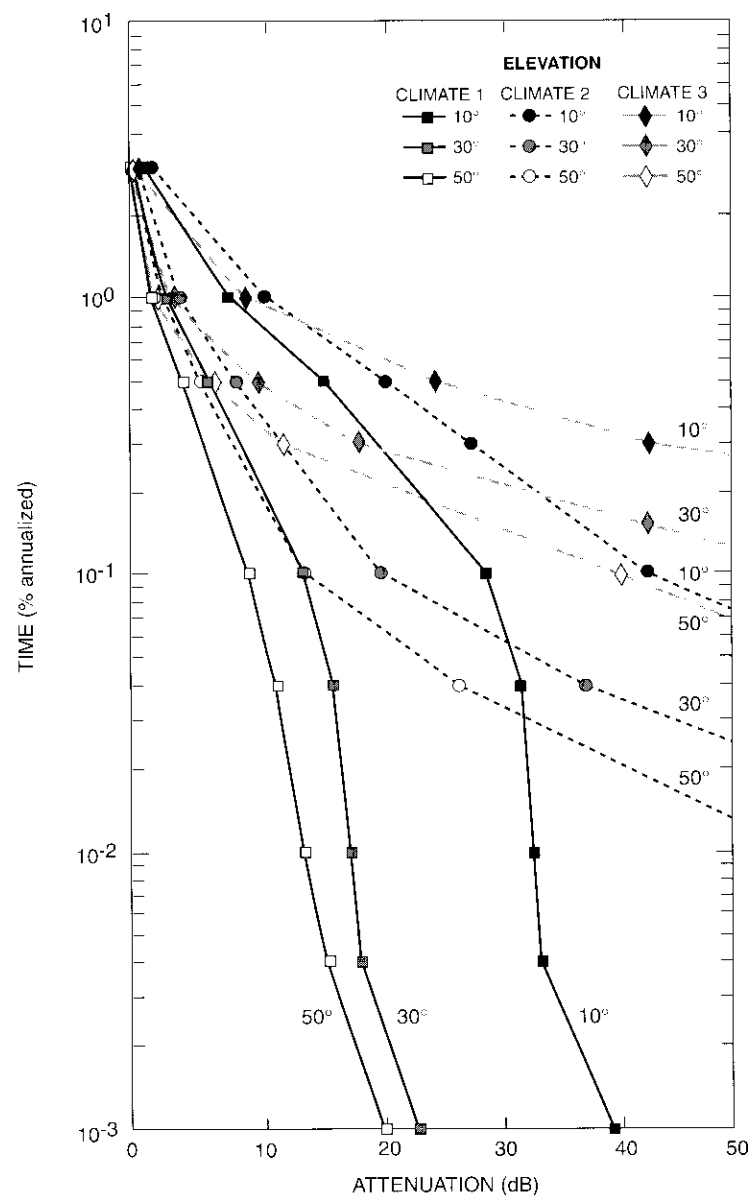


Figure 2. Rain Attenuation Data

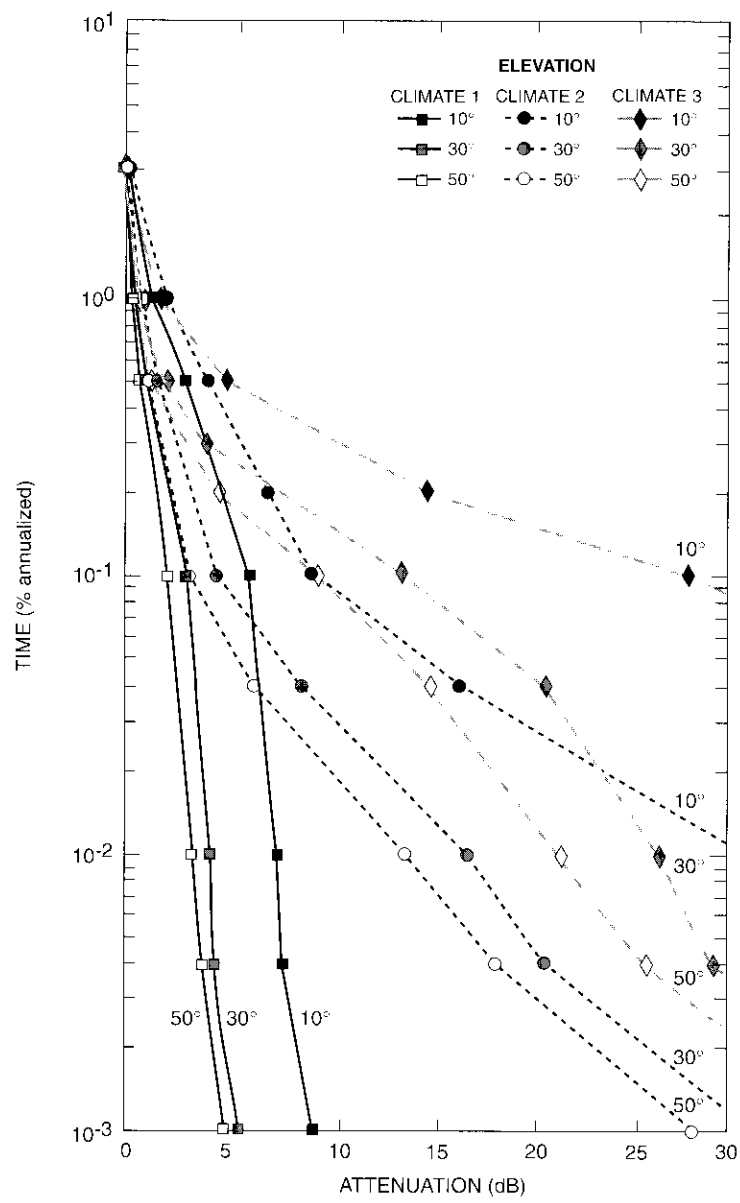


Figure 2. Rain Attenuation Data (Cont'd)

Using the information given in Figure 2, required SNG uplink margins were computed using two availability definitions:

- a. Margin necessary to provide service for all but 1 percent of the worst month.
- b. Margin necessary to ensure that the chance of having a rain fade during a 60-minute transmission will be 10 percent or less, given that the transmission occurs during the worst part of the day during the worst month.

Definition (a) has a basis in public switched telephone network (PSTN) system planning methodology, and definition (b) was selected as a comparison example for this study. Table 2 gives the results of these margin computations. Since the PAP program uses a Rice-Holmberg rain rate model to describe different rain climates, the coefficients used by this model—annual rain fall in millimeters,  $m$ , and the thunderstorm coefficient,  $\beta$ —are also given in the table. The results indicate that availability definition (b) is more stringent than definition (a). In addition, there is wide variation in the margin required for different locations, elevation angles, and frequencies. For some locations and elevation angles, especially for Ka-band, the estimated margins required are very large. As will be seen later, the requirement for a large margin is a major factor in determining the modulation, access scheme, and transponder architecture for the preferred SNG system architecture.

Because of the severity of rain impairments at Ka- and Ku-band, a number of rain fade mitigation techniques were examined, as summarized in Table 3. However, these techniques were found not to be broadly applicable to a general SNG service. This part of the study also revealed, in quantitative terms, that rain impairments at Ka-band are significantly worse than at Ku-band. However, as discussed below, SNG service at Ka-band may still be preferable for other reasons.

Due to differing rain climates and elevation angles, an SNG system operating with uplink frequencies at either Ku- or Ka-band requires large variations in uplink margin to meet a specified availability from different uplink locations. This implies that transponders having channelized AGC have a distinct advantage over conventional transponders in that they can provide more uplink margin (as shown below) and can permit a mix of different-sized SNG uplink earth stations to operate within a system. For example, earth stations with low effective isotropically radiated power (EIRP) can be used in regions having high elevation angles and/or dry climates, with larger earth station EIRP values being required for low-elevation-angle or high-rain climates.

TABLE 2. REQUIRED MARGINS FOR TWO EXAMPLE AVAILABILITY DEFINITIONS

CLIMATE NO.	ANNUAL RAINFALL, $m$ (mm/yr)	THUNDER-STORM COEFF., $\beta$	FREQ. (GHz)	ELEV. ANGLE (deg.)	DEF. (b) MARGIN* (dB)	DEF. (a) MARGIN** (dB)	
1	600	0.0	30	10	21	21	
				30	9	9	
				50	6	6	
			14	10	4	4	
					30	2	2
					50	1	1
2	1,000	0.3	30	10	58	28	
				30	30	12	
				50	20	8	
			14	10	13	6	
					30	7	2
					50	5	2
3	1,500	0.7	30	10	>100	43	
				30	78	19	
				50	55	12	
			14	10	37	9	
					30	19	4
					50	13	3

\*Worst 1-hr period applies to climates 2 and 3.

\*\*1% of month corresponds to 438 min, or 7.3 hr.

TABLE 3. UPLINK RAIN FADE MITIGATION ALTERNATIVES

TECHNIQUE	COMMENT
Site Diversity	Not appropriate for most SNG applications.
Uplink Power Control	Potentially applicable, especially at Ku-band, but at high cost. Cost may be too high and practical range too low at Ka-band.
Reduced Transmission Rates With Added FEC	Potentially applicable but may have limited range, may require excessive codec complexity, and may not be attractive to SNG operators.
Time Shift—Store and Forward	Not suitable for many SNG applications.
Frequency Diversity or Alternative Transmission Media	Potentially applicable to the limited number of SNG operators who have alternative satellite links operating at lower frequency bands or have alternative terrestrial transmission facilities available.

**Baseline parameters for system tradeoffs**

To analyze and compare the performance of the 36 candidate architectures identified in Table 1 and Figure 1, a judiciously selected design was assumed for each. Table 4 summarizes the key link parameters assumed for each candidate architecture. These values form a baseline around which parametric tradeoffs for each scheme were computed, and these tradeoffs in turn form the basis for selecting preferred architectures.

Figure 3 summarizes the results of a survey of video codec technology which led to the baseline assumption of a 5-Mb/s data rate for digitally compressed TV (as given in Table 4). The values of other parameters listed in the table are realistic, based on current system designs. Parametric data that reflect the cost considerations associated with the selection of the up- and downlink frequencies are given in Tables 5 and 6.

**Parametric study results and recommendations**

The results of the parametric tradeoff phase of the study, summarized here, form the basis for the narrower investigations conducted in phase 2. Figures 4a and 4b illustrate examples of the primary parametric tradeoffs that were performed on each of the 36 candidate system architectures. The figures show the variation of uplink margin with SNG high-power amplifier (HPA) power and satellite receive antenna beamwidth, respectively, for various system architectures. As discussed later, these results formed the basis for the

TABLE 4. KEY BASELINE LINK PARAMETERS

PARAMETER	VALUE
TV/I-M	30 MHz
Digitally Compressed TV— QPSK	5 Mb/s
Downlink EIRP (Saturated)	
C-Band	36 dBW
Ku-Band	44 dBW
SNG Antenna Diameter	1.8 m
Broadcast Center Antenna Diameter	
C-Band	9 m
Ku-Band	8 m
Spacecraft Uplink Antenna Beamwidth	Variable (or 1°)
SNG HPA Power	Variable (or 100 W)
Uplink Margin	Variable

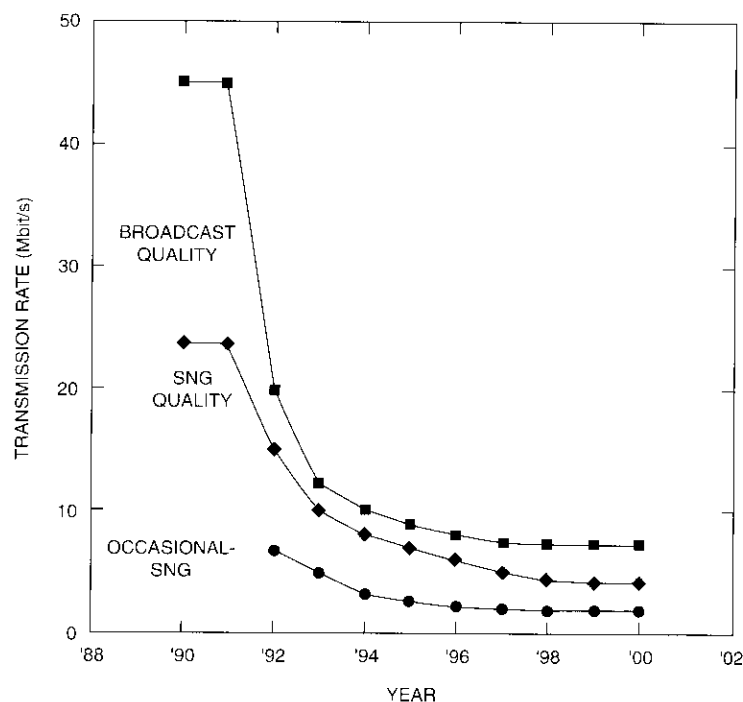


Figure 3. Transmission Rate Projections (Actual and estimated rates for compressed video, assuming redundancy due to FEC < 20%)

TABLE 5. APPROXIMATE COSTS FOR SNG HPAs\*

RF POWER (W)	COST (\$K)	EFFICIENCY (%)
<b>(a) Ka-Band (30 GHz)</b>		
200	120	10
70	60	10
<b>(b) Ku-Band (14 GHz)</b>		
600	100	15
200	30	15
50	15	15

\*At time of study.

TABLE 6. BROADCAST CENTER (EARTH STATION)  
ROUGH COST ESTIMATES\*

PARAMETER	C-BAND	KU-BAND
Antenna Size	9 m	8 m
Antenna Cost		
Auto-tracking	\$197K	\$180K
No auto-tracking	\$67K	\$62K
HPA Cost (2 for 1) (250 W)	\$55K	\$91K
{Antenna + HPA} Cost		
Auto-tracking	\$252K	\$271K
No auto-tracking	\$122K	N/A

\*At time of study.

ultimate selection of FDMA schemes that use digitally compressed video signals, and transponder architectures with channelized AGC (either with or without OBR), as the preferred system architectures.

Other parametric tradeoffs and sensitivity analyses were performed in this phase of the study to ensure that the basic conclusions recorded were applicable over a range of realistic system designs, as well as to illustrate quantitative parametric relationships. Tradeoffs of this type included:

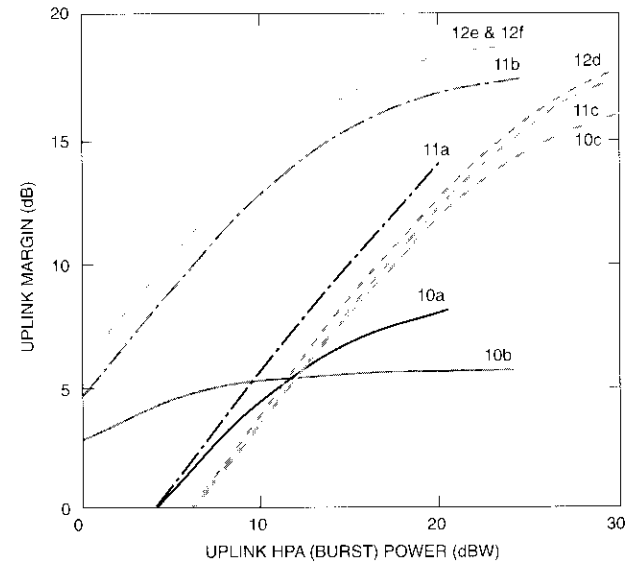
- Uplink and downlink margin vs downlink carrier-to-noise power density ratio,  $C/N_0$
- Uplink margin vs downlink  $C/N_0$  vs intermodulation noise
- Off-axis emission margins vs SNG antenna diameter
- Uplink margin vs video codec rate vs uplink carrier-to-interference ratio,  $C/I$
- Uplink and downlink margin vs transponder output backoff
- Uplink HPA size vs satellite receive antenna beamwidth for fixed uplink margin.

The results of these preliminary analyses and tradeoffs were used to develop specific recommendations regarding elements of preferred SNG system design.

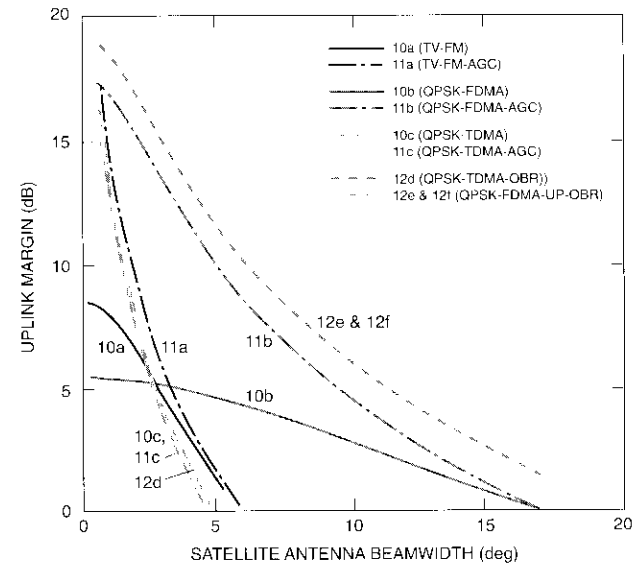
#### MODULATION, MULTIPLE ACCESS, AND TRANSPONDER ARCHITECTURE SELECTION

The modulation, multiple-access technique, and transponder architecture for an SNG system are highly interrelated, and their selection is influenced by the following considerations:

- Uplink margin
- Downlink margin



(a) 1.8-m SNG Terminal with 1° Spacecraft Antenna Beam



(b) 1.8-m Terminal with 100-W (Peak) HPA Power

Figure 4. SNG TV (Ku-band uplink and downlink)  
for 1.8-m SNG Terminals

- Spectrum utilization
- Earth station and spacecraft power requirements
- Spacecraft technology
- Transmission format flexibility
- Routing flexibility.

The propagation studies showed that, at both Ka- and Ku-band, a large uplink fading margin is essential to ensure maximum availability. In light of a requirement for a large uplink fade margin, the types of tradeoffs shown in Figures 4a and 4b illustrate that the use of FDMA on the uplink with digitally compressed video carriers, and the use of channelized transponders with AGC, results in uplink margins that are superior by several dB to those of the other candidate schemes.

Channelized AGC improves the margin against uplink rain fades because increasing the transponder gain during an uplink fade maintains the downlink EIRP at a constant value. Hence, given that there is sufficient excess margin on the uplink to maintain an acceptable uplink carrier-to-noise ratio ( $C/N$ ) during a fade, the AGC protects against the fade by ensuring that the downlink  $C/N$  does not degrade. Without AGC, the downlink EIRP would fade in proportion (or nearly in proportion) to the uplink fade. Therefore, since a satellite system has limited downlink margin due to spacecraft power resource limitations, the amount of uplink margin would be limited by downlink parameters. Without an excessively large downlink earth station or an excessive demand on spacecraft resources, the downlink margin typically is limited to only a few dB.

In terms of maximizing uplink margin, the study tradeoffs indicated that the best system architecture uses uplink FDMA with digitally compressed carriers, in combination with transponders that provide both OBR and AGC for individual carriers. With this scheme, the downlink could be either frequency-division multiplexed (FDM) or time-division multiplexed (TDM).

A system architecture that provides slightly worse (by about 1.5 dB) uplink margins also uses uplink FDMA with digitally compressed carriers, where carriers are individually channelized with AGC, but OBR is not used. In this case, the downlink must have an FDM format.

The two system architectures identified above were selected for further evaluation in phase 2 of this study. For the case where OBR is used, FDM is the preferred downlink format, primarily to keep the downlink transmission scheme compatible with current INTELSAT transmission schemes and to maximize both spacecraft power and bandwidth resources under conditions of light loading.

The technology necessary to implement the two preferred transponder architectures (*i.e.*, individual carrier OBR or channelized AGC without OBR) was investigated in detail in phase 2. A transponder with OBR must be implemented with onboard digital processing, while a transponder architecture that channelizes carriers on an individual basis and applies AGC, but does not use OBR, can be implemented with either onboard digital processing or passive filters (in which case, surface acoustic wave [SAW] filtering is the most appropriate technology for space implementation).

For digital processing architectures, most of the computational power is needed to achieve channelization, and OBR can be achieved with little additional mass and power penalty. Thus, it is reasonable to assume that OBR will be used if digital processing is employed, and if there is a benefit to be realized by using OBR. The use of forward error correction (FEC) coding on the satellite channel is an important factor in assessing the benefit of OBR, as discussed later.

#### CHOICE OF UPLINK FREQUENCY BAND

Although rain impairments are substantially more serious at Ka-band than at Ku-band, Ka-band may still be attractive for future SNG service. The reasons include the ability to use smaller SNG and spacecraft antennas, and the likelihood of an operating environment with fewer restrictions and less co-channel interference. (If SNG uplinks with large fading margins are to be implemented, uplink interference must be kept at low levels.) Furthermore, there are sites where large margins are not necessary to ensure high Ka-band availability, and there are types of SNG service that can tolerate service interruptions due to rain fades. Hence, both uplink frequencies were considered for the SNG-to-satellite link.

#### CHOICE OF DOWNLINK FREQUENCY BAND

The parametric phase of this study provided information (such as that presented in Table 6) regarding the differences among systems that use either C- or Ku-band for the downlink to the broadcast center. The downlink band preferred will depend on the specific design of the spacecraft upon which the SNG payload is to be placed, as discussed later. The results of this study are essentially independent of whether C- or Ku-band is used for the downlink.

#### SPACE SEGMENT ALTERNATIVES

Although the studies and quantitative tradeoffs considered in phase 1 are generally applicable to systems where either dedicated spacecraft or add-on

payload "packages" are used, it was decided to limit the architectures investigated in phase 2 to add-on payloads. This restriction was prompted by the desire to orient the study results toward startup SNG systems. Hence, the spacecraft-related issues treated in phase 2 address how add-on packages can be implemented within the mass, power, and mechanical constraints associated with such packages. However, many of the issues discussed are also applicable to larger payloads that would require a dedicated spacecraft.

#### CHANNELIZATION BANDWIDTHS

A minimum channelization bandwidth of 6 MHz was selected for this study, and the transponder architectures investigated (*i.e.*, SAW filters and digital processors) are required to be capable of switching to combinations that include wider bandwidth segments.

### **Phase 2: Detailed study of recommended architecture**

The objective of phase 2 of the study was to conduct a detailed investigation of the basic architecture recommended in phase 1. Major issues addressed in this phase were spacecraft antenna design, channelization techniques, transponder connectivity, and the two-way auxiliary coordination channel needed for SNG operations.

In response to the requirement that the antenna be an add-on to a future INTELSAT spacecraft, a variety of spacecraft antenna designs were also examined. Thus, the recommendations resulting from phase 2 are expressed in terms of antenna descriptions and power and mass estimates. These are given for a number of different antenna designs that cover two frequency bands (Ku- and Ka-band), various beamwidths (in the 1° to 3° range), and have either one or two beams.

In examining transponder channelization issues, both SAW and digital processing technology implementations were considered. Power and mass estimates are given for both approaches, and other implementation issues are discussed. Further, various OBR options were evaluated and compared in terms of their relative performance. These consisted of several demodulation/remodulation configurations, with and without decoding and recoding.

Regarding transponder architectures, various connectivity and switching options for connecting one or more SNG uplinks to existing downlink transponder beams were examined.

In terms of the auxiliary channel, alternative approaches are described, spacecraft EIRP requirements are given in parametric terms, and the issues involved in modifying an add-on SNG uplink spacecraft antenna to include a transmit function are discussed.

The architectures selected in this phase of the study were driven by the following key requirements:

- Use of satellite spot beams for uplink user access.
- Use of FDMA on the uplinks, with most accesses having a bandwidth of 6 MHz and some being multiples of 6 MHz.
- Onboard channelization of the individual uplink access signals by either AGC or OBR. Compared to "bent-pipe" transponder methods, this approach tends to maximize uplink fading margins and the efficiency of downlink power usage by allowing the downlink margins to be smaller than the uplink fading margins. It also circumvents the issue of power allocation to, and policing of, the SNG uplink user network.
- The concept of an SNG package as an add-on payload to an existing or future satellite design.
- Use of either Ku- or Ka-band for the SNG uplink frequency.
- Use of existing onboard resources for downlink transmission of SNG signals by employing existing transponder pathways.

Based on these considerations, four fundamental architectures bounded the study: channelized AGC using SAW filters for both Ku- and Ka-band uplinks, and channelized AGC implemented digitally, also for Ku- and Ka-band uplinks. For the purposes of this study, frequency-band-related elements were separable from signal processing elements. For example, a SAW filter channelization subsystem has the same design detail, whether it is driven by a Ku- or Ka-band uplink signal. Any modest difference in the frequency conversion components can be incorporated into the RF front end.

Figure 5 illustrates the SNG link and coverage concept. SNG service can be provided via dedicated steerable spot beam(s), or with a fixed spot beam having one or more transponders dedicated to SNG service.

The broad concept for an SNG payload element add-on to an INTELSAT satellite communications payload is depicted in Figure 6. SNG uplink signals may be received either on existing fixed-uplink Ku-band spot beams, or via an optional SNG steerable beam add-on package. SNG downlink signals are transmitted via existing downlink paths (*e.g.*, area or spot beams at either C- or Ku-band). The design can provide for any predetermined number of INTELSAT transponder channels to be selectable for SNG use. Transponder channels may bypass the SNG payload by ground command for the reallocation of resources.

As shown in Figure 6, the INTELSAT payload permits existing Ku-band uplink spot beams to be used for SNG in those cases where the coverage areas are applicable. The figure illustrates an SNG add-on which does not include an

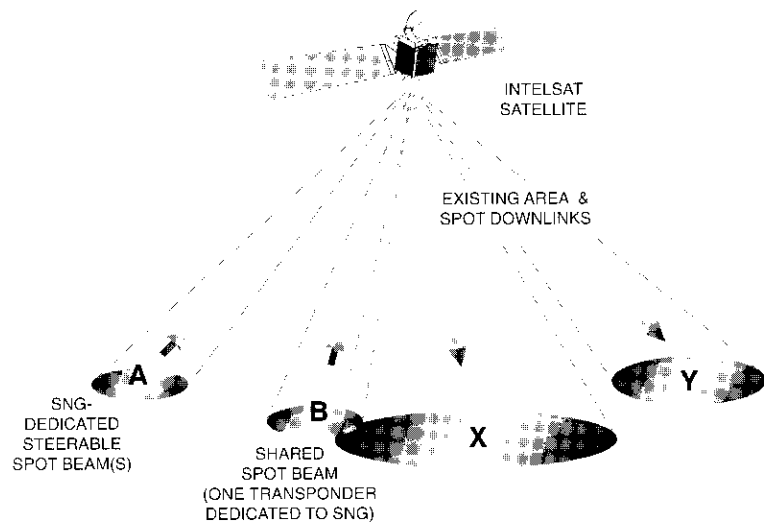


Figure 5. SNG Link and Coverage Concept

SNG-dedicated spot beam antenna. This alternative could be considered if the cost in terms of mass and mounting area would be too great to justify the additional aperture.

Important issues in considering an SNG add-on payload are how much power and mass can be budgeted for it, and what mechanical constraints must be imposed on it. Reasonable power and mass budgets were estimated using an INTELSAT VIIA spacecraft as an example.

**Channelization approaches**

As determined in phase 1 of the study, the two candidate approaches to channelization are SAW filter demultiplexing combined with AGC for subchannel power regulation, and a form of digital processing to accomplish the same goal (as well as, perhaps, to perform OBR). Figure 7 shows the channelization of the uplink subchannels by the demultiplexer and illustrates the occupancy by signals of different bandwidths.

To briefly review, SNG channelization has three major purposes. First, to accept one or more composite groups of narrowband FDMA uplink signals from a number of SNG users. Second, to separate and process individual SNG user signals in order to maximize uplink fading margins while balancing their power demand on the spacecraft's downlink transmitters. Third, as an added

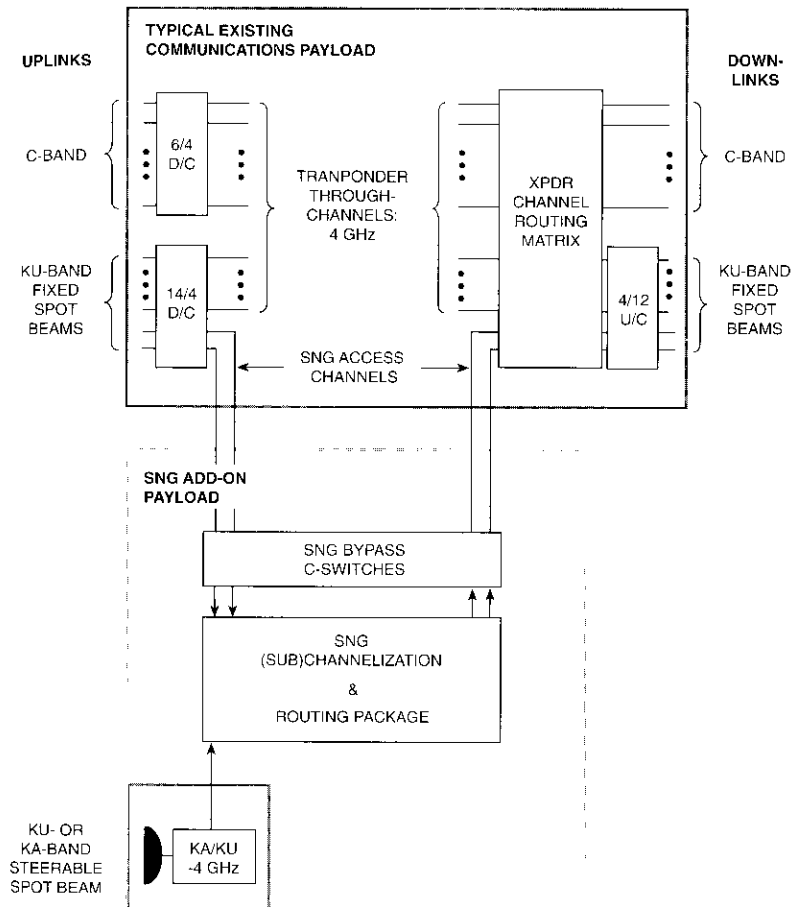


Figure 6. SNG Add-On Payload Concept

benefit, where more than one uplink channel or beam carries SNG accesses, channelization can route the SNG carriers between uplink and downlink channels, and possibly concentrate sparse populations of uplink SNG carriers occupying multiple uplink channels into (for instance) one downlink channel.

CHANNELIZATION BY SAW FILTER DEMULTIPLEXING

The following basic configurations, representing three levels of flexibility for SAW demultiplexer channelization, were examined during phase 2:

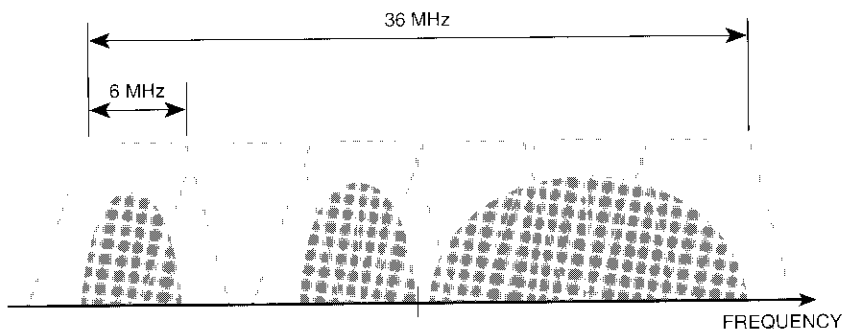


Figure 7. Contiguous Channel Filters in Demultiplexer

Case 1. Single uplink transponder beam

Case 2. Selectable uplink beam

Case 3. Selection of beams and rerouting between beams.

Figure 8 illustrates the most complex of these, case 3.

Figures 9 and 10 show two alternate subchannel routing switch configurations which provide permutations of the same  $M$  frequency channels among  $N$  uplink/downlink paths. For simplicity,  $N = 2$  beams up and down, and  $M = 6$  subchannels, are shown. Either of these configurations would provide the switch matrix function depicted as a simple box in Figure 8 for the six-subchannel, two-beam case.

Figure 11 shows a typical design for a fully redundant six-channel SAW demultiplexer with AGC. The approach is based on similar units without the AGC function which are under procurement for the N-STAR S-band Mobile Satellite Service payload. (N-STAR is a Japanese domestic communications satellite being built by Space Systems/Loral for NTT.) The use of SAW filters allows high adjacent channel rejection with very narrow transition bands between the mux/demux subchannels, thereby permitting the use of almost the entire allocated band without wide, spectrally inefficient guard bands. SAW devices synthesized on quartz substrates are inherently temperature-stable. Since the SAW filter pattern is printed on the quartz substrate, the devices are easily and accurately reproducible at low cost once a successful prototype is achieved. (The prototype process typically requires several iterations to realize a device that meets specifications.) As shown in Figure 11, a redundancy capability is provided by applying power to the desired unit. External control of the AGC loop bias gives a measure of flexibility to the level-setting concept.

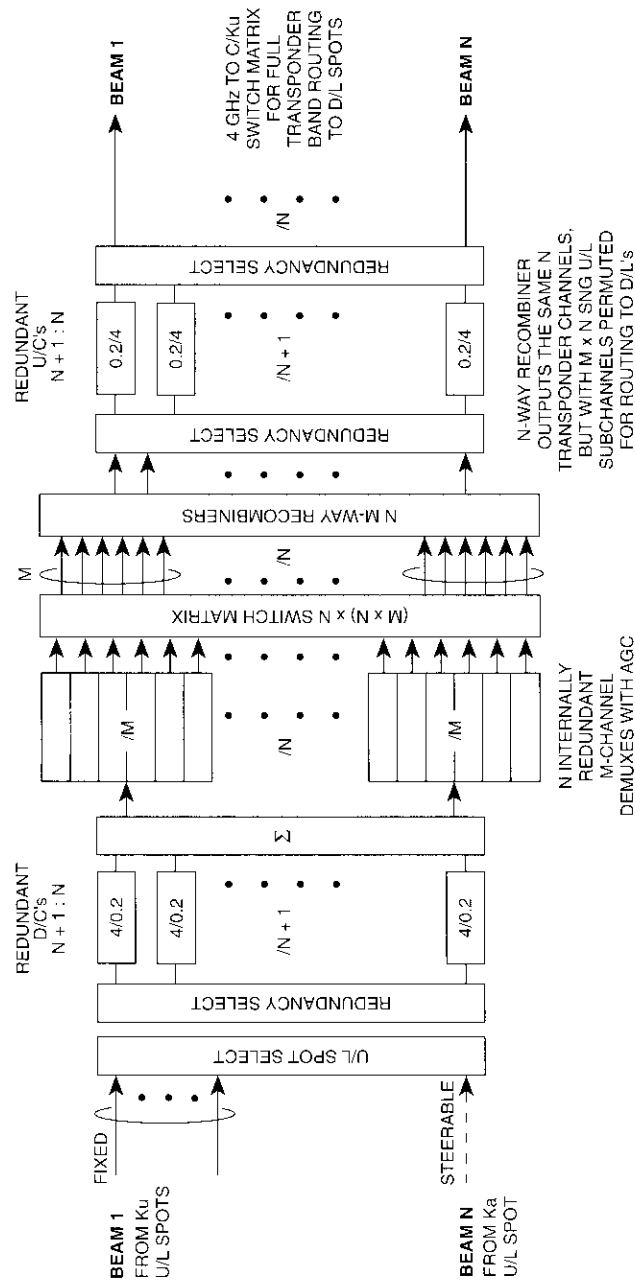


Figure 8. SAW Filter Demultiplexing, Selection of Uplink and Downlink Beams, and Rerouting Between Beams (Case 3)

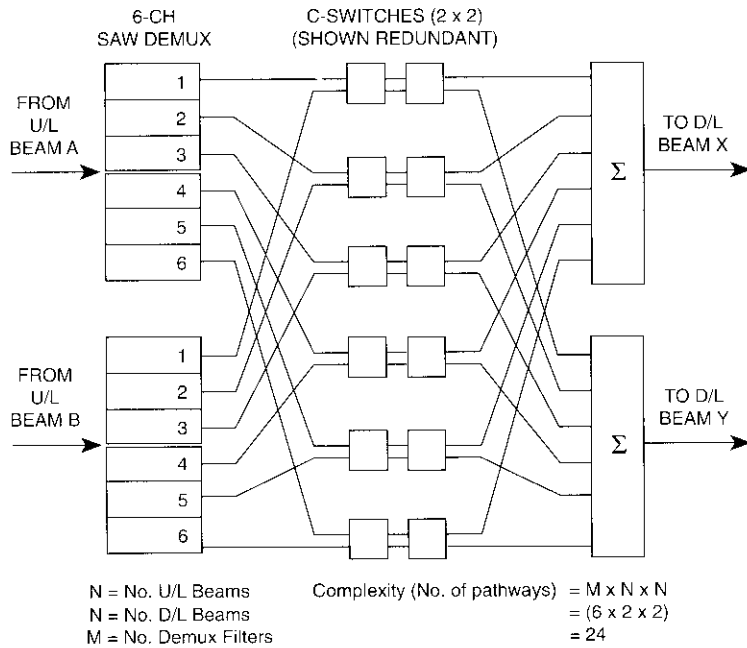


Figure 9. SNG Subchannel Routing Switch Matrix

In addition to providing low mass and high stability, SAW filter technology has another significant advantage in realizing a bandwidth-flexible demultiplexer. SAW filters exhibit an inherently linear phase response, and highly accurate characteristics are achievable at the crossover of the contiguous filters. Consequently, a signal which overlaps contiguous subchannel filters (as shown in Figure 7) will emerge after summing with almost no distortion, provided that the gain of the summed channels is equalized [1].

Mass and power estimates for a SAW filter AGC channelizer are based on similar equipment being procured for the N-STAR satellite program. There is very high confidence in the values used for the major components.

Mass and power estimates for the three cases identified above are given in Table 7. Table 8 presents a detailed mass and power breakdown for case 3 for two selectable uplink beams.

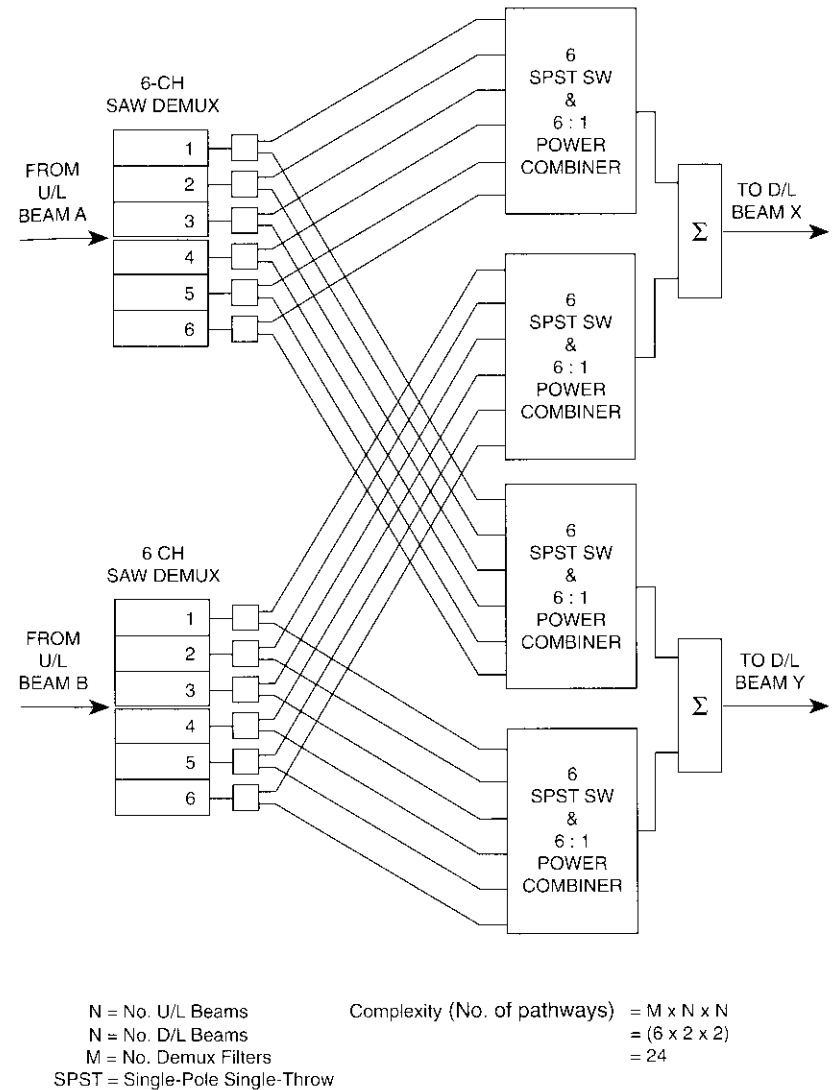


Figure 10. SNG Subchannel Routing Switch Matrix (Alternate)

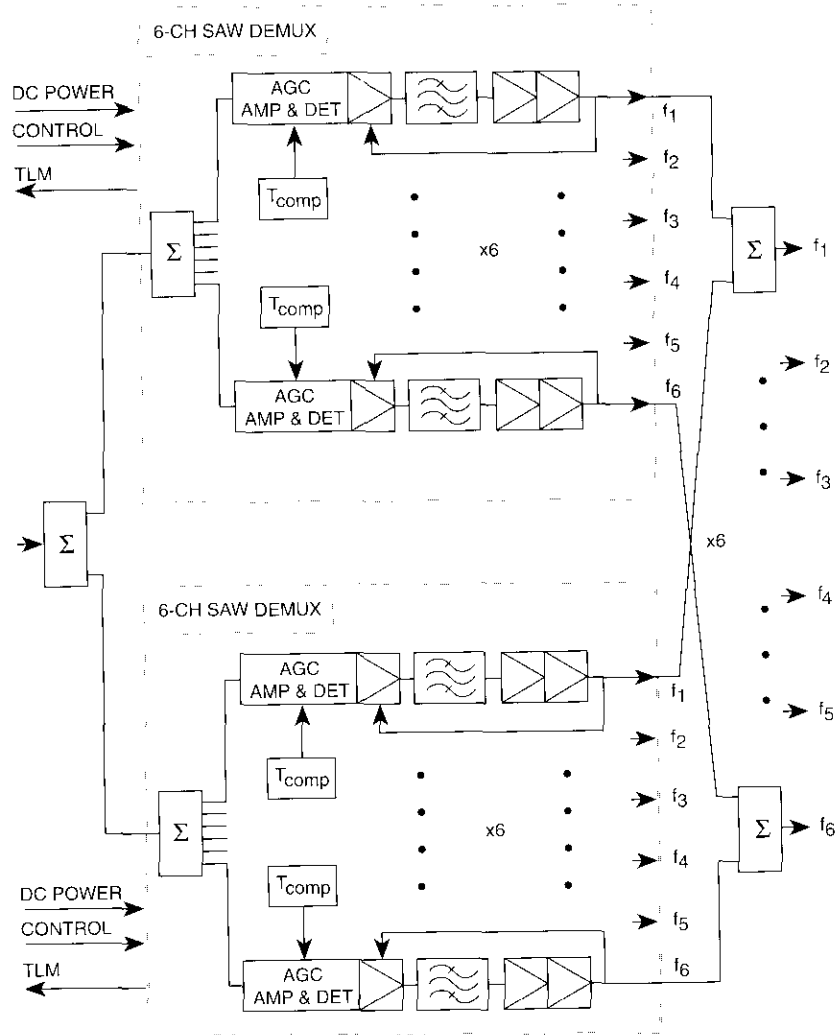


Figure 11. SNG Redundant SAW Demultiplexer Detail

TABLE 7. MASS AND POWER ESTIMATES FOR SAW FILTER DEMULTIPLEXING CASES

CASE	DESCRIPTION	MASS (kg)	POWER (W)
1	Single-Beam, Hard-Wired	8	18
2	One Beam, Selectable From Two Uplink Beams	11	18
3	Two Selectable Uplink Beams Operating Simultaneously, With Subchannel Routing to Two Downlink Beams	15	36

DIGITAL DEMULTIPLEXER AND DEMODULATOR

The second generic technique of filtering the subchannels and adjusting their power levels on the downlinks employs digital technology. In principle, the uplink channel carrying multiple SNG signals, after down-conversion to below 1 GHz, is sampled and digitized with an analog-to-digital converter of perhaps 8-bit resolution. To be directly equivalent to the analog demultiplexer approach, the digital approach would consist of the demultiplexer function alone. However, the demodulator section represents only a small addition in power and mass over the demultiplexer section alone, and the improvement in uplink margin due to onboard regeneration can be substantial. Thus, it is reasonable to consider that the digital alternative to the analog approach may include either demod/remod alone, or both demod/remod and decode/recode functions. A performance comparison of the various processing options is given later.

Figure 12 is a block diagram of a multicarrier demultiplexer/demodulator (MCDD) implementation in which the demultiplexer supports flexible data rates. The demultiplexing process begins with in-phase and quadrature (*I* and *Q*) sampling of the IF signal. The time domain samples are then applied in 50-percent overlapped blocks to a fast Fourier transform (FFT) to obtain the signals in the frequency domain. Demultiplexing is accomplished by multiplying the frequency domain samples by the desired filter coefficients for the particular subchannel frequency plan in use, thereby isolating each subchannel in the frequency domain. Next, the weighted frequency domain samples of the individual subchannels are applied in sequence to an inverse FFT (IFFT) processor in an order such that the size of the IFFT can be sequentially altered as required by the bandwidth of the individual subchannel. The output of the IFFT consists of overlapped data blocks; the 50 percent of aliased samples are discarded at the input to the interpolator. The interpolator adjusts the number of samples per symbol for each carrier from an arbitrary value near 2 to

TABLE 8. MASS AND POWER ESTIMATES FOR A ONE- AND TWO-BEAM SAW FILTER

## (a) Mass Estimates

ITEM	QTY	ITEM MASS (g)	TOTAL MASS (kg)
SNG Bypass Switch Assembly			
Coax T Switches	4	112	0.448
Coax Switch Bracket	1	60	0.060
Uplink Wideband Redundancy Ring Switch Matrix			
Coax T Switches	6	112	0.672
Coax Switch Bracket	2	60	0.120
Down-Converter $12/f_0$ (or $4/f_0$ )	3	1,120	3.360
6-Channel SAW Demux. Internally Dual Redundant	2	1,689	3.378
Narrowband Routing Switch Matrix			
Coax C Switches	12	110	1.320
Coax Switch Bracket	4	60	0.240
6-Way Power Combiner	2	150	0.300
Power Combiner Mounting Bracket	1	60	0.060
Up-Converter $f_0/12$ (or $f_0/4$ )	3	1,120	3.360
Downlink Wideband Redundancy Ring Switch Matrix			
Coax Switches	6	112	0.672
Coax Switch Bracket	2	60	0.120
Coaxial Cable	As req'd	500	0.500
Harness (DC, Tlm, Cmd)	As req'd	500	0.500
TOTAL MASS			15.110

exactly 2, and adjusts the sampling points to coincide with the peaks and zero crossings of the symbols.

The demodulator itself operates on the multiple quadrature phase shift keying (QPSK) modulated carriers in TDM, processing a few symbols from one carrier, storing the resulting demodulated symbols, processing the next carrier, and repeating the sequence. For the downlink FDMA transmissions assumed in the SNG system, the output demodulated TDM data must be demultiplexed into parallel paths, buffered, and released to the separate downlink modulators in continuous streams.

Although the characteristics of the MCDD described here may differ somewhat from the MCDD actually implemented, they are close enough to permit

TABLE 8. MASS AND POWER ESTIMATES FOR A ONE- AND TWO-BEAM SAW FILTER (CONT'D)

## (b) Power Estimates

ITEM	QTY ON	ITEM POWER (W)	TOTAL POWER (W)
Uplink Wideband Redundancy Ring Switch Matrix	N/A	—	—
Coax T Switches	—	—	—
Coax Switch Bracket	—	—	—
Down-Converter ( $4/f_0$ )	2	8.0	16.0
6-Channel SAW Demux. Internally Dual Redundant	2	3.0	6.1
Narrowband Routing Switch Matrix	N/A	—	—
Coax C Switches	—	—	—
Coax Switch Bracket	—	—	—
6-Way Power Combiner	N/A	—	—
Up-Converter ( $f_0/4$ )	2	6.7	13.4
Downlink Wideband Redundancy Ring Switch Matrix	N/A	—	—
Coax Switches	—	—	—
Coax Switch Bracket	—	—	—
TOTAL POWER			35.5

power and mass estimates. Based on an estimate that an MCDD processor would consume about 25 W and have a mass of about 2 to 3 kg [2], the estimated mass and power of an SNG payload are given in Table 9. In an actual implementation, different architectures (e.g., a tree demultiplexer or a polyphase FFT) are possible, and might be preferable depending on specific requirements. Since the estimates given in the table are relatively low, the effect of using a different architecture should be very small. It should be noted that interpolating filters would probably not be used in any future MCDD implementation, and would instead be replaced by a demodulator operating on a fractional number of samples per symbol.

## ASSESSMENT OF ONBOARD DEMOD/REMOD AND DECODE/RECODE FOR SNG SERVICES

The use of onboard digital processing to achieve channelization offers the opportunity for carrier demodulation and remodulation, as well as decoding and recoding, with only a modest increase in processing requirements over

TABLE 9. MCDD MASS AND POWER BUDGETS

(a) Mass Budget			
ITEM	QTY	ITEM MASS (g)	TOTAL MASS (kg)
SNG Bypass Switch Assembly			
Coax T Switches	4	112	0.448
Coax Switch Bracket	1	60	0.060
Uplink Wideband Redundancy Ring Switch Matrix			
Coax T Switches	6	112	0.672
Coax Switch Bracket	2	60	0.120
Down-Converter $12f_0$ (or $4f_0$ )	3	1,120	3.360
6-Channel MCDD, Internally Dual Redundant	2	2,273	4.546
Modulator to $f_0$ and Transmit Subchannel Synthesizer			
• Modulators	8	10	0.080
• Six-Step Synthesizer	8	20	0.160
6-Way Power Combiner	2	150	0.300
Power Combiner Mounting Bracket	1	60	0.060
Up-Converter $f_0/12$ (or $f_0/4$ )	3	1,120	3.360
Downlink Wideband Redundancy Ring Switch Matrix			
Coax Switches	6	112	0.672
Coax Switch Bracket	2	60	0.120
Coaxial Cable	As req'd	500	0.500
Harness (DC, Tlm, Cmd)	As req'd	500	0.500
TOTAL MASS			14.958

those required for demultiplexing. The benefits to be realized by various onboard processing options were assessed for the alternative configurations shown in Figure 13, and are summarized as follows:

- Case 1.* Channelization with AGC, no demod/remod, no decode/decode—baseline link budget with relatively low intermodulation and downlink thermal noise.
- Case 1a.* Same as case 1, except that intermodulation noise and downlink thermal noise are higher.
- Case 2.* Same as case 1, except that a rate 3/4 convolutional FEC code is applied to the SNG carrier.

TABLE 9. MCDD MASS AND POWER BUDGETS (CONT'D)

(b) Power Budget			
ITEM	QTY	ITEM POWER (W)	TOTAL POWER (W)
Uplink Wideband Redundancy Ring Switch Matrix	N/A	—	—
Down-Converter ( $4/f_0$ )	2	8.0	16.0
6-Channel MCDD, Internally Dual Redundant	2	25.0	50.0
Modulator to $f_0$ and Transmit Subchannel Synthesizer			
• Modulators	6	N/A	—
• 6-Step Synthesizer	6	0.2	1.2
6-Way Power Combiner	N/A	—	—
Up-Converter ( $f_0/4$ )	2	6.7	13.4
Downlink Wideband Redundancy Ring Switch Matrix	N/A	—	—
TOTAL POWER			80.6

- Case 3.* Same as case 1, except that onboard demod/remod is used.
- Case 4.* Same as case 3, except that a rate 3/4 convolutional FEC code is applied to the SNG carrier.
- Case 5.* Same as case 4, except that decode/decode is performed onboard the satellite.

Commercial compressed-video digital modems use a variety of source and FEC coding schemes, such that the satellite channel coding used for cases 2, 4, and 5 (as shown in Figure 13) is in addition to the coding used in the video modem. To permit the use of an extra satellite FEC code, it is assumed that the satellite codecs employ interleaving of sufficient depth to enable the video modem coding schemes to operate satisfactorily.

Because of the importance of uplink margin in an SNG service operating at either Ku- or Ka-band, this margin was used to compare cases 1 through 5. That is, an option's relative worth was determined based on the amount of fading (due primarily to rain) that can be tolerated in the SNG uplink. Figure 14 illustrates the uplink margin vs uplink  $C/N_0$  for each of the five cases described above. Figure 15 plots the difference in uplink margin between case 1 and each of the other cases.

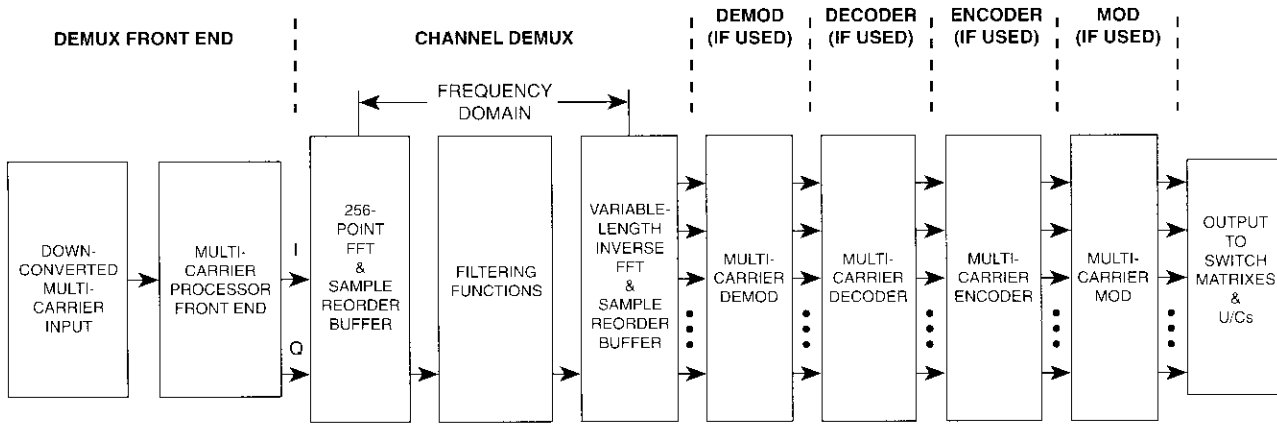


Figure 12. Functional Block Diagram of MCDD

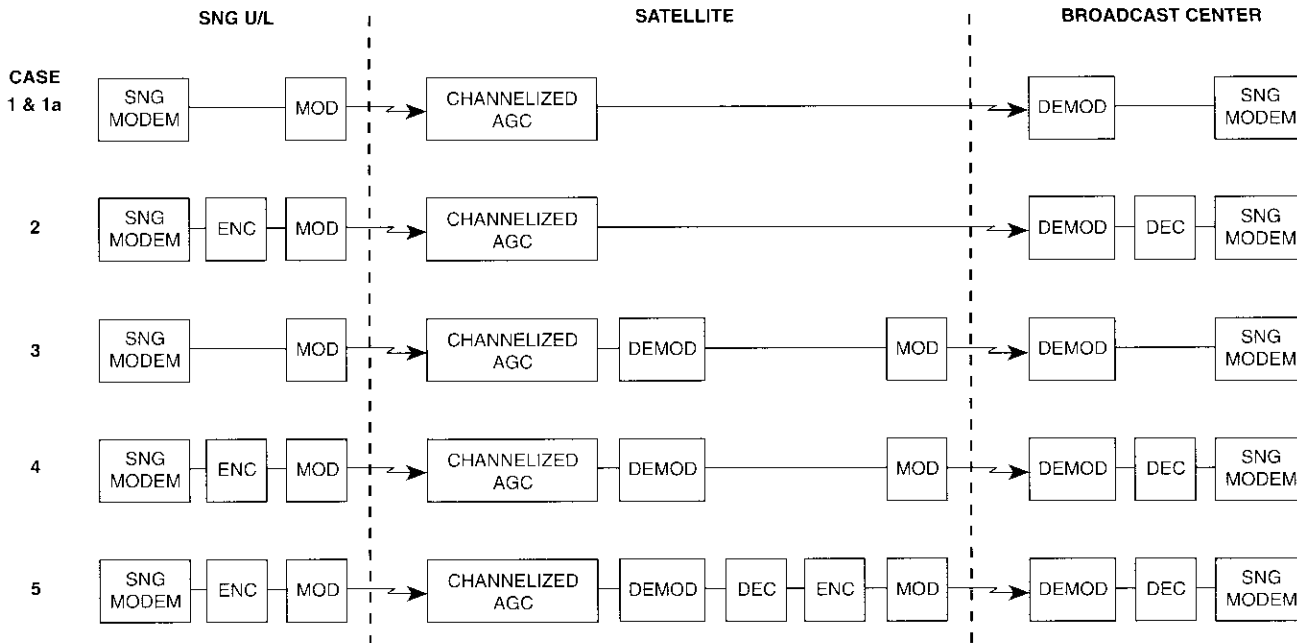


Figure 13. Onboard Processing Options

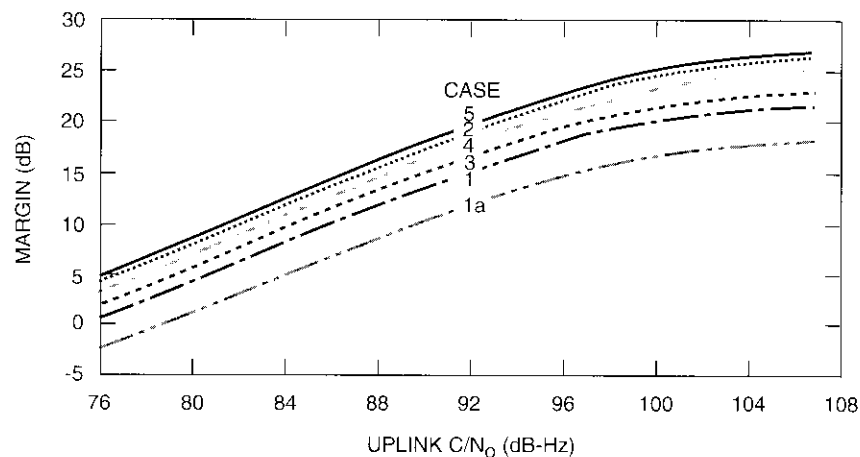


Figure 14. Uplink Margins for Various Onboard Processing Options

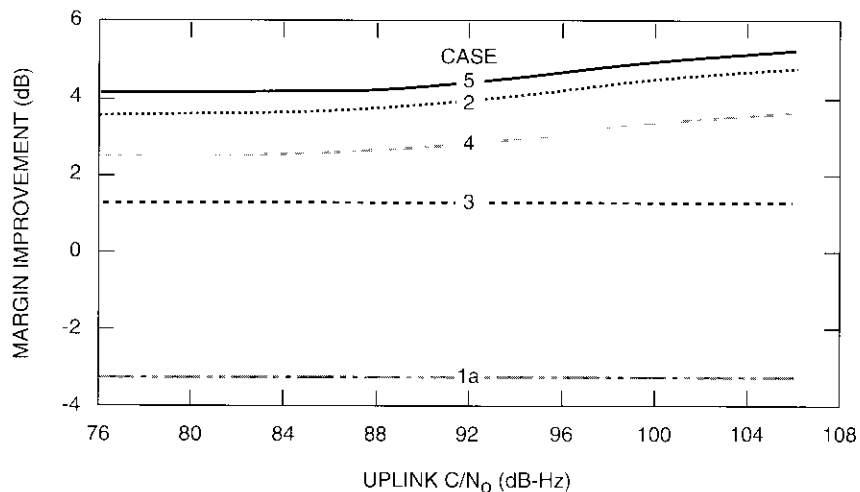


Figure 15. Improvement in Uplink Margin With Respect to Case 1

Figure 14 shows that, for all cases, uplink margin increases proportionally with increasing uplink  $C/N_0$  for low levels of  $C/N_0$ , and then "flattens" for higher values of  $C/N_0$  as the link becomes uplink-interference-limited. Figures 14 and 15 together reveal that the amount of uplink margin improvement provided by onboard demod/remod (case 3) vs channelized AGC alone (cases 1 and 1a) depends on the downlink parameters. Figure 15 shows that case 3 provides about 1.3 dB improvement when the downlink is relatively good, and about 4.6 dB when the downlink is relatively poor (case 3 minus case 1a). Indeed, the performance of channelized AGC alone (case 1) is highly sensitive to the condition of the downlink, as illustrated by case 1a. This is in contrast to the performance of onboard regeneration configurations (cases 3 through 5), where the uplink margin is insensitive to the downlink condition unless the downlink is operating near threshold.

The fact that the curves in Figure 15 for the cases with coding are not flat, but increase slightly with  $C/N_0$ , is due to the use of lower required energy-per-bit to noise-power density ratio ( $E_b/N_0$ ) values for these cases. It is also attributable to the use of a constant uplink  $C/I$ , rather than carrier-to-interference power density ratio,  $C/I_0$ , for all cases.

All of the cases with channel coding (cases 2, 4, and 5) result in better performance than those without channel coding (cases 1 and 3). The use of channel coding with onboard demod/remod, but without onboard decode/recode (case 4), results in an improvement of between 1 and 2 dB over case 3, where no coding is used. This is due to the loss of soft-decision information in case 4.

Channel coding without onboard regeneration (case 2) performs more than 1 dB better than channel coding with onboard demod/remod only (case 4). This implies that, if channel coding is used in combination with onboard regeneration, then the onboard regeneration should include both demod/remod and decode/recode (or decode only, without downlink channel coding, as mentioned previously), as in case 5, in order to take advantage of the additional gain realized by soft-decision decoding. Case 2 also results in uplink margins nearly as good (0.5-dB smaller) as for the use of channel coding with onboard demod/remod and decode/recode (case 5), assuming that a good-quality downlink is available.

Another issue regarding onboard regeneration (especially where onboard decoding is employed) is that its use may restrict the flexibility with which various video digital compression codecs and rates can be used. However, this problem may be alleviated by onboard reprogramming, or by turning off regenerative functions.

It is difficult to recommend one of the five onboard configurations compared herein without more specific knowledge of system requirements, particularly regarding the importance of flexibility and the nature of the system's downlink parameters. However, conditional recommendations are as follows:

- If channel coding with interleaving is compatible with the formats used by the digital compression video codecs, then channel coding should be used and a rate 3/4 convolutional code ( $k = 7$ ) is recommended. For reasons discussed earlier, if coding is used, then onboard demod/remod without onboard decoding/recoding (case 4) should not be used. This leaves cases 2 and 5 as the preferred candidates.
- If the downlink design is known to be robust, then the relative simplicity of case 2 (no onboard regeneration) is preferable. On the other hand, if protection is required for a downlink where intermodulation and thermal noise are significant, and where downlink fading may also be significant, then case 5 is preferable. A variation of case 5 which requires less downlink protection would omit onboard recoding, and thus channel coding would not be used on the downlink.

#### The spacecraft uplink antenna

A major factor in evaluating the viability and achievable performance of an SNG add-on payload is the antenna subsystem—not only because of mass requirements, but also because of the mechanical constraints and restrictions inherent in adding a new antenna capability to an existing spacecraft design. The elements that can be accommodated in a spacecraft as add-on payload are highly dependent on the specific spacecraft model. Therefore, in this study antenna mass estimates were compiled for a range of configurations of interest for this type of application.

The estimates include one- and two-beam configurations, where the antenna's beamwidth ranges between  $1^\circ$  and  $3^\circ$  for Ku-band, and between  $1^\circ$  and  $1.5^\circ$  for Ka-band. In general, while a more narrow spacecraft antenna beamwidth would require a larger spacecraft antenna and reduce the size of the coverage footprint, it has the important advantage of providing a higher  $G/T$  value, which permits smaller SNG earth stations and/or larger uplink rain fade margins.

Specific design approaches for the add-on SNG payload antennas considered in this study included concepts where additional antennas are placed on the spacecraft, and concepts where existing antennas are modified with additional feeds. In the former category, antenna types considered included mechanically steerable parabolic reflectors, multiple-feed nonmechanically steerable reflectors, and phased arrays.

Concepts employing existing reflectors included those using frequency-selective surfaces (FSSs), which would be part of a Ka-band feed system and would be transparent at lower frequencies. The FSS would move mechanically to steer a Ka-band spot beam. Another antenna in this category uses electronically switched multiple feeds integrated with the existing feeds used by the reflector for its original purpose (*i.e.*, Ku-band or C-band spot beams).

Consideration was also given to the problems associated with placing additional antenna apertures on an existing spacecraft. For purposes of illustration, the earth-facing deck layout of the INTELSAT VIIA spacecraft was examined, and it was concluded that the spacecraft would have to undergo a major redesign in order to accommodate an extra SNG aperture.

Evaluation of independently steered receive antennas for an add-on SNG payload led to the following observations:

- With the new conventional apertures, it is assumed that the present redundant INTELSAT payload receivers could be used for the Ku-band SNG function, thereby realizing a significant savings in mass and power over Ka-band operation, which would require the addition of low-noise amplifiers (LNAs) and down-converters to the payload. Depending on the redundancy philosophy adopted, it is possible that only one additional Ku-band receiver would be required for two added SNG beams.
- In the case of a phased array implemented at either Ku- or Ka-band, LNAs are integral to the antenna; however, extra down-converters would be required for Ka-band operation. The phased array is deemed to represent higher development risk due to its monolithic microwave integrated circuit (MMIC) implementation and lack of design heritage. Moreover, it consumes the most power of all of the options.
- In cases where it is required to add an aperture to the present INTELSAT payload, there is a high risk of being unable to benefit from the satellite and bus design heritage due to already congested antenna farms.
- A low-risk option is to use steerable FSSs in front of the apertures being employed for the normal INTELSAT services at Ku- and C-band. This option is applicable only for SNG operation at Ka-band, and is not particularly low in mass or power.
- A low-mass option of only moderate development risk would use electronic beam-forming as an added feed in the usual INTELSAT Ku- and C-band apertures. Both the Ku- and Ka-band versions would include integral LNAs; however, the Ka-band version would require additional down-converters and more power.

A tradeoff that could be considered would examine whether the aperture-bandwidth product (with the bandwidth assumed to be only 36 MHz) for a separate aperture could be economically exploited for SNG service. Factors could be weighed to determine whether the revenue derived from dedicating an entire aperture to 36-MHz SNG service justifies the investment, compared with other possible services that use from hundreds of megahertz to more than a gigahertz of bandwidth per aperture.

In summarizing the possible approaches to antenna design for an SNG add-on option, the more difficult task of providing two independently steered beams is presented first, followed by a less detailed description of approaches that cover both one and two beams and wider beamwidths. Table 10 summarizes the most feasible approaches for realizing two independently steerable beams, while Table 11 provides mass and power estimates for the antenna options that can provide such beams.

To describe the SNG add-on antenna options parametrically, in terms of the number of beams and beamwidth, Tables 12 and 13 identify the preferred antenna type and estimate the mass and power for a number of options that include both one and two beams, with beamwidths ranging from 1° to 3° for the Ku-band options, and from 1° to 1.5° for the Ka-band options. For completeness, the tables also include the mass and power of the onboard demultiplexer, so that the total estimate provided is essentially for the entire add-on package. Although SAW filter technology is assumed for the estimates provided, this assumption does not necessarily imply that SAW technology is generally preferred, as will be discussed later.

#### The auxiliary channel

In an SNG operation, two-way communications links are required between the SNG site and the broadcast center (and possibly other locations as well), in addition to the basic requirement of providing uplink video and audio from the

TABLE 10. SUMMARY OF APPROACHES FOR TWO STEERABLE BEAMS

APPROACH	POWER (W)	MASS (kg)	COMMENTS
Phased-Array Antenna	100	45	Highest risk and power. Estimates apply to both bands.
Movable FSSs	nil	15	Ka-band only.
Electronic Beam Steering	0.5	45	SNG beams cannot overlap main communications beams. Estimates apply to both bands.

TABLE 11. MASS AND POWER SUMMARY OF ANTENNA AND RF OPTIONS TO PROVIDE TWO INDEPENDENTLY STEERED RECEIVING BEAMS

ANTENNA OPTION	ITEM	MASS (kg)	POWER (W)
<b>(a) Ku-Band</b>			
Two Additional Apertures (Assumes use of existing receivers)	2 antenna assemblies	34.48	0.0
	Totals	34.48	0.0
One Additional Aperture (Assumes use of existing receivers) (Assumes electronic switched feed array)	1 antenna assembly	17.24	—
	Feeds	4.50	0.5
	Totals	21.74	0.5
Phased Array (Uses existing receiver after phased array)	Phased-array antenna & LNAs	45.00	100.0
	Totals	45.00	100.0
Steerable FSS (Not a viable option for Ku-band)	—	—	—
Electronic Beam-Forming on Current INTELSAT Reflectors (Assumes use of existing receiver after BFN)	Feeds & LNAs	45.00	0.5
	Totals	45.00	0.5
<b>(b) Ka-Band</b>			
Two Additional Apertures	2 antenna assemblies	34.48	0.0
	2 LNAs	0.89	2.2
	2 down-converters	2.36	20.0
	Totals	37.73	22.2
One Additional Aperture (Assumes use of electronic switched feed array)	1 antenna assembly	17.24	0.0
	Feeds	4.50	0.5
	2 LNAs	0.89	2.2
	2 down-converters	2.36	20.0
	Totals	24.99	22.7
Phased Array	Phased-array antenna & LNAs	45.00	100.0
	2 down-converters	2.36	20.0
	Totals	47.36	120.0
	Steerable FSS	FSSs	15.00
Electronic Beam-Forming on Current INTELSAT Reflectors	2 LNAs	0.89	2.2
	2 down-converters	2.36	20.0
	Totals	18.25	22.2
	Feeds & LNAs	45.00	0.5
	2 down-converters	2.36	20.0
Totals	47.36	20.5	

TABLE 12. MASS AND POWER OF SNG PAYLOAD OPTIONS WITH ADDITION OF DEDICATED STEERABLE REFLECTORS<sup>a</sup>

PREFERRED ANTENNA TYPE	APERTURE DIAMETER (m)	NO. BEAMS	BEAM-WIDTH	ITEM	MASS <sup>b</sup> (kg)	POWER (W)
<b>Ku-Band</b>						
Two Additional Reflecting Apertures	1.83	2	1°	Demux	15.0	36.0
				Antenna	35.4	0.0
				Totals	50.4	36.0
	0.915	2	2°	Demux	15.0	36.0
				Antenna	33.0	0.0
				Totals	48.0	36.0
	0.61	2	3°	Demux	15.0	36.0
				Antenna	32.0	0.0
				Totals	47.0	36.0
One Additional Reflecting Aperture	1.83	1	1°	Demux	8.0	18.0
				Antenna	17.7	0.0
				Totals	25.7	18.0
	0.915	1	2°	Demux	8.0	18.0
				Antenna	16.5	0.0
				Totals	24.5	18.0
	0.61	1	3°	Demux	8.0	18.0
				Antenna	16.0	0.0
				Totals	24.0	18.0
<b>Ka-Band</b>						
Two Additional Reflecting Apertures	0.915	2	1°	Demux	15.0	36.0
				LNAs & D/Cs	3.3	22.2
				Antenna	33.0	1.0
Totals	51.3	59.2				
One Additional Reflecting Aperture	0.915	1	1°	Demux	7.5	18.0
				LNAs & D/Cs	1.7	11.1
				Antenna	16.5	0.0
Totals	25.7	29.1				

<sup>a</sup>SAW filter demultiplexer assumed for purpose of illustrating mass estimate.  
<sup>b</sup>Main reflector masses for 1° and 3° Ku-band antenna estimated from 2° aperture.

TABLE 13. MASS AND POWER OF SNG PAYLOAD OPTIONS USING EXISTING REFLECTORS<sup>a,b</sup>

NO. OF BEAMS	BEAM-WIDTH <sup>c</sup>	ITEM	MASS (kg)	POWER (W)
<b>Ku-Band</b>				
2	3°	Demux	15.0	36.0
		Switched Feeds	9.0	1.0
		Totals	24.0	37.0
1	3°	Demux	8.0	18.0
		Switched Feeds	4.5	0.5
		Totals	12.5	18.5
<b>Ka-Band</b>				
2	1.5°	Demux	15.0	36.0
		LNAs & D/Cs	3.3	22.2
		Switched Feeds	9.0	1.0
Totals	27.3	59.2		
1	1.5°	Demux	7.5	18.0
		LNAs & D/Cs	1.7	11.1
		Switched Feeds	4.5	0.5
Totals	13.7	29.6		

<sup>a</sup>New antenna design of the same diameter as the present INTELSAT VII antennas.  
<sup>b</sup>Approach has moderate to low technological risk, using SAW demux and beam-switched feeds in front of current INTELSAT payload antennas. SAW filter demux assumed for purpose of illustrating mass estimate.  
<sup>c</sup>Current INTELSAT VII spot Ku-band antennas produce noncircular coverage beams of approximately 3° at Ku-band. Approximately the same beamwidth could be realized by using an antenna having the C-band spot antenna diameter at Ku-band. At Ka-band, an antenna of this diameter (0.51 m) would have a 1.5° beamwidth.

SNG site to the center. These auxiliary channel requirements were examined with an emphasis on how they might affect add-on SNG payload concepts.

In an SNG operation, auxiliary two-way links are required in order to schedule SNG programming transmissions, to ensure that transmission quality is acceptable and that the uplink is not interfering with other services, and to permit communications among programming personnel [3],[4]. The requirements for auxiliary links range from a single voice channel to multiple voice channels, and can also include data transmission at T1 carrier rates (1.544 Mb/s) over channels that may require symmetrical two-way transmission. For

example, data may be transmitted from the broadcast center to the SNG site to provide limited-motion video to programming personnel.

In the inbound direction (*i.e.*, the SNG-site-to-broadcast-center link), the transmission requirements for the auxiliary channels can be satisfied relatively easily by multiplexing the auxiliary channel (in digital form) with the programming signal. The major problem in providing auxiliary channels in an SNG system lies in the outbound link. Here, it is preferable if the auxiliary link can be designed to use the same SNG antenna and satellite used for the inbound link. If this is not possible, other satellites (including other satellite systems such as Inmarsat) or terrestrial facilities must be used, requiring extra equipment at the SNG site and/or added complexity and cost for setup and operation. A desirable solution to this problem is to include a transmit function in the spacecraft antenna used for the SNG uplink receiver. In this case, the auxiliary link is not limited by the coverage regions of the satellite's other antennas, and does not require limited spectrum from a global transponder.

If the downlink portion of the outbound link cannot use the SNG uplink spacecraft antenna, the next best alternative is to use the same satellite and the same SNG earth station antenna. Furthermore, if the SNG uplink is at Ku-band, it would be preferable to use Ku-band for the outbound link, to minimize the expense of fitting the SNG uplink antenna with a C-band receive feed. There are, however, small antennas available that transmit at Ku-band (14 GHz) and receive at both Ku-band (11–12 GHz) and C-band (4 GHz), and it is technically feasible to design SNG antennas that would transmit at Ka-band (30 GHz) and receive at either Ku- or C-band.

If an SNG service's uplink and broadcast center lie within the coverage regions of certain transponders, then a portion of only one transponder on the SNG satellite need be used for the outbound link. However, if this is not possible, then it may be feasible to reserve slots on several transponders for the SNG outbound link, where the transponder used would depend on the location of the SNG and the broadcast center.

Because the coverage regions of Ku-band transponders are limited in area, it is likely that a C-band downlink will be preferable for the SNG outbound auxiliary link. In this case, zone, hemi, and possibly global beams may be available, thus giving the SNG system either a wide area from which to operate or, if a global beam is available, a virtually unlimited area (except for polar regions). Use of C-band for the SNG outbound downlink does make it more difficult to use a small antenna, due to spacecraft EIRP limitations and adjacent satellite interference. However, spread spectrum modulation can be used to alleviate the interference problem.

If it is assumed that the auxiliary channel transmission rate requirement will be between 5 kb/s (the approximate rate of a single-channel, low-rate

voice codec) and 3 Mb/s (representing approximately two T1 carriers), then it is of interest to know what demands will be placed on space segment resources (*i.e.*, EIRP) for various link design options. Link tradeoffs of required spacecraft EIRP vs data rate for the auxiliary channel outbound downlink were evaluated in the phase 2 study for C-, Ku-, and Ka-band downlinks.

Table 14 gives an example of the resources of several satellite transponders that would be required for a 64-kb/s auxiliary channel outbound link. In general, significantly larger portions of the C-band transponder power are required for this type of service, compared to the Ku-band transponder power, which is a consequence primarily of the larger saturated EIRP values of the Ku-band transponders. This result is unfortunate, but reasonable, in the sense that Ku-band spot beams offer much smaller geographical coverage than the C-band transponders.

Regarding the incorporation of an auxiliary channel outbound link in an SNG add-on package, this study has shown that, while the high antenna gain

TABLE 14. EXAMPLES OF C- AND KU-BAND TRANSPONDER POWER REQUIREMENTS FOR A 64-KB/S AUXILIARY DOWNLINK TO AN SNG ANTENNA

TRANSPONDER	BAND	SATURATED EIRP (BEAM EDGE) (dBW)	0.8-m ANTENNA		1.8-m ANTENNA	
			EIRP (dBW)	APPROX. % OF XPDR POWER	EIRP (dBW)	APPROX. % OF XPDR POWER
INTELSAT VII-A Zone A (also approx. hemi)	C	32.7	24.5	15	17.5	3.0
INTELSAT VII-A Global, Transponder 10–12	C	29	24.5	35	17.5	7.0
INTELSAT VII-A Global, Transponder 9B	C	26	24.5	71	17.5	14.0
INTELSAT VII-A Spot 1, Normal, Outer	Ku	44.7	26.7	1.6	19.0	0.27
INTELSAT VII A Spot 1, High-Power, Inner	Ku	49.5	26.7	0.5	19.0	0.09
INTELSAT VIII Global	C	29	24.5	35	17.5	7.0
INTELSAT VIII Hemi	C	36	24.5	7	17.5	1.4
INTELSAT VIII Spot, Outer	Ku	44	26.7	1.9	19.0	0.3

would reduce the power and mass required for the downlink RF amplifier, the provision of a transmit capability could present significant design complications and added mass, depending on the SNG uplink antenna design. Also, depending on the requirements for broadcast center location, additional switching capability in the outbound direction might need to be added to the spacecraft.

The added complexity and mass required by the SNG add-on package is primarily due to the antenna subsystem, but also, to a lesser extent, to the onboard interconnections and the added RF power requirement necessary for incorporating an outbound link. The decision whether or not to include this function depends heavily on such factors as the inbound SNG antenna subsystem requirements and design, the power and mass available on board the spacecraft for such a function, and the availability of alternative links for the auxiliary channel.

### Conclusions and recommendations

Phase 1 of this study examined issues that lead to the selection of a basic SNG system architecture, while phase 2 addressed the implementation of the preferred architecture as an add-on payload. The recommended system was a digitally compressed video FDMA format employing channelized transponders that apply AGC on a per-carrier basis and may use OBR. This type of architecture provides the largest uplink margin against rain fades, given a reasonable SNG uplink earth station size and power.

The propagation data and rain fade margin requirements determined in phase 1 provided guidance as to how well links will perform, in terms of availability, for earth stations located in various climates and at various elevation angles for both Ku- and Ka-band frequencies. The link tradeoffs, sensitivity analyses, and other parametric data (such as the survey of digitally compressed video codec rates and earth station costs) performed in this phase are a resource that can be used in future SNG system definition efforts.

The objective of phase 2 of the study was to examine issues related to the placement of an add-on SNG payload, operating with either a Ka- or Ku-band uplink and with a channelized AGC transponder that may or may not use OBR. It was determined that a major issue in the design of an SNG add-on package is the antenna subsystem, because of the mass it requires and the effect it may have on the design of other spacecraft antennas and on the spacecraft packaging, deployment, and launch vehicle shroud. However, depending on the limitations of the specific spacecraft, its existing transponder antenna coverages, and the requirements of the SNG system, an SNG add-on package that uses the existing spacecraft's antenna subsystem, with little or no modifica-

tion, may also be a viable option. In this case, extra power and mass would be required only for transponder channelization and connectivity. Figure 16 summarizes the power and mass requirements for the various options considered in phase 2.

Two approaches to transponder channelization were examined: SAW filters and digital processing. Because the demands on spacecraft resources for both approaches are relatively small compared to, for example, the requirements of an add-on antenna, and because both approaches are satisfactory, there is no clear preference for one approach over the other. For the application analyzed, in which a 36-MHz transponder is divided into six 6-MHz channels, both approaches will use approximately the same mass (15 kg), but the digital processing option will require 80 W of power, while the SAW filter version requires 35 W.

The SAW filter approach has a space-qualified heritage and is considered reliable, temperature-stable, and accurately reproducible, once a successful prototype has been developed. Thus, this approach may be the desirable choice, especially for the near term, on the basis of both a smaller power requirement and a more mature technology. However, depending on the requirements of the specific application and the time frame available, the digital processing approach may offer significant advantages. Such advantages

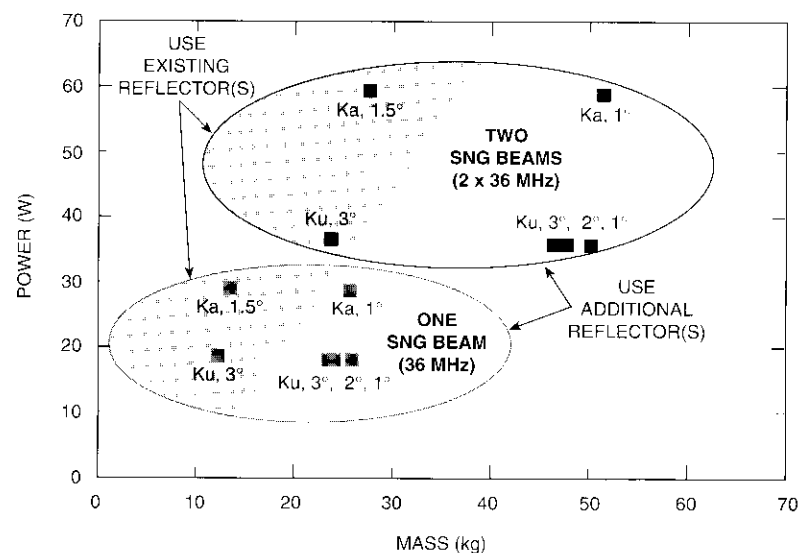


Figure 16. Summary of Payload Options

include flexibility and reprogrammability where, for example, the smallest channelization bandwidth could be reduced from 6 MHz to a smaller value, and finer resolution could be obtained for intermediate-sized channelization segments.

Another advantage of digital processing is offered by OBR. The phase 2 study demonstrated that, if the SNG downlink to the broadcast center is of high quality, then the benefits of OBR (relative to channelized AGC) in terms of increased uplink margin are relatively small—on the order of a dB or less. However, if the downlink transmission quality is not good, or the downlink requires a high fading margin, then the benefits of OBR are significant. (The use of satellite channel FEC coding on the SNG-to-broadcast-center link can also provide significant benefits. However, if OBR is used in an SNG link with FEC coding, then the OBR should include a decoding function as well as demodulation/remodulation functions.)

In the future, another factor to consider when choosing between SAW and digital processing technology for a specific application will be that both the power and mass of digital processors are likely to be reduced somewhat from the estimates given here. State-of-the-art onboard digital processors are currently under development for advanced mobile service satellites having channelization requirements far more complex than those assumed in this study. Also, INTELSAT is currently studying onboard processing that has processing requirements substantially greater than those assumed here.

Alternative implementations of the two-way auxiliary channel were also described. Whether or not it is desirable to include a transmit function on the spacecraft's SNG uplink receive antenna is highly dependent on the coverage and availability of other transponders, as well as SNG antenna subsystem design constraints.

The purpose of this study was to narrow the recommended options for elements of an SNG system design as much as possible without having access to specific payload and system requirements. The study results can be used to develop specifications for an actual SNG system and add-on payload, using the method illustrated in Figure 17. Specific steps in this process are as follows:

- Step 1.* Identify the specific spacecraft on which the SNG add-on package would be installed, and determine the power, mass, space, and mechanical configuration constraints for the SNG add-on package.
- Step 2.* Define the gross performance requirements of the SNG service to be provided, in terms of the frequency band, coverage,

transmission rate, link parameters, fade margins, and auxiliary channel requirements.

- Step 3.* Using the phase 1 results to perform transmission and link parameter tradeoffs, and the phase 2 results primarily for spacecraft subsystem mass and power estimates, refine the SNG system features originally defined in step 2 until the constraints specified in step 1 can be satisfied. Since some of these constraints may themselves represent cost and performance tradeoffs involving other spacecraft subsystem features, this process may also involve iterations and modifications of the constraints originally specified in step 1.

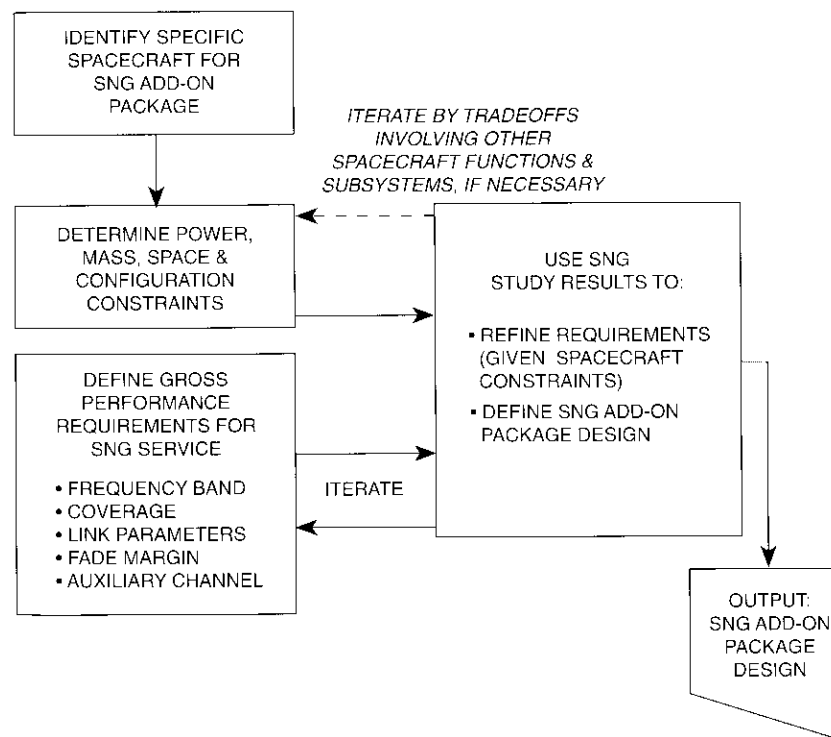


Figure 17. *Follow-On Steps*

### Acknowledgments

The contributions of A. Dissanayake, N. Mathews, and S. Sayegh are gratefully acknowledged. Dr. Dissanayake provided information on rain impairments. Dr. Mathews helped in defining modulation and multiple-access issues. Dr. Sayegh provided expert advice on onboard digital processing issues.

### References

- [1] R. C. Peach *et al.*, "SAW Based Systems for Mobile Communications Satellites," 3rd International Mobile Satellite Conference, Pasadena, California, June 1993, *Proc.*, pp. 53-58. JPL Publication 93-009.
- [2] S. Sayegh *et al.*, "An Overview of COMSAT Work in Multicarrier Demultiplexer/Demodulators," AIAA 14th International Communication Satellite Systems Conference, Washington, D.C., March 1992, *A Collection of Technical Papers*, Pt. 2, pp. 1234-1244. AIAA Paper No. 92-1971-CP.
- [3] J. J. Wengryniuk and C. A. Sederquist, "Auxiliary Digital Communications Channels for Transportable Satellite News Gathering Earth Station Coordination and Control," 9th International Conference on Digital Satellite Communications, Copenhagen, May 1992, Session B, *Proc.*, pp. 329-332.
- [4] CCIR, "Satellite News Gathering," Document CMTT/1008-E, 17th Plenary Assembly, January 31, 1990.



William A. Sandrin received a BSEE from the University of Vermont in 1963, and an MEE from Rensselaer Polytechnic Institute in 1966. From 1966 to 1971, he worked for the Boeing Company, Aerospace Group, where he was involved in space communications system design and the development of phased-array antennas. In 1971, he joined COMSAT Laboratories, where he has been engaged in multibeam antenna studies; transponder linearizer development; transmission impairments analysis; modulation and multiple-access studies; earth station design activities; propagation studies; spacecraft architecture studies; frequency coordination studies; studies of domestic, maritime, and aeronautical satellite systems; studies of adaptive phased-array antennas for spacecraft and small-terminal applications; frequency planning studies; computer modeling and simulation; and transmission software development. He is currently a Senior Scientist in the Communications Technology Division. Mr. Sandrin is a Senior Member of IEEE.

Tarek H. Abdel-Nabi received a BSEE in 1968, and an MSc degree in 1972, both from Alexandria University, Alexandria, Egypt, and a PhD in electrical engineering from the University of Ottawa, Canada, in 1982. Since joining INTELSAT in 1982, Dr. Abdel-Nabi has initiated several R&D projects which have led to the development of TCM modems at 64 kb/s and 140 Mb/s, and FEC codecs for INTELSAT digital services. His work has included the definition of communications parameters for the INTELSAT VII/VIIA and VIII series of satellites. He is currently Manager of System Planning, leading a group which analyzes and defines plans for the evolution of the INTELSAT system. The group's most recent accomplishment was the finalization of concepts for the replacement of the INTELSAT VI satellites. Dr. Abdel-Nabi is a member of IEEE.





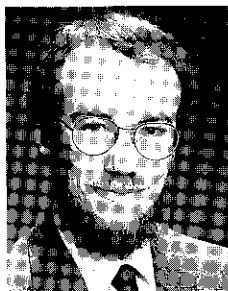
*Stephen A. Ames received a BSEE from Carnegie Mellon University in 1960, and an MSFE from Drexel University in 1964. In 1983 he completed the majority of requirements toward a PhD in electrical engineering at Arizona State University. Mr. Ames joined Space Systems/Loral (formerly Ford Aerospace Corporation) in 1985, where he has specialized in satellite communications repeater engineering. His special interest is in communications on-board processing (OBP), including satellite modems, codecs, digital demultiplexers, and SS/TDMA subsystems. He recently performed design, analysis, and simulation tasks*

*for the communications transponders on the INTELSAT VIIA, N-STAR, Globalstar, and Cyberstar programs, and conducted R&D related to various OBP concepts.*

*Prior to joining SS/L, Mr. Ames was with Motorola Government Electronics Group where he specialized in satellite communications and electronic support measures. He is a Senior Member of IEEE and the IEEE Communications Society, and a member of Eta Kappa Nu.*

*David V. Haschart received a BSEE from Ohio University in 1986 and an MSFE from the University of Toledo in 1991. He is currently a Senior Member of the Technical Staff in the Systems Studies Department of the Communications Technology Division at COMSAT Laboratories.*

*Since joining COMSAT in 1991, Mr. Haschart has worked primarily in the areas of system studies and computer modeling. In the systems area, he has been involved with comprehensive transmission analysis/trade-offs and system architecture definition for various fixed and mobile communications scenarios (including a satellite-based digital-audio distribution system, a Ka/L-band hybrid satellite-based personal communications concept, an advanced satellite newsgathering system, and various mobile satellite system configurations). In the area of computer modeling, he has been responsible for a number of computer simulations of non-geosynchronous satellite systems—examining various interference scenarios, the dynamics of system coverage, and other measures of system suitability.*



*Kent M. Price received a BS in physics from Yale University and an MS in physics from the University of Sydney, New South Wales, Australia. From 1966 to 1982, he was a member of the Radioscience Laboratory, Electrical Engineering Department, at Stanford University, where he participated in and directed a number of radioscience projects, particularly in the field of radio astronomy. He joined Ford Aerospace in 1982 in the Antenna Systems Department, where he directed a number of advanced technology development programs for IR&D and external customers. Mr. Price joined the Advanced Systems Department*

*in 1986, and has managed and been a significant technical contributor to a broad range of advanced satellite communications studies. (Ford Aerospace became Space Systems/Loral in 1989.)*

*Mr. Price is currently Program Manager for Space Systems/Loral's Future Military Communications Satellite Architecture Study, which has considered how national and international (French, U.K., and U.S.) MILSATCOM requirements can be met in the future. He was also Program Manager of the Commercial Satellite Communications Initiatives Study (1992) of mobile satellite service (MSS) systems, which proposes a commercial MSS network made up of existing and proposed MSS systems, to meet government requirements. Mr. Price is a member of AIAA and a Senior Member of IEEE.*

*Ashok K. Rao received a BTech degree in electrical engineering from the Indian Institute of Technology, Delhi, in 1984, and an MS and PhD in electrical engineering from the University of Notre Dame in 1987 and 1989, respectively. He joined COMSAT Laboratories in 1989 as a Member of the Technical Staff in the Communications Technology Division, where he is currently Manager of the Image Processing Department. He has been active in the development of algorithms and hardware for the compression of conventional and high-definition television signals, and is currently involved in developing MPEG-2 standard-based video encoders and set-top boxes. Dr. Rao has published more than 20 journal and conference articles, holds two patents, and has two others pending. He is currently serving as an Associate Editor for IEEE Signal Processing magazine.*



## ***Bandwidth on demand for the INTELSAT network***

T. R. HENDERSON

(Manuscript received January 17, 1995)

### ***Abstract***

Bandwidth-on-demand (demand-assigned multiple access) techniques have been used extensively in the design of both private satellite networks and national hybrid terrestrial/satellite networks. A new signaling protocol has been developed which will enable a new kind of bandwidth-on-demand system in the international satellite telecommunications environment.

### ***Introduction***

Since the inception of satellite communications, international circuit routes—and particularly intercontinental routes—for telephony and data have been in short supply, and hence relatively expensive. Since this situation is expected to continue into the future, several techniques and network architectures have evolved to maximize the number of telephony circuits in use per unit bandwidth of the satellite link.

International traffic has historically been dominated by voice and voiceband data such as facsimile. In terrestrial networks, a digital hierarchy has evolved based on 64-kb/s time-division multiplexing (TDM), and voice (although nominally only a 4-kHz baseband signal) has been encoded into 64-kb/s time slots. Over the past 25 years, a number of techniques related to digital speech interpolation (DSI) [1] and low-rate encoding (LRE) [2] have been developed to reduce the bit rate of voice calls. DSI takes advantage of the fact that the average activity level in a conversation is only 40 percent [3], while LRE uses a more optimized encoding technique to achieve a lower bit rate—sometimes as low as a few kilobits per second. In addition,

demodulation and remodulation are used with voiceband data to achieve bandwidth compression by transmitting the information content of the voiceband data signal in digital form. Advances in digital signal processing continue to progress these technologies.

Because the greatest speech compression gains can be achieved if the above techniques are used on an aggregate number of circuits, digital circuit multiplication equipment (DCME) has been developed and widely deployed. In DCME, a number of voice channels are compressed into a reduced number of bearers, with circuit compression ratios of up to eight or ten to one now achievable. This technique has the added advantage of spreading the effects of overload over random channels in a manner that forestalls service degradation. An overview of DCME technology has been provided by Onufry [4].

DCME should continue to be quite attractive for telephony; however, it has limited applicability to digital data traffic and requires that the gateway switch groom voice traffic for the DCME and seek alternate routes for other calls. For example, DCME is not designed to handle 384-kb/s integrated services digital network (ISDN) calls. In response, manufacturers have developed packetized circuit multiplication equipment (PCME) [5], which uses packetized voice protocols to combine voice with data traffic. As with DCME, PCME input trunks must be provisioned (and balanced) by the network operator, and the signaling designed to support such equipment does not support on-demand circuit assignment for data calls.

Circuit multiplication techniques rely on maximizing throughput for a fixed amount of bandwidth. This approach is most attractive for "thick route" traffic, that is, for routes on which the average traffic load is great enough to fully populate the input trunks to the DCME. Also, for a number of administrative reasons, it has historically been easier to approach the utilization problem from this angle. An alternative is to vary the occupied bandwidth on an as-needed basis. Called bandwidth-on-demand (BOD) or demand-assigned multiple access (DAMA), this approach can be particularly attractive for network scenarios such as "thin" routes, in which the traffic load does not justify circuit multiplication, and for routes with heavier traffic loads consisting of multirate (greater than 64-kb/s) data traffic in addition to basic rate (64-kb/s) traffic. Such a technique may prove feasible as international networks transition toward providing ISDN.

This paper presents a new signaling protocol that will enable the BOD technique to be used on the international ISDN interface. First, two existing public switched networks based on DAMA are introduced. A newly standardized signaling protocol known as International Telecommunication Union-Telecommunications Sector (ITU-T) Recommendation Q.768 [6] is then described, and some extensions to the basic BOD capabilities are elaborated

upon. An example of a network architecture that uses Rec. Q.768 signaling is provided. Finally, some thoughts are presented as to how Rec. Q.768 and circuit multiplication may evolve to complement each other in making maximum efficient use of satellite circuit capacity.

### **Existing DAMA systems in the public switched networks**

DAMA systems in the Fixed Satellite Service have been deployed in many private and public switched networks. In the public sector, such systems may be used nationally to complement the terrestrial-based network. A notable example of the use of DAMA in the public switched network is NTT's DYANET system [7]. A contrasting example is the SPADE distributed DAMA system developed by INTELSAT for public switched telephone network (PSTN) traffic.

#### **NTT DYANET**

In commercial use since 1988, DYANET was designed to carry light and variable traffic dispersed over a wide area. It is equivalent to a widely dispersed transit switch for the integration of satellite and terrestrial networks, and is used to carry overflow traffic in the NTT network. The system is engineered such that the cost of the satellite system is less than the cost of the number of terrestrial circuits needed to achieve the same probability of blocking.

Architecturally, DYANET consists of a centralized network architecture interconnecting many traffic terminals, each of which is connected to a transit switch in the PSTN. The multiple-access system used is transponder-hopping, demand-assigned, time-division multiple access (TDMA), and the network control center (NCC) is integrated into the common channel Signaling System 7 (SS7) network. Call control at the NCC employs "farthest-end routing" to ensure that the traffic terminal closest to the destination subscriber is selected, and "alternative routing" to ensure network diversity in coping with propagation outages. Figure 1 illustrates the signaling relationship between the SS7 network, the national transit switches, two communications satellites, and the network control system (NCS). In addition to providing flexibility and reliability for the national network, DYANET has been an economic success as a complementary system to the terrestrial network [7].

#### **INTELSAT SPADE**

In contrast to DYANET, INTELSAT SPADE [8] was developed as a distributed DAMA system for PSTN traffic. In addition to being one of the first digital satellite systems, SPADE was also the first DAMA system to be implemented.

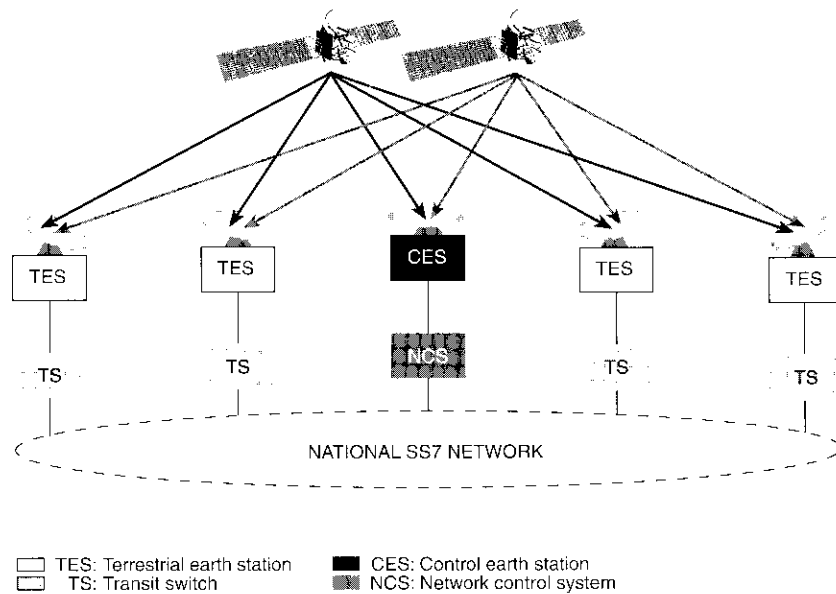


Figure 1. Signaling Relationships in DYANET [6]

SPADE is based on single-channel-per-carrier (SCPC) frequency-division multiple access (FDMA), providing demand assignment with distributed control. In the SPADE system, incoming call requests are provisionally assigned to a pair of transmit/receive frequencies, and a call request is put through to the destination station via a common signaling channel (CSC). If the destination station does not detect any contention for the requested frequencies, the request is acknowledged and all of the stations in the system will avoid seizing the frequencies until they are released by the participating stations. If contention arises during a call request, the contending stations register a "busy" on the frequencies and try a new request on a different frequency pair.

Figure 2 illustrates the signaling relationship between the international signaling network, the gateway international switching center (ISC), and the SPADE terminal. SPADE was designed to handle a number of signaling systems, including ITU-T [formerly International Telephone and Telegraph Consultative Committee (CCITT)] signaling systems 1: R2, 4, 5, and 5bis. INTELSAT SPADE was operational for over a decade, but was ultimately unsuccessful, due in part to relatively high terminal expense as compared to DCME-based solutions.

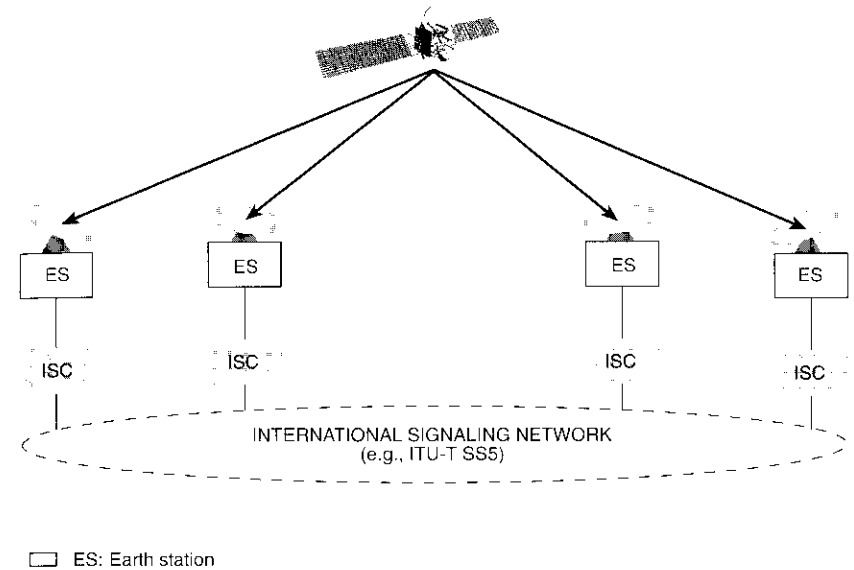


Figure 2. Signaling Relationships in INTELSAT SPADE

While SPADE is attractive from the standpoint of distributed control, it relies on international signaling information being available at the satellite terminals (which is not often the case for out-of-band signaling such as SS7), and it is not well designed to handle multirate ISDN calls. Although a DYANET-like architecture could be technically feasible for providing multirate 64-kb/s DAMA in the INTELSAT system, administrative constraints would preclude the INTELSAT system from functioning as a signaling code point in the international SS7 network. Hence, a new satellite architecture has been developed in which the satellite network is not integrated into the SS7 network and does not rely on signaling information being available at the earth station (*i.e.*, it does not perform switching), but in which satellite bandwidth is dynamically used to connect fixed correspondent trunk pairs. The signaling interface for this architecture has been standardized as Rec. Q.768 [6].

**Bandwidth-on-demand based on Rec. Q.768 signaling**

The basic function of Rec. Q.768 signaling is to inform an earth station when a trunk circuit is being put into use. Upon receiving such a request, the

satellite system assigns unused bandwidth and interconnects the correspondent trunk pairs. The architecture offers higher system utilization than a pre-assigned system, at the expense of a probability of blocking which can be engineered to the desired low level. Rec. Q.768 allows interaction between the gateway ISC and the satellite connection manager (SCM) in the traffic terminal. Rec. Q.768 is not part of SS7, nor does it require any protocol changes to the existing signaling network. The satellite network performs no switching, since all inter-ISC correspondent trunk pairs are fixed; however, the satellite circuits are tied to the trunk pairs on an on-demand basis. Figure 3 depicts a Rec. Q.768-based satellite system from a signaling standpoint.

Rec. Q.768 defines a signaling interface across which a number of standardized protocols are employed to perform different functions. Figure 4 illustrates the protocol relationship between Rec. Q.768 and SS7. The message transfer part (MTP) forms a reliable transport system for signaling packets. The ISDN user part (ISUP) protocol [9] is the application protocol that allows call control functions in a network to set up, release, and maintain circuits and calls. The satellite ISDN user part (SIUP) is similar to the ISUP, but is specifically tailored to support satellite circuits and is much less complex. A simplified version of the MTP for small systems, Rec. Q.710 [10], is used to deliver messages reliably between the network elements. The call control processes at the ISC and SCM employ the protocols defined by Rec. Q.768 to coordinate the on-demand insertion and removal of satellite channels.

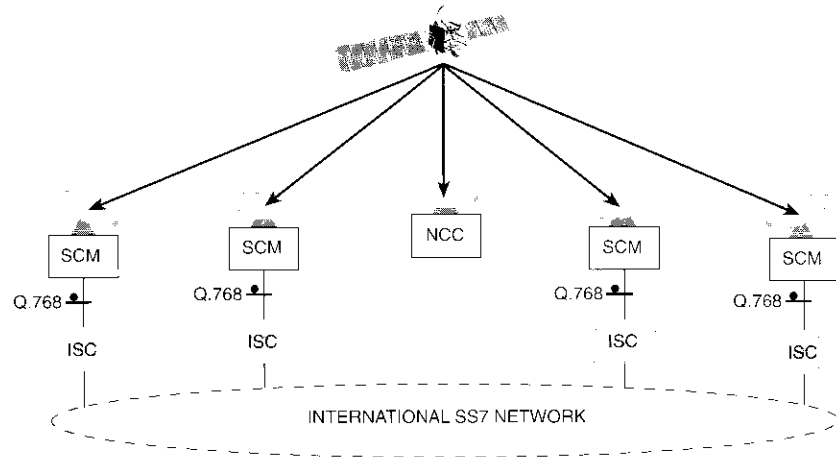


Figure 3. Signaling Relationships Between Network Elements Based on Rec. Q.768

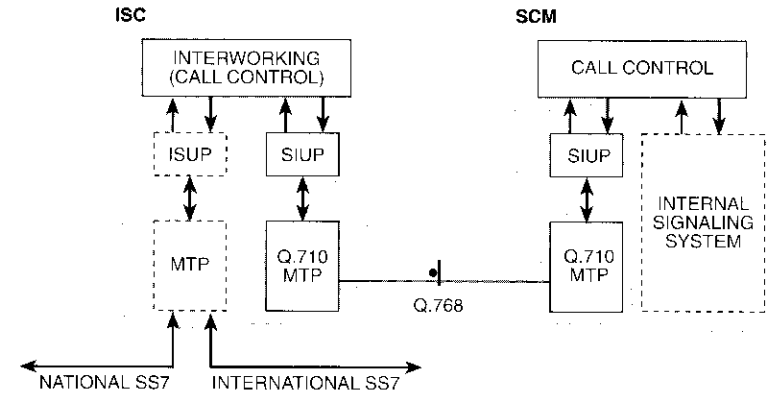


Figure 4. Protocol Architecture of Rec. Q.768

The example in Figure 5 shows how Rec. Q.768 signaling relates to SS7 signaling. SS7 system elements and messages are shown with solid lines, and Rec. Q.768 signaling and elements are shown with dashed lines. The receipt of an Initial Address Message (IAM) at an outbound ISC initiates the circuit selection process within the ISC. If a satellite route served by Rec. Q.768 is selected, the ISC forms an SIUP Setup message and sends it to the SCM. The call control of the satellite network then attempts to assign a circuit to the channel. If successful, the SCM returns a Setup Acknowledge message to the ISC and begins to set up the satellite path. Upon receipt of this positive acknowledgment, the ISC forwards the IAM to the destination international exchange. After information transfer is complete, the ISC will receive a Release (REL) message. It then forwards an SIUP Release message to the SCM, and the satellite network returns the circuit to the DAMA pool.

This approach to on-demand circuit setup does not require changes to the SS7 protocols, but does require that the ISC modify its call control procedures. International exchanges are not accustomed to holding an IAM while an additional network is polled for its bandwidth availability. Even though Rec. Q.50 [11], which specifies signaling for control of DCME, suggests that the ISC hold the IAM whenever a clear channel is seized through the DCME, ISCs typically do not do this in practice, since bits can be robbed from voice channels in the overload scenario if necessary. The IAM should be held in the Rec. Q.768 case, however, since if the ISC assumes that bandwidth is available and forwards the request—and the call subsequently cannot be assigned bandwidth—no overload procedures exist and there is a high probability that the call attempt will

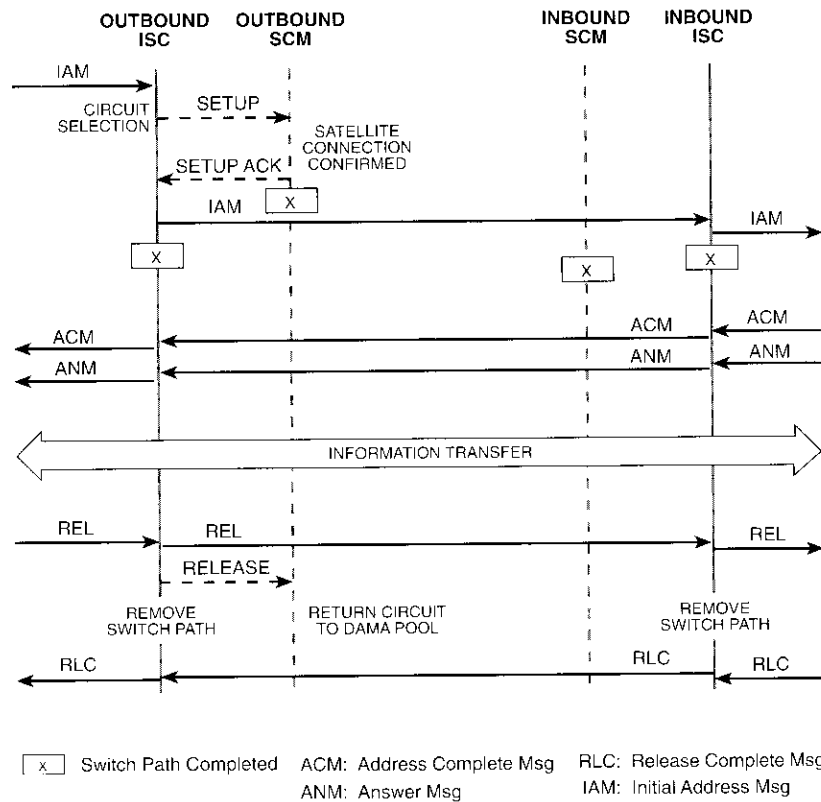


Figure 5. Example of the Relationship Between Rec. Q.768 and SS7 Signaling Flows

be lost. An alternative to holding the IAM is to provide ISCs with dynamic load information as to circuit availability; however, this would place additional processing burdens on ISCs. Based on these considerations, it was decided to allow the satellite subnetwork up to 1 second to reply to a Rec. Q.768 Setup message. This interval allows for the possibility of centralized call acceptance, although in practice there will be some advantages to performing distributed call acceptance at the SCMs and minimizing the IAM holding time.

Although holding an IAM does not cause any ISUP-related protocol timers to expire, it does increase the post-dialing delay of call setup, and thus there is interest in expediting the call-acceptance decision. Once the call has been

accepted, this information can be relayed to the ISC so that SS7 call setup can proceed in parallel with satellite circuit setup.

### Additional features of Rec. Q.768 signaling

Rec. Q.768 is based on a 64-kb/s link between the ISC and the SCM. This communications link has much greater capacity than is required for the simple request/release of ISDN circuits. Rec. Q.768 has been defined to further utilize this signaling capacity by including protocol information in its messages. This capability can be exploited to perform other useful functions in addition to simple call setup and release.

### Protocol conversion

Certain data communications protocols are subject to throughput and delay degradation when operated over the satellite link. This degradation is due to both the protocol semantics (which may incorporate procedures that do not work well over long round-trip delays) and the protocol syntax (which may not have enough space in the protocol fields to accommodate the coding of satellite-efficient parameters). An example is Rec. X.75 [12], which incorporates a go-back-N procedure at the link layer, and which in many implementations can accommodate a maximum window size of only seven data frames. Both of these characteristics can cause throughput degradation when the protocol is operated over a satellite link. Kaul [13] discusses this problem in detail.

In the ISDN, SS7 signaling can carry identifiers for the particular in-band protocols in use across the link. With knowledge of the protocols being used by the end terminals, the satellite network can insert protocol converters into the circuit to improve the user-perceived throughput and delay. This conversion can be made transparent to the end user. Figure 6 illustrates some of the throughput gains that can be achieved by substituting a satellite-efficient selective retransmission protocol for a go-back-N protocol across the satellite link.

The Rec. Q.768 Setup message is defined to carry such protocol identifiers to the SCM so that conversion can be performed if appropriate. The international gateway switch simply extracts the relevant SS7 signaling information and sends it to the SCM, where it is interpreted. If the protocol being used is one that could benefit from conversion (such as X.75 or Group 4 Facsimile [14]), and if the SCM has an appropriate converter available, the SCM attempts to set up the call with protocol conversion. The insertion and removal of

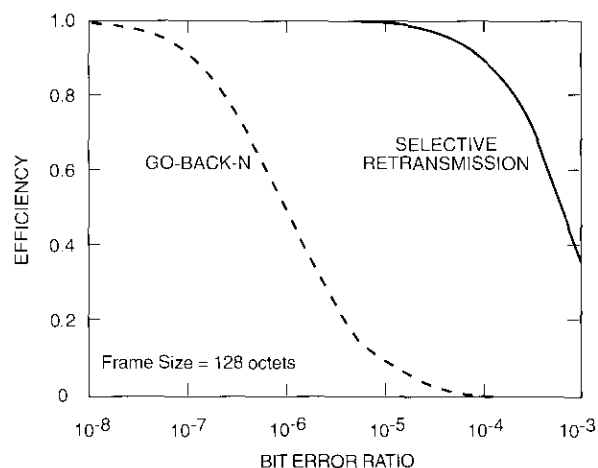


Figure 6. Throughput Efficiency Benefits of Protocol Conversion

protocol conversion across the satellite network is coordinated via internal signaling.

#### Packet/frame concentration

Packet/frame concentration techniques also can be used to achieve further statistical gains. For example, data frames from a number of different connections can be statistically multiplexed onto a common channel. This approach is efficient for thin-route traffic if each station can receive the aggregate channel and extract only those frames addressed to it. When a new data call is requested, the SCM can examine the protocol information contained in the Rec. Q.768 Setup message and consider assigning the call to an existing multiplexed channel.

#### Integration with circuit multiplication

Packet/frame concentration is very similar to the data handling capability of PCME. This highlights the fact that equipment providing DAMA based on Rec. Q.768 may eventually evolve to encompass circuit multiplication techniques as well, or that next-generation PCME could include a Rec. Q.768 interface. As Figure 7 illustrates, Rec. Q.768 was initially specified as being separate from circuit multiplication equipment (CME) traffic, to avoid disturbing existing implementations of CME. However, since Rec. Q.768 is capable of supporting the CME signaling traffic requirements [11], it could be used to

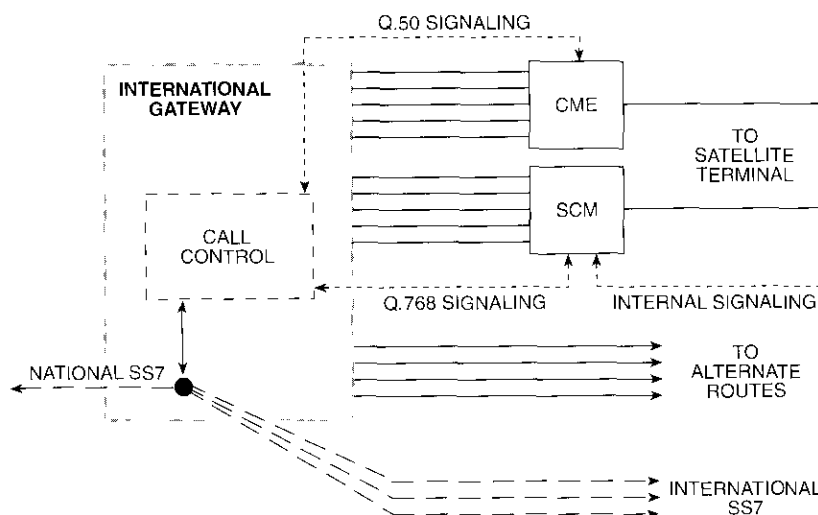


Figure 7. Independence of CME and SCM

reduce the number of signaling interfaces that must be supported at the international gateway exchange. Figure 8 shows the potential evolution of satellite transmission equipment to incorporate both circuit multiplication techniques for voice and packet data calls, with the added efficiency of on-demand circuit assignment to account for variations in overall traffic intensity.

#### On-demand network architecture using Rec. Q.768

Figure 5 illustrated the Rec. Q.768 signaling flow for call setup, but did not show the internal signaling needed to complete the satellite channel assignment. Figure 9 provides one example of how Rec. Q.768 could be used to design the signaling information flows of an on-demand satellite network. The scenario of Figure 5 is depicted from the satellite network perspective. SS7 system elements and messages are indicated by dashed lines, and Rec. Q.768 signaling and network elements, along with internal signaling, are indicated by solid lines. In this example, centralized control is used, and an NCC coordinates the channel assignments. When the SCM receives a Rec. Q.768 Setup message, it relays the signaling information to the NCC via a satellite IAM. In this case, the NCC is able to assign suitable network capacity to the call and forwards the circuit assignment to the inbound (originating) SCM via the IAM, and to the outbound (destination) SCM via the Answer message (ANM). The

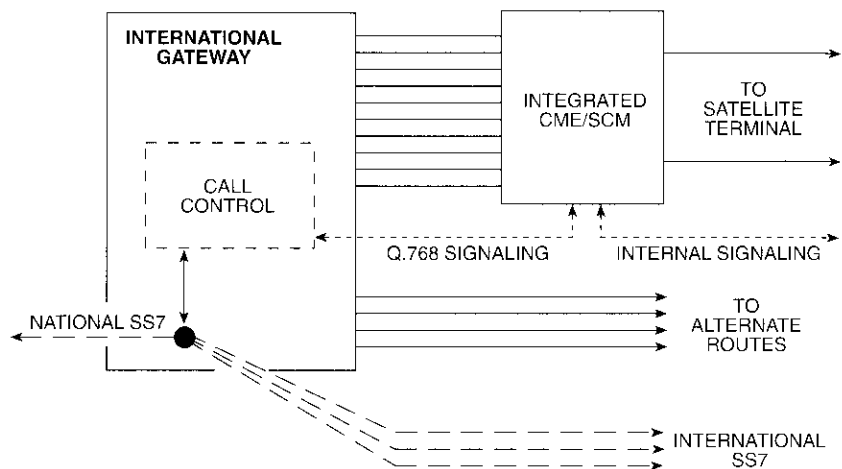


Figure 8. Circuit Multiplication Integrated With Rec. Q.768 Signaling

inbound SCM acknowledges the assignment with its own ANM. If the circuit assignment had been unsuccessful, the NCC would have sent a Release message to the outbound SCM, which would have followed with a Rec. Q.768 Release message indicating no network capacity. The ISC would then have had to consider an alternate route for the call.

In Figure 9, SS7 signaling flows (dashed lines) occur in parallel with internal satellite signaling. Note, however, that the SS7 IAM is not relayed to the inbound ISC until a Rec. Q.768 Setup Acknowledge is received from the satellite network.

#### Advance notification

Because the wait incurred in querying for bandwidth availability (while nominally less than 1 s) will add to the post-dialing delay of the user, some administrations may want to obtain an earlier acknowledgment of the call setup. A satellite network can be designed to offer advance notification to the ISC, based on circuit availability information disseminated from the NCC. In Figure 9, the signaling flow would be modified by placing the Rec. Q.768 Setup Acknowledge above the internal IAM signaling. Two drawbacks of this approach are that it introduces the possibility of erroneous decisions at the SCM due to the latency of the distributed information, and an extra internal signaling load is incurred. A tradeoff exists between the granularity of the control information (*e.g.*, how often it is updated and how much information

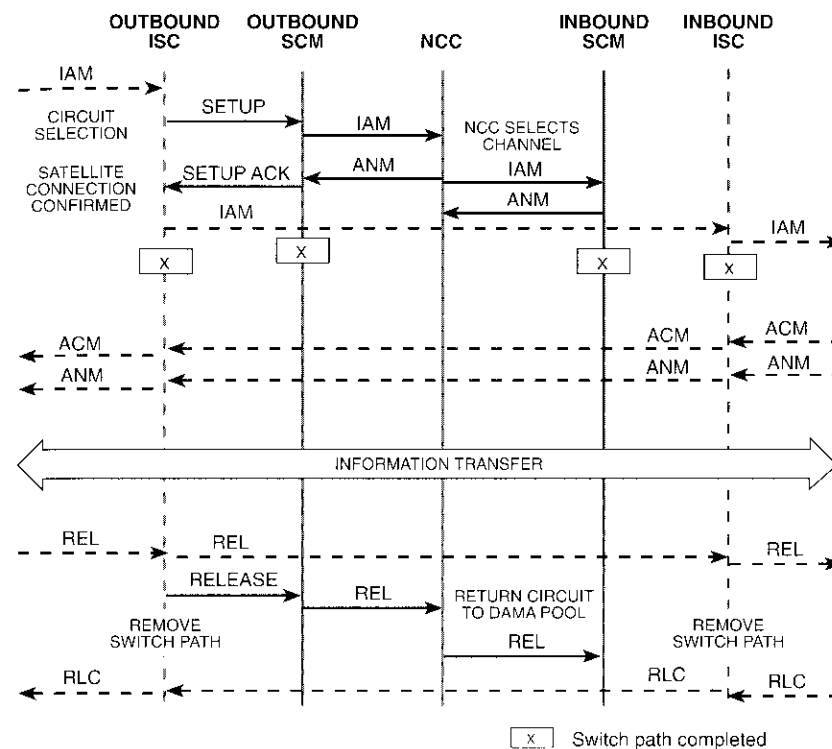


Figure 9. Example of an On-Demand Signaling System Based on Rec. Q.768

is conveyed) and the load on the internal signaling system. However, by strategically determining when to provide advance notification (*e.g.*, when the system load is light) and when to forward the request to the NCC (*e.g.*, when the load is heavy), the probability of an incorrect decision can be reduced to acceptable levels.

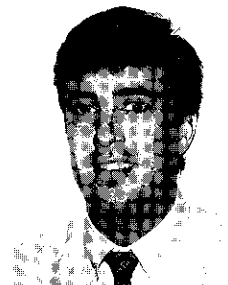
#### Conclusions

The implementation of ITU-T Recommendation Q.768 will permit the development of a new kind of DAMA satellite architecture in a common channel signaling environment. A new INTELSAT network architecture based on this signaling interface will allow dynamic bandwidth assignment for the whole range of ISDN connection types.

BOD circuit assignment offers an alternative to circuit multiplication for efficient satellite capacity assignment. A key challenge in the use of BOD will be to determine how it can be optimally combined with packet and circuit multiplication to provide the most flexible and efficient ISDN service.

## References

- [1] S. Campanella, "Digital Speech Interpolation." *COMSAT Technical Review*, Vol. 6, No. 1, Spring 1976, pp. 127-158.
- [2] CCITT Rec. G.726, "40, 32, 24, 16 kbit/s Adaptive Differential Pulse Code Modulation (ADPCM)," Geneva, Switzerland, 1991.
- [3] ITU-T Rec. G.763, "Digital Circuit Multiplication Equipment Using ADPCM (Rec. G.726) and Digital Speech Interpolation." Geneva, Switzerland, latest version published 1994.
- [4] M. Onufry *et al.*, "DCME in the INTELSAT VI Era." *COMSAT Technical Review*, Vol. 22, No. 1, Spring 1992, pp. 19-55.
- [5] ITU-T Rec. G.765, "Packet Circuit Multiplication Equipment," Geneva, Switzerland, 1993.
- [6] Draft ITU-T Rec. Q.768, "Signalling Interface Between an International Switching Center (ISC) and an ISDN Satellite Subnetwork." COM 11-R X, Geneva, Switzerland, 1994.
- [7] M. Ohnuki *et al.*, "A New Satellite Communication System Integrated into Public Switched Networks—DYANET." *IEEE Journal on Selected Areas in Communications*, Vol. 10, No. 2, February 1992, pp. 447-464.
- [8] J. Puente and A. Werth, "Demand-Assigned Service for the INTELSAT Global Network." *IEEE Spectrum*, January 1971, pp. 59-69.
- [9] ITU-T Rec. Q.764, "ISDN User Part." Geneva, Switzerland, latest version published 1994.
- [10] CCITT Rec. Q.710, "Simplified MTP Version for Small Systems." Geneva, Switzerland, 1988.
- [11] ITU-T Rec. Q.50, "Signalling Between Circuit Multiplication Equipment (CME) and International Switching Centres (ISC)," Geneva, Switzerland, latest version published 1994.
- [12] ITU-T Rec. X.75, "Packet-Switched Signaling System Between Public Networks Providing Data Transmission Services," Geneva, Switzerland, latest version published 1993.
- [13] A. K. Kaul, "Performance of High-Level Data Link Control in Satellite Communications," *COMSAT Technical Review*, Vol. 8, No. 1, Spring 1978, pp. 41-87.
- [14] CCITT Rec. T.90, "Characteristics and Protocols for Terminals for Telematic Services in ISDN." Geneva, Switzerland, latest version published 1992, pp. 41-87.



*Thomas R. Henderson received the BS and MS degrees in electrical engineering from Stanford University in 1990 and 1991, respectively. From 1991 to 1995 he was a Member of the Technical Staff in the Network Systems group within the Network Technology Division at COMSAT Laboratories. During that time, he worked on several INTELSAT and NASA system architecture studies, participated in a number of satellite ATM demonstrations and field trials, and represented COMSAT at national and international standards meetings. He served as vice-chairman of the ATM/ATM sub-working group of standards committee TISI; as Rapporteur for Q.29/13, "Integration of Satellites With the Terrestrial ISDN and B-ISDN," within ITU-T Study Group 13; and as editor of several ANSI and ITU-T standards. He is currently pursuing a PhD in electrical engineering at the University of California, Berkeley.*

## ***Acoustic echo control considerations for video teleconferencing***

C. S. RAVISHANKAR AND M. ONUFRY

(Manuscript received March 24, 1995)

### ***Abstract***

The occurrence of acoustic echo in video teleconferencing environments that employ satellite links is analyzed, and alternative measures are recommended for alleviating the condition. The echo problem is analyzed for point-to-point and point-to-multipoint configurations representing the different network scenarios typically encountered in video teleconferencing applications. The echo control measures recommended are directed toward providing the greatest end-user satisfaction with minimal impact on total system cost.

### ***Introduction***

Acoustic echoes are generated in a video teleconferencing (VTC) environment as a result of the feedback path provided between the loudspeaker and the microphone at the customer premises. This path can be direct or indirect, or both, depending on the orientation of the loudspeaker and microphone. In general, the characteristics of the acoustic echo path (typically described by its impulse response, assuming the path is linear) are significantly different from those of the echo path provided by the hybrid and associated circuitry (often referred to as the network echo path) in the public switched telephone network (PSTN).

An acoustic echo path tends to exhibit a reverberating (slowly decaying) impulse response characteristic, while a network echo path tends to exhibit a nondispersed (rapidly decaying) impulse response characteristic. This indicates that the impulse response duration of acoustic echo is significantly

longer than that of network echo. Consequently, echo cancellers designed for acoustic echo control should have a much wider processing window (a larger number of coefficients) than those designed for network echo control. This requirement is further exacerbated by the fact that the audio bandwidth used in videoconferencing applications is much wider than that used in telephony. In a telephone network, speech is typically band-limited at about 3,400 Hz at the higher end of the spectrum. For VTC applications, bandwidths on the order of 7 kHz or more are usually preferred. Therefore, the sampling rate used for input speech should be more than twice that used for speech over the telephone network—and consequently the impulse response of the echo path should be modeled with more than twice the number of coefficients.

An echo canceller for acoustic echo control must perform a convolution between the input speech samples and the coefficients of the adaptive filter (both of which are twice as long as those encountered in network echo control for the same processing window size) in half the time (due to doubling of the sampling rate) required in network echo control. This combination of a wider processing window and reduced processing time means that the requirements for an acoustic echo control device differ significantly from those for a PSTN echo control device.

The use of VTC is increasing, and it is often used to interconnect facilities within a local area. With success comes the desire to add more locations that are often further away. As the distance and resulting propagation delay increase, the problems of acoustic echo control in the VTC environment become more complex and more difficult to resolve because additional attenuation of the echo is required. This paper examines several aspects of VTC system performance that are directly affected by the complexity of an expanding VTC network.

Highlights of the nature and perception of acoustic echo typically experienced in VTC applications are presented first, followed by observations based on the analysis of point-to-point and multipoint VTC configurations. An alternate set of recommendations is then outlined which is aimed at providing the greatest satisfaction to the end user with minimal impact on total system cost. Details of the analyses for point-to-point and multipoint VTC configurations are provided in an Appendix.

### **The acoustic echo problem**

To understand the problem of echo in VTC applications, including its perception by the end user, it is important to first examine the conditions under which such problems are noticeable. Figure 1 is a highly simplified

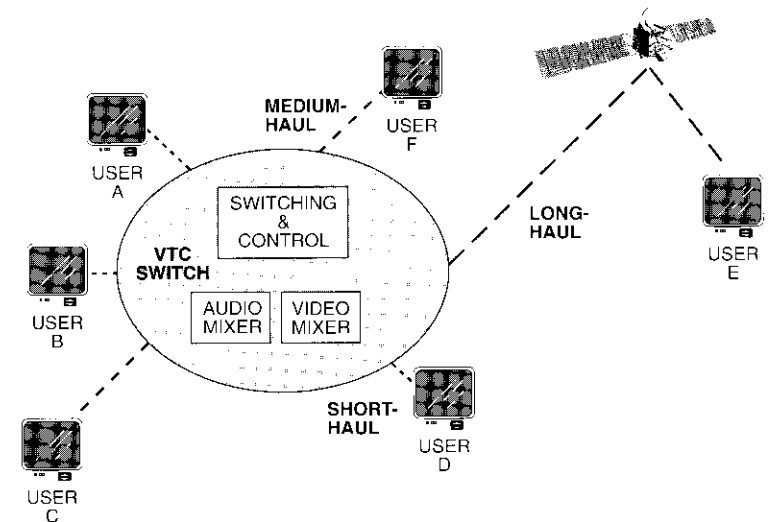


Figure 1. Typical VTC Network Configuration

diagram of a generic VTC network. The VTC terminals can be linked to the switch via short-haul, medium-haul, or long-haul links, depending on the geographical separation between the terminals and the switch. Further, one or more of these links could be a trunk that interconnects one or more VTC networks. The level of echo that a user can tolerate depends directly on the type of links connected to the switch, and on the acoustic echo return loss (AERL) at each customer's premises. Several studies have shown that the echo level that can be tolerated by a user decreases almost exponentially as the delay encountered by the echo in the network increases [1],[2]. That is, for acceptable performance, the amount of echo attenuation necessary for tolerable performance increases with delay.

Figure 2 is a plot of the minimum echo attenuation necessary for just-tolerable conditions to prevail, as a function of round-trip delay. The curve shows the average tolerance of a large sample of listeners to talker echo, although individuals may have a slightly different tolerance curve. The data indicate that echoes are most objectionable when the amount of echo attenuation is significantly less than that required for a given amount of delay. For example, referring to Figure 1, the amount of echo attenuation necessary when any combination of users A, B, and D are engaged in a VTC is less than that necessary when C, E, or F is one of the participants.

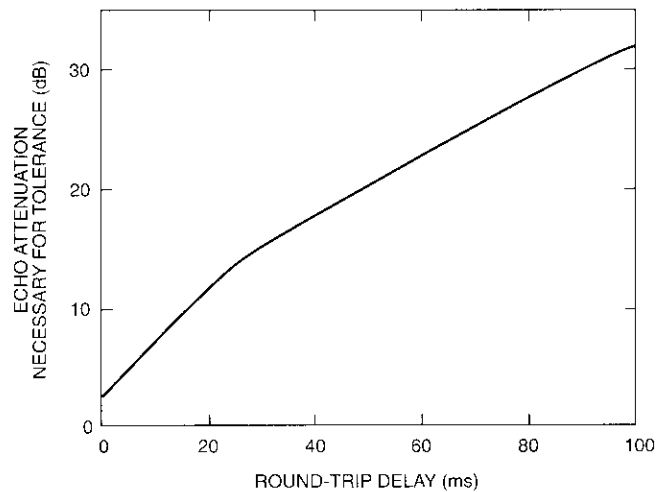


Figure 2. Average Tolerance of Echo

Apart from its switching and control functions, the VTC switch also performs video mixing and audio mixing to cater to multiple-user teleconferencing. Video mixing allows a user to watch all other users simultaneously on the video monitor in a split-screen configuration, and audio mixing permits a user to listen to all other users when talking simultaneously. Since the operation of the audio mixer plays a critical role in the nature of acoustic echoes and their perception by the user, the operation of a typical audio mixer will be briefly described.

**The audio mixer**

Figure 3 diagrams a generic audio mixer with four inputs and outputs. As mentioned with respect to Figure 1, the inputs could be from a local VTC terminal or from a trunk carrying traffic from a different VTC network. Here, audio signals from three users are combined and transmitted to the fourth user. It should be noted that although Figure 3 shows four inputs and outputs from four users (commonly referred to as "quad" operation), the basic operation of the audio mixer is the same for any number of users. If  $N$  users are engaged in a VTC, then the audio signal received by any user is a combination of the signals of all the other  $N - 1$  users. For example, in a point-to-point operation where only two users are engaged in a VTC, each receives the audio signal generated by the other. An audio mixer is referred to as lossless if it combines the input signals without introducing any loss to the signals, and lossy if it

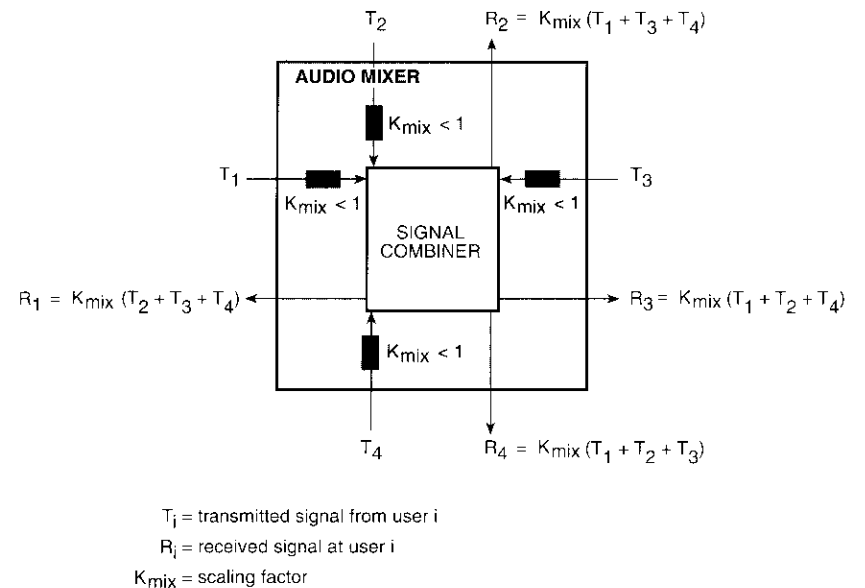


Figure 3. A Generic Audio Mixer

introduces a loss to each signal and then combines them. For the lossy mixer shown in Figure 3, the combiner is such that

$$R_i(t) = \sum_{\substack{j=1 \\ j \neq i}}^4 K_{mix} T_j(t); \quad i = 1, 2, 3, 4 \quad (1)$$

where  $R_i$  is the speech signal received by user  $i$ , and  $T_j$  is the speech signal from talker  $j$ . The introduction of loss,  $K_{mix}$ , is usually motivated by the need to align the network in terms of acceptable signal levels and avoid possible instabilities, or "singing," of echoes generated in the network.

**Echo perception in a VTC network**

A number of parameters that contribute to the auditory perception of a VTC network are analyzed in the Appendix. The parameters considered include delay, AERL, listening level, talking level, and loss introduced by the audio mixer. Point-to-point and multipoint operating modes are considered separately. The results of the analysis are summarized below, and the reader is referred to the Appendix for their derivation. It should be noted that the analyses in the

Appendix deal only with the effects of direct acoustic echo path. The following symbols, used in the Appendix, are also used in discussing the observations presented here:

- $\tau_i$  = delay encountered by a signal originating from user  $i$  in reaching the audio mixer
- $t_{di}$  = delay encountered by the acoustic signal in traversing from the loudspeaker to the microphone at the premises of user  $i$
- $AERL_i$  = acoustic echo return loss at the premises of user  $i$
- $L_{mix}$  = loss (in dB) introduced by the audio mixer to each of the input signals before they are combined ( $20 \log K_{mix}$ ).

**Point-to-point configurations**

Figure 4 diagrams a point-to-point configuration where user 1 is engaged in a VTC with user 2. The analysis presented in the Appendix led to the following observations regarding the impact of  $\tau_i$ ,  $t_{di}$ ,  $AERL_i$ , and  $L_{mix}$  on the echo level perceived by the VTC participants:

- Echo can be objectionable if the attenuation of the first talker/echo reflection of user 1, after  $2\tau_1 + 2\tau_2 + t_{d2}$  time units, is less than that specified by the curve in Figure 2. Similarly for user 2, echo can be objectionable if the attenuation of the first talker/echo reflection, after  $2\tau_1 + 2\tau_2 + t_{d1}$  time units, is less than that specified by the curve in Figure 2.
- Subsequent echo reflections can be objectionable if the rate of increase of echo attenuation as a function of delay (*i.e.*,  $2L_{mix} + AERL_1 + AERL_2$ )/ $2\tau_1 + 2\tau_2 + t_{d1} + t_{d2}$ ) is less than that required for the dashed line shown in Figure 5 to stay above the curve shown in Figure 2.
- Tolerable echoes can be maintained by proper adjustment of  $L_{mix}$ ,  $t_{di}$ , and  $AERL_i$ .
- The rate of decrease of talker echo levels heard by both users subsequent to the first reflection is the same, regardless of how far or close each user is to the switch, and the individual room acoustics.
- Echo control will be necessary whenever the echo attenuation is significantly less than that specified by the curve in Figure 2. This is especially true when one or both users are connected via a

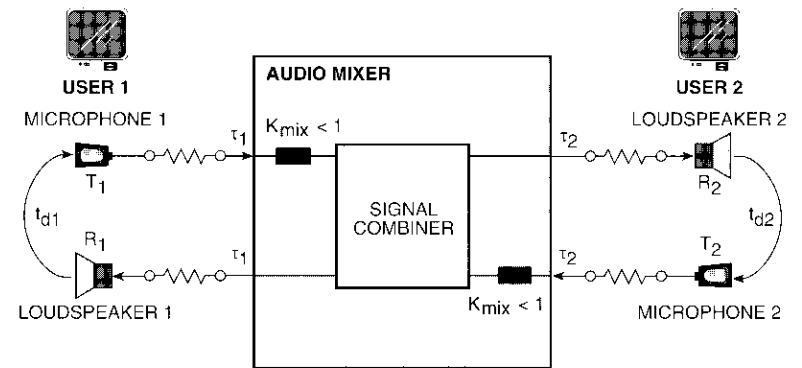


Figure 4. Schematic of Signals in a Point-to-Point Configuration

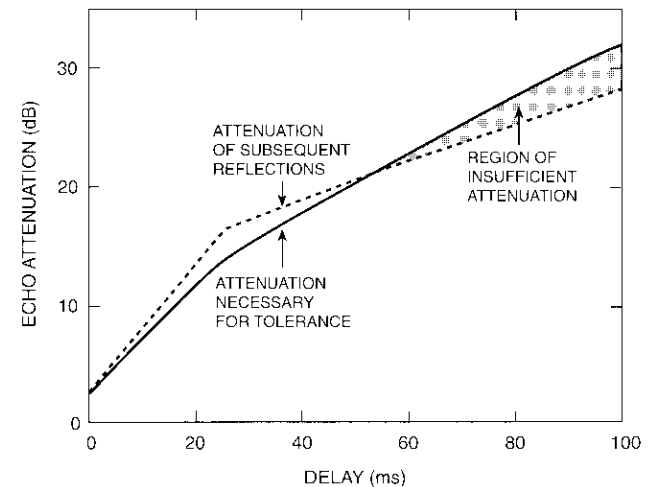


Figure 5. Echo Attenuation vs Delay for a Point-to-Point Configuration

long-distance link, since for fixed values of  $L_{mix}$ ,  $t_{di}$ , and  $AERL_i$ , the echo attenuation required for large values of  $\tau_i$  is far greater than that for small values of  $\tau_i$ .

- The problem of echo can be more severe with lossless mixers ( $L_{mix} = 0$  dB). Under such circumstances, the network requirements regarding the minimum values of  $AERL_i$  and maximum values of  $\tau_i$  and  $t_{di}$  will be more stringent.
- It is advisable to use lossy mixers to maintain the alignment of signal power levels and operate the network in tolerable echo regions.

The analyses implicitly assumed that talking and listening levels at the individual premises were adjusted to normal and comfortable levels. However, it is not unusual for teleconference participants to want to adjust signal levels and, when the controls are accessible, to do it frequently. While the reasons may be legitimate (e.g., unexpected background noise, a soft talker, or a participant with a hearing impairment), the effects on echo levels of adjusting loudspeaker or microphone gain are usually not fully understood by those making such adjustments.

IMPACT OF LOUDSPEAKER GAIN ON ECHO LEVELS

If the loudspeaker gain at the premises of user 1 (as shown in Figure 6a) is increased beyond nominal levels by  $G_{R1}$  dB (where  $G_{R1} = 20 \log K_{R1}$ ), the following consequences can be anticipated based on the analysis presented in the Appendix.

Increasing the gain of the loudspeaker at the premises of user 1 will decrease the attenuation of the first reflected talker echo of both users by  $G_{R1}$  dB; or equivalently, the level of the first reflected talker echo of both users increases by  $G_{R1}$  dB. While both users are affected equally in terms of echo levels, their perceptions can differ. Assuming that both are speaking at approximately the same level, during a double-talk situation the ratio of desired signal to echo level is unaffected for user 1 (see equation A-9), whereas for user 2 the desired level degrades by  $G_{R1}$  dB (equation A-10). Hence, increasing the loudspeaker gain of user 1 has a more negative impact on user 2 than on user 1 in this situation.

For both user 1 and user 2, the attenuation in subsequent reflections will be the same and is equal to  $2L_{mix} + AERL_1 - G_{R1} + AERL_2$  dB. Subsequent reflections will occur every  $2\tau_1 + 2\tau_2 + t_{d1} + t_{d2}$  time units. As a result, the rate of increase of the attenuation of echo reflections decreases compared to when  $G_{R1}$  was zero. This implies that the echo attenuation could fall below the tolerance curve of Figure 2 for the given amount of delay.

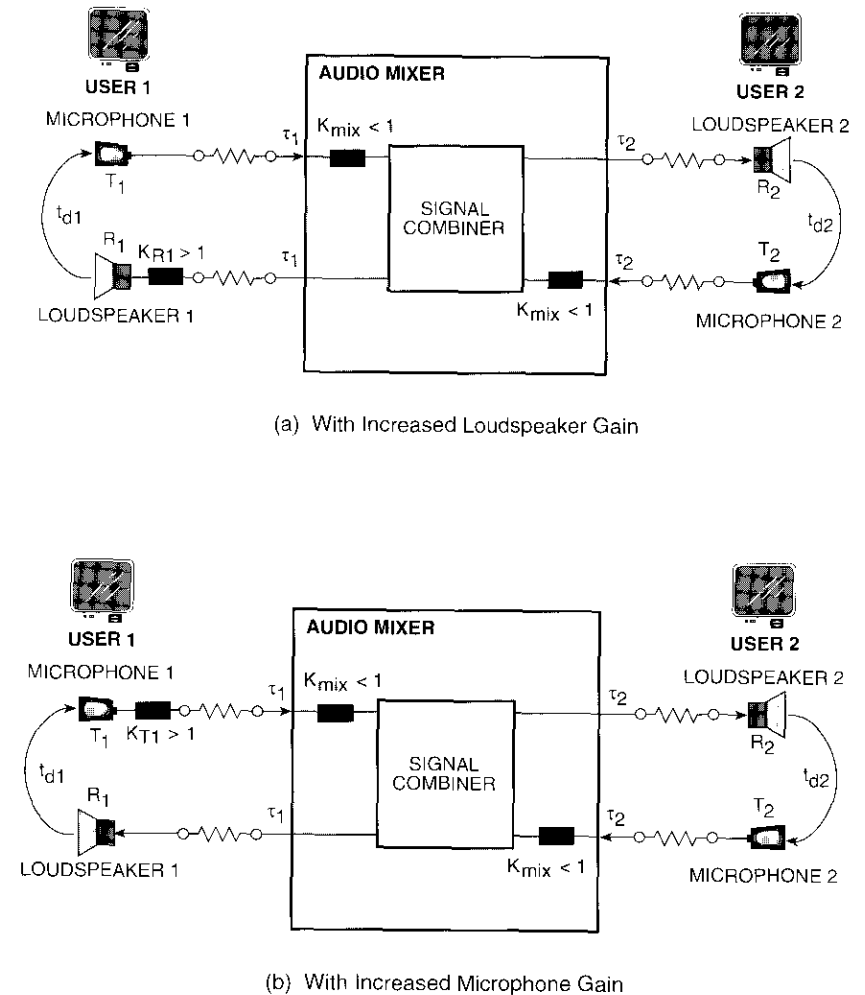


Figure 6. Schematic of Signals in a Point-to-Point Configuration With Increased Gain

IMPACT OF MICROPHONE GAIN ON ECHO LEVELS

If the microphone gain at the premises of user 1 (as shown in Figure 6b) is increased beyond nominal levels by  $G_{T1}$  dB, where  $G_{T1} = 20 \log K_{T1}$ , several consequences can be anticipated based on the analysis presented in the Appendix. First, increasing the gain of the microphone at the premises of user 1 will decrease the attenuation of the first reflected talker echo of both users by  $G_{T1}$  dB; or equivalently, the level of the first reflected talker echo of both users will increase by  $G_{T1}$  dB. During a double-talk situation, the ratio of desired signal to echo level is degraded for user 1 by  $G_{T1}$  dB (see equation A-12), whereas for user 2 the desired level is unaffected (equation A-13). Hence, increasing the microphone gain of user 1 has a more negative impact on user 1 than on user 2 during double-talk situations.

For both user 1 and user 2, the attenuation in subsequent reflections will be the same and is equal to  $2L_{mix} - G_{T1} + AERL_1 + AERL_2$  and will occur every  $2\tau_1 + 2\tau_2 + t_{d1} + t_{d2}$  time units. Consequently, the rate of increase of attenuation of echo reflections decreases compared to when  $G_{T1}$  was zero. This implies that the echo attenuation could fall below the tolerance curve of Figure 2 for the given amount of delay.

While the impact of increasing loudspeaker gain and microphone gain beyond nominal levels is to increase echo levels, decreasing the loudspeaker and/or microphone gain below nominal levels can improve the echo situation. While this rule of thumb can be used in certain situations when noticeable echoes are heard, the extent to which the gain can be reduced below normal levels is limited in practice by the hearing ability of the users and the ambient noise in the VTC room.

**Multipoint configuration**

Once point-to-point VTC has been successfully accomplished, the next step is to expand to multipoint teleconferencing. This involves three or more locations simultaneously participating in the teleconference. For simplicity, the minimum-size multipoint configuration will be considered.

Assuming that users 1, 2, and 3 are engaged in a VTC, as shown in Figure 7, the analysis given in the Appendix reveals that the initial reflection of the talker echo of user 1 arrives after

$$t_1 = \min(2\tau_1 + 2\tau_2 + t_{d2}, 2\tau_1 + 2\tau_3 + t_{d3}) \quad (2)$$

time units. The corresponding echo attenuation will be

$$2I_{mix} + AERL_2 ; \quad \text{if } t_1 = 2\tau_1 + 2\tau_2 + t_{d2} \quad (3a)$$

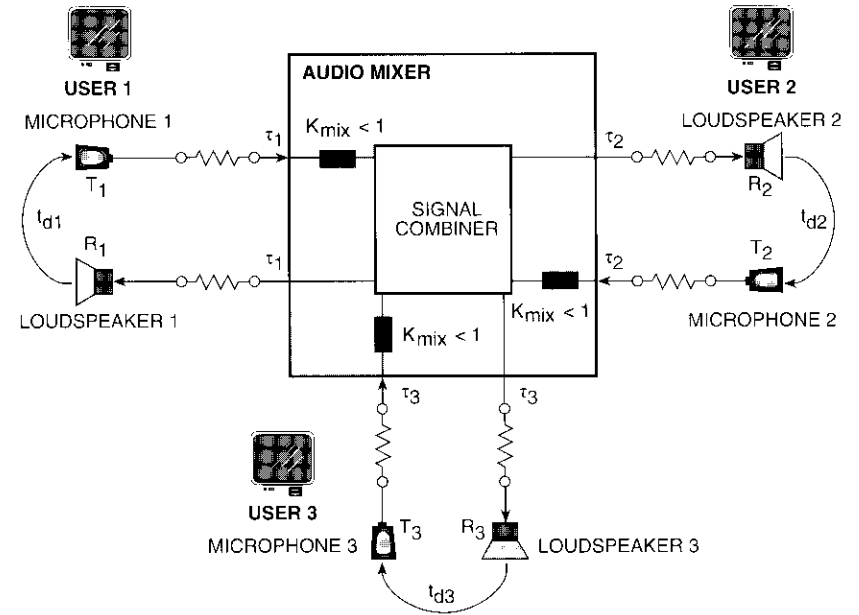


Figure 7. Schematic of Signals for a Multipoint Configuration

or

$$2L_{mix} + AERL_3 ; \quad \text{if } t_1 = 2\tau_1 + 2\tau_3 + t_{d3} \quad (3b)$$

When  $\tau_2$  and  $t_{d2}$  are comparable to  $\tau_3$  and  $t_{d3}$ , the second reflection of talker echo of user 1 arrives after

$$t_2 = \max(2\tau_1 + 2\tau_2 + t_{d2}, 2\tau_1 + 2\tau_3 + t_{d3}) \quad (4)$$

time units, with the corresponding attenuation. However, when  $\tau_2$  and  $t_{d2}$  are significantly different from  $\tau_3$  and  $t_{d3}$  [i.e.,  $(\tau_2 + t_{d2}) > 2(\tau_3 + t_{d3})$  or  $(\tau_2 + t_{d2}) < 0.5(\tau_3 + t_{d3})$ ], the second reflection of the talker echo of user 1 can arrive with either of the two delays and paths (see Figure 7) given in Table 1, rows A and B. Thus, the time of arrival of the second reflection,  $t_2$ , is given by

$$t_2 = \min \left[ \begin{matrix} \max(2\tau_1 + 2\tau_2 + t_{d2}, 2\tau_1 + 2\tau_3 + t_{d3}), & 4\tau_1 + 4\tau_2 + 2t_{d2} + t_{d1}, \\ 4\tau_1 + 4\tau_2 + 2t_{d3} + t_{d1} \end{matrix} \right] \quad (5)$$

TABLE 1. DELAY AND ATTENUATION ASSOCIATED WITH DIFFERENT ECHO PATHS

ROW	DELAY	PATH	ATTENUATION (dB)
A	$4\tau_1 + 4\tau_2 + 2t_{d2} + t_{d1}$	T1-R2-T2-R1-T1-R2-T2-R1	$4L_{mix} + 2AERL_2 + AERL_1$
B	$4\tau_1 + 4\tau_3 + 2t_{d3} + t_{d1}$	T1-R3-T3-R1-T1-R3-T3-R1	$4L_{mix} + 2AERL_3 + AERL_1$
C	$2\tau_1 + 2\tau_2 + 2\tau_3 + t_{d2} + t_{d3}$	T1-R2-T2-R3-T3-R1	$3L_{mix} + AERL_2 + AERL_3$

with the corresponding attenuation given in Table 1. Subsequent reflections of talker echoes can arrive via increasingly greater numbers of paths, with corresponding attenuations. The third reflection path (Table 1, row C) may be more critical because it may encounter less attenuation than the other two paths.

From the information given above, it can be seen that, unlike in point-to-point configurations, the arrival times of echo reflections are irregularly spaced, as determined by the propagation delays of the transmission paths to each location, plus their acoustic path delays, and various combinations thereof. Consequently, the rate of change of echo attenuation as a function of delay is no longer constant in a multipoint configuration (again, in contrast to the echo attenuation characteristics in the point-to-point configuration).

The rate of change in a multipoint mode can be negative; that is, the attenuation of the reflected echo at  $\tau_1$  may be greater than at  $\tau_2$ . In other words, the second reflected echo may have a higher power level than the first. Such situations can adversely impact the echo tolerance of the end user, as illustrated in Figure 8. Echo control will be necessary whenever the attenuation of the reflected echo falls below the tolerable levels for a given amount of delay. This is more likely to occur with multipoint configurations due to the irregular nature of the arrival times of reflected echoes, and their corresponding attenuation.

For convenience, this analysis was limited to three users in a multipoint configuration; however, it could be extended along similar lines to any number of users. The arrival times, paths, and attenuations that the reflected echoes encounter become increasingly complicated as more users are engaged in the same VTC.

### Recommendations

From analysis of the point-to-point and multipoint configurations, it is clear that echo control will be necessary whenever one or more users are on

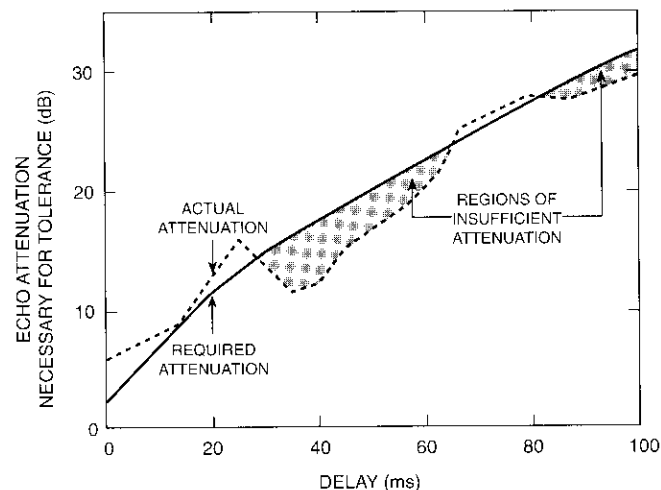


Figure 8. Irregularly Spaced Arrival Times of Reflected Echoes and Possible Negative Slopes

long-distance links. This is because, for fixed values of  $AERL$  and  $L_{mix}$ , the amount of delay that the echo signal can encounter and still be tolerable is limited by the curve of Figure 2. Hence, long-distance links will require an echo control device that can effectively improve the  $AERL$  of the individual echo return paths. It should be noted that the level of the first reflected talker echo is entirely dependent on the  $AERL$ s of the other users. Therefore, providing an echo control device at the premises of user  $i$  will reduce echo levels for all other users except user  $i$ .

Another important distinction between the point-to-point and multipoint configurations applies to the situation of double-talk, where two parties talk simultaneously. In the point-to-point case, any distortion introduced by the echo canceller during double-talk tends to be masked by the talker. If only one person is involved in the teleconference at each end, the distortion is less noticeable. In the case of a multipoint configuration, if two participants talk at the same time, the remaining participants are cast as "third-party" listeners who will hear the distortion produced during double-talk without the benefit of any masking, since they are not speaking. This places an even greater performance requirement on the echo canceller during double-talk to satisfy the remaining listeners.

### Complexity of the acoustic echo problem

It was stated conclusively above that acoustic echo control is necessary when one or more users are connected to the VTC network via a long-distance link. However, some VTC environments pose a particular challenge to effective acoustic echo control and require alternative echo control measures.

Traditionally, two types of echo control devices have been widely used to control electric echo in the PSTN: echo suppressors [3], which are considered obsolete, and echo cancellers [4]. An echo suppressor uses sophisticated logic to compare the signals in two directions and decide which user is talking at any given instant. When speech signal is present only in the receive path, the suppressor places a very high loss in the send path, thus blocking the echo from reaching the far end. Whenever speech signal is present in the send path, the loss is removed from the send path and a smaller loss is inserted in the receive path to reduce the level of the received signal, and hence the resulting echo. Thus, when both parties are actively conversing, the echo suppressor is continually inserting and removing losses. When this insertion and removal mechanism is imperfect, it can lead to chopping of send-side speech and level modulation of the receive speech. As the circuit delay is increased, the speech mutilation becomes subjectively more annoying. Further, during double-talk there is really no echo control except for the loss in the receive side, which is insufficient in most cases.

An echo canceller is more sophisticated than an echo suppressor. Rather than interrupt the return path to stop the echo, the canceller creates a replica of the echo which it then subtracts from the actual echo. Figure 9 is a highly simplified block diagram of an echo canceller. An adaptive filter is used to model the echo path. The input signal is the receive-path signal, and the signal that is desired to be canceled is the actual echo. During double-talk—which is identified by a double-talk detector—the coefficients of the adaptive filter are frozen (*i.e.*, the adaptation of coefficients is discontinued), but echo cancellation continues to be performed using the frozen coefficients. This is not a severe limitation since, for circuit-assigned connections, the echo path characteristics typically change only slowly with time. Thus, unlike with suppressors, echo control in an echo canceller continues even during double-talk. Further, eliminating the insertion and removal of losses on transmit and receive paths helps reduce the chopping effect noticed with suppressors. Overall, it is well recognized that echo cancellers generally outperform echo suppressors. For these reasons, the discussion that follows will address echo cancellers only.

As stated in the previous section, if even one user in a multipoint videoconference is connected via a long-distance link, effective echo control is neces-

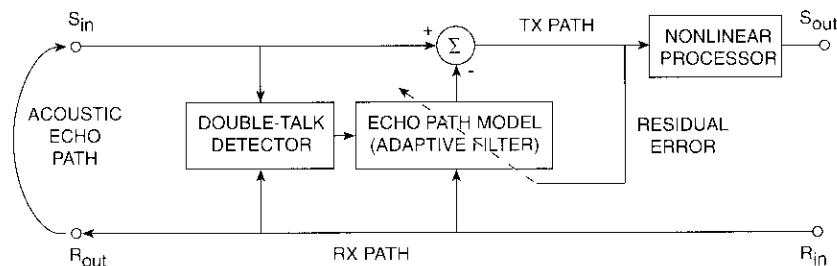


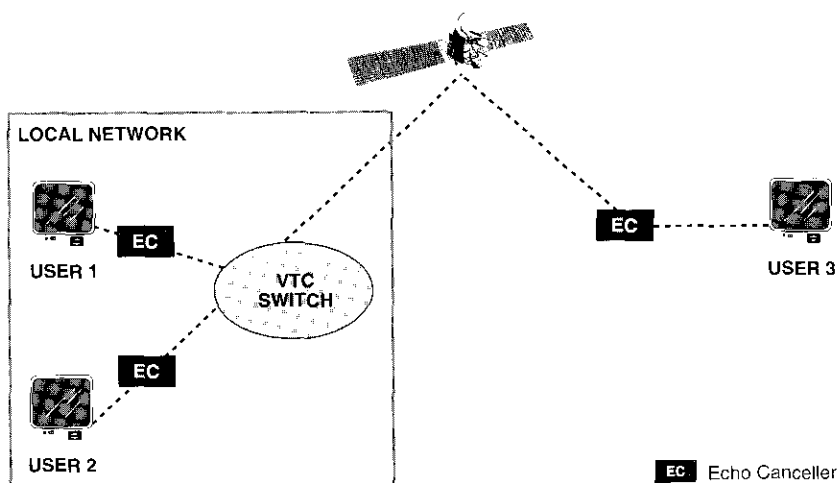
Figure 9. Echo Canceller Simplified Block Diagram

sary to enhance the AERI of all users, regardless of how close the other users might be to the VTC switch. One solution is to provide an echo canceller for each user (both local and long distance) in the network to reduce the echo levels generated at the premises of the individual users. An alternative, and less expensive, solution is to use one echo canceller that protects the long-distance user from the echo of all the users in the local network, and another to control the echo generated at the long-distance user's location. These two scenarios are illustrated in Figures 10a and 10b. The echo control requirements for these scenarios are analyzed and compared below.

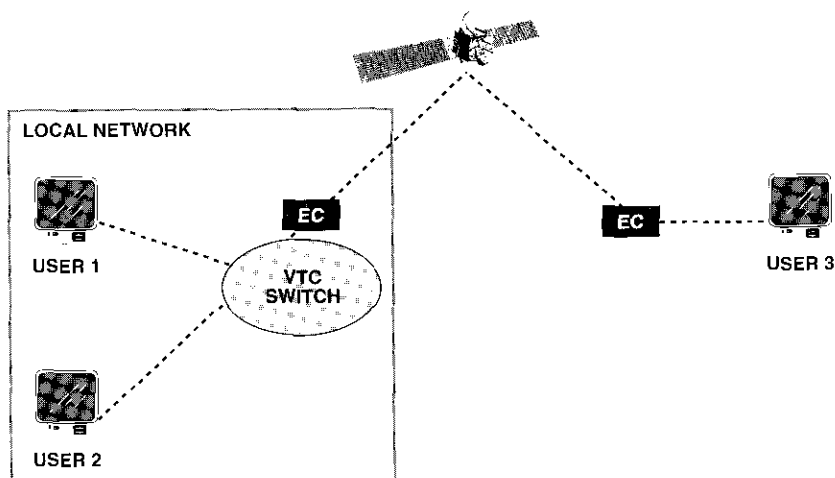
#### Acoustic echo control for individual users

Let the impulse response of the acoustic echo path of user  $i$  be given by  $h_i(n)$ , where  $n = 0, 1, \dots, L_i - 1$ . Also, assume that  $h_i(n) = 0$  for  $n < 0$  (causal system), and that  $h_i(n)$  is negligibly small for  $n \geq L_i$ . Let the nominal delay encountered by the signal at the  $R_{out}$  terminal of the echo canceller be equivalent to  $n_{di}$  samples. It should be noted that when the echo canceller is located at the customer premises, this delay is approximately equal to the delay encountered by the acoustic signal in traveling from the loudspeaker to the microphone, which was denoted in a previous section by  $t_{di}$  ( $t_{di} = n_{di} / f_s$ , where  $f_s$  is the sampling frequency) (see Figure 11). Further, when the echo canceller is located close to the customer premises, the  $R_{out}$  signal of the echo canceller is the loudspeaker signal of user  $i$ , namely  $R_i(t)$ , and the  $S_{in}$  signal of the canceller is the microphone signal of user  $i$ , namely  $T_i(t)$ .

To focus on reducing the echo generated at user  $i$ , we will assume no interruption (single-talk) from user  $i$ . Under these conditions,  $T_i(N) \approx E_i(n)$ , assuming room noise is negligible. If  $\hat{T}_i(n)$  is the output of the echo canceller's



(a) Cancellor for Each User



(b) Cancellor for More Than One User on Local Network

Figure 10. Two Scenarios for VTC Networks Employing Echo Cancellers

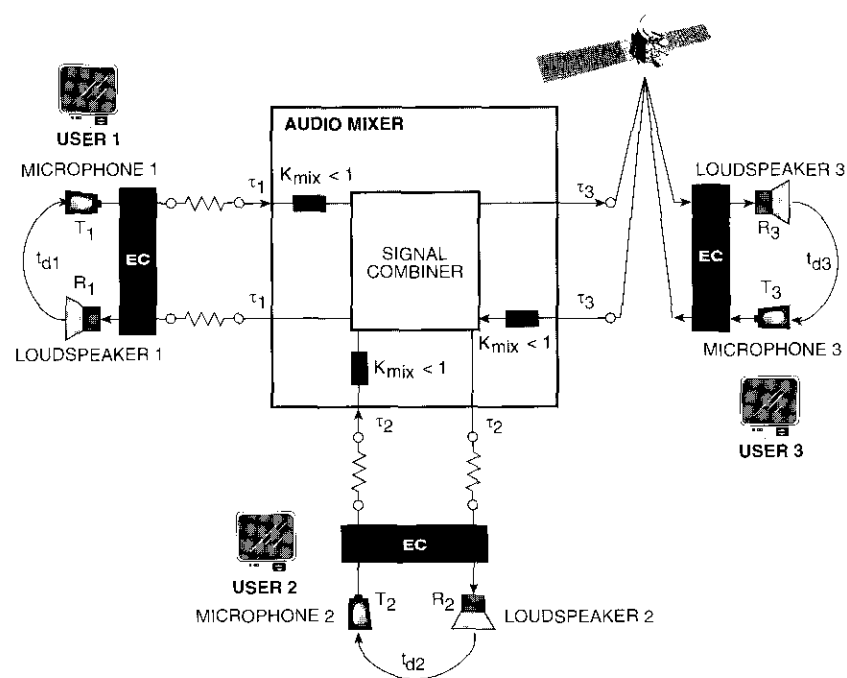


Figure 11. Schematic of Signals in a Cancellor-per-User Configuration

adaptive filter, then the coefficients of the adaptive filter,  $c(m)$ ,  $m = 1, 2, \dots, L - 1$ , are chosen such that

$$E\left\{\left[T_i(n) - \hat{T}_i(n)\right]^2\right\}$$

is minimum, where

$$T_i(n) \approx E_i(n) = \sum_{j=0}^{L_i-1} h_i(j) R_i(n - n_{di} - j) \quad (6)$$

and

$$\hat{T}_i(n) = \sum_{j=0}^{L-1} c(j) R_i(n - j) \quad (7)$$

Substituting  $n_{di} + j = j'$  in equation (6) gives

$$T_i(n) = \sum_{j'=n_{di}}^{L_i + n_{di} - 1} h_i(j' - n_{di}) R_i(n - j')$$

$$= \sum_{j=0}^{L_i + n_{di} - 1} h_i(j' - n_{di}) R_i(n - j') \quad (8)$$

since  $h_i(m) = 0$ , where  $m < 0$ .

Comparing equation (8) with equation (7) reveals that, in order to reasonably model the acoustic echo path at the premises of user  $i$ , the length of the adaptive filter of the echo canceller (sometimes referred to as the processing window of the canceller) should be at least  $L_i + n_{di}$ , and  $c(m) = h_i(m - n_{di})$ . This suggests that the echo canceller should model a flat delay component (a string of  $n_{di}$  zeroes) and the actual echo path. Consequently, for a given fixed number of coefficients of the adaptive filter, the number of coefficients used to model the actual echo path is limited by  $n_{di}$ . Hence, for larger rooms where the separation between microphone and speaker can be wide, the processing window of the canceller needs to be wider as well. An alternative is to employ some flat delay compensation to account for the flat delay component, thereby utilizing the adaptive filter coefficients to better represent the dispersion in the echo path.

**Acoustic echo control for several users in a local network**

An alternate means of controlling echo when one user in a VTC is on a long-distance link is to use one echo canceller to prevent the echoes generated at the premises of all users in the local network from reaching the far end. This configuration is depicted in Figure 12, where a single echo canceller (EC) is used to control echo generated by users 1 and 2. For this analysis, it is assumed that the signal combiner is a linear device that does not use any gating of the signals in the echo path of the EC' canceller.

Further analysis will reveal that the requirements for such an echo canceller are different from those described in the previous section. As shown in Figure 12, this canceller is denoted EC' to differentiate it from the canceller provided at the premises of user 3. (The requirements of canceller EC in Figure 12 are the same as those derived previously, since it is dedicated for user 3).

Before proceeding with the analysis, it is important to note that the echo path that EC' is required to model is the path encountered by the signal  $T'_3(t)$

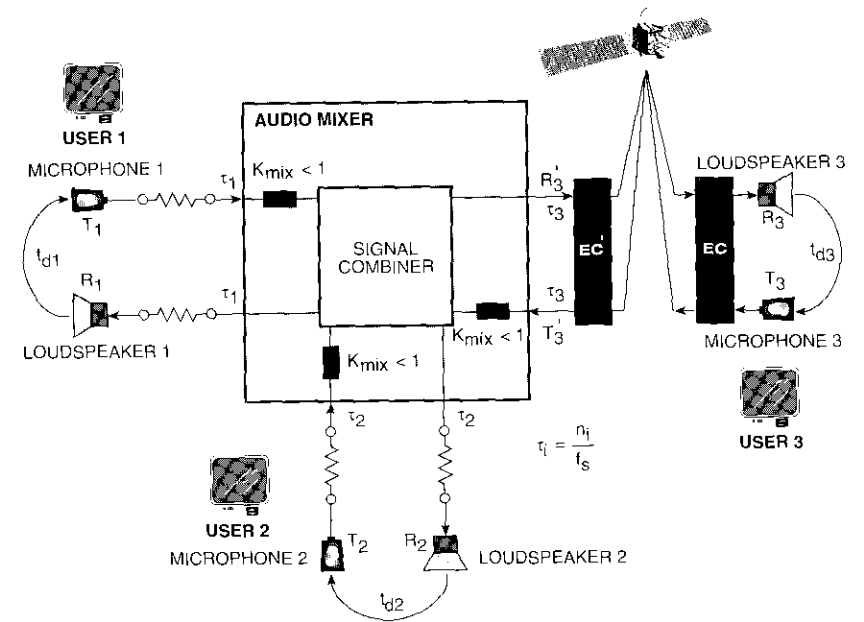


Figure 12. Schematic of Signals in Canceller-Per-Multiusers Configuration

through the premises of users 1 and 2, which will return as an echo denoted by  $R'_3(t)$ . Thus,  $T'_3(t)$  is the signal exiting the  $R_{out}$  port of EC', and  $R'_3(t)$  is the signal entering the  $S_{in}$  port of EC'. This is different from the roles played by  $T_i(t)$  and  $R_i(t)$  in the previous section. Let EC' be located in the network such that it takes an equivalent of  $n'_3$  samples for a signal from the canceller/mixer to reach the mixer/canceller. From the basic operation of the audio mixer, we have

$$R_i(n) = \sum_{\substack{j=1 \\ j \neq i}}^3 K_{mix} T_j(n - n_i - n_j) \quad (9)$$

Assuming that EC' is in the single-talk mode (i.e.,  $S_1(t)$  and  $S_2(t) \approx 0$ ) and that the ambient noise is negligibly small, then

$$T_i(n) = E_i(n); \quad i = 1, 2 \quad (10)$$

$$E_i(n) = \sum_{j=0}^{L_i - 1} h_i(j) R_i(n - n_{di} - j); \quad i = 1, 2 \quad (11)$$

From the basic operation of the mixer, we have

$$R'_3(n) = K_{\text{mix}} E_1(n - n_1 - n'_3) + K_{\text{mix}} E_2(n - n_2 - n'_3) \quad (12)$$

Substituting for  $E_i(t)$  from equation (11) gives

$$\begin{aligned} R'_3(n) &= K_{\text{mix}} \sum_{i=0}^{L_1-1} h_1(i) R_1(n - n_1 - n'_3 - n_{d1} - i) \\ &\quad + K_{\text{mix}} \sum_{i=0}^{L_2-1} h_2(i) R_2(n - n_2 - n'_3 - n_{d2} - i) \\ &= K_{\text{mix}}^2 \sum_{i=0}^{L_1-1} h_1(i) T'_3(n - 2n_1 - 2n'_3 - n_{d1} - i) \\ &\quad + K_{\text{mix}}^2 \sum_{i=0}^{L_2-1} h_2(i) T'_3(n - 2n_2 - 2n'_3 - n_{d2} - i) \\ &\quad + K_{\text{mix}}^2 \sum_{i=0}^{L_1-1} h_1(i) T_2(n - 2n_1 - n_2 - n'_3 - n_{d1} - i) \\ &\quad + K_{\text{mix}}^2 \sum_{i=0}^{L_1-1} h_2(i) T_1(n - 2n_2 - n_1 - n'_3 - n_{d2} - i) \end{aligned} \quad (13)$$

At this point, equation (13) indicates that the effective echo path provided by the combination of users 1 and 2 has an infinite-duration impulse response, although the individual acoustic echo paths could be having finite-duration impulse response. This is because in equation (13) it is possible to substitute for  $T_1(t)$  and  $T_2(t)$  repeatedly in terms of  $T'_3(t)$ , thus leading to an effective infinite impulse response. This can be envisioned intuitively by referring to Figure 12, which shows that a signal originating at  $R_{\text{out}}$  of EC' [i.e.,  $T'_3(t)$ ] can take an infinite number of paths (each associated with a different delay) before reaching the  $S_{\text{in}}$  port of EC'. This is essentially due to the functionality of the mixer.

Although the effective impulse response duration is infinite, the presence of higher powers of  $K_{\text{mix}} (< 1)$  associated with longer delay reflections makes the corresponding impulse response coefficients negligibly small. This is another significant advantage of using a lossy mixer which, in addition to avoiding the

singing effect, also helps to reduce the processing window that would be necessary in order for the canceller to model the echo path reasonably well. Notice that  $K_{\text{mix}}$  does not play any role in the requirements of a dedicated echo canceller, as discussed previously. Thus the equation for  $R'_3(t)$  can be rewritten approximately as

$$R'_3(n) = \sum_{i=0}^{L_{3\text{ecq}}-1} h_{3\text{ecq}}(i) T'_3(n - n_{d3\text{ecq}} - i) \quad (14)$$

where

$$\begin{aligned} L_{3\text{ecq}} &= \max(L_1, L_2) \\ n_{d3\text{ecq}} &= \max(2n_1 + 2n'_3 + n_{d1}, 2n_2 + 2n'_3 + n_{d2}). \end{aligned}$$

Let the adaptive filter output of the canceller be

$$\hat{R}_3(n) = \sum_{j=0}^{L-1} c(j) T'_3(n - j) \quad (15)$$

Performing algebra on equation (14) similar to that done in the Appendix, and comparing it with equation (15), reveals that an echo canceller designed to control echoes generated from users 1 and 2 requires a processing window of at least:

$$L = \max(L_1 + 2n_1 + 2n'_3 + n_{d1}, L_2 + 2n_2 + 2n'_3 + n_{d2}) \quad (16)$$

This differs significantly from the requirements for a dedicated acoustic echo canceller described in the previous section because the mixer is part of the acoustic echo path, and the delays associated with the link connected to users 1 and 2 will add to the flat delay component of the overall acoustic echo path. In addition, combining the two acoustic echo paths with the functionality of the mixer creates a complex echo path that is difficult for the acoustic canceller to model.

For the network configuration of Figure 10a, with a canceller at each teleconference location, when double-talk occurs at least two cancellers are involved, and the distortions produced by both will be audible to the third (or more) parties. For the network configuration of Figure 10b, double-talk may occur between users 1 and 2, but no canceller will be placed in the double-talk mode because the combined speech of users 1 and 2 will appear as a transmit signal to the canceller closest to the VTC switch. While this latter network

configuration reduces the number of combinations that give rise to double-talk, it is more probable that double-talk will involve the remote long-haul participant (user 3) and one of the other short- or medium-haul users.

### **Conclusions and recommendations**

The complexity of the echo control problem in the VTC environment as network operating range is extended beyond a local area has been analyzed. Because of the variability of user transmit and receive levels, equipment placement, and room acoustics, it does not appear that reasonable engineering-level controls can be placed on the network. The room and its acoustic characteristics are now part of the network, and customers who adjust their own levels may not recognize that they are affecting performance for other participants in the conference.

The possibility of using a single canceller to control the echo from a number of rooms simultaneously (as in a quad conference) is enticing because it greatly reduces the number of cancellers required. However, this mode of operation is not considered to be sufficiently stable for widespread application. It is expected that the cost of customer complaints, with the repeated service required, would soon outweigh the lower initial cost of the single shared canceller approach.

The use of cancellers at all locations is recommended as the best performance approach. Recognizing that this may not be economically acceptable, the following specific recommendations are made for providing the highest overall system grade of service at the lowest cost.

1. *For small-room applications, design the loudspeaker and microphone into a single unit with the microphone located at a fixed position in a minimum-strength acoustic field. Care must be taken to minimize mechanical-acoustical coupling.*

This will control one variable of delay—the loudspeaker-to-microphone distance—and maximize the range of a local network that may operate without active echo control. Note that a loudspeaker-to-microphone separation of 3 m provides the equivalent of a 2,150-km round-trip fiber connection delay.

In addition (and perhaps even more importantly), fixing the location of the microphone will greatly reduce the variability of the acoustic echo path model that must be tracked by the canceller, which is expected to be particularly important for quad operation. If a lapel microphone is used, for example, and the participant changes physical position so that the microphone is moved even 15 cm with respect to the loudspeaker, this results in a 0.5-ms delay change which, at a 16-kHz

sample rate, represents a position shift of eight coefficients in the canceller model. This places a heavy demand on the acoustic echo canceller to keep reconverging during intervals where no double-talk is detected. In some VTC environments where background music may be playing, very little time is available for the canceller to reconverge.

2. *Ensure that the acoustic mixer introduces a loss (on the order of 2 dB).*

This will help to prevent singing and provide a means of dissipating echo more rapidly to minimize the probability of it being heard, especially when the echo return loss is bad on a longer delay connection. It also reduces the processing range required for the echo canceller.

3. *Use a dedicated canceller for larger conference rooms.*

Controlling echo in a larger room is a more difficult task. Operation of the canceller can be optimized to a single room and provide its best performance. With echo control in place for a larger room, that room could participate in local network connections involving longer range without the need for echo control in all rooms.

4. *If the above recommendations have been implemented, then consider introducing a single canceller at the switch to provide echo control for more than one room. However, if such a configuration is selected, extensive testing will be necessary and user control of transmit and receive levels must be disabled in order to maintain system alignment and ensure acceptable performance for all VTC participants.*

Items 1 and 3 both serve to constrain the range of operating environments presented to a single canceller attempting to provide echo control from a common network point. Operation of the large-room canceller in tandem with the network canceller is not expected to cause a problem; however, further testing is recommended. With the large-room echo control already provided, the common canceller performance may now be optimized for smaller rooms.

5. *To provide the highest quality of multipoint service, give particular attention to the performance of the selected echo cancellers in the double-talk mode.*

Echo cancellers are only able to adapt their model when an active signal is present at the receive input port and a resulting echo is present at the send input port in the absence of an interfering near-talker signal (receive speech single-talk mode). Interrupting near-talker speech

distorts the echo signal used for adaptation. The echo canceller must detect this near-talker speech and disable the adaptation process in order to maintain the proper model for estimating echo. Once double-talk is detected, the model will be frozen in its current (distorted) state and used for the duration of the double-talk interval. The nonlinear processor of the canceller is removed during double-talk, allowing the residual echo level to be transmitted. In multipoint teleconferencing, two cancellers will produce distorted residual echoes which will be heard by all participants at nonspeaking locations. Thus, it is important to maintain maximum cancellation and minimize the distortion produced by the cancellers during double-talk intervals.

6. *Considering that some rooms will continue to operate with non-fixed microphones, take the following actions to resolve echo problems when they occur:*

- Move the loudspeaker closer to the microphone to reduce delay around the loop and make echo less noticeable.
- Lower the output level of the loudspeaker to improve the AERL, and try to locate the microphone at a sound pressure level minimum. (Note: Some commercially available echo cancellers automatically adjust the effective output level of the loudspeaker in order to train with a degraded echo return loss; in which case the user has less ability to improve the effective AERL.)
- Try to operate with a fixed microphone where possible.

7. *If a single canceller (as recommended in item 4) does not provide adequate service, consider using a pool of cancellers located at the switch as an alternative to using echo cancellers in every room.*

In the pooled approach, the switch would route audio traffic via cancellers on all calls where the link delay requires echo control. This would involve the introduction of some type of class marking to identify long-delay links and would, of course, consume additional switch ports to provide for four-wire connections to the echo cancellers.

To reiterate, the use of an acoustic echo canceller is recommended for each VTC location. If cost containment is the driving mechanism, then a dedicated canceller for every large room and a shared canceller for smaller rooms—or a pool of cancellers with class marking, as recommended in item 7—may be employed. This could involve a tradeoff of some user flexibility, and possibly some quality of service.

## References

- [1] S. J. Campanella and D. Chitre, "Assessment of Satellite Communications Quality Study," Final Report to NASA from COMSAT Laboratories, NASA Document No. NAS3-23790, November 1988.
- [2] ITU-T Recommendation G.131, IXth Plenary Assembly, Melbourne, November 1988, *Blue Book*, Fascicle III.1, pp. 143–154.
- [3] ITU-T Recommendation G.164, IXth Plenary Assembly, Melbourne, November 1988, *Blue Book*, Fascicle III.1, pp. 186–221.
- [4] ITU-T Recommendation G.165, IXth Plenary Assembly, Melbourne, November 1988, *Blue Book*, Fascicle III.1, pp. 221–243.

## Appendix: Analysis of point-to-point and multipoint configurations

An analysis is presented of the impact of delay, AERL, listening level, talking level, orientation of the microphone with respect to the loudspeaker, and loss factor of the audio mixer (if any) on the level of acoustic echo and its perception by the end user in a VTC network. Although the treatment is general in nature, any simplification or assumptions made in order to demonstrate points of interest are clearly stated. For clarity of discussion, point-to-point and multipoint VTC are treated separately. For simplicity and ease of understanding, only direct acoustic paths are addressed in the analyses. The effects of complicated acoustic multipaths are ignored, assuming that their contribution to the problem under consideration is less severe.

### Analysis of point-to-point configurations: A general framework

Referring to Figure 4, let user 1 be engaged in a VTC with user 2. Also, let the delay encountered by a signal from user  $i$  to the audio mixer be  $\tau_i$ , where  $i = 1, 2$ , and let the transmitted and received (microphone and loudspeaker) signals for the two users be  $T_i(t)$  and  $R_i(t)$ , respectively, where  $i = 1, 2$ . In general, then

$$T_i(t) = S_i(t) + E_i(t) + N_i(t); \quad i = 1, 2 \quad (\text{A-1})$$

where  $S_i(t)$ ,  $E_i(t)$ , and  $N_i(t)$  are the speech signal (interchangeably referred to as the audio signal), acoustic echo signal, and room noise respectively, generated at the premises of user  $i$ .

Let  $L_{\text{mix}}$  be the loss in dB introduced by the audio mixer to each input signal before the inputs are combined, and let  $-20 \log K_{\text{mix}} = L_{\text{mix}}$ . This implies that  $K_{\text{mix}} < 1$ .

To see the effects of delay, listener levels, talker levels,  $L_{\text{mix}}$ , and AERLs on echo levels, it will be assumed that all links and all echo paths are ideal (*i.e.*, have a flat frequency response in the region of interest). This eliminates the dependency of the impulse responses of links and echo paths on the level of echoes generated in the network and simplifies the analysis. From the basic operation of the mixer, as described previously, we have

$$R_i(t) = K_{\text{mix}} T_j(t - \tau_1 - \tau_2); \quad \begin{array}{l} i=1, j=2 \\ i=2, j=1 \end{array} \quad (\text{A-2})$$

For the moment, consider the impact of talker echo on user 1. The analysis for user 2 is very similar. Let  $t_{di}$  be the nominal delay encountered by the acoustic signal when it traverses from the loudspeaker to the microphone at the premises of user  $i$ . Then,

$$E_i(t) = K_{\text{ERL},i} R_i(t - t_{di}); \quad i=1, 2 \quad (\text{A-3})$$

where  $K_{\text{ERL},i}$  is such that  $-20 \log K_{\text{ERL},i}$  equals the AERL at the premises of user  $i$ , denoted by  $\text{AERL}_i$ . From equations (A-1) and (A-2), therefore,

$$R_1(t) = K_{\text{mix}} [S_2(t - \tau_1 - \tau_2) + E_2(t - \tau_1 - \tau_2) + N_2(t - \tau_1 - \tau_2)] \quad (\text{A-4})$$

Substituting for  $E_i(\cdot)$  from equation (A-3) yields

$$R_1(t) = K_{\text{mix}} \left[ \begin{array}{l} S_2(t - \tau_1 - \tau_2) + K_{\text{ERL},2} R_2(t - \tau_1 - \tau_2 - t_{d2}) \\ + N_2(t - \tau_1 - \tau_2) \end{array} \right] \quad (\text{A-5})$$

Using equation (A-2) gives

$$R_1(t) = K_{\text{mix}} \left[ \begin{array}{l} S_2(t - \tau_1 - \tau_2) + K_{\text{ERL},2} K_{\text{mix}} T_1(t - 2\tau_1 - 2\tau_2 - t_{d2}) \\ + N_2(t - \tau_1 - \tau_2) \end{array} \right] \quad (\text{A-6})$$

Since we are interested in the level of talker echo of user 1, we explicitly extract only the term that involves  $S_1(\cdot)$  in  $R_1(t)$ . Substituting for  $T_1(\cdot)$  from equation (A-1), and rearranging the terms, yields

$$R_1(t) = K_{\text{mix}}^2 K_{\text{ERL},2} S_1(t - 2\tau_1 - 2\tau_2 - t_{d2}) + \text{terms involving } S_2(\cdot), N_2(\cdot), E_1(\cdot), \text{ and } N_1(\cdot) \quad (\text{A-7})$$

From the above equation, it is clear that the first reflection of the talker echo of user 1 arrives after a delay of  $2\tau_1 + 2\tau_2 + t_{d2}$  time units, and the attenuation encountered by this first reflection is equal to  $-(40 \log K_{\text{mix}} + 20 \log K_{\text{ERL},2})$  or  $2L_{\text{mix}} + \text{AERL}_2$  dB.

It is important to note that, upon arrival of the first reflection of the talker echo of user 1 after  $2\tau_1 + 2\tau_2 + t_{d2}$  time units, this echo is fed back to the microphone from the loudspeaker at the premises of user 1. Similar to the analysis carried out above, it is easy to see that the second and subsequent reflections of echo will arrive at the premises of user 1 every  $2\tau_1 + 2\tau_2 + t_{d1} + t_{d2}$  time units, and each time echo will be attenuated by an amount equal to  $2L_{\text{mix}} + \text{AERL}_1 + \text{AERL}_2$  dB. Similarly for user 2, the first reflection of talker echo arrives after  $2\tau_1 + 2\tau_2 + t_{d1}$  time units, and subsequent reflections arrive every  $2\tau_1 + 2\tau_2 + t_{d1} + t_{d2}$  time units.

#### IMPACT OF LOUDSPEAKER GAIN ON ECHO LEVELS

Referring to Figure 6a, let the power gain of the loudspeaker at the premises of user 1 be increased by  $G_{R1}$  ( $>0$ ) dB, and let  $G_{R1} = 20 \log K_{R1}$ . Note that  $K_{R1} > 1$ , since  $G_{R1} > 0$ . From the figure, it can be seen that the basic equations governing the analysis are the same as in the general point-to-point framework above, except for  $R_1(t)$ , which is now

$$R_1(t) = K_{R1} K_{\text{mix}} T_2(t - \tau_1 - \tau_2) \quad (\text{A-8})$$

Conducting an analysis along similar lines as in the previous section for  $R_1(t)$ , we obtain

$$R_1(t) = K_{\text{mix}}^2 K_{R1} K_{\text{ERL},2} S_1(t - 2\tau_1 - 2\tau_2 - t_{d2}) + K_{\text{mix}} K_{R1} S_2(t - \tau_1 - \tau_2) + \text{terms involving } N_1(\cdot), N_2(\cdot), \text{ and } E_1(\cdot) \quad (\text{A-9})$$

A similar analysis for the talker echo received by user 2, namely the content of  $S_2(\cdot)$  in  $R_2(t)$ , yields

$$R_2(t) = K_{\text{mix}}^2 K_{R1} K_{\text{ERL},1} S_2(t - 2\tau_1 - 2\tau_2 - t_{d1}) + K_{\text{mix}} S_1(t - \tau_1 - \tau_2) + \text{terms involving } N_1(\cdot), N_2(\cdot), \text{ and } E_2(\cdot) \quad (\text{A-10})$$

IMPACT OF MICROPHONE GAIN ON ECHO LEVELS

Referring to Figure 6b, let the microphone gain at the premises of user 1 be increased beyond nominal levels by  $G_{T1}$  dB. Also let  $G_{T1} = 20 \log K_{T1}$ . Note that  $K_{T1} > 1$ , since  $G_{T1} > 0$ . From the figure, it can be seen that the basic equations governing the analysis are the same as in the general point-to-point framework, except for  $R_2(t)$ , which is now

$$R_2(t) = K_{\text{mix}} K_{T1} T_1(t - \tau_1 - \tau_2) \tag{A-11}$$

Carrying out the analysis along similar lines as in the previous section for  $R_1(t)$ , we obtain

$$R_1(t) = K_{\text{mix}}^2 K_{T1} K_{\text{ERL}2} S_1(t - 2\tau_1 - 2\tau_2 - t_{d2}) + K_{\text{mix}} S_2(t - \tau_1 - \tau_2) + \text{terms involving } N_1(\cdot), N_2(\cdot), \text{ and } E_1(\cdot) \tag{A-12}$$

Similarly, for  $R_2(t)$  we obtain

$$R_2(t) = K_{\text{mix}}^2 K_{T1} K_{\text{ERL}2} S_2(t - 2\tau_1 - 2\tau_2 - t_{d1}) + K_{\text{mix}} K_{T1} S_1(t - \tau_1 - \tau_2) + \text{terms involving } N_1(\cdot), N_2(\cdot), \text{ and } E_2(\cdot) \tag{A-13}$$

**Analysis of multipoint configurations: A general framework**

Referring to Figure 7, let users 1, 2, and 3 be engaged in a video teleconference. The analysis will be conducted in a manner similar to that for the point-to-point configurations.

From Figure 7, the basic equations governing the analysis are:

$$T_i(t) = S_i(t) + E_i(t) + N_i(t); \quad i = 1, 2, 3 \tag{A-14}$$

$$R_i(t) = \sum_{\substack{j=1 \\ j \neq i}}^3 K_{\text{mix}} T_j(t - \tau_i - \tau_j); \quad i = 1, 2, 3 \tag{A-15}$$

$$E_i(t) = K_{\text{mix}} R(t - t_{di}); \quad i = 1, 2, 3 \tag{A-16}$$

Concentrating for the moment on the talker echo received by user 1 in such a configuration, we can write

$$R_1(t) = \sum_{j=2}^3 K_{\text{mix}} T_j(t - \tau_1 - \tau_j) \tag{A-15}$$

$$= \sum_{j=2}^3 K_{\text{mix}} \left[ \begin{array}{l} S_j(t - \tau_1 - \tau_j) + E_j(t - \tau_1 - \tau_j) \\ + N_j(t - \tau_1 - \tau_j) \end{array} \right] \tag{A-14}$$

$$= \sum_{j=2}^3 K_{\text{mix}} \left[ \begin{array}{l} S_j(t - \tau_1 - \tau_j) + K_{\text{ERL}j} R_j(t - \tau_1 - \tau_j - t_{dj}) \\ + N_j(t - \tau_1 - \tau_j) \end{array} \right] \tag{A-16}$$

$$= \sum_{j=2}^3 K_{\text{mix}} \left[ \begin{array}{l} S_j(t - \tau_1 - \tau_j) \\ + K_{\text{ERL}j} \sum_{\substack{k=1 \\ k \neq j}}^3 K_{\text{mix}} T_k(t - \tau_1 - 2\tau_j - t_{dj} - \tau_k) \\ + N_j(t - \tau_1 - \tau_j) \end{array} \right] \tag{A-17}$$

Substituting for  $T_k(\cdot)$  from equation (A-14) and extracting terms containing  $S_1(\cdot)$ , we obtain

$$R_1(t) = K_{\text{mix}}^2 K_{\text{ERL}2} S_1(t - 2\tau_1 - 2\tau_2 - t_{d2}) + K_{\text{mix}}^2 K_{\text{ERL}3} S_1(t - 2\tau_1 - 2\tau_3 - t_{d3}) + \text{terms involving } S_2(\cdot), N_2(\cdot), S_3(\cdot), N_3(\cdot), \text{ and } N_1(\cdot) \tag{A-18}$$

We have explicitly shown only those terms involving  $S_1(\cdot)$ , since we are interested in the talker echo of user 1.

While the analysis was limited to three users in a multipoint configuration for convenience, it can be extended along similar lines to any number of users. Obviously, the arrival times, paths, and attenuations that the reflected echoes encounter will become increasingly complicated as more users are engaged in the same VTC.



*Chammasandra Ravishankar received a BE degree in electronics engineering from Bangalore University, India, in 1985; an MTech degree in communications engineering from the Indian Institute of Technology, Bombay, in 1987; and a PhD in communications and signal processing from Purdue University in 1991. Starting in 1987, he was with the R&D division of Indian Telephone Industries, and subsequently was a Member of the Technical Staff at COMSAT Laboratories. Since November 1995, Dr. Ravishankar has been working as a Principal Engineer at Hughes Network Systems, Germantown, Maryland. His*

*interests are in the areas of low-bit-rate speech coding, echo cancellation, and voice and voiceband data transmission for wireless and mobile satellite communications systems. He is a member of IEEE and Eta Kappa Nu.*

*Michael Onufry received a BS degree from Pennsylvania State University in 1962, and performed graduate work at both Northeastern University and George Washington University. He is currently Assistant to the President of COMSAT Laboratories. His experience includes echo canceller development, 64-kb/s PCM and 32-kb/s ADPCM, digital speech interpolation development, and speech encoding. He has been active in planning and implementing international field trials in the INTELSAT network, and was responsible for subjectively assessing various speech processing devices. From 1977 to 1993, Mr. Onufry was a COMSAT representative to CCITT Study Group XV, where he was a leader in echo canceller activities and a Special Rapporteur for questions concerning syllabic companders and digital circuit multiplication equipment. Mr. Onufry previously held the positions of Manager of the Voice Band Processing Department and Associate Executive Director of the Communications Technology Division at COMSAT Laboratories. He is a member of IEEE, and past president of the Maryland Chapter of the ASSP.*



Index: frequency reuse, INTELSAT, performance specifications, polarization, transponders

## **Communications performance of the INTELSAT VII and VIIA satellites**

S. JAMSHIDI AND C. B. COTNER

(Manuscript received June 27, 1995)

### **Abstract**

This paper describes the performance characteristics of the C-band and Ku-band transponders on board the INTELSAT VII and VIIA satellites, which are currently entering service. Emphasis is placed on parameters of interest to potential users, including effective isotropically radiated power (EIRP), gain-to-noise temperature ratio (G/T), and transponder gain. Coverages of various beams are shown for typical Atlantic, Pacific, and Indian Ocean Region locations. The interconnection capabilities among the different transponders—a key source of flexibility—are also described. A comprehensive bibliography of publications addressing the INTELSAT VII/VIIA satellites is included.

### **Introduction**

The INTELSAT VII/VIIA series satellites are technically advanced, commercial communications satellites whose impact will be felt well into the next century. With increased power, coverage, and connectivity, they will provide voice, data, and video services through a new generation of smaller, less expensive ground stations. While the INTELSAT VII program was tailored to meet the requirements of INTELSAT system users in the Pacific Ocean Region, elements of the design reflect capabilities that make the satellite suitable for use in other ocean regions as well.

Payload configuration flexibility is a key design feature of the INTELSAT VII/VIIA series satellites. Steerable spot beams in C- and Ku-band allow the

transmission of high-power signals in both bands to any point on the earth's surface. Providing transmission from several INTELSAT orbital locations, INTELSAT VII series satellites will cover the vast Atlantic, Indian, and Pacific ocean regions (AOR, IOR, and POR) with higher power transponders than the INTELSAT V/VA series satellites they are replacing.

The INTELSAT VII satellite series comprises six spacecraft: flight models 701 through 705, and 709. The INTELSAT VIIA satellite series comprises three spacecraft: flight models 706, 707, and 708. This paper discusses the communications payloads of these satellites, including the transponder configurations, beam connections, and transponder radio frequency plans. Key design features of the INTELSAT VII satellites are as follows:

- Increased transponder power levels to facilitate operation of small ground segment antennas, coupled with increased receiver sensitivity to reduce earth station transmit power requirements.
- Flexible connectivity provided by an in-orbit reconfiguration capability.
- Enhanced Ku-band coverage and bandwidth.
- Availability of 12-GHz bands for international business services (IBS) into urban-based antennas, with minimal interference.

INTELSAT VII/VIIA satellites have some new features that make them unique compared to the INTELSAT V/VA series. They are the first INTELSAT series satellites to employ only solid-state power amplifiers (SSPAs) at C-band, and all-high-power linearized traveling wave tube amplifiers (LTWTAs) at Ku-band, resulting in improved linearity in these bands. They are also the first INTELSAT satellites with four-times frequency reuse at Ku-band, employing dual polarization in the spot 1 and spot 2 (S1 and S2) antennas.

### **Program summary**

INTELSAT issued the request for proposals (RFP) for the INTELSAT VII series spacecraft in October 1987. One year later, the contract for the first five INTELSAT VII satellites (701 through 705) was awarded to Ford Aerospace Corporation (FAC) (now Space Systems/Loral).

The INTELSAT VII contract was amended in December 1989 to increase operational flexibility. The modification improved coverage by broadening the hemispheric (hemi)/zone beams in the IOR on INTELSAT VII (704 onward), with not more than 0.7-dB reduction in effective isotropically radiated power (EIRP). Also,

beginning with INTELSAT 703, a separate modification was incorporated to add in-orbit polarization switchability to the Ku-band spot 3 (S3) antenna.

In response to new service requirements, INTELSAT VII satellites were modified to provide a more extensive Ku-band payload, resulting in the INTELSAT VIIA series. In December 1990, a contract for the first two INTELSAT VIIA satellites (706 and 707) also was let to Space Systems/Loral by INTELSAT.

The INTELSAT VIIA contract was amended in March 1991 to increase operational flexibility, especially in providing television services. This modification enlarged the Ku-band S3 beamwidth and added Ku-band-to-C-band connectivity in channel 12 on all INTELSAT VIIA series satellites, to facilitate satellite newsgathering (SNG).

Increased service requirements led INTELSAT to procure one more INTELSAT VIIA (708) in September 1992, and an additional INTELSAT VII (709) in March 1993. Thus, a total of six INTELSAT VII (701 through 705, and 709) and three INTELSAT VIIA (706 through 708) satellites have been procured by INTELSAT.

The first INTELSAT VII (701) satellite was delivered in September 1993 (5 years after contract award), launched on October 22, 1993, and began providing service to the POR at the 174°E orbital location on January 15, 1994, replacing an INTELSAT VA satellite. To date, there have been five successful INTELSAT VII launches (701 through 705) and two successful INTELSAT VIIA launches (706 and 707), providing INTELSAT service in all three ocean regions. The INTELSAT 701 through 705 satellites have been deployed at 174°, 359°, 177°, 66°, and 310°E, respectively, while INTELSAT 706 is deployed at 307°E. As of April 9, 1996, INTELSAT 707 has been deployed at 359°E, replacing INTELSAT 702. The remaining INTELSAT VII satellite (709) is scheduled for launch around mid-1996.

### **Launch vehicle considerations**

INTELSAT VII satellites are being launched on Ariane 4 (Ariane 44 LP and Ariane 44 P) launch vehicles from Kourou, French Guiana, or on Atlas II-AS vehicles from Cape Canaveral, Florida, resulting in different orbital maneuver lifetimes (OMLS). For example, based on a spacecraft dry mass of 1,490 kg for INTELSAT VII spacecraft, an Ariane 44 LP launch is estimated to result in an OML of 17 years. If launched by an Atlas II-AS, however, a 12-year life is expected, although the precision of the Atlas launches to date has resulted in OMLS of about 14.5 years. The larger INTELSAT VIIA satellites are launched on Ariane 4 (Ariane 44 LP). Based on a spacecraft dry mass of 1,830 kg for

INTELSAT VIIA spacecraft, an Ariane 44 LP launch is estimated to result in an OMI of 15 years.

### **INTELSAT VII/VIIA modes of operation in different roles**

INTELSAT VII/VIIA satellites will be maintained within a north-south and east-west stationkeeping box of  $\pm 0.05^\circ$ . Depending on the requirements of various orbital locations, INTELSAT VII/VIIA satellites can be operated in either normal pitch, roll, and yaw attitude, or in an inverted attitude (*i.e.*, rotated  $180^\circ$  along the yaw axis). The latter results in a change in the geographical orientation of the physical beam patterns. Depending on the operational requirements, the normal attitude (yaw =  $0^\circ$ ) is intended for use at certain locations (such as  $174^\circ$ ,  $177^\circ$ , and  $307^\circ\text{E}$ ), while the coverages required for other locations (such as  $342^\circ$  and  $359^\circ\text{E}$ ) are best provided with an inverted attitude (yaw =  $180^\circ$ ). The hemi and zone beam coverages of INTELSAT VII/VIIA satellites are given below for both the normal and inverted attitude modes from various orbital locations.

<b>Normal Mode</b> (yaw bias = $0^\circ$ )	<b>Inverted Mode</b> (yaw bias = $180^\circ$ )
Operation from $174^\circ$ , $177^\circ$ , $180^\circ$ , $183^\circ$ , $307^\circ$ , $310^\circ$ , $325.5^\circ$ , and $328.5^\circ\text{E}$	Operation from $359^\circ$ , $342^\circ$ , $63^\circ$ , $66^\circ$ , $91.5^\circ$ , and $95^\circ\text{E}$
Hemi 1 (H1) = West Hemi (WH)	Hemi 1 (H1) = East Hemi (EH)
Hemi 2 (H2) = East Hemi (EH)	Hemi 2 (H2) = West Hemi (WH)
Zone 1 (Z1) = Northwest (NW)	Zone 1 (Z1) = Southeast (SE)
Zone 1A (Z1A) = Southeast (SE)	Zone 1A (Z1A) = Northwest (NW)
Zone 2 (Z2) = Northeast (NE)*	Zone 2 (Z2) = Northeast (NE)*
Zone 2A (Z2A) = Southwest (SW)*	Zone 2A (Z2A) = Southwest (SW)*

\*The northeast and southwest zone beams are always labeled Z2 and Z2A, respectively, regardless of attitude mode (normal or inverted).

The INTELSAT VII/VIIA series are the first INTELSAT satellites designed with an attitude error-correction capability to alleviate variations in coverage during inclined orbit operation. They can compensate for the equivalent spacecraft body pitch, roll, and yaw errors in the antenna beam pointing when operating with up to  $3^\circ$  inclination. Both pitch (east-west) and roll (north-south) biases may be employed to meet coverage requirements.

### **General characteristics of INTELSAT VII/VIIA spacecraft**

The INTELSAT VII/VIIA is a three-axis-stabilized hybrid (C- and Ku-band) communications satellite. The FS-1300 spacecraft bus, employed on both series, is a modular design based on earlier FAC designs, including INTELSAT V, INSAT-1, ARABSAT, and SUPERBIRD. The INTELSAT VII/VIIA satellites have an orbital design life (ODL) of 10.9 years. However, due to improved switching and transponder redundancy, they are expected to function reliably for 13 to 15 years.

The INTELSAT VII satellites, with their frequency reuse design, provide 1,542 MHz of C-band and 896 MHz of Ku-band spectrum, resulting in a total bandwidth of 2,432 MHz. INTELSAT VIIA satellites have the same C-band spectrum as the INTELSAT VII SATELLITES, but 1,498 MHz of Ku-band spectrum, for a total usable bandwidth of 3,040 MHz.

### **INTELSAT VII/VIIA frequency band, channelization, and beam connectivity**

The INTELSAT VII/VIIA communications payloads consist of two independent, cross-strapable communications systems operating at C- and Ku-bands. Greater flexibility is introduced with the INTELSAT VII's three independently steerable Ku-band spot beams and one independently steerable C-band spot (C-spot) beam, which can be steered over the entire visible portion of the earth to accommodate changing traffic patterns and service requirements.

At C-band, INTELSAT VII/VIIA satellites employ shaped-beam antennas and polarization isolation to achieve up to four-times frequency reuse. INTELSAT VII/VIIA C-band hemispheric, zone, global, and spot beams operate in circular polarization in either A or B polarization. The circular polarization of the C-band beams of INTELSAT VII/VIIA satellites can be defined as follows:

- *A Pol Satellite Receive/Uplink*: Left-hand circular polarization (LHCP)
- *A Pol Satellite Transmit/Downlink*: Right-hand circular polarization (RHCP)
- *B Pol Satellite Receive/Uplink*: RHCP
- *B Pol Satellite Transmit/Downlink*: LHCP.

At Ku-band, INTELSAT VII satellites employ three independently steerable spot beam antennas to achieve two-times frequency reuse through sharing two sets of transmitters/TWTAs among the three spot beams. INTELSAT VIIA series satellites also employ three independently steerable spot beam antennas, but

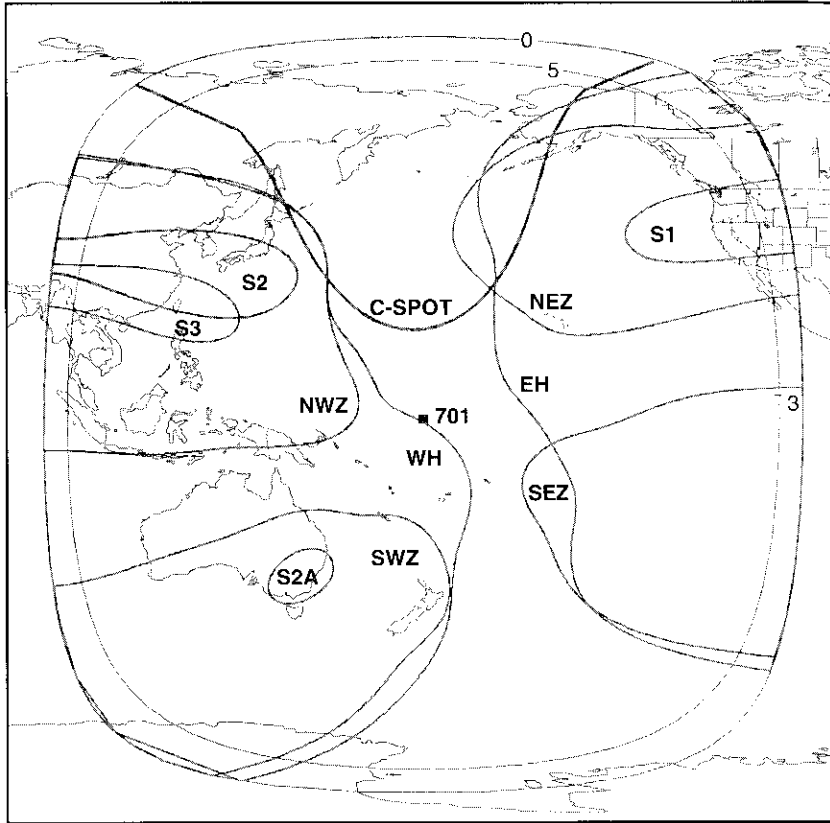


Figure 1. *INTELSAT 701 at 174°E: Composite Coverage*  
(pitch = -0.46°E, tilt = 0.0°N, normal mode)

can achieve up to four-times frequency reuse through cross-polarization isolation. The two sets of transmitters/TWTAs are shared among up to three spot beams, where two of the three beams are cross-polarized.

Figures 1 through 4 show representative satellite antenna pattern coverages for INTELSAT 701 at 174°E in the normal attitude, INTELSAT 702 at 359°E in the inverted attitude, INTELSAT 704 at 66°E in the inverted attitude, and INTELSAT 706 at 307°E in the normal attitude.

Figures 5 and 6 show the transponder layout and channelization for INTELSAT VII and VIIA series, respectively. The 500-MHz C-band (6/4-GHz) spectrum accessed by INTELSAT VII/VIIA satellites is 5.925–6.425 GHz receive/uplink

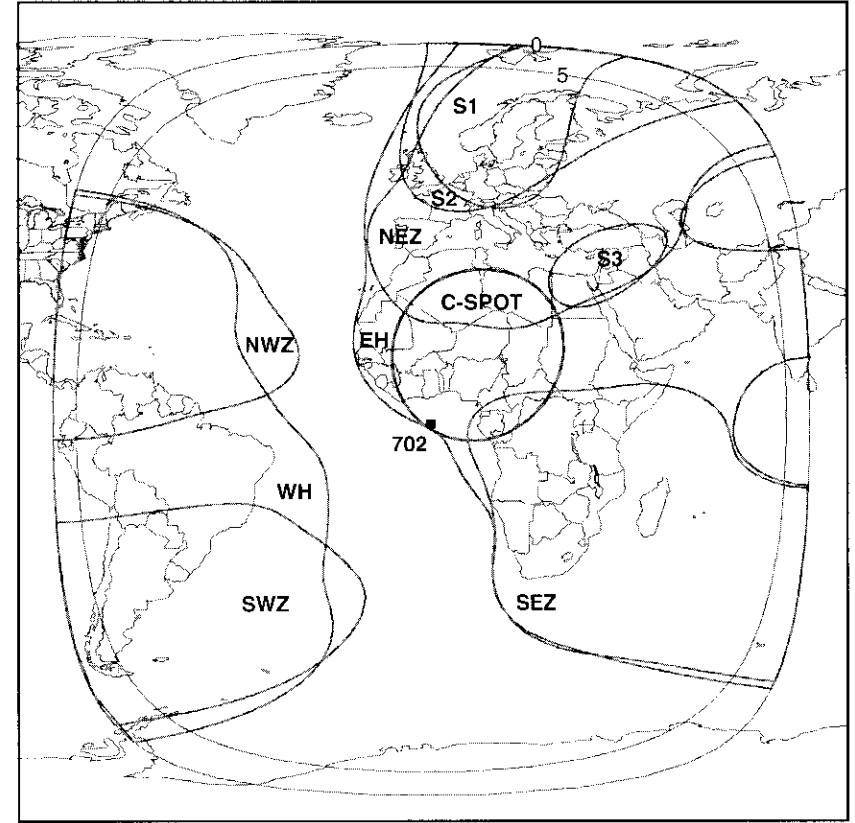


Figure 2. *INTELSAT 702 at 359°E: Composite Coverage*  
(pitch = -0.6°E, tilt = 0.0°N, inverted mode)

band and 3.7–4.2 GHz transmit/downlink band. The 500-MHz Ku-band (14/11- or 14/12-GHz) spectrum accessed by the INTELSAT VII/VIIA satellites is 14.0–14.5 GHz receive/uplink band and 10.95–12.75 GHz (band A is 10.95–11.20 GHz, band B is 11.45–11.70 GHz, band C is 11.70–11.95 GHz, and band D is 12.50–12.75 GHz) transmit/downlink band. Bands C and D make it possible to exploit satellite-specific frequency allocation in all three International Telecommunication Union (ITU) regions.

INTELSAT VII/VIIA satellites have the capability to interconnect earth stations operating at C-band with those operating at Ku-band. This is known as cross-strapped operation. INTELSAT VII/VIIA satellites can be configured via

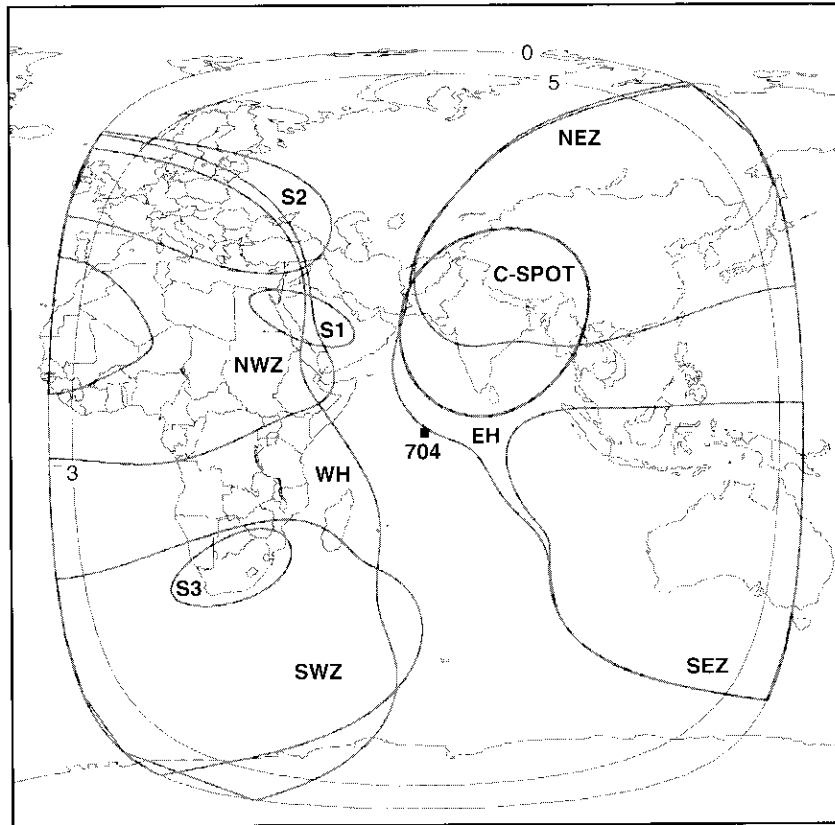


Figure 3. *INTELSAT 704 at 66°E: Composite Coverage*  
(pitch = 1.0°E, tilt = 0.3°N, inverted mode)

ground command for a 12-GHz (instead of 11-GHz) downlink on any Ku-band spot beam channel independently, in the lower 241 MHz of the 500-MHz frequency band. Therefore, for the six Ku-band transponders in channels (1-2), (3-4), and (5-6) of band A, one can select among three downlink frequency bands of "11 GHz" (10.95–11.2 GHz), "ITU Region 2" (11.7–11.95 GHz), or "ITU Regions 1 and 3" (12.5–12.75 GHz).

The RF spectrum of the INTELSAT VII/VIIA satellites is partitioned into segments of 34, 36, 41, 72, 77, and 112 MHz, depending on the frequency and beam connections employed. C-band spectrum is divided into segments of 34, 36, 41, 72, and 77 MHz, while Ku-band spectrum is divided into segments of

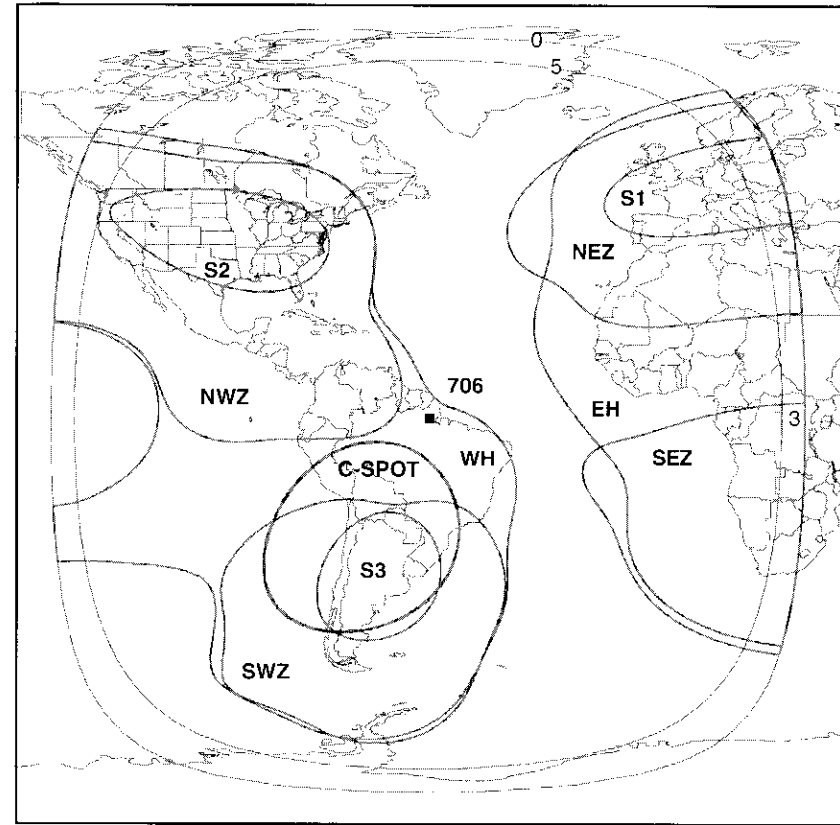
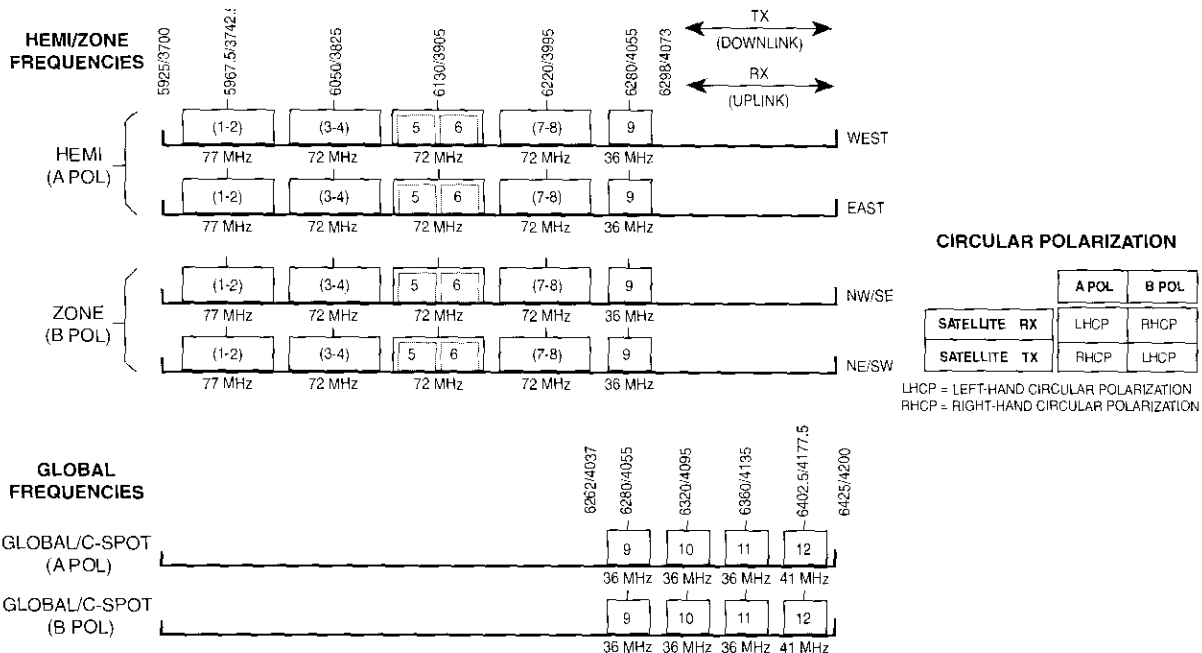


Figure 4. *INTELSAT 706 at 307°E: Composite Coverage*  
(pitch = 1.0°E, tilt = 0.3°N, normal mode)

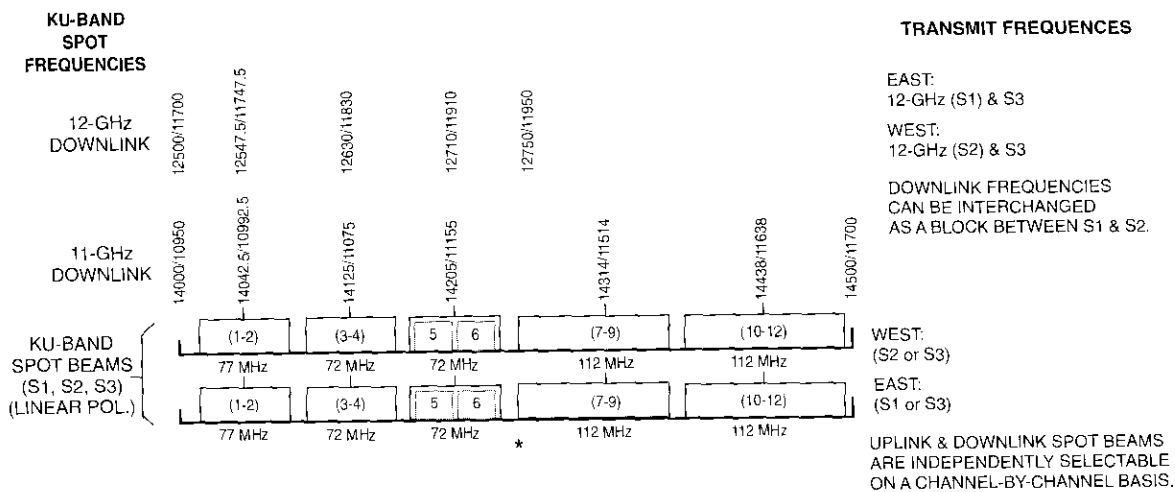
34, 72, 77, and 112 MHz. INTELSAT VII satellites have 26 C-band and 10 Ku-band transponders, resulting in 42 C-band and 20 Ku-band 36-MHz units of capacity, for a total of 62 units of 36-MHz bandwidth. INTELSAT VIIA satellites have the same number of C-band transponders, plus four additional Ku-band transponders. This results in 42 C-band and 28 Ku-band 36-MHz units of capacity, for a total of 70 units of 36 MHz.

Extensive flexibility in connectivity is provided through static switch matrices. Tables 1 and 2 give connectivity matrices for INTELSAT VII and VIIA, respectively. On INTELSAT VII satellites, there are five 6 × 6 switch matrices interconnecting channels (1-2), (3-4), 5, 6, and (7-8)/(7-9) received from the



Note: 1. C-band beacons are available at 3947.5, 3948.0, 3950.0, 3952.0, and 3952.5 MHz. With the exception of the 3950.0-MHz tracking-only beacon, which is linear (V Pol), all telemetry/tracking beacons are RHCP.

(a) INTELSAT VII C-Band



Notes: 2. The 11-GHz Ku-band beacons at 11198 and 11452 MHz are RHCP. The 12-GHz Ku-band beacons at 11701 and 12501 MHz are Linear Pol.

- 3. The 11-GHz or 12-GHz Ku-band spot frequencies may be selected independently for each beam and each transponder.
- 4. The polarization of the S3 beam may be changed via ground command to be orthogonal to either S1 or S2 for flight models 703 and onward.

\* There is a 250-MHz gap (11200–11450 MHz) between (5-6) and (7-9) on the 11-GHz downlink.

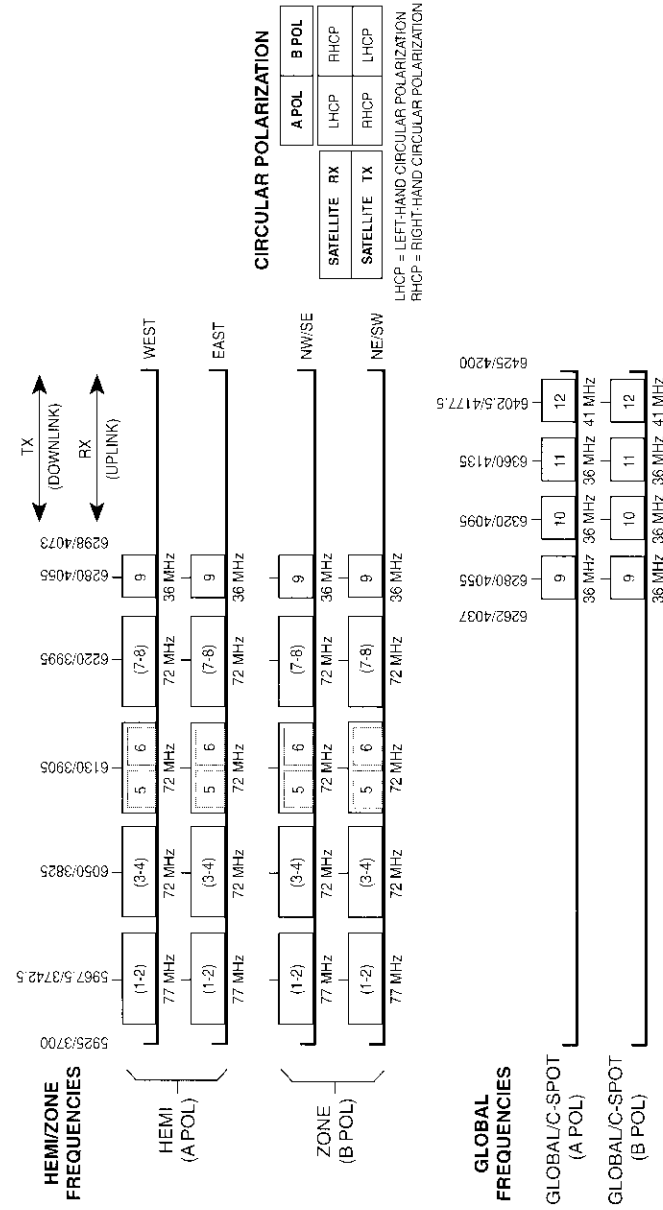
(b) INTELSAT VII Ku-Band

Figure 5. Transponder Frequency Plan for INTELSAT VII

hemi/zone antennas and two of the three Ku-band spot uplinks. The 4 × 6 switch matrix interconnects the four channel 9 hemi/zone uplinks. All global and C-spot channels can be interchanged on a channel-by-channel basis on both the uplink and downlink. Therefore, INTELSAT VII satellites can accommodate changing traffic requirements by routing individual channel 9, 10, 11, and 12 signals from either the global or the C-spot uplink in either A or B polarization (a total of four receivers) to either global or C-spot downlinks of corresponding polarization. To avoid interference, each channel is precluded from serving both global and C-spot beams of the same polarization simultaneously. Switchability between the C-spot beams and the corresponding global beams is provided for transponders in channels 10, 11, and 12 on a transponder-by-transponder basis. Global and C-spot interconnectivity allows signals from transponders to be routed to downlinks of corresponding polarization. Specifically, channel 9, 10, 11, and 12 signals from either the global or the C-spot uplink can be routed to either the global or the C-spot downlinks. Channel 9 is switchable among C-spot, global, hemi, and zone beams.

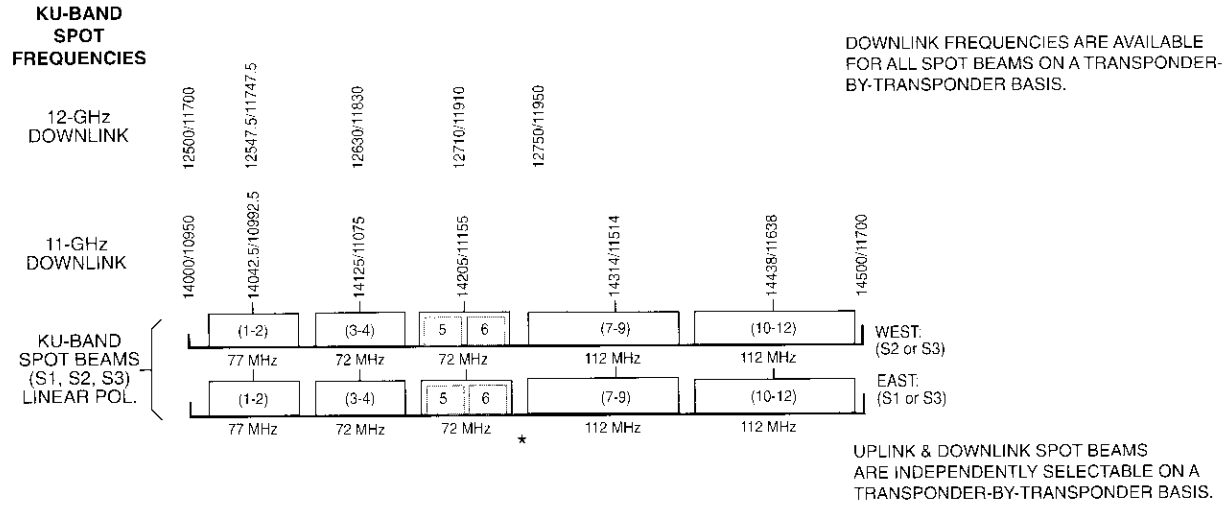
The C-band SSPAs on INTELSAT VII satellites have four different power level options: 10, 16, 20, and 30 W. The different power levels are utilized to keep oppositely polarized transponder EIRPs approximately equal, in order to maintain the polarization isolation necessary for successful frequency reuse operation. Ku-band TWTAs on INTELSAT VII satellites have two different power level options, with five 35-W TWTAs and five 50-W TWTAs. INTELSAT VII/VIIA satellites use LTWTAs to improve repeater transmit linearity and allow more linear operation over a wide range of output backoff levels. However, it is possible to bypass the linearizer independently for each channel, so signals may be routed directly to TWTAs. As mentioned earlier, INTELSAT VII/VIIA satellites have sufficient redundancy to provide reliable communications throughout the life of the satellite.

Tables 3 and 4 provide detailed communications payload parameters for the INTELSAT VII and VIIA series satellites, respectively. C-band saturation flux densities vary from -87 to -73 dBW/m<sup>2</sup> in 1-dB steps, and Ku-band saturation flux densities vary from -90 to -76 dBW/m<sup>2</sup> in 1-dB steps. This ability to adjust saturation flux density in small steps allows the tailoring of individual transponder gain for best overall link performance. In addition, the variety of earth stations now accessing the INTELSAT system can be better accommodated, and interbeam isolation can be maximized. Note that satellites prior to INTELSAT VII/VIIA allowed only three gain states at most, separated by nominally 7.5 dB.

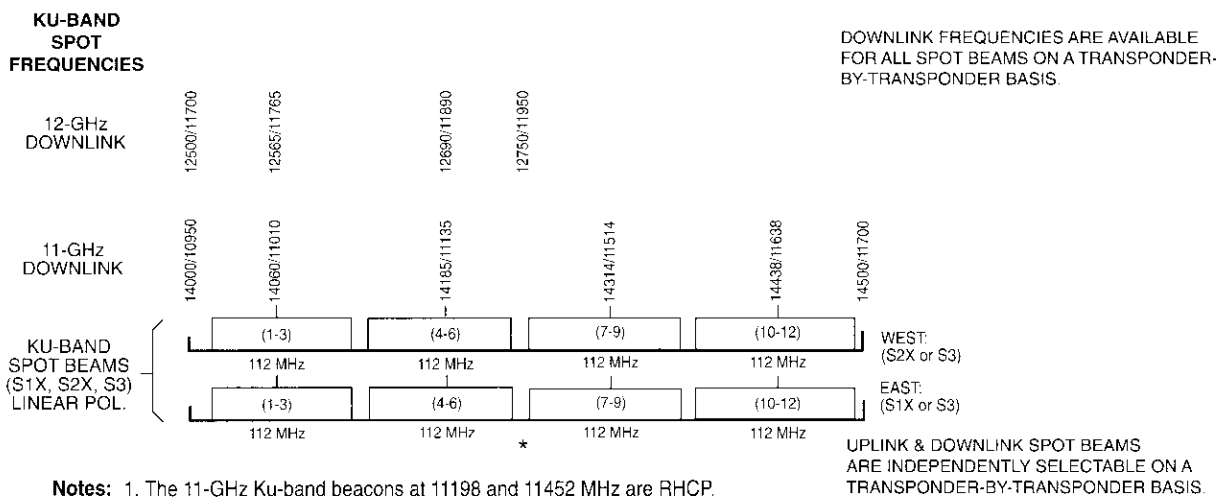


(a) INTELSAT VIIA C-Band

Figure 6. Transponder Frequency Plan for INTELSAT VIIA



(b-1) INTELSAT VIIA Ku-Band, Part 1



- Notes:**
- The 11-GHz Ku-band beacons at 11198 and 11452 MHz are RHCP. The 12-GHz Ku-band beacons at 11701 and 12501 MHz are Linear Pol.
  - The 11-GHz or 12-GHz Ku-band spot frequencies may be selected independently for each beam and each transponder.
  - The polarization of the S3 beam may be changed via ground command to be orthogonal to either S1 or S2 for flight models 703 and onward.
  - S3 operation in transponders (1-3) and (4-6) is limited to bandwidth defined by transponders (1-2) and (5-6), respectively.
  - S3 may operate with the 41-MHz portion of the uplink in transponder (10-12) corresponding to the bandwidth defined by the downlink A or B Pol Global/C-Spot transponder in channel 12.
- \* There is a 250-MHz gap (11200-11450 MHz) between (5-6) and (7-9) on the 11-GHz downlink.

(b-2) INTELSAT VIIA Ku-Band, Part 2

Figure 6. Transponder Frequency Plan for INTELSAT VIIA (Cont'd)

TABLE 1. INTELSAT VII (701 THROUGH 705, AND 709)  
CONNECTIVITY MATRIX

UPLINK BEAM	CHANNEL NO.	DOWNLINK BEAM	UP/DOWN FREQUENCY BAND			
			C-BAND (6/4 GHz)	KU-BAND (14/11 or 14/12 GHz)	CROSS-STRAPPED	
					(6/11 or 6/12 GHz)	(14/4 GHz)
GA	9	III, GA, or CSA	X			
GA	10, 11, 12	GA or CSA	X			
GB	9	H2, GB, or CSB	X			
GB	10, 11, 12	GB or CSB	X			
CSA	9	H1, GA, or CSA	X			
CSA	10, 11, 12	CSA or GA	X			
CSB	9	H2, GB, or CSB	X			
CSB	10, 11, 12	CSB or GB	X			
H1	(1-2), (3-4), 5, 6, (7-8)	H1, H2, Z1, or Z2	X			
III	9	III, H2, Z1, Z2, GA, or CSA	X			
H1	(1-2), (3-4), 5, 6, (7-8)	S1 or S2 or S3			X	
H2	(1-2), (3-4), 5, 6, (7-8)	H1, H2, Z1, or Z2	X			
H2	9	H1, H2, Z1, Z2, GB, or CSB	X			
H2	(1-2), (3-4), 5, 6, (7-8)	S1 or S2 or S3			X	
Z1	(1-2), (3-4), 5, 6, (7-8), 9	H1, H2, Z1, or Z2	X			
Z1	(1-2), (3-4), 5, 6, (7-8)	S1 or S2 or S3			X	
Z2	(1-2), (3-4), 5, 6, (7-8), 9	III, H2, Z1, or Z2	X			
Z2	(1-2), (3-4), 5, 6, (7-8)	S1 or S2 or S3			X	
S1	(1-2), (3-4), 5, 6, (7-9), (10-12)	S1 or S2 or S3		X		
S1	(1-2), (3-4), 5, 6, (7-9)/(7-8)	H1, H2, Z1, or Z2				X
S2	(1-2), (3-4), 5, 6, (7-9), (10-12)	S1 or S2 or S3		X		
S2	(1-2), (3-4), 5, 6, (7-9)/(7-8)	H1, H2, Z1, or Z2				X
S3	(1-2), (3-4), 5, 6, (7-9), (10-12)	S1 or S2 or S3		X		
S3	(1-2), (3-4), 5, 6, (7-9)/(7-8)	H1, H2, Z1, or Z2				X

### Input multiplexer filters for channel (5-6)

The transponder in channel (5-6) is split into two segments, each with a usable bandwidth of 34 MHz, by a two-channel multiplexing filter at the input to the transponder power amplification section. This filter allows two separate independent beams, corresponding to channels 5 and 6, to be connected to a single transponder power amplifier, which in turn is connected to either a C-band hemi/zone downlink beam or a Ku-band spot beam downlink. On the uplink, connectivity provided in channel 5 is independent from that provided in channel 6. For example, using this flexibility for the hemi beam it is possible to uplink from the west hemi beam in the lower half of a hemi transponder (channel 5) and uplink from the east hemi beam in the upper half of the same transponder (channel 6). The traffic from both these sources is then routed to a common downlink for the entire channel (5-6).

### INTELSAT VII/VIIA hemi/zone beams

The two spatially isolated C-band hemi beams have the same sense of circular polarization (A pol). The larger hemi coverage is called hemi 1 (H1); the smaller hemi coverage is hemi 2 (H2). The two spatially isolated C-band zone beams also have the same circular polarization (B pol), which is of opposite sense to the hemi beams. Four-times frequency reuse is accomplished in the hemi and zone beams through spatial isolation of the beams, with circular polarization of opposite senses between the hemi and zone beams. INTELSAT VII/VIIA hemi and zone beams are not steerable; however, a platform bias can be applied to achieve desired coverages from given orbital locations. Note that the two zone beams on the INTELSAT VII/VIIA satellites are split, with each offering a basic zone coverage [referred to here as zone 1 (Z1) and zone 2 (Z2)] and an "extension" zone coverage, referred to as Z1A and Z2A.

On INTELSAT VII/VIIA satellites, the hemi beam transponders use 30-W (H1) and 20-W (H2) SSPAs, delivering an EIRP of 33 dBW at the edge of coverage. It should be noted that INTELSAT 704 and onward were modified to broaden the hemi beam coverages for use in the IOR. This resulted in 32.8-dBW EIRP for H1 transponders and 32.3-dBW EIRP for H2 transponders.

The zone beam transponders on INTELSAT VII/VIIA satellites use 16-W (Z1/Z1A) and 10-W (Z2/Z2A) SSPAs to deliver an EIRP of 33 dBW at the edge of coverage. As above, the INTELSAT VII/VIIA satellites (again from 704 onward) were modified to broaden the zone beam coverages in the IOR. This resulted in 32.9-dBW EIRP for Z1/Z2 and 32.7-dBW EIRP for Z1A, while 33.0 dBW for Z2A was maintained.

TABLE 2. INTELSAT VIIA (706 THROUGH 708) CONNECTIVITY MATRIX

UPLINK BEAM	CHANNEL NO.	DOWNLINK BEAM	UP/DOWN FREQUENCY BAND			
			C-BAND (6/4 GHz)	KU-BAND (14/11 or 14/12 GHz)	CROSS-STRAPPED	
					(6/11 or 6/12 GHz)	(14/4 GHz)
GA	9	H1, GA, or CSA	X			
GA	10, 11, 12	GA or CSA	X			
GB	9	H2, GB, or CSB	X			
GB	10, 11, 12	GB or CSB	X			
CSA	9	H1, GA, or CSA	X			
CSA	10, 11, 12	CSA or GA	X			
CSB	9	H2, GB, or CSB	X			
CSB	10, 11, 12	CSB or GB	X			
H1	(1-2), (3-4), 5, 6, (7-8)	III, H2, Z1, or Z2	X			
H1	9	H1, H2, Z1, Z2, GA, or CSA	X			
H1	(1-2), (3-4), 5, 6, (7-8)	S1 or S2 or S3		X		
H2	(1-2), (3-4), 5, 6, (7-8)	H1, H2, Z1, or Z2	X			
H2	9	H1, H2, Z1, Z2, GB, or CSB	X			
H2	(1-2), (3-4), 5, 6, (7-8)	S1 or S2 or S3		X		
Z1	(1-2), (3-4), 5, 6, (7-8), 9	H1, H2, Z1, or Z2	X			
Z1	(1-2), (3-4), 5, 6, (7-8)	S1 or S2 or S3		X		
Z2	(1-2), (3-4), 5, 6, (7-8), 9	III, H2, Z1, or Z2	X			
Z2	(1-2), (3-4), 5, 6, (7-8)	S1 or S2 or S3		X		
S1	(1-2), (3-4), 5, 6, (7-9), (10-12)	S1 or S2 or S3		X		
S1	(1-2), (3-4), 5, 6, (7-9)/(7-8)	H1, H2, Z1, or Z2			X	
S1X	(1-3)/(7-9), (4-6)/(10-12)	S1X or S2X		X		
S1X	(1-3), (4-6), (7-9), (10-12)	S3		X		
S2	(1-2), (3-4), 5, 6, (7-9), (10-12)	S1 or S2 or S3		X		

TABLE 2. INTELSAT VIIA (706 THROUGH 708) CONNECTIVITY MATRIX (CONT'D)

UPLINK BEAM	CHANNEL NO.	DOWNLINK BEAM	UP/DOWN FREQUENCY BAND			
			C-BAND (6/4 GHz)	KU-BAND (14/11 or 14/12 GHz)	CROSS-STRAPPED	
					(6/11 or 6/12 GHz)	(14/4 GHz)
S2	(1-2), (3-4), 5, 6, (7-9)/(7-8)	III, H2, Z1, or Z2				X
S2X	(1-3)/(7-9), (4-6)/(10-12)	S1X or S2X		X		
S2X	(1-3), (4-6), (7-9), (10-12)	S3		X		
S3	(1-2), (3-4), 5, 6, (7-9), (10-12)	S1 or S2 or S3		X		
S3	(1-2), (3-4), 5, 6, (7-9)/(7-8)	III, H2, Z1, or Z2				X
S3	(1-2), (5-6), (7-9), (10-12)	S1X or S2X		X		
S3	12	GA, CSA, or GB, CSB				X

The zone beams Z1 and Z2 are each split to cover smaller areas. For example, zone 1 provides split coverage consisting of regions "zone (Z1)" and "extension zone (Z1A)". These two components of the zone 1 beam illuminate diagonally opposite quadrants (northwest and southeast) of the east and west hemispheres, as seen from the satellite. The two components of the zone 2 beam (Z2 and Z2A) cover the remaining two diagonally opposite quadrants (northeast and southwest).

On the uplink, a zone receiver can be connected to either of the two coverages of a set (Z1 or Z1A), or to a combination of the two coverages (Z1 and Z1A), for all channels in the five-transponder set. Therefore, uplink coverage of Z1, Z1A, or (Z1 + Z1A) can be selected on a channel-by-channel basis, or all channels can be combined. A channel may be a 77-MHz transponder for channel (1-2), or a 72-MHz transponder for channels (3-4) and (7-8), or a 34-MHz unit for channels 5 and 6, or a 36-MHz transponder for channel 9. This capability does not exist on the downlink. When the receiver operates with the combined coverage uplink, this is called enhanced zone operation. In this mode, on the downlink, a zone transmitter can be connected to one of the two coverages of a set (Z1 or Z1A) on a transponder-by-transponder (channel-by-channel) basis. Enhanced zone 1 operation allows transponders normally associated with Z1 to be switched on the downlink to the diagonally opposite

TABLE 3. INTELSAT VII (701 THROUGH 705, AND 709) PARAMETERS

BEAM CONNECTIVITY (UP/DOWN)	BANDWIDTH (MHz)	SATURATION EIRP (dBW)	SATURATION FLUX DENSITY (dBW/m <sup>2</sup> )		
			HIGHEST	LOWEST	G/T (dB/W)
Global/Global	36	26-29 <sup>a</sup>	-87	-73	-12
Hemi/Hemi	72	33	-87	-73	-8.5 (H1) or -7.5 (H2)
Hemi/Hemi (Ch 9)	36	33	-87	-73	-8.5 (H1) or -7.5 (H2)
Zone/Zone	72	33	-87	-73	-9.2 to -4.0
Zone/Zone (Ch 9)	36	33	-87	-73	-9.2 to -4.0
C-Spot/C-Spot	36	33.3-36.5 <sup>b</sup>	-87	-73	-5.0
Any Ku-Band Spot/S1	72/112	45.4 (35 W) or 46.7 (50 W)	-90	-76	0.5-4.5 <sup>c</sup>
Any Ku-Band Spot/S2	72/112	44.5 (35 W) or 45.8 (50 W)	-90	-76	0.5-4.5 <sup>c</sup>
Any Ku-Band Spot/Enhanced S2	72/112	44.1 (50 W)	-90	-76	0.5 4.5 <sup>c</sup>
Any Ku-Band Spot/S3	72/112	46.0 (35 W) or 47.8 (50 W)	-90	-76	0.5 4.5 <sup>c</sup>

<sup>a</sup> EIRP of global beam transponders:

GA, Ch 9	28.5 dBW
GB, Ch 9	26.0 dBW
GA/GB, Ch 10/11	26.0 dBW
GA/GB, Ch 12	29.0 dBW

<sup>b</sup> EIRP of C-spot beam transponders:

CSA, Ch 9	36.5 dBW
CSB, Ch 9	34.3 dBW
CSA/CSB, Ch 10/11	33.3 dBW
CSA/CSB, Ch 12	36.3 dBW

<sup>c</sup> G/T of Ku-band spot beams, for inner contour:

S1	4.5 dB/K
S2	2.5 dB/K
Enhanced S2	0.5 dB/K
S3	3.8 dB/K

All Ku-band EIRP values are edge-of-coverage for inner contour.

TABLE 4. INTELSAT VIIA (706 THROUGH 708) PARAMETERS

BEAM CONNECTIVITY (UP/DOWN)	BANDWIDTH (MHz)	SATURATION EIRP (dBW)	SATURATION FLUX DENSITY (dBW/m <sup>2</sup> )		
			HIGHEST	LOWEST	G/T (dB/W)
Global/Global	36	26-29 <sup>a</sup>	-87	-73	-12.0
Hemi/Hemi	72	33	-87	-73	-8.7 (H1) or -7.5 (H2)
Hemi/Hemi (Ch 9)	36	33	-87	-73	-8.5 (H1) or -7.5 (H2)
Zone/Zone	72	33	-87	-73	-9.2 to -4.0
Zone/Zone (Ch 9)	36	33	-87	-73	-9.2 to -4.0
C-Spot/C-Spot	36	33.2 36.1 <sup>b</sup>	-87	-73	-5.0
Any Ku-Band Spot/S1	72 112	47.0 (49 W) 49.5 (2 × 49 W)	-90 -90	-76 -76	-0.6-4.2 <sup>c</sup> -0.6-4.2 <sup>c</sup>
Any Ku-Band Spot/S1X	112 112	47.1 (49 W) 49.4 (2 × 49 W)	-90 -90	-76 -76	1.0-4.2 <sup>c</sup> 1.0-4.2 <sup>c</sup>
Any Ku-Band Spot/S2	72 112	47.0 (73 W) 49.4 (2 × 73 W)	-90 -90	-76 -76	1.0 4.2 <sup>c</sup> 1.0-4.2 <sup>c</sup>
Any Ku-Band Spot/S2X	112 112	46.7 (73 W) 48.9 (2 × 73 W)	-90 -90	-76 -76	1.0-4.2 <sup>c</sup> 1.0 4.2 <sup>c</sup>
Any Ku-Band Spot/Enhanced S2	72 112	45.2 (73 W) 47.6 (2 × 73 W)	-90 -90	-76 -76	-0.6-4.2 <sup>c</sup> -0.6-4.2 <sup>c</sup>
Any Ku-Band Spot/S3	72 72	42.8 (49 W) or 44.5 (73 W) 45.0 (2 × 49 W) or 46.7 (2 × 73 W)	-90 -90	-76 -76	-0.6-4.2 <sup>c</sup> -0.6-4.2 <sup>c</sup>

<sup>a</sup> EIRP of global beam transponders:

GA, Ch 9	28.0 dBW
GB, Ch 9	26.0 dBW
GA/GB, Ch 10/11/12	29.0 dBW

<sup>b</sup> EIRP of C-spot beam transponders:

CSA, Ch 9	35.2 dBW
CSB, Ch 9	33.2 dBW
CSA/CSB, Ch 10/11/12	36.1 dBW

<sup>c</sup> G/T of Ku-band spot beams, for inner contour:

S1/S1X	4.2 dB/K
S2	1.1 dB/K
S2X	1.5 dB/K
Enhanced S2	-0.6 dB/K
S3	1.0 dB/K

All Ku-band EIRP values are edge-of-coverage for inner contour.

Z1A coverage. Enhanced zone 2 operation is similar, but uses the other pair of diagonally opposite quadrant coverages. As an example, enhanced zone operation is very attractive in the POR (see Figure 1), where traffic uplinked from the U.S. in Z2 (NW) and Australia in Z2A (SW) can be combined in the Z2 + Z2A (NE + SW) coverage and downlinked to Japan/Korea in the Z1 (NW) beam using one transponder. Alternatively, the above uplink can be downlinked via the Z2 (NE) or Z2A (SW) beams. This design feature helps to tailor INTELSAT VII/VIIA capacity to match the east/west traffic imbalance in the POR, resulting in improved loading efficiency in this region.

To summarize, the INTELSAT VII/VIIA satellites have two sets of five zone-beam C-band transponders, in channels (1-2), (3-4), (5-6), (7-8), and 9, and four zone coverage areas (Z1, Z2, Z1A, and Z2A), grouped into two sets (Z1/Z1A and Z2/Z2A). Five zone transponders are assigned to each of the two sets of zone coverages. Also, the Z1/Z1A coverages are always associated with the northwest and southeast zone coverages of INTELSAT VII/VIIA, and Z2/Z2A coverages are always associated with the northeast and southwest zone coverages, whether the satellite is in normal or inverted orientation.

#### **INTELSAT VII global/C-spot beams**

At C-band (6/4 GHz), two-times frequency reuse is achieved in the global and C-spot beams, with the signals being transmitted in orthogonal senses of circular polarization. The two global, or earth, coverages are achieved by using a horn antenna (with the usual 18° beamwidth) to illuminate the entire visible earth. These coverages are identified as global A (GA) and global B (GB). The global beams may be steered, but only in azimuth, to compensate for possible spacecraft (platform) east-west pitch bias used to optimize the hemi/zone beam coverages.

Two INTELSAT VII/VIIA congruent C-spot coverages are achieved by orthogonal polarization frequency reuse, and with an antenna having 6° beamwidth. These coverages, identified as C-spot A (CSA) and C-spot B (CSB), are mechanically fully steerable anywhere on the visible earth, as shown in Figure 1 for INTELSAT 701 at 174°E. There are up to eight global/C-spot transponders (four in A pol and four in B pol) on an INTELSAT VII/VIIA satellite, although it is highly unlikely that more than six would ever be so used. To meet various service requirements, any of these transponders can be switched to the C-spot beams.

On INTELSAT VII, global transponders in channel 12 use 30-W SSPAs and deliver 29-dBW EIRP at the edge of coverage, while the global transponders in channels 10 and 11 use 16-W SSPAs and deliver 26 dBW EIRP. If C-spot transponders are used in channel 12, however, a 30-W SSPA will deliver

36.3-dBW EIRP at the edge of coverage, while those C-spot transponders in channels 10 and 11 using 16-W SSPAs will deliver 33.3-dBW power.

#### **INTELSAT VIIA global/C-spot beams**

At C-band, INTELSAT VIIA differs from INTELSAT VII only in the power levels of the global and C-spot transponders. The downlink EIRP of the global and C-spot transponders in channels 10 and 11 are increased to be equal to those transponders in channel 12. All INTELSAT VIIA global transponders use 30-W SSPAs and deliver 29-dBW EIRP at the edge of coverage. However, if C-spot transponders are activated using the same 30-W SSPAs, an EIRP of 36.1 dBW will be delivered at the edge of coverage of the 6° C-spot beam.

#### **INTELSAT VII Ku-band spot beams**

There are three independently (of one another and the C-spot beam) steerable Ku-band spot beams on the INTELSAT VII series satellites: spot 1 (S1), spot 2 (S2), and spot 3 (S3). As an example, the pointings of the Ku-band spot beams of INTELSAT 701 at 174°E are shown in Figure 1. The S1 and S2 coverages operate with orthogonal linear polarization, either vertically or horizontally as referenced to the spacecraft coordinate system. Vertical orientation places the E-field vector parallel to the spacecraft's pitch axis (north-south); horizontal orientation places the E-field vector parallel to the spacecraft's roll axis (east-west). Two-times frequency reuse is accomplished at Ku-band by spatial isolation of the Ku-band spot beams, which in normal operation have orthogonal linear polarization between the S1/S3 beams on the one hand and the S2 beam on the other. The linear polarization of the Ku-band spot beams of INTELSAT VII is as follows:

- *Spot 1 and Spot 3:* Satellite receive/uplink is horizontal, and satellite transmit/downlink is vertical.
- *Spot 2:* Satellite receive/uplink is vertical, and satellite transmit/downlink is horizontal.

However, to provide additional operational flexibility, the polarization of S3 may be changed via ground command to be orthogonal to either S1 or S2 on INTELSAT 703 and onward. This allows the S1 and S3 coverages to overlap.

Note that the only exception to fully independent steerability is the enhanced spot 2 (S2A) beam, which is intended for use only in the POR. Enhanced beam S2A has a one-to-one steering relationship with the S2 beam because S2A is generated using a second feed with the S2 antenna reflector. In the S2A mode,

S2 and S2A function as a single beam on both the uplink and downlink. The primary feed of S2, which forms the S2 beam, provides an elliptical beam that covers Japan, Korea, and Hong Kong when the satellite is deployed in the POR. However, if additional coverage is required, this feed may be combined with the second feed on the S2 reflector to obtain the S2A configuration. The S2A beam provides simultaneous coverage of the main business areas and population centers in southeast Australia.

The S1 and S3 beams, which are each generated using a single feed horn with their respective reflectors, are elliptical and circular, respectively. The S1 beam is a simple elliptical beam with a  $2.7^\circ \times 1.3^\circ$  inner contour. The S3 beam is a simple  $2.2^\circ$  inner contour circular beam. On the other hand, the S2 beam is elliptical with a  $3.5^\circ \times 2.0^\circ$  inner contour. Note that inner contour is defined to be 4-dB down from beam peak, except for S2A where the inner contour is 3-dB down from beam peak.

A key Ku-band feature of INTELSAT VII series satellites is the addition of the S3 beam, whereby unused transponders on the S1 or S2 may be allocated to S3 to provide Ku-band coverage to a different geographical area. For INTELSAT VII satellites, up to five transponders may be assigned to S3 on a channel-by-channel basis, and can be operated in any of the downlink frequency bands, again channel-by-channel. The use of the Ku-band S3 beam in any uplink or downlink channel excludes the availability of the corresponding uplink or downlink channel for either Ku-band S1 or S2. Only two Ku-band spot coverages out of three are simultaneously available for each channel.

The 10 Ku-band transponders on an INTELSAT VII satellite (five with 35-W LTWTAs and five with 50-W LTWTAs) can be individually assigned on an as-needed basis among the three Ku-band spot beams. The elliptical S1 beam can be assigned either a 35- or a 50-W TWTA, to achieve EIRP values of 45.4 or 47.0 dBW, respectively. The elliptical S2 beam achieves a 44.5 or 45.8 dBW with 35- and 50-W LTWTAs, respectively. It should be noted that, when S2 is operated in the S2A mode, only the 50-W LTWTAs can be assigned, resulting in an EIRP of 44.1 dBW. The circular S3 beam can also be assigned to either a 35- or 50-W LTWTA, achieving a 46.0- or 47.8-dBW EIRP, respectively. Table 5 summarizes INTELSAT VII/VIIA Ku-band spot beam sizes, TWTA options, and the resulting EIRP values.

The 35- and 50-W LTWTAs on INTELSAT VII were specifically constructed to operate across the entire 10.95- to 12.75-GHz frequency range. INTELSAT VII can be configured via ground command to independently select downlink frequencies either between 11.7 and 11.95 GHz, or between 12.5 and 12.75 GHz, on a transponder-by-transponder basis [*i.e.*, channels (1-2), (3-4), and/or (5-6) only]. It is also possible to exchange, as a block and by ground

TABLE 5. INTELSAT VII/VIIA KU-BAND BEAM, TWTA SIZE, AND EIRP<sup>a</sup>

DOWNLINK BEAM	BEAM SHAPE	BEAM SIZE	TWTA (W)	DOWNLINK EIRP (dBW)
<b>INTELSAT VII (701 through 705, and 709) Satellites<sup>b</sup></b>				
S1	Elliptical	$2.7^\circ \times 1.3^\circ$	35	45.4
			50	46.7
S2	Elliptical	$3.5^\circ \times 2^\circ$	35	44.5
			50	45.8
Enhanced S2 and S2A <sup>c</sup>	Elliptical	$3.5^\circ \times 2^\circ$ Plus S2A	50	44.1
S3	Circular	$2.2^\circ \times 2.2^\circ$	35	46.0
			50	47.5
<b>INTELSAT VIIA (706 through 708) Satellites<sup>d</sup></b>				
S1/S1X	Elliptical	$2.7^\circ \times 1.3^\circ$	Single 49-W tube	47.0
			Two 49-W parallel tubes	49.5
S2/S2X	Elliptical	$3.5^\circ \times 2^\circ$	Single 73-W tube	47.0
			Two 73-W parallel tubes	49.4
S3	Circular	$3.3^\circ \times 3.3^\circ$	Single 49-W tube	42.8
			Single 73-W tube	44.5
			Two 49-W parallel tubes	45.0
			Two 73-W parallel tubes	46.7

<sup>a</sup> Beam size and downlink EIRP are based on inner contour (defined to be 4-dB down from beam peak for all INTELSAT VII/VIIA Ku-band spot beams except S2A, where the inner contour is 3-dB down from beam peak).

<sup>b</sup> INTELSAT VII satellites have 10 Ku-band TWTAs ( $5 \times 35$  W and  $5 \times 50$  W) to be shared among three spot beams (S1, S2, and S3).

<sup>c</sup> Only on 701 at 174°E.

<sup>d</sup> INTELSAT VIIA satellites have 14 Ku-band TWTAs ( $7 \times 49$  W and  $7 \times 73$  W) to be shared among three spot beams (S1/S1X, S2/S2X, and S3).

command, the downlink frequencies associated with S1 with those of all the transmission channels associated with S2, except when S2 is operated in the S2A mode in the POR.

On INTELSAT VII satellites, cross-strapped operation is only possible between C-band hemi/zone transponders and Ku-band S1/S2/S3 transponders in channels (1-2), (3-4), (5-6), and/or (7-8). Cross-strapped operation with transponder (7-8) at C-band can only take place in the corresponding 72-MHz portion of the 112-MHz-wide Ku-band transponder (7-9). Note that the Ku-band transponders occupying the 11.45–11.70 GHz and 14.25–14.50 GHz

frequency band segments are each 112-MHz wide. This was done, in part, to allow the possibility of rate 3/4 forward error correction (FEC) coded quadrature phase shift keyed (QPSK) transmission of 140- and 155-Mb/s high-speed digital bit streams.

### **INTELSAT VIIA Ku-band payload enhancements**

INTELSAT VIIA Ku-band transponder power is higher than on INTELSAT VII because 49- and 73-W LTWTAs, again designed for operation over the full 10.95–12.75 GHz frequency band, replace the 35- and 50-W LTWTAs. Also, INTELSAT VIIA has 14 Ku-band transponders, compared to 10 on INTELSAT VII. The four additional Ku-band transponders are accommodated through improved bus prime power capability, larger spacecraft size, and by the introduction of orthogonal polarization isolation at Ku-band.

The INTELSAT VIIA satellites are the first INTELSAT satellites to employ dual polarized Ku-band spot beams. The four-times frequency reuse is accomplished in the 14/11-GHz or 14/12-GHz band by spatial isolation between the S1 and S3 beams on the one hand, and the S2 beam on the other. Polarization isolation, in the form of orthogonal linear polarization, is also used between the S1 and the S1 cross-polarized (S1X) beams, as well as between the S2 and the S2 cross-polarized (S2X) beams. The S1 and S1X beams offer congruent coverage, as do S2 and S2X.

As shown in Figure 6b, the four additional Ku-band transponders on INTELSAT VIIA are each 112-MHz wide. They are provided in two sets of two spot beam transponders. One set is associated with the S1X beam, the other with the S2X beam. One of the S1X transponders can operate in either channels (1-3) or (7-9), upon ground command. The other S1X transponder can operate in either channels (4-6) or (10-12), again on command from the ground. A similar capability is available for the two S2X transponders. This flexible transponder assignment feature provides frequency agility to facilitate both frequency planning and intersystem coordination. Note that there is no enhanced S2A mode of operation for the cross-polarized S2X transponders.

On INTELSAT VIIA series satellites, in addition to the increased traveling wave tube power, a switchable "high-power" mode of operation has been added. This allows up to four pairs of selected Ku-band LTWTAs to be operated in a parallel (phase-combined) mode. In this mode, the power amplifier in each transponder can be paralleled with the corresponding, co-polarized transponder [channels (7-9) or channels (10-12)] to provide 49.5-dBW EIRP to either polarization. The parallel (phase-combined) operation is accomplished by combining the output of the two LTWTAs in a hybrid located in the output multiplexer and feeding the input signals to both amplifiers through a hybrid

in the input multiplexer. Phase-combining will provide about 2.5 dB more output power than using a single tube. This high-power mode is available to a total of four transponders: in up to two S1 (or S1X) transponders, up to two S2 (or S2X) transponders, or up to two S3 transponders. Additionally, high-power operation may be employed in transponders (1-3) and (4-6) in the S1X and S2X beams only, and in transponders (1-2) and (5-6) in the S3 beam. Note that phase-combining in microwave tube amplifiers is a fairly common practice in earth stations, and two INTELSAT VA (IBS) satellites have a limited phase-combining capability at Ku-band. When undertaking phase-combined operation, it is important to establish the proper phase and amplitude relationships between the signal paths. On INTELSAT VIIA, ground-commandable phase shifters are used in conjunction with the gain step attenuators and a detector on the fourth port of the output combining hybrid to establish and maintain this relationship.

The circular S3 beam on INTELSAT VIIA is broadened from the 2.2° inner contour beamwidth on INTELSAT VII, to 3.3°. On INTELSAT VIIA, up to four high-power mode transponders, or various combinations of single and parallel transponders, can be assigned to S3. The polarization of S3 may be changed via ground command to be orthogonal to either S1 or S2. It is possible to assign various combinations of S1, S1X, S2, and S2X transponders to the S3 beam to provide up to five S3 transponders.

In channel 12, it is possible to connect the Ku-band S3 uplink to either the global/CSA or global/CSB 41-MHz transponder downlink. The intended application is to provide SNG services using small Ku-band uplink antennas to large C-band earth stations anywhere on the earth's surface visible from the orbital location of a particular INTELSAT VIIA. Of course, this also offers the possibility of a coordination channel from the C-band station to the newsgathering station. Otherwise, on INTELSAT VIIA, cross-strapped operation is possible between C-band hemi/zone transponders and Ku-band S1/S2/S3 transponders in channels 1 through 8, just as on INTELSAT VII.

### **Conclusions**

The INTELSAT VII/VIIA satellites were designed with higher power and better communications parameters than their predecessors (the INTELSAT V/VA and VI series). These satellites possess great flexibility in connectivity, coverage, and transponder performance, and INTELSAT expects them to meet the needs of existing and new system users through the 1990s and into the 21st century. This detailed description of the INTELSAT VII/VIIA communications payload features should amply demonstrate that a wide range of services can be provided via cost-effective ground segment facilities.

## Bibliography

- Abdel-Nabi, T., E. Koh, and D. Kennedy, "INTELSAT VII Communications Capabilities and Performance," 13th AIAA International Communications Satellite Systems Conference, Los Angeles, California, March 1990, *A Collection of Technical Papers*, Pt. 1, pp. 84-94.
- Abdel-Nabi, T., and P. Nadkarni, "The Planning and Service Utilization Aspects of the INTELSAT VII-A Spacecraft," 14th AIAA International Communications Satellite Systems Conference, Washington, D.C., March 1992, *A Collection of Technical Papers*, Pt. 2, pp. 1019-1024.
- Edridge, M., F. Dietrich, and K. Betaharon, "Features of the INTELSAT VII Repeater," 13th AIAA International Communications Satellite Systems Conference, Los Angeles, California, March 1990, *A Collection of Technical Papers*, Pt. 1, pp. 111-119.
- INTELSAT Earth Station Standard, IESS-409 (Rev. 3), "INTELSAT VII Satellite Characteristics," May 29, 1995.
- INTELSAT Earth Station Standard, IESS-415 (Rev. 2), "INTELSAT VIIIA Satellite Characteristics," August 15, 1995.
- INTELSAT Earth Station Standard, IESS-410 (Rev. 4), Appendix D (INTELSAT VII) and Appendix E (INTELSAT VIIA), "INTELSAT Space Segment Leased Transponder Definitions and Associated Operating Conditions," November 10, 1995.
- Madon, P. J., and D. K. Sachdev, "INTELSAT VII Program and the Future," 13th AIAA International Communications Satellite Systems Conference, Los Angeles, California, March 1990, *A Collection of Technical Papers*, Pt. 1, pp. 74-77.
- Nadkarni, P., *et al.*, "INTELSAT VII Planning and Evolution," 13th AIAA International Communications Satellite Systems Conference, Los Angeles, California, March 1990, *A Collection of Technical Papers*, Pt. 1, pp. 78-83.
- Neyret, P., *et al.*, "The INTELSAT VII Spacecraft," 13th AIAA International Communications Satellite Systems Conference, Los Angeles, California, March 1990, *A Collection of Technical Papers*, Pt. 1, pp. 95-110.
- Neyret, P., *et al.*, "INTELSAT VII-A Spacecraft," 14th AIAA International Communications Satellite Systems Conference, Washington, D.C., March 1992, *A Collection of Technical Papers*, Pt. 2, pp. 1025-1030.
- Sachdev, D. K., *et al.*, "INTELSAT VII: A Flexible Spacecraft for the 1990s and Beyond," *Proc. IEEE*, Vol. 78, No. 7, July 1990, pp. 1057-1074.
- Schennum, G., *et al.*, "The INTELSAT VII Antenna Farm," 13th AIAA International Communications Satellite Systems Conference, Los Angeles, California, March 1990, *A Collection of Technical Papers*, Pt. 1, pp. 120-125.
- Thompson, P. T., and R. Silk, "INTELSAT VII—Another Step in the Development of Global Communications," *Journal of the British Interplanetary Society*, Vol. 43, No. 8, August 1990, pp. 353-364.
- Thompson, P. T., *et al.*, "The INTELSAT VII/VIIA Generation of Global Communications Satellites," *International Journal of Satellite Communications*, Vol. 13, 1995, pp. 39-48.

## Acknowledgments

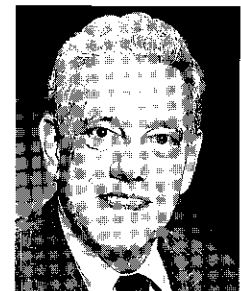
*The authors wish to thank J. Mattingly, C. Jeffcoat, and E. Wells of COMSAT World Systems for their encouragement and support, as well as K. Betaharon and L. Khoo of INTELSAT for their helpful guidance.*



*Simin Jamshidi received the BSEE and MSEE degrees from George Washington University in 1978 and 1980, respectively. From 1980 to 1988 she was with INTELSAT, where she had systems planning and service development responsibilities. As Manager, Digital Services, at INTELSAT, she was heavily involved in developing IBS, IDR, and INTELNET services. From 1988 to 1990, she served as Product Manager, Satellite Data Services, at GTE Spacenet Corporation, where she managed partial transponder services for the full spectrum of domestic customers.*

*Ms. Jamshidi joined COMSAT World Systems in 1990 as a Senior Systems Planner, and is currently participating in planning the next generation of INTELSAT satellites. She also serves as Chairman of the INTELSAT Board of Governors Advisory Committee on Planning.*

*Cal Cotner received a BS in electrical engineering (cum laude) from Princeton University in 1962, and an MSEE from Cornell University in 1964. He has been with COMSAT since 1967, and is currently Director of Customer Technical Support in COMSAT World Systems. His primary technical interests are in the areas of transmission analysis, earth station design, and high-power amplifiers. Mr. Cotner has held several technical management positions at COMSAT Laboratories, COMSAT General, and COMSAT World Systems, including representing the U.S. Signatory on the INTELSAT Board of Governor's Technical Advisory Committee for 5 years. He recently retired from the U.S. Army Reserve as a Colonel, Signal Corps. A Commandant's List Graduate of the Command and General Staff College, his reserve assignments have been oriented toward satellite communications, including a 5-year tour on The Joint Staff. He is a Senior Member of AIAA.*



## **A BISDN-compatible 140/155-Mbit/s modem/codec**

S. P. MILLER, F. HEMMATI, D. H. LAYER, AND P. N. JOHNSON

### **Abstract**

Coded modulation techniques for development of a broadband integrated services digital network (BISDN)-compatible modem/codec are investigated. The selected baseband processor system supports data transmission at a rate of 155.52 Mbit/s over an INTELSAT 72-MHz transponder. Performance objectives and fundamental system parameters, including channel symbol rate, code rate, and the modulation scheme are discussed. From several candidate codes, a concatenated coding system is selected which consists of a coded octal phase shift keying modulation as the inner code and a high-rate Reed-Solomon code as the outer code. The bit error rate performance results from the computer simulation are presented and analyzed. The hardware implementation of the selected concatenated coding system is also described, and laboratory test results are examined.

### **Introduction**

Current INTELSAT VVA time-division multiple access (TDMA) links use quadrature phase shift keying (QPSK) modulation with a transmission rate of 60 Msymbol/s. The INTELSAT VVA system has a transponder frequency spacing of 80 MHz and a usable bandwidth of 72 MHz per transponder. With forward error correction (FEC) coding of rate 7/8, the bandwidth efficiency of the QPSK TDMA system is about 1.31 bit/s/Hz of the allocated bandwidth.

COMSAT Laboratories recently developed a 140-Mbit/s coded octal phase shift keying (COPSK) modem with an operating symbol rate of 60 Msymbol/s. The implemented 140-Mbit/s modem/codec consists of a 16-state trellis code of rate 7/9 and an OPSK modem [1]. Transatlantic field tests of the system

were conducted which effectively demonstrated that restoration of the TAT-8 fiber optic cable via satellite is feasible. The bandwidth efficiency of the 140-Mbit/s CQPSK system is 1.75 bit/s/Hz with respect to the allocated bandwidth, which is an improvement of 33 percent over the QPSK TDMA system.

The integrated services digital network (ISDN) will provide broadband services, including broadcast television, high-definition television, high-speed transmission of database files, and inter-computer communications. To effectively support this range of services, broadband ISDN (BISDN) uses a new transmission and switching technique termed asynchronous transfer mode (ATM). ATM employs the capabilities of time-division multiplexing to permit the efficient transport and switching of the wide variety of information services characteristics envisioned for BISDN. For the synchronous optical network (SONET), ATM packets are embedded in a synchronous time-multiplexed bit stream which supports the standard BISDN H4 rate of 155.52 Mbit/s.

Given the high reliability of satellites, it is advantageous for network operators to have available economical, BISDN-compatible links via the INTELSAT system which use a single 72-MHz transponder. Such satellite links can interconnect BISDN networks and provide for early introduction of this service. Satellites also offer worldwide interconnectivity, and their support is essential if BISDN is to prosper in many areas of the world. Additionally, satellites can act as a "safety valve" in optical fiber networks. In the case of fiber failure or network congestion, traffic can be routed through a satellite channel on a demand-assigned basis.

This paper investigates the design, performance, and implementation of a BISDN-compatible modem/codec. System performance objectives and parameters are briefly reviewed, and QPSK is selected as the modulation format because of its constant envelope and the high power efficiency achievable when combined with an appropriate code. Coded modulation techniques, including Ungerboeck codes and Imai-Hirakawa codes are briefly reviewed. The selected code is an Imai-Hirakawa code with block/convolutional component codes, concatenated with a high-rate Reed-Solomon (RS) code to achieve good performance. The hardware implementation and bit error rate (BER) performance of the code over an additive white Gaussian noise (AWGN) channel and a typical INTELSAT V nonlinear channel are presented, and the flexibility of the decoder for transmission at 140 Mbit/s is examined.

### **System performance and performance objectives**

The fundamental parameters for a coded modulation system operating at a given information rate include the channel symbol rate, the code rate ( $R$ ), the

modulation scheme, and the expected error performance. A transmission symbol rate of close to 60 Msymbol/s is preferable because the QPSK TDMA system is operating at this rate, and hence the available subsystems such as transmit and receive filters and equalizers can also be used in the BISDN system, thus reducing the overall unit cost. Selecting an operating symbol rate near 60 Msymbol/s for the BISDN system will also minimize its interference with existing 120-Mbit/s TDMA QPSK channels. Also, high-level modulation schemes are very sensitive to phase noise, which mainly arises from the group delay distortion of pulse-shaping and satellite-multiplexing filters, AM/AM and AM/PM nonlinearities, residual phase modulation in high-power amplifiers (HPAs), and carrier phase noise. Group delay distortion of filters can be almost perfectly equalized when the channel symbol rate is near 60 Msymbol/s; however, an equalizer for much higher channel symbol rates might not perform as well.

International standards for the error performance of BISDNs are not yet available. However, it is expected that a BER of approximately  $10^{-10}$  for 90 percent of the available time will be adopted by the International Telegraphy and Telephony Consultative Committee (CCITT) for broadband service. Extensive link analysis, laboratory hardware measurements, and field trials have indicated that the INTELSAT V transponders are primarily interference-limited (not thermal noise limited) when supporting very high-data-rate services [2]. Bandwidth-efficient coded modulation schemes suitable for high-speed implementation do not afford sufficient power efficiency to correct all the errors caused by link interference. The BER vs the energy-per-bit to noise-power density ratio,  $E_b/N_o$ , performance curves exhibit unresolvable errors at BERS of  $10^{-7}$  and less. Therefore, a concatenated coding system, consisting of a power- and bandwidth-efficient inner code and a high-rate RS outer code, was selected to achieve the required BER performance of  $10^{-10}$ . Performance objectives and system parameters for the BISDN codec/modem are summarized in Table I.

### **Candidate modulation schemes**

The transmission of 155.52 Mbit/s over INTELSAT V transponders requires a bandwidth efficiency of about 1.94 bit/s/Hz, which is an improvement of nearly 48 percent over the QPSK TDMA system. Because this required bandwidth efficiency cannot be achieved by QPSK modulation, higher level modulation schemes such as OPSK, 16-ary PSK, and 16-ary quadrature amplitude modulation (QAM) were considered.

Octal PSK (OPSK) modulation was selected as the most viable modulation method for this system because of its demonstrated ability to achieve good

TABLE 1. SYSTEM PERFORMANCE GOALS

PARAMETER	GOALS	
Information Rate (Mbit/s)	155.52	139.264
OPSK Symbol Rate (Msymbol/s)	60.414	60.281
Bandwidth Efficiency (bit/s/Hz)	2.1	2.0
Channel Bandwidth (MHz)	72	72
Multistage Inner Code Rate	13/15	7/9
Inner Decoder Type	Viterbi/parity mixed mode at 60 Msymbol/s	
Outer RS Code Rate	239/255	175/195
System BER Performance	<2 dB from theory at BER = $10^{-7}$	
Probability of Miss and False UW Detect	$<1 \times 10^{-8}$	$<1 \times 10^{-8}$
Sync/Status Overhead (%)	1	1
Slip Recovery Time (ms)	<1	<1
BER (Modem hard-decision)	<1.4 dB from ideal at $10^{-3}$	
Carrier Cycle Slip Rate	$<1 \times 10^{-4}$ slips/s at $C/N_o = 87.8$ dB-Hz	
IF Carrier Offset (kHz)	$\pm 25$	$\pm 25$
Input Signal Level Range	12 dB (+2 to -10 dB relative to nominal)	

power and bandwidth efficiency over a satellite channel. In the past, it has been shown that OPSK modulation is readily implemented for high-speed applications [2].

Although 16-ary PSK is a bandwidth-efficient modulation scheme, it is very difficult to implement for high-speed applications. The performance of 16 PSK is very sensitive to phase noise, and its demodulator requires fine resolution to distinguish between the 16 points closely packed on the circumference of a circle. Also, the complexity of the synchronization circuits for symbol timing, carrier, and clock recovery is much greater than that for OPSK. Sixteen-ary QAM is also a power- and bandwidth-efficient modulation scheme, but is most suitable for linear channels. Since this application requires that the earth station HPAs, and particularly the satellite traveling wave tube amplifiers (TWTAs), operate in the nonlinear region, near their saturation point, the 16-QAM BER performance would not be satisfactory.

OPSK modulation, together with a suitable code, appears to be the best candidate modulation method. The COPSK modulation techniques that were considered for this application are discussed in the next section.

### COPSK modulation techniques

The area of power- and bandwidth-efficient coded modulation has been of great research interest for several years. In addition to the class of coded continuous-phase frequency shift keying (CPFSK) modulation schemes, research in this area has focused in two closely related areas known as Ungerboeck codes and Imai-Hirakawa codes. CPFSK modulation schemes, which include the class of multi- $h$  codes, are not suitable for the present application because of their low power efficiency and the unmanageable complexity of their modem and codec hardware implementation operating at the required speed.

After carefully considering a number of candidate Ungerboeck and Imai-Hirakawa codes that could be used for this application, a rate 13/15 Imai-Hirakawa, or multistage, code was identified as the most appropriate for fulfilling the system's performance and flexibility goals. The following sections summarize the theory of the particular code selected and describe its implementation.

### The selected Imai-Hirakawa code

The multilevel coding method proposed in 1977 by Imai and Hirakawa [3] is convenient for high-speed implementation and, for a selected modulation signal space, allows a wide range for the code rate. In a multilevel/phase signal space, the Euclidean distances between a particular signal point and the remaining points in the signal set are not equal; the distance between adjacent signal points is much smaller than the maximum distance between elements in the signal space. Therefore, channel noise is more likely to cause a particular signal point to be received as an adjacent signal point, than as a signal point that is further away in the signal space. The structure of the class of Imai-Hirakawa codes exploits this concept. Codes in this class use several different encoders to encode the different bits within the signal points. Lower rate codes are placed on bits which distinguish between adjacent signal points in the signal space, and codes with less redundancy, or no coding at all, are used on the bits which select between points that are at a greater distance from each other in the signal space. Both block codes and convolutional codes may be used as the constituents of a multistage coding system.

Generalized versions of the Imai-Hirakawa codes have been designed by Ginzburg [4] and Sayegh [5]. In particular, Sayegh has described an efficient multistage decoding procedure in which the most error-prone information bits are estimated first, using *a posteriori* probabilities based on the received channel symbols and the code structure. These estimates are then used in later decoding stages to estimate the successively less error-prone information bits.

Among several candidate QPSK modulation schemes, a block/convolutional Imai-Hirakawa code of rate 13/15, affording an asymptotic coding gain of 3.58 dB over uncoded QPSK, was selected as the inner code [6]. This multistage code is depicted in Figure 1. While other CQPSK modulation schemes could potentially yield higher power/bandwidth efficiency, this particular code was chosen mainly because of its simplicity of hardware implementation.

In the specific multistage code selected for operation at 155 Mbit/s, a different code is responsible for encoding each of the 3 bits of the QPSK symbol. The most significant bit of the symbol, which differentiates between signal points at the maximum (or BPSK) distance from each other, is universally encoded (or uncoded). The middle bit of the QPSK symbol, which differentiates between the signal points at QPSK distance from each other, is protected by a single parity check code of length 15. The least significant bit of each QPSK symbol, which differentiates between signal points that are closest (or at QPSK distance from each other), is encoded by a rate 2/3 punctured convolutional code.

The three component encoders of the QPSK system jointly encode blocks of 39 bits at a time. The outputs of the encoders are arranged in a 3-row by 15-column array. To create the first row, 10 information bits are supplied to the rate 2/3 encoder, and the corresponding 15 consecutive encoded output bits become the first row of the array. Fourteen information bits are supplied to the parity check encoder, and the single encoded 15-bit output block becomes the second row of the array. The last row of the array is filled with 15 consecutive uncoded information bits. The 39-bit block encoding process produces 45 output bits, for an overall code rate of 39/45 (or 13/15). Each 3-bit column in the encoded array represents one of the points in the QPSK signal space. With an information rate of 155 Mbit/s and a code rate of 13/15, the transmit rate is approximately 180 Mbit/s, or 60 Msymbol/s when QPSK modulation is used.

After analyzing the burst error statistics of the inner code, an eight-symbol error-correcting (255, 239) RS outer code was found suitable for achieving the

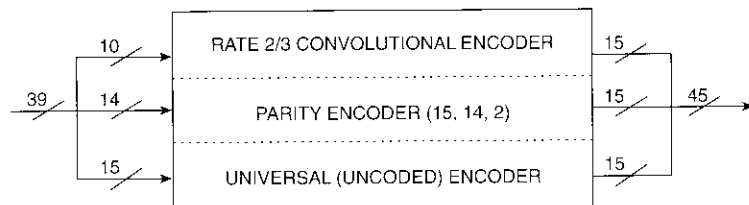


Figure 1. Rate 13/15 Selected Multistage Code

required BER performance. The overall rate of this concatenated coding system is approximately 13/16 and requires a channel symbol rate of 64 Msymbol/s to support 155.52-Mbit/s data and synchronization overhead bits.

The required channel symbol rate can be reduced to 62.4 MHz by using a (15, 15, 1) universal code instead of the (15, 14, 2) parity check code in the second encoding stage. In this case, the inner code operates at 58.5 MHz. Finally, a 140-Mbit/s codec can be realized if the inner code of rate 13/15 is concatenated with a (195, 175) 10-error-correcting shortened RS code requiring a channel symbol rate of 60 MHz.

### Performance analysis

The BER performance of the concatenated coding system was evaluated by computer simulation by first examining the performance of the inner code, without the RS outer code, under various link conditions. System performance was then evaluated under worst-case link conditions. The system environment and performance parameters considered in the computer simulation are summarized in Table 2.

In the computer simulation, the received channel symbols were first quantized by a 64-level quantizer, and then compressed to 3 bits by nonlinear mapping, to model the potential hardware realization. Over an AWGN channel and at a BER of  $10^{-5}$ , the BER performance of this quantization scheme is within 0.2 dB of the theoretical performance of the coded system using unquantized channel symbols.

BER performance results over an AWGN channel and over a typical INTELSAT V nonlinear channel are shown in Figure 2. For the AWGN channel,

TABLE 2. COMPUTER SIMULATION SYSTEM VARIABLES AND ASSUMPTIONS

PARAMETER	VALUE
No. of Samples/Symbol	16
HPA IBO	10 dB
Satellite TWTA IBO	2 dB
CCI Level	-18.5 dB
Separation Between Adjacent Channels	80 MHz
Rolloff Factor for Square Root Nyquist Modem Filters	40%
Ideally Group-Delay-Equalized Filters	
Perfect Symbol Phase and Symbol Timing	

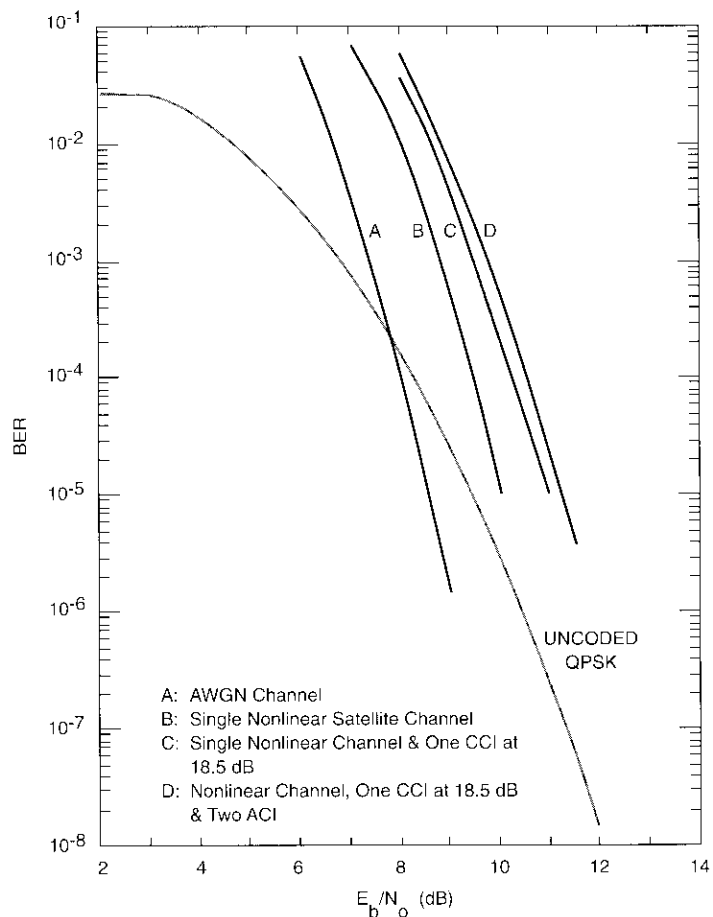


Figure 2. Simulated BER Performance of the Rate 13/15 Code Over the Nonlinear Satellite Channel

a coding gain of about 1.2 dB over uncoded QPSK is observed at a BER of  $10^{-5}$ . Extrapolating the BER performance curve of Figure 2 reveals that an effective coding gain of about 2.5 dB is expected at a BER of  $10^{-8}$ . The 1.08-dB discrepancy between the 3.58-dB asymptotic coding gain for this code and the effective coding gain of 2.5 dB is due to the multiplicity of the neighboring paths, the suboptimum multistage decoding, and finite eight-level symbol metric quantization.

The computer simulation also shows that at a BER of  $10^{-4}$ , link nonlinearities and intersymbol interference degrade the performance of the single nonlinear satellite channel by about 1.5 dB relative to the AWGN channel performance. The BER performance degrades by an additional 1 dB with one entry of co-channel interference (CCI) at a power level of -18.5 dB with respect to the desired channel. The two 60-Msymbol/s adjacent channels located at +80 and -80 MHz relative to the center frequency of the desired channel degrade the BER performance by an additional 0.3 dB. These results are obtained by assuming that the group delay distortion of the modem filters and satellite multiplexing filters is ideally equalized. In a real channel, phase noise caused by the carrier oscillator, link nonlinearities, and group delay distortion of filters degrades system performance. For example, at a BER of  $10^{-4}$ , degradations due to unequalized group delay distortion can be as much as 0.8 dB.

The BER performance of the concatenated coding system was also evaluated by computer simulation. The results are shown in Figure 3 for the nonlinear channel with two adjacent channel interference (ACI) and one CCI at -18.5 dB. The dashed curves show the BER performance of the inner code, without the RS outer coding. The performance of the concatenated coding system with channel symbol rates of 64 and 62.4 Msymbol/s, corresponding to the inner codes with and without parity check coding in the second stage, are depicted as solid curves. Because of its lower channel symbol rate, the 62.4-Msymbol/s system outperforms the 64-Msymbol/s system by about 1 dB. The 62.4-Msymbol/s system is expected to achieve a BER of  $10^{-10}$  at less than 12 dB, which allows sufficient margin for modem implementation loss and the transmission link.

### Hardware implementation

Detailed design, construction, and laboratory testing of the multistage inner coding system has been completed, as has hardware design of the RS outer codec. Testing and integration with the outer codec and modem are under way and will be completed in early 1992.

To implement the concatenated multistage inner code and the RS outer code, the concatenated coding system uses five circuit boards housed in a common chassis with backplane intercommunications. The circuit boards employ an efficient mixture of high-speed emitter-coupled logic (ECL), intermediate-speed complementary metal-oxide semiconductor (CMOS) and transistor-transistor logic (TTL) circuitry, and analog phase-locked loop components. The first circuit board implements the high-speed data interfaces to the system, the phase-locked loop timing circuits, and the serial-to-parallel

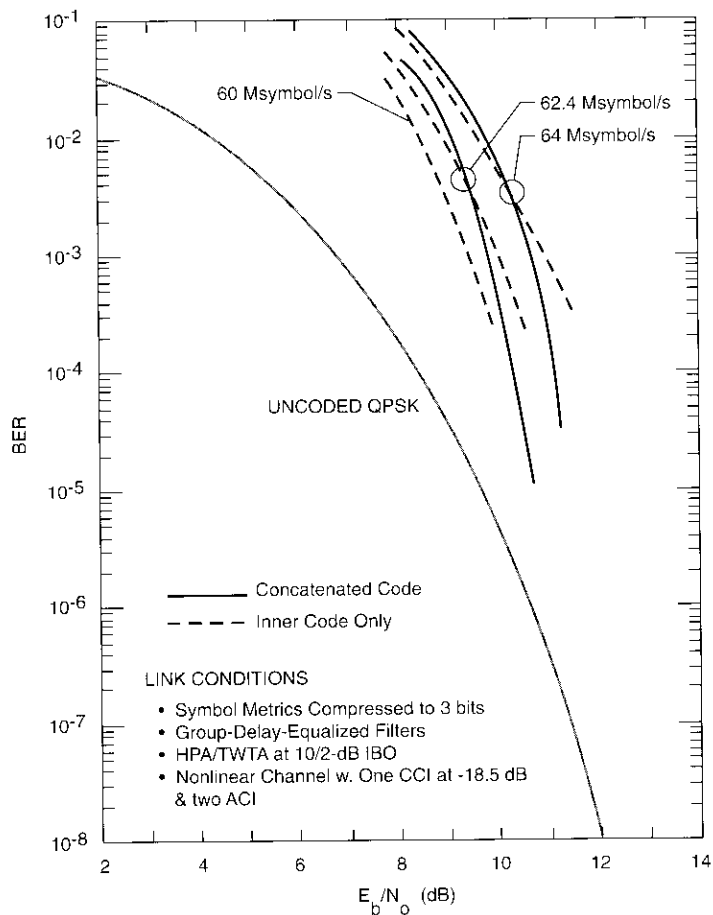


Figure 3. Simulated BER Performance of the Concatenated Coding System Over the INTELSAT V Transponders

data conversion function. The CMOS/TTL design of the second board executes the outer code RS encoding, decoding, interleaving, and block code synchronization functions. Parallel use of off-the-shelf RS codec chips supports the system's high-data-rate throughput. A combination of the parallel RS coding devices and auxiliary codeword memory serves to implement the depth-of-four interleaving that is necessary for the RS code to effectively combat the system's burst errors. An efficient combination of programmable gate array devices and discrete logic and memory comprises the rest of the second board

design. The third board uses programmable and discrete CMOS logic to implement the transmit functions for the inner coding system, including multistage encoding, data scrambling, unique word insertion, data frame construction, and interface to the OPSK modulator.

The fourth and fifth boards are responsible for the inner code receive-side processing. In particular, the fourth board operates at a symbol rate of 62.4 Msymbol/s and uses high-speed ECL circuitry to perform OPSK phase ambiguity resolution, inner decoder synchronization, Viterbi metric calculation, parity decoding, universal decoding, and overall decoder timing and control. The fifth board uses a parallel array of commercially available Viterbi codec chips, with a mixture of CMOS discrete and programmable logic, to implement the Viterbi decoding portion of the multistage decoder, the data alignment function, and the Doppler buffering.

The OPSK modulator accepts 3-bit symbols from the encoder and creates one of the eight phase states in the OPSK signal space. The OPSK demodulator receives the incoming IF signal, makes gain adjustments to the signal path, removes the modulation to recover the carrier, generates symbol timing, and demodulates the data into soft-decision quadrature baseband streams. In the past, COMSAT Laboratories developed a 180-Mbit/s OPSK modem for use in its 140-Mbit/s rate 7/9 COPSK system [2]. The basic structure of this design was incorporated into the modem design for the present system, with enhancements for additional alarms and operational features.

A number of alarms and operational features from relevant CCITT Recommendations were incorporated into the proof-of-concept hardware model, which renders the system design suitable for manufacturing and field deployment. Included among the operational enhancements are the ability to generate an alarm indication signal (AIS) when a fatal error is present in the coded modulation system, on-line BER monitoring capability, a high-BER alarm, standard coded mark inverse (CMI) high-speed interface compatibility, and plesiochronous/Doppler buffering for operation with satellites in inclined orbits up to 3°. The most prominent maintenance features include baseband loop-back capability, clock and data activity detectors and indicators, power supply indicators, and ample test points.

### Laboratory test results

Laboratory tests were performed in mid-1991 on the 155-Mbit/s BISDN modem/codec, utilizing the OPSK modem and the inner codec described above, to establish the performance of the system prior to applying the RS outer code. This test configuration was also motivated by the fact that the inner code hardware was completed early enough in the program to be integrated with the



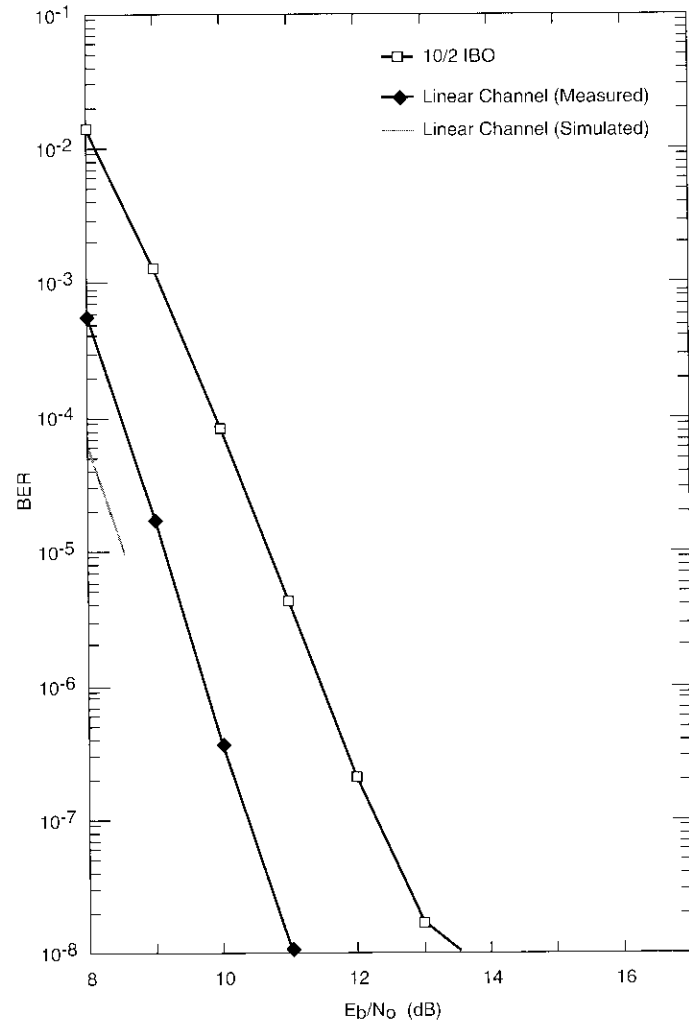


Figure 5. 155-Mbit/s System BER: No Interference

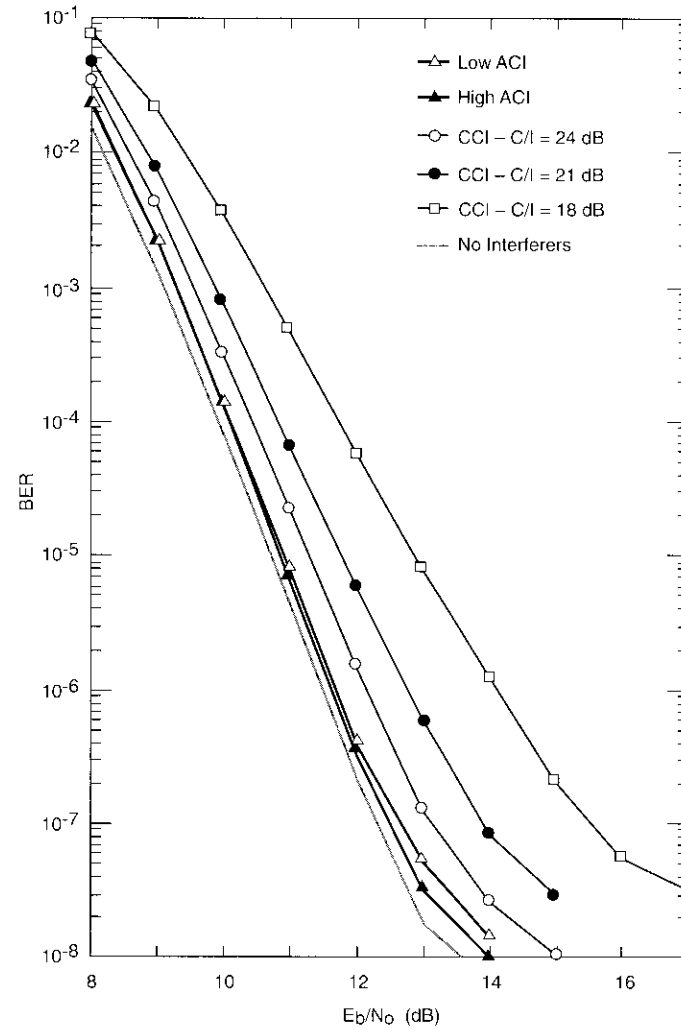
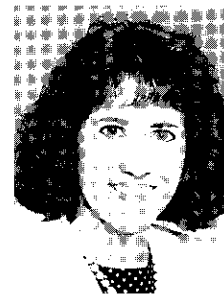


Figure 6. 155-Mbit/s System BER: Nonlinear Channel With Interference

The same interfering carrier used in the CCI was employed to measure the effect of ACI on 155-Mbit/s system performance. Because of time constraints and the unavailability of a second up-converter, these measurements were limited to only a single adjacent channel carrier per measurement. Figure 6 shows the resulting system performance when an adjacent carrier of equal power is placed in either the high-side (desired frequency plus 80 MHz) or low-side (desired frequency minus 80 MHz) adjacent channel. Comparing these results with the no-interference data, which are also plotted, it is apparent that the degradation in system performance due to the single adjacent channel is slight, on the order of 0.2 to 0.4 dB.

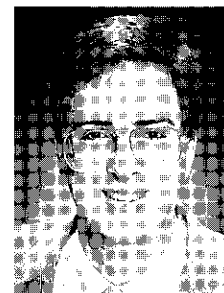
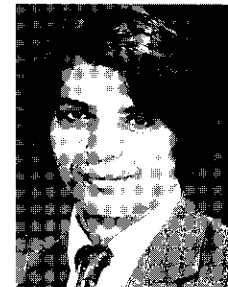
### References

- [1] F. Hemmati and R. J. F. Fang, "Low-Complexity Coding Methods for High-Data-Rate Channels," *COMSAT Technical Review*, Vol. 16, No. 2, Fall 1986, pp. 425-447.
- [2] D. H. Layer, J. M. Kappes, and C. B. Cotner, "140-Mbit/s COPSK Modem Laboratory Tests and Transatlantic Field Trials," *COMSAT Technical Review*, Vol. 20, No. 1, Spring 1990, pp. 63-96.
- [3] H. Imai and S. Hirakawa, "A New Multilevel Coding Method Using Error-Correcting Codes," *IEEE Transactions on Information Theory*, Vol. IT-23, No. 3, May 1977, pp. 371-377.
- [4] V. V. Ginzburg, "Multidimensional Signals for a Continuous Channel," *Problemy Peredachi Informatsii (Problems of Information Transmission)*, Vol. 20, No. 1, 1984, pp. 28-46.
- [5] S. I. Sayegh, "A Class of Optimum Block Codes in Signal Space," *IEEE Transactions on Communications*, Vol. COM-34, No. 10, October 1986, pp. 1043-1045.
- [6] F. Hemmati, "A BISDN-Compatible Modem/Codec," IEEE Global Telecommunications Conference, San Diego, California, December 1990, *Conf. Rec.*, pp. 907.4.1-907.4.5.
- [7] INTELSAT, *Satellite System Operating Guide*, Vol. 3, Book 2, Sec. 3 and 7, October 1986.



*Susan P. Miller received a BSEE from the Rensselaer Polytechnic Institute in 1983, and an MSEE from the University of Southern California in 1986. She is currently Manager of Advanced Business Applications for COMSAT World Systems, responsible for developing and implementing new services in the areas of ATM networks, bandwidth-on-demand systems, frame relay networks, and ISDN interfaces to satellite networks. Prior to joining COMSAT World Systems, Ms. Miller was Associate Manager, Digital Techniques Department, at COMSAT Laboratories where she held design and project management responsibility for the study, analysis, and development of advanced digital satellite communications equipment, specializing in forward error correction and signal processing applications for increased bandwidth efficiency and improved performance.*

*Farhad Hemmati received an MSEE and PhD from the Illinois Institute of Technology in 1973 and 1977, respectively. Since joining COMSAT Laboratories in 1982, he has worked on power- and bandwidth-efficient coded modulation techniques and various signal processing methods for satellite channels. He is currently a Senior Scientist in the Communications Technology Division, where his primary interests are portable and mobile satellite communications, spread spectrum, and multiple access.*



*David H. Layer received a BSEE degree from the University of Maryland, College Park, and an MSEE from Purdue University. He was with COMSAT Laboratories, Clarksburg, Maryland, for more than 10 years, most recently as Associate Manager of the Transmission and Channel Processing Department. While at COMSAT, Mr. Layer designed numerous digital PSK modems for satellite transmission—most notably a variable-rate modem for MPEG-2 video distribution—and was responsible for burst-mode implementation of a 180-Mbit/s, 8-PSK modem designed for cable restoration. In addition, he was the chief designer of the MSP-10 modem ASIC, which performs virtually all of the transmit and receive baseband signal processing functions of a QPSK modem over a 64-kbit to 20-Mbit data rate range. His other technical areas of interest at COMSAT included*

satellite link equalization and differential GPS—in particular, the distribution of DGPS correction signals via satellite.

Mr. Layer is currently a Senior Engineer in the Science and Technology Department of the National Association of Broadcasters, Washington, D.C. Since joining NAB in August 1995, he has worked primarily with the NRSC's DAB and high-speed FM subcarrier subcommittees toward the establishment of technical standards and technical recommendations in these areas.



Peter N. Johnson is a Staff Communications Engineer in the Advanced Projects and Applications Division at Enscor, Inc., Springfield, Virginia, where he is responsible for the design and implementation of military and commercial portable land-based spread spectrum communications systems utilizing various multiple-access methods. Prior to joining Enscor, Mr. Johnson was a Member of the Technical Staff in the Transmission Processing and Digital Techniques Department at COMSAT Laboratories, where his responsibilities focused on the research and development of high-speed, bandwidth-efficient satellite communications

systems and equipment. He received a BA in music education from Berklee College of Music, Boston, Massachusetts, in 1980.

## Translations of Abstracts

### Caractéristiques de fonctionnement de la plate-forme du satellite INTELSAT-K

K. RAGHUNATHAN, T. RUSH ET A. OZKUL

#### Sommaire

Le satellite INTELSAT-K est monté sur une plate-forme GE-Martin Marietta 5000 à stabilisation triaxiale dont les quatre batteries de 50 Ah à 22 éléments permettent au générateur solaire de fournir 3,5 kW d'énergie après 10 années sur orbite. Le corps principal du satellite renferme le cylindre central ainsi que les propulseurs et leurs réservoirs. Le système propulsif comprend deux moteurs d'apogée bimodes de 45 kg à ergols liquides et quatre propulseurs électrothermiques améliorés à hydrazine pour le contrôle d'inclinaison. La masse du satellite s'élevait à 2 925 kg au décollage et son poids à vide était de 1 250 kg. Les caractéristiques fondamentales du modèle INTELSAT-K sont décrites en mettant l'accent sur les capacités du satellite en tant qu'elles se rapportent aux opérations du satellite sur l'orbite.

### La charge utile de l'INTELSAT-K

R. A. PETERS, F. L. KHOO ET A. OZKUL

#### Sommaire

Dans le domaine des télécommunications intercontinentales, le satellite INTELSAT-K se prête à des applications telles que la distribution vidéo, l'utilisation de micro-terminaux, le service international de communications d'entreprises et le reportage d'actualités par satellite, qui font appel à des terminaux de réception économiques et de taille réduite, ce qui exige une p.i.r.e. élevée sur la liaison descendante. La charge utile de ce satellite se compose de seize répéteurs de 60 W et 54 MHz qui couvrent l'Europe et l'Amérique du Nord en mode émission et réception, et l'Amérique du Sud en mode émission. La souplesse du dispositif d'interconnexion des faisceaux permet de varier les connexions sur les liaisons montante et descendante, et même de combiner les trois faisceaux. Les amplificateurs dans un panneau du répéteur ont des circuits limiteurs destinés à compenser les affaiblissements du signal sur la liaison montante, comme ceux causés par les évanouissements dus à la propagation. L'article décrit en détail les caractéristiques de cette charge utile et passe en revue les essais de vérification de performance du satellite.

## **Desempeño de las comunicaciones de los satélites INTELSAT VII y VIIA**

S. JAMSHIDI Y C. B. COTNER

### **Abstracto**

En este artículo se describen las características de desempeño de los transpondedores de banda C y Ku instalados en los satélites INTELSAT VII y VIIA, que recién comienzan a prestar servicios. Se hace hincapié en parámetros de interés para usuarios potenciales, incluida la potencia isotropa radiada efectiva (P.I.R.E.), la relación ganancia-temperatura de ruido ( $G/T$ ) y la ganancia de los transpondedores. Se muestran las coberturas de varios haces para lugares típicos en las regiones de los océanos Atlántico y Pacífico. También se describe la capacidad de interconexión entre los diferentes transpondedores, que es una fuente clave de flexibilidad. Se incluye una bibliografía completa de referencias en las que se discuten los satélites INTELSAT VII/VIIA.

## **Un módem/códec de 140/155 Mbit/s compatible con la RDSIBA**

S. P. MILLER, F. HEMMATI, D. H. LAYER Y P. N. JOHNSON

### **Abstracto**

Se investigan técnicas de modulación codificada para desarrollar un módem/códec que sea compatible con la red digital de servicios integrados de banda ancha (RDSIBA). El sistema de procesador de banda de base seleccionado respalda la transmisión de datos a una velocidad de 155,52 Mbit/s por un transpondedor INTELSAT de 72 MHz. Se discuten los objetivos de desempeño y los parámetros fundamentales de este sistema, incluida la velocidad de símbolos por canal, la relación de codificación y el plan de modulación. Entre los varios códigos disponibles se seleccionó un sistema de codificación concatenada con modulación octal por desfase como código interior y un codificador Reed-Solomon de alta velocidad como código exterior. Se presentan y analizan los resultados de la simulación en computadora del desempeño de la tasa de errores en los bits. También se describe la implementación de los equipos del sistema seleccionado de codificación concatenada, y se examinan los resultados de las pruebas hechas en el laboratorio.

## **Author Index, CTR 1993**

The following is a list of articles that appeared in *COMSAT Technical Review* for 1993. The list is cross-referenced based on COMSAT authors (only). The code number at the end of each entry should be used when ordering reprints from Corporate Records, COMSAT Corporation, 22300 COMSAT Drive, Clarksburg, MD 20871-9475 USA.

- ALLISON, G., see Ramos, A.  
 CHITRE, D. M., and W. S. Oei,\* "Architectures for INTELSAT Communications Systems in the ISDN Era," *COMSAT Technical Review*, Vol. 23, No. 1, Spring 1993, pp. 1-33. [CTR93/393]  
 COOK, W. L., "INTERIM System Planning Computer," *COMSAT Technical Review*, Vol. 23, No. 2, Fall 1993, pp. 295-316. [CTR93/401]  
 ESTEP, G. C., see Upshur, J. I.  
 FULLETT, K. D.,\* B. J. Kasstan,\*\* W. D. Kelley, V. E. Riginos, P-H. Shen, S. L. Teller, and Y. Tharaud,\*\* "The EUTELSAT In-Orbit Test System," *COMSAT Technical Review*, Vol. 23, No. 1, Spring 1993, pp. 61-99. [CTR93/395]  
 FULLETT, K. D.,\* W. D. Kelley, V. E. Riginos, P-H. Shen, and S. L. Teller, "Microwave Measurement System Software," *COMSAT Technical Review*, Vol. 23, No. 1, Spring 1993, pp. 101-137. [CTR93/396]  
 GUPTA, R. K., see Upshur, J. I.  
 HAMPSCH, T., see Ramos, A.  
 HARE, F. W., see Ramos, A.  
 HASCHART, D. V., see Sandrin, W. A.  
 KELLEY, W. D., see Fullett, K. D. (two papers)  
 KEMP, L. W., and D. C. May, "Geostationary Communications Satellite Log for Year-End 1992," *COMSAT Technical Review*, Vol. 23, No. 1, Spring 1993, pp. 139-206. [CTR93/397]  
 KHALONA, R. A., "Performance of M-ary FSK Modulation in a Shadowed Land Mobile Satellite Communications Channel," *COMSAT Technical Review*, Vol. 23, No. 2, Fall 1993, pp. 225-236. [CTR93/398]  
 KROLL, R. T., see Upshur, J. I.  
 MAY, D. C., see Kemp, L. W.  
 OPIEKUN, J. W., see Ramos, A.  
 RAMOS, A. R., L. Minciotti,\*\* T. Hampsch, G. Allison, E. W. Hare, and J. W. Opiekun, "Design and Validation of the ITALSAT AOCs Flight Simulator," *COMSAT Technical Review*, Vol. 23, No. 1, Spring 1993, pp. 35-60. [CTR93/394]  
 RIGINOS, V. E., see Fullett, K. D. (two papers)

\* INTELSAT author.

\*\* Non-COMSAT author.

- SANDRIN, W. A., and D. V. Haschart, "Availability Prediction for Handheld Communications Systems Using Non-Geosynchronous Satellites," *COMSAT Technical Review*, Vol. 23, No. 2, Fall 1993, pp. 237-270. [CTR93/399]
- SHEN, P-H., see Fullett, K. D. (two papers)
- TELLER, S. L., see Fullett, K. D. (two papers)
- UPSHUR, J. I., R. K. Gupta, G. C. Estep, and R. T. Kroll, "1-W Ku-Band MMIC SSPAs for Communications Satellite Phased-Array Antenna Applications," *COMSAT Technical Review*, Vol. 23, No. 2, Fall 1993, pp. 271-294. [CTR93/400]

## **Index of 1993/1994 Publications by COMSAT Authors**

The following is a list of 1993/1994 publications by authors at COMSAT Corporation. The list is cross-referenced based on COMSAT authors (only). Copies of these publications may be obtained by contacting the COMSAT authors at: COMSAT Corporation, 22300 COMSAT Drive, Clarksburg, MD 20871-9475 USA.

- ALBRIGHT, G., see Kelly, W.
- ARNSTEIN, D., R. Garlow, and M. Lieberman, "Frequency Sharing Between MSS and FS/FSS: Transmission and Coordination Issues," IEEE Military Communications Conference (MILCOM '93), Boston, MA, October 1993, Classified Session 17, *Classified Conf. Rec.*, Paper No. 17.4.
- ARNSTEIN, D., T. Czerner, and J. Buzzelli, "Broadband Signal Processing for AJ and RFI Reduction in Spread Spectrum Systems," IEEE Military Communications Conference (MILCOM '94), Ft. Monmouth, NJ, October 1994, Unclassified Session 16, *Conf. Rec.*, Vol. 2, pp. 421-429, Paper No. 16.6.
- ARNSTEIN, D., see Smith, D. R.
- ASSAL, F., and R. Mott, "In-Orbit Test Transponder (IOTT) for On-Board Regenerative Satellite," 24th General Assembly of the International Union of Radio Science (URSI), Kyoto, Japan, August/September 1993, *Abstracts*, p. 555.
- ASSAL, F., see Ekelman, E.; Estep, G.; Gupta, R. (two papers); and Zaghoul, A. I. (two papers)
- ATIA, A. E., C. Chen, S-W. Chen, G. Estep, and K. Peterson, "Development of Low Cost High Performance C-Band VSAT Outdoor Transceiver," AIAA 15th International Communications Satellite Systems Conference, San Diego, CA, February/March 1994, *A Collection of Technical Papers*, Pt. 2, pp. 660-665, AIAA Paper No. 94-0998-CP.
- BHARGAVA, S., see Rao, A. K.
- BHASKAR, B. R. U., see Ravishankar, C. S.; and Tzeng, F. F.
- BONETTI, R. R., "Microwave Ceramic Filters for Mobile Communication Systems," American Ceramic Society, *Abstracts*, April 1993, p. 33.
- BONETTI, R. R., and A. E. Williams, "Advances in Microwave Active Filters," SBMO International Microwave Conference, São Paulo, Brazil, August 1993, *Proc.*, Vol. 1, pp. 23-28.
- BONETTI, R. R., and A. E. Williams, "New Design Techniques for Coupled-Line Filters With Transmission Zeros," European Microwave Conference, September 1993, *Proc.*, pp. 240-243.
- BONETTI, R. R., see Yao, S-J. (two papers)
- BUZZELLI, J., see Arnstein, D.
- CHEN, C., see Atia, A. E.; and Estep, G.